Separation of Hexane Isomers in Metal-Organic Frameworks (MOFs)

Patricia Alexandra Pinto Mendes

Thèse de doctorat

De l'université de Versailles Saint-Quentin-en-Yvelines
Institut Lavoisier de Versailles

Specialité : Chimie du Solide et des Matériaux

Présenté par

Patrícia Alexandra Pinto Mendes

Pour le titre de
Docteur de l'Université de Versailles Saint-Quentin-en-Yvelines

Séparation des isomères de l'hexane par des solides hybrides poreux (MOFs)

Thèse soutenue publiquement le 9 Septembre 2014 devant la commission d'examen:

Joeri Denayer	Pr., Vrije Universiteit Brussel	Rapporteur
Franck Launay	Pr., Université Pierre et Marie Curie	Rapporteur
François Couty	Pr., Université de Versailles St Quentin	Examinateur
José Silva	Pr., Instituto Politécnico de Bragança	Codirecteur de thèse
Christian Serre	Dr., Université de Versailles St Quentin	Directeur de thèse

To my parents

And my sister

There are special persons that are special not only due the wonderful persons that are, but also due the love inside them.

All that is “made in love” has more value.

Patrícia Mendes

Acknowledgements

To my supervisors, Prof. Alírio Rodrigues and Prof. José Silva, by the opportunity, scientific support and friendship; a big thanks by the confidence and dedication. To the supervisor from *Institut Lavoisier* Dr. Christian Serre and to Dr. Patricia Horcajada by their excellent scientific support and help with the synthesis of MOFs, welcome, hospitality and friendship. To Florence by her friendship, sympathy and time spent in the lab. And to all exceptional team members Thomas, Denise, Nissem, Hubert, Farid,...by their friendship, sympathy and good moments during my stay in Versailles which was great.

To Isabel Patrícia, Maria João and Paula by their sympathy, friendship, laboratories LQA/ LPQ availability and temporary lending of vacuum oven. To all my colleagues, Virgínia, Miguel, Isabel, Mariana, Catarina and Rita from LSRE (IPB pole) by their friendship and great moments, which create an excellent workplace.

Very special thanks to my parents, José and Perpétua, and my sister Susana by their sacrifice, worry, love, kindness, strength and confidence every day. To my all family by their worry and kindness. To my friends and Tona-Tuna by their friendship, kindness and positive energy. To Marco by their friendship, kindness, great support in all moments, happiness and good moments.

To *Faculdade de Engenharia-Universidade do Porto*, LSRE, and *Instituto Politécnico de Bragança* by the opportunity and good financial resources allocated. To Carla Silva from academic services FEUP by their great support and patience. To *Université de Versailles et Saint Quentin-en-Yvelines, Institut Lavoisier de Versailles*, France, by the opportunity and technical conditions needed to perform this work.

To *Fundação da Ciência e Tecnologia* (FCT), Prof. José Silva and Prof. Alírio Rodrigues by the financial support spent in the scientific research fellowship in support to Ph.D.

Life is like a porous solid, it can be amorphous or crystalline. It will be amorphous if we close the doors to the world and to the motivation that origins a life without direction. It will be crystalline if we allow that our life be defined and lapidated by experiences, errors, knowledge and will, that open the mind and make the skyline shine.

Patrícia Mendes

Abstract

The main goals of this research are the synthesis of new specific adsorbents named Metal-Organic Frameworks (MOFs) for the separation of hexane isomers in order to improve the octane number of the gasoline. The laboratories involved here are: the Laboratory of Separation and Reaction Engineering - LSRE (experimental and modelling work on isotherms, diffusion and design of cyclic adsorption industrial processes) and the *Institute Lavoisier de Versailles* - ILV (synthesis of new MOFs). MOFs are crystalline materials with an inorganic sub-unit coordinated to organic complexing molecules (carboxylates, azotates …) forming a porous solid two- or three-dimensional framework with an internal pore system resulting from these connections. These materials, which possess a wide structural and chemical diversity, pore sizes ranging from 2 Å to 60 Å and BET surface areas up to 6500 $m^2.g^{-1}$, have various applications, where, the principal are in catalysis, gas purification/separation or gas storage.

The separation of hexane isomers is actually performed using the conventional Total Isomerization Processes (TIP) for the improvement of the octane rating of the gasoline. The process typically involves isomerizing «normal hydrocarbons» (with low RON) in a reactor using a proper catalyst prior to or following an adsorption-desorption cycle using zeolite 5A which isolates «non-normal paraffins». The success of the process is in part due to the capacity of zeolite 5A to completely separate normal from branched paraffins. In LSRE, it was demonstrated recently that zeolite BETA can be used for to upgrade the actual TIP processes by separating mono form di-branched hexane isomers, where the RON number of the final stream can be improved from 86 to 92 using zeolite Beta as the final separator of di- from mono-branched paraffins. However, this actual process suffers the disadvantage that in the final stream there are still low RON molecules such as the mono-branched isomers of hexane. In order to test another alternative flexible and rigid frameworks were synthesized, performing a set of breakthrough curves with hexane isomers *n*HEX, 3MP and 22DMB 23DMB with the purpose of obtaining adsorption equilibrium isotherms and further analysis of their performances in order to find new frameworks that offer better results. This concerned first the rigid frameworks UiO-66(Zr) functionalized with the functional groups –Br, $–NO_2$, and $–NH_2$; the mesoporous MIL-100(Cr) and its functionalized analogue MIL-100(Cr) grafted

with alkylamines, the microporous Ti MOF MIL-125 functionalized with the functional group $–NH_2$ and the iron tetracarboxylate MIL-127(Fe). The flexible frameworks were the Zn imidazolate ZIF-8, the iron(III) dicarboxylates MIL-53(Fe) functionalized with the functional groups $–(CF_3)_2$ and $–2CH_3$ and the MIL-88B functionalized with the functional group $–2CF_3$. The characterization of these crystalline adsorbents was achieved by X-Ray Powder Diffraction (XRPD), Infra-Red spectroscopy (IR), Thermogravimetric Analysis (TGA) and nitrogen surface area measurement.

In the breakthrough experiments, the functionalized Zr terephthalate UiO-66(Zr) MOFs exhibit between 343 and 423 K and partial pressure up to 10 kPa for the forms Br, NO_2 and NH_2 an uptake reaching 15 wt%, keep the sorption selectivity of the UiO-66(Zr) solid non functionalized with a reverse hierarchy: 22DMB>23DMB>3MP>*n*HEX. The 22DMB/*n*HEX selectivity reaches a maximum of 2.6 at low uptake for UiO-66(Zr)–Br, while the 22DMB/3MP selectivity of UiO-66(Zr)–NO_2 is nearly constant (1.3). The MIL-100(Cr) and the MIL-100(Cr) functionalized with ethylamine or MEDA, demonstrate maximum amounts adsorbed around 27 wt% for the MIL-100(Cr) and maximum selectivities of $S_{n\text{HEX/22DMB}} = 3$ for the MIL-100(Cr) ethylamine sample. The MIL-127(Fe) demonstrated an affinity for the linear isomer *n*HEX relatively to the other isomers with a maximum selectivity of 18 for to the ratio *n*HEX/22DMB and an adsorption maximum around 7 wt%. MIL-125–NH_2 presents an uptake maximum also of 15 wt% with a maximum selectivity of 2.6 for the ratio *n*HEX/22DMB. The ZIF-8 material, demonstrate a similar behaviour relatively to the MIL-127(Fe) but with a better loading of the *n*HEX reaching the 25 wt% and near zero for the other hexane isomers, conferring to this material a remarkable behaviour.

MIL-53(Fe)–$2CH_3$ does not show adsorption neither separation of the hexane isomers in the column experiments. On the other side, MIL-53(Fe)–$(CF_3)_2$ exhibits interesting results in terms of separation. The capacity of adsorption reaches around 6.5 wt%, with however, through the binary experiments (22DMB/3MP) and (22DMB/*n*HEX), a good adsorption of linear and mono branched isomer (*n*HEX and 3MP) in comparison with the di-branched isomer (22DMB). Data from binary mixtures clearly shows that 22DMB is excluded from the framework. This behaviour is true at low temperatures and disappeared close to 423 K. Finally, MIL88B–$2CF_3$ has a maximum adsorption (6 wt%) similar to the MIL-53(Fe)–$(CF_3)_2$, but with lower selectivities ($S_{n\text{HEX/22DMB}} = 4$, $S_{3\text{MP/22DMB}} = 1.3$).

Résumé

Introduction

Dans l'industrie du pétrole, la séparation des isomères de l'hexane pour l'enrichissement de l'indice d'octane recherche (RON) de l'essence est un procédé important. Appliqué aux combustibles, l'indice d'octane est un paramètre essentiel de la qualité du produit parce qu'un indice d'octane élevé réduit la tendance d'une détonation rapide et inefficace des hydrocarbures lors de la combustion et élimine les ondes de choc associées générant un cliquetis caractéristique [1]. Pour la séparation des isomères de l'hexane, la méthode de la distillation fractionnée est normalement utilisée. Toutefois, en raison des très faibles différences entre les points d'ébullition de ces isomères, elle est consommatrice d'une énergie élevée. Donc, il est essentiel de trouver des alternatives pour la séparation des isomères d'alcanes à fin d'améliorer le processus. Des technologies comme les *Total Isomerization Processes* (TIP) ont été développées [2]. Ces procédés impliquent généralement l'isomérisation des «hydrocarbures normaux» (à faible RON) dans un réacteur en utilisant un catalyseur approprié, avant ou après un cycle d'adsorption - désorption basé sur l'utilisation de la zéolite 5A qui permet d'isoler les paraffines «non normales». Le succès de ce processus est en partie dû à la capacité de la zéolite 5A à séparer complètement les paraffines normales des ramifiées. La table 1 présente l'indice d'octane de quelques hydrocarbures normaux et de leurs isomères. Cela reste néanmoins à ce jour insuffisant étant donné la présence d'une teneur encore trop importante en isomères mono-ramifié de l'hexane.

Table 1 - Comparaison de l'indice d'octane entre les hydrocarbures normaux et de leurs isomères [2].

Hydrocarbures	RON
n-Butane	93,8
i-Butane	100,4
n-Pentane	61,7
i-Pentane	92,3
n-Hexane	24,8
2-Methylpentane (2MP)	73,4
3-Methylpentane (3MP)	74,5
2,2-Dimethylbutane (22DMB)	91,8
2,3-Dimethylbutane (23DMB)	101,0

Au LSRE, il a été démontré récemment que la zéolite bêta peut être utilisée pour l'amélioration des processus TIP ; en particulier la séparation des isomères de l'hexane mono-ramifié des di-ramifié. Le nombre RON du flux final pouvant ainsi passer de 86 à 92 [3] ; la zéolite bêta agissant comme séparateur final des paraffines mono-ramifiées. Toutefois, cette procédé a aussi l'inconvénient présence des isomères mono-ramifiés de l'hexane. Il est donc nécessaire de trouver de nouveaux solides adsorbants ayant une meilleure sélectivité entre mono et di-ramifié de l'hexane.

En ce sens, les solides poreux hybrides cristallisés avec cadres métal-organiques (MOF) représentent une nouvelle famille d'adsorbants intéressants combinant une grande richesse structurale et une grande variété de tailles et topologies de pores, susceptibles de donner lieu à des propriétés de séparation très différentes des zéolites. Ils sont constitués par un assemblage d'entités inorganiques (Fig. 1a) reliées entre elles par des ligands organiques (Fig. 1b) possédant des fonctions complexantes (carboxylates, azotates…) et forment une structure (Fig. 1c) bi- ou tri- dimensionnelle avec un système de pores internes, résultat des interactions fortes (forces ioniques et covalentes) [4, 5]. Cela conduit à la formation de solides poreux d'une grande diversité de structures et de compositions, avec des tailles des pores pouvant aller jusqu'à 60 Å et des surfaces spécifiques (BET) jusqu'à 6500 $m^2.g^{-1}$ [6, 7].

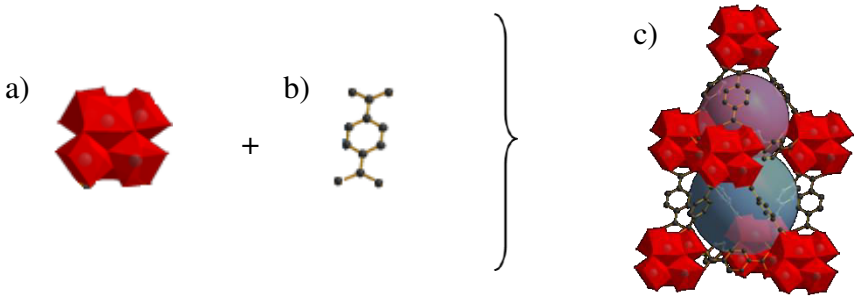

Figure 1 - La combinaison de l'unité (a) inorganique et (b) organique forme la structure (c) UiO-66(Zr) avec huit briques inorganiques et deux types de cage, une super cage octaèdre (sphère bleu) et une super cage tétraèdre (sphère violette) [8].

Les MOFs sont une bonne alternative pour la séparation des isomères de l'hexane en raison de la facilité de moduler leurs propriétés physico-chimiques en intégrant différents groupes fonctionnels sur les ligands organiques et, ainsi, offrant un système hautement adaptable pour résoudre des problèmes spécifiques de séparation [9, 10]. Ces solides ont été à ce jour étudiés pour une large gamme d'applications potentielles : principalement en catalyse, purification/séparation ou stockage de gaz [11-15].

Les méthodes synthétiques les plus utilisées sont: le chauffage conventionnel hydro/solvothermale, les conditions hydro/solvothermales assistée par micro-ondes ou par la pression ambiante à partir d'un précurseur inorganique et organique dans un solvant polaire. Généralement, les MOFs sont caractérisés en utilisant différentes techniques: diffraction des rayons X (XRPD), Spectroscopie Infrarouge (IR), Analyse Thermogravimétrique (TGA), l'analyse élémentaire et l'analyse d'adsorption d'azote et porosité au porosimètre qui permettent de fournir des informations importantes sur leurs structures cristallines, leurs compositions et propriétés texturales.

Objectifs

L'objectif de cette recherche est l'évaluation de nouveaux adsorbants spécifiques nommés *Metal-Organic Frameworks* (MOF) pour la séparation des isomères de l'hexane afin d'améliorer l'indice d'octane de l'essence. Donc, le principal objectif est d'identifier de nouveaux solides poreux hybrides cristallisés capables de mieux séparer les alcanes dibranchés des alcanes monobranchés et linéaires. Cela permettra d'augmenter l'indice d'octane de l'essence. Les laboratoires impliqués sont: le *Laboratory of Separation and Reaction Engineering* - LSRE (travaux expérimentaux et de modélisation sur isothermes, la diffusion et la conception de procédés industriels cycliques d'adsorption) et l'Institut Lavoisier de Versailles - ILV (synthèse de nouveaux MOF).

Plan de Travail

Afin de réaliser cette étude, des structures de solides poreux hybrides (MOF) flexibles et rigides avec une taille de pore proche de celle des alcanes branchés ont été synthétisées et caractérisées à l'Institut Lavoisier de Versailles. Dans un premier temps, les structures rigides UiO-66(Zr) fonctionnalisées par des groupes fonctionnels –Br, $–NO_2$, et $–NH_2$, les solides mésoporeux MIL-100(Cr) et son analogue fonctionnalisé avec des alkylamines, le solide

microporeux MIL-125(Ti) fonctionnalisé avec un groupe $–NH_2$ et le tétracarboxylate de fer(III) microporeux MIL-127(Fe) ont été évalués. La fonctionnalisation utilisée pour moduler la taille des pores des matériaux a permis de limiter ou d'augmenter les cages et les fenêtres afin d'améliorer la séparation des isomères de l'hexane. Dans un second temps, les structures flexibles à base d'imidazolate de Zn ZIF-8, les dicarboxylates de fer(III) MIL-53(Fe) fonctionnalisés ($–(CF_3)_2$, $–2CH_3$) et un polymorphe MIL-88B(Fe) fonctionnalisé ($–2CF_3$) ont été évalués pour cette application. La caractérisation de ces adsorbants cristallins a finalement été réalisée par une combinaison de diffraction des rayons X (XRPD), spectroscopie infrarouge (IR), analyse thermogravimétrique (TGA) et par porosimétrie d'adsorption d'azote. Ensuite, ils ont été évalués au *Laboratory of Separation and Reaction Engineering* (LSRE) pour la séparation des isomères de l'hexane à travers d'une série de courbes de perçage avec des mélanges d'isomères de l'hexane *n*HEX, 3MP et 22DMB 23DMB afin de tester la capacité d'adsorption et la sélectivité. Cela a permis d'obtenir des isothermes d'adsorption à l'équilibre et une analyse plus approfondie de leurs performances a permis de trouver les structures les plus performantes.

Résultats

Avant l'étude de courbes de perçage de chaque solide, les échantillons dans leur forme en poudre (particules ayant un diamètre jusqu'à 0,03 mm) ont été activés par chauffage sous vide (10 kPa) à une température de calcination spécifique de chaque matériau pendant 15 heures. Ensuite, les échantillons activés ont été empaquetés dans une colonne en acier inoxydable (diamètre = 4,3 mm, longueur = 80 mm) pour la détermination des courbes de perçage. La séparation par chromatographie en phase gazeuse utilisé mélanges équimolaires avec les isomères de l'hexane (hexane (*n*HEX), 3-méthylpentane (3MP), 2,2-diméthylbutane (2,2DMB), 2,3-diméthylbutane (2,3DMB).

Chapitre 3 *- UiO-66(Zr)*

Dans les expériences de perçage, les téréphtalates de zirconium UiO-66 (Zr) fonctionnalisés avec -Br, -NO_2 et -NH_2 ont démontré, entre 343 et 423 K, et une pression partielle jusqu'à 10 kPa, une capacité d'adsorption proche de 15 pds%. Ces matériaux ont montré la même hiérarchie inverse que celle affichée avec le solide UiO-66(Zr) non fonctionnalisé: 22DMB > 23DMB > 3MP > *n*HEX [8]. La sélectivité d'adsorption 22DMB/*n*HEX atteint un maximum de 2,6 pour le composé UiO-66(Zr)–Br tandis que la sélectivité d'adsorption pour le couple 22DMB/3MP reste à peu près constant (1,3) pour l'UiO-66(Zr)–NO_2. Le Figure 2 présente la sélectivité des matériaux en fonction du chargement total du mélange.

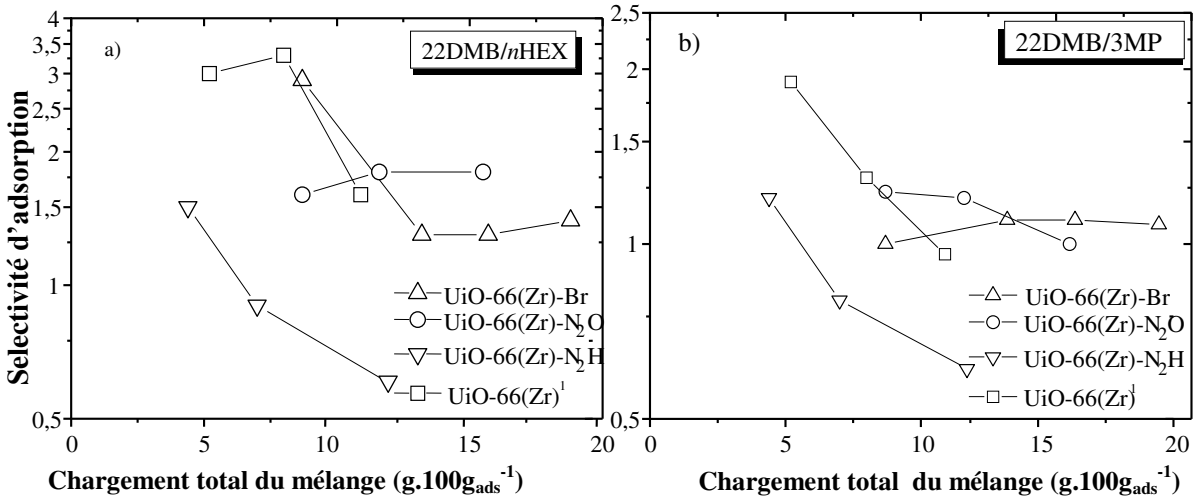

Figure 2 - Sélectivité d'adsorption en fonction du chargement total pour les MOFs fonctionnalités et le MOF signalé. Comparaison entre (a) 22DMB/ *n*HEX et (b) 22DMB/3MP. [1] Référence [8].

En général, les figures 2a et 2b démontrent que la sélectivité semble diminuer lorsque la quantité totale adsorbée augmente. Une possible explication de ce comportement est l'effet d'entropie de ce solide résultant de la limitation des molécules linéaires dans les cages tétraédriques plus petites (qui conduise à leur exclusion). Cet effet est aussi responsable pour la forme inverse de la sélectivité observée. Pour une faible quantité adsorbée, la sélectivité entre les paraffines linéaires et ramifiées est plus grande parce que les molécules ramifiées peuvent accéder aux cages tétra et octaédriques. Thermodynamiquement, les petites cages tétraédriques sont remplies en premier. Aux pressions partielles élevées (hauts chargements), seulement les cages octaédriques continuent l'adsorption des molécules [16]. Néanmoins, dans ce cas, les molécules linéaires sont adsorbées avant que les ramifiés (effet classique) en raison des constantes de Henry supérieure. Par conséquent, la diminution de la sélectivité ramifiée/linéaire de sorption suggère la présence de deux mécanismes de sorption différents: un équilibre mené à faibles charges et un contrôle cinétique dans les charges élevées.

Un autre solide étudié a été l'imidazolate de zinc cubique microporeux ZIF-8 [17], qui possède un réseau unidimensionnel de pores hexagonaux de 12 Å, connectés par des ouvertures de petite taille (3,5 Å). Fig. 3 montre les courbes de perçage d'adsorption ternaires obtenues aux températures de 313, 373 et 423 K, à une pression de 2 et 20 KPa (environ).

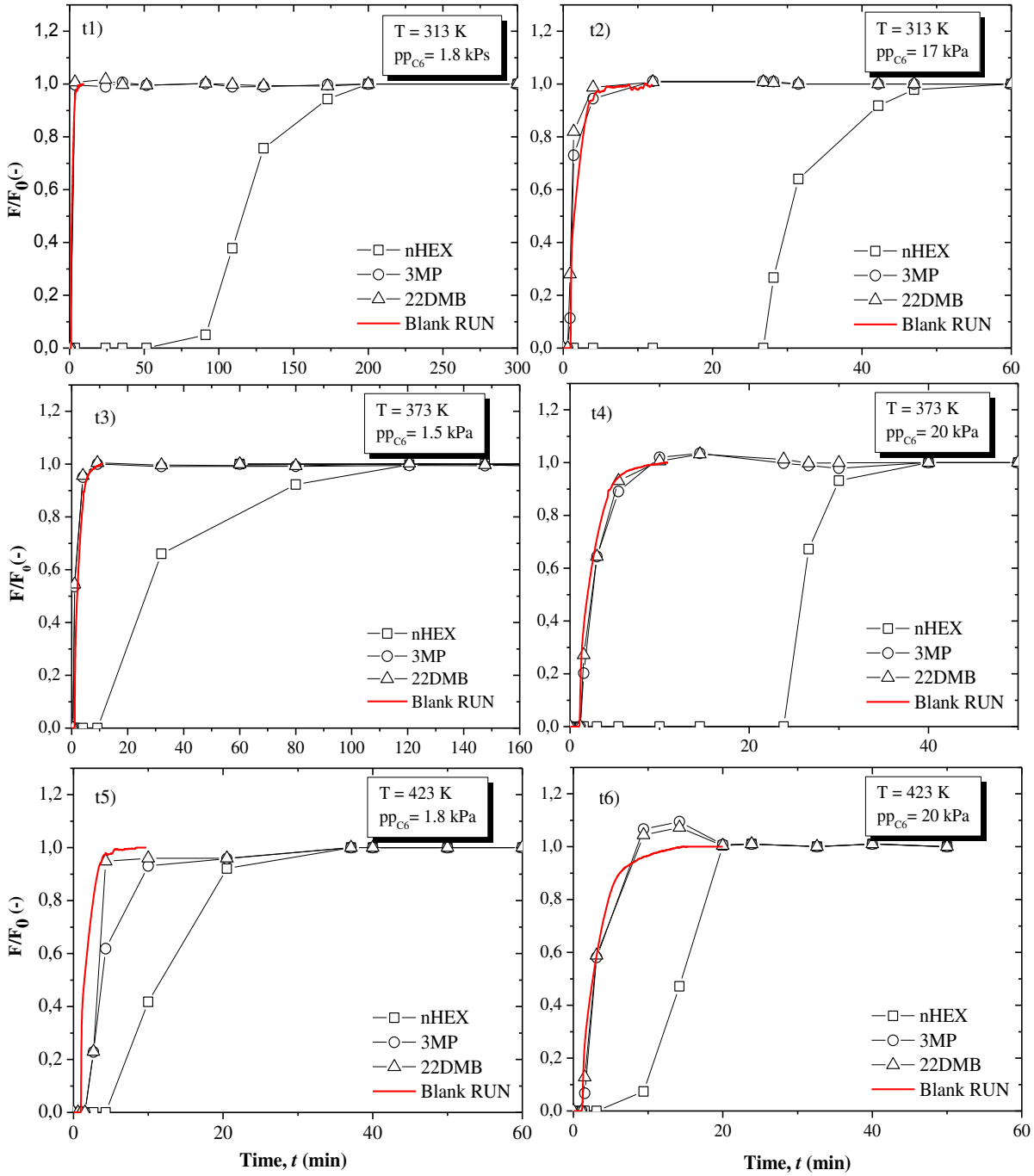

Figure 3 - Comparaison des courbes de perçage d'adsorption ternaire pour les mélanges *n*HEX/3MP/22DMB dans le ZIF-8. (t1) pp = 1,8 kPa, T = 313 K; (t2) pp = 17 kPa, T = 313 K; (t3) pp = 1,5 kPa; T = 373 K; (t4) pp = 20 kPa, T = 373 K; (t5) pp = 1,8 kPa, T = 423 K; (t6) pp = 20 kPa, T = 423K. Les lignes rouges dans la figure montrent un essai à blanc dans les mêmes conditions expérimentales mais avec la colonne remplie de billes de verre.

Le solide ZIF-8 a les fenêtres d'accès aux pores flexibles et, comme constaté dans la Fig. 3, seul le *n*HEX est adsorbé (comportement similaire relativement au MIL-127(Fe), mais avec un meilleur résultat) avec une capacité proche de 25 pds% et proche de zéro pour les autres isomères de l'hexane. La grande capacité liée à l'importante porosité, ainsi que la taille de fenêtres, légèrement modulable par la torsion des ligands organiques, font du ZIF-8 un candidat intéressant pour la séparation des isomères de l'hexane. De façon remarquable, ce matériau a montré une séparation complète de n-HEX, similaire à la zéolite 5A, mais avec des capacités d'adsorption de l'ordre de 25%pds, beaucoup plus importantes que celles obtenues en utilisant la zéolite 5A (13 %pds) [18].

Chapitre 5 - *MIL-53(Fe) and -88B(Fe)*

Plusieurs solides flexibles de fer MIL-53, ou leur polymorphe MIL-88B, ont été synthétisés : MIL-53(Fe)-$(CF_3)_2$, MIL-53(Fe)-$2CH_3$ and MIL-88B-$2CF_3$. La famille des téréphtalates de fer flexible du type MIL-53(Fe) [19], constituée de chaines d'octaèdres de fer (III) connectées par des ligands téréphtalates définissant une structure tridimensionnelle avec un système de tunnels unidimensionnels (ϕ libre = 8,5 Å), a été étudiée. Ces solides possèdent une porosité importante, qui peut être modulée de façon réversible en fonction d'un *stimuli* externe, tel que la température, la pression ou l'adsorption de molécules (phénomène de respiration). En particulier, le solide fonctionnalisé 2,5-diperfluorotéréphtalate de fer MIL-53(Fe)–$2CF_3$ [20] a été sélectionné afin de bloquer partiellement la respiration, diminuer la taille des pores pour les rendre à la fois plus accessibles aux isomères de l'hexane et de les séparer en fonction de leurs dimensions respectives. De plus, les atomes de fluor sont susceptibles d'interagir plus fortement avec les molécules adsorbées. Pour comparer l'influence de la fonctionnalisation avec le groupe CF_3 sur la séparation des isomères de l'hexane, un autre solide mais avec le groupe fonctionnel CH_3 a aussi été préparé.

Les études de séparation ont prouvé le grand potentiel du matériau MIL-53(Fe)–$2CF_3$ pour la séparation des paraffines ramifiées des linéaires. La Fig. 4 montre les courbes de perçage ternaires pour les composants 22DMB/3MP/*n*HEX dans le MIL-53(Fe)–$(CF_3)_2$ à la température de 313 K et à des pressions entre 0,5 kPa et 20 kPa.

En effet, à basse température (313 K) et pression partielle (1 kPa), une bonne séparation entre le 22DM, 3MP et *n*HEX a été observée, pour la première fois sur un solide microporeux, avec

une sélectivité importante (3,2). Il existe néanmoins une diminution, voir une perte, de la séparation à des températures élevées. En conséquence, les expériences binaires (22DMB/3MP) et (22DMB/*n*HEX) montrent une bonne adsorption de l'isomère linéaire et mono-ramifié (*n*HEX et 3MP) par rapport à l'isomère di-ramifié (22DMB). Ces expériences ont démontré clairement que le 22DMB était exclu de la structure.

Il a été observé pour le MIL-53(Fe)-2CH_3 que les isomères de l'hexane ne sont pas adsorbés dans la structure. Par contre, son polymorphe MIL88B–2CF_3 conduit à une adsorption importante (6 pds%), similaire au MOF MIL-53$(CF_3)_2$, mais sans aucun degré notable de séparation.

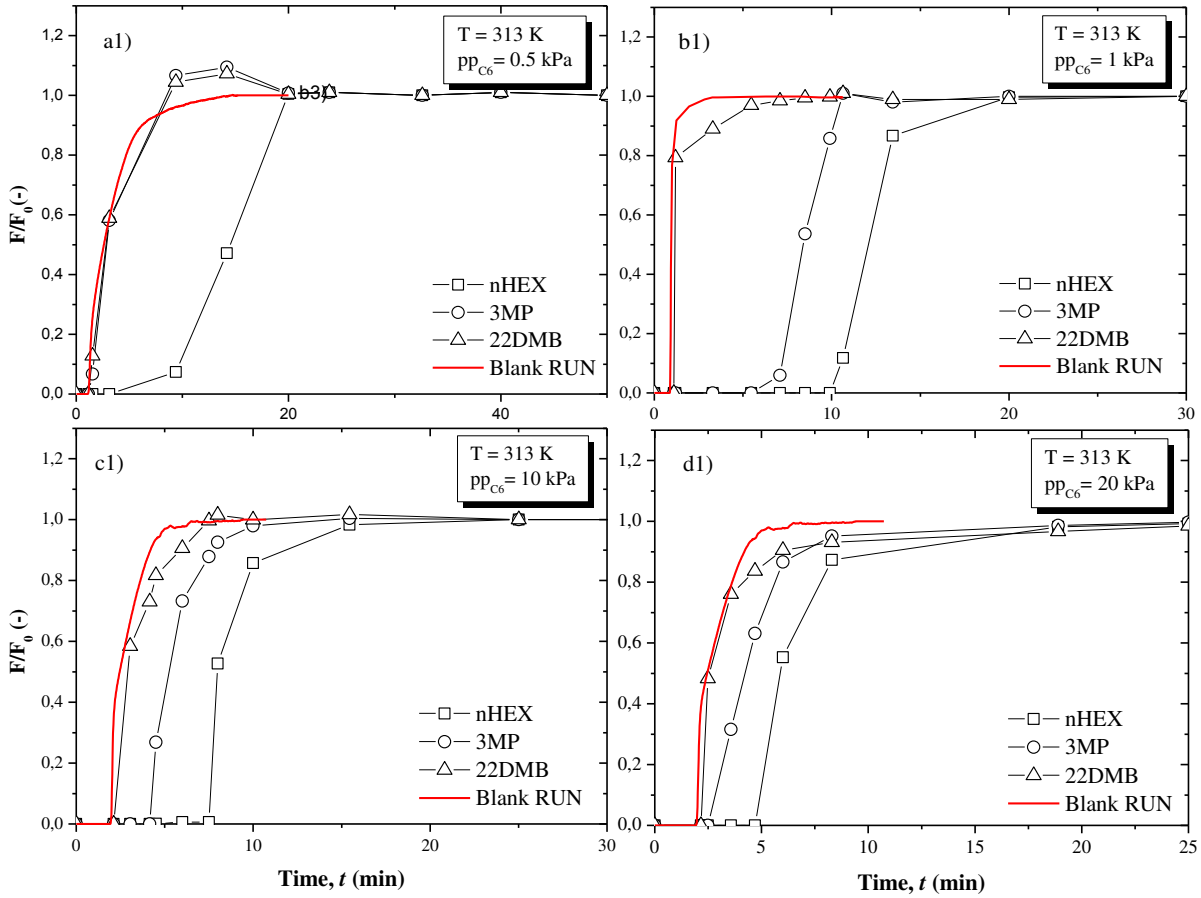

Figure 4 - Courbes de perçage ternaires pour les composants 22DMB/3MP/*n*HEX dans le MIL-53(Fe)–$(CF_3)_2$ à la température de 313 K. (a1) pp = 0,5 kPa; (b1) pp =1 kPa; (c1) pp = 10 kPa et (d1) pp = 20 kPa.

Chapitre 6 - *MIL-100(Cr), -127(Fe) and -125(Ti)-NH_2*

Plusieurs MOFs micro- et mésoporeux rigides ont été synthétisés et caractérisés avec succès comme le MIL-100 (Cr) et le MIL-100 (Cr) fonctionnalisés par une modification post-synthétique (PSM) avec des amines, le MIL-125-NH_2 et le MIL-127 (Fe). Le MIL-100 (Cr)

ou [Cr_3F $(H_2O)_2[(CO2)_3$-$C_6H_3]_2.nH_2O$, n~28] a une structure cristalline cubique hybride 3D [21] avec des trimères à base de chrome (III) octaédrique et des ligands trimésates, définissant deux types de cages mésoporeuses (25 et 29 Å), accessibles par des fenêtres microporeuses (≈ 9,5 Å). Le fer (III) 3,3', 5,5-azobenzenetetracarboxate MIL-127(Fe) est un MOF avec une phase isostructurelle à base de blocs de Indian Soc-MOF [6]. Le Fe (III) partage trimères octaédriques central μ3 anion-oxo et formule blocs similaire à leMIL-100 (Fe) trimérique. La structure de MIL-127 (Fe) est un cristal cubique à l'architecture rigide microporeuse. Cette structure définit les micropores (5-7 Å) du système 3D, où la taille de la cage est supérieure à 10 Å. Le téréphtalate de titane MIL-125 ou $Ti_8O_8(OH)_4$-$(O_2C$-C_6H_4-$CO_2)_6$ présente une structure rigide tétragone quasi cubique [22], avec des paramètres de maille a = b = 18,654 (1) Å et c = 18,144 (1) Å , un volume de cellule unitaire = 6313,9 (1) A^3 et de groupe d'espace 4/mmm I (n ° 139). La connexion 3D des oxo-clusters Ti et les anions téréphtalates délimite deux types de cages microporeuses qui correspondent à une cage octaèdrique et une autre tétraédrique avec des diamètres de 12,55 et 6,13 Å, respectivement [17]. Les cages sont accessibles à travers des fenêtres triangulaires avec une ouverture libre dans la gamme des 5-7 Å. Les surfaces estimées par la méthode BET et Langmuir sont: S_{BET} = 1550 (20) $m^2.g^{-1}$ et S_{Lang} = 1,950 (10) $m^2.g^{-1}$, respectivement.

Les études de la séparation des isomères de l'hexane ont montré que ces structures organométalliques ont une ordre d'adsorption standard qui est égale à l'ordre de leurs points d'ébullition: *n*HEX> 3MP> 23DMB> 22DMB. Les solides trimésates de chrome MIL-100(Cr) et MIL-100(Cr) fonctionnalisés (éthylamine ou MEDA) possèdent une capacité d'adsorption élevée, atteignant un maximum de 27 pds%. (MIL-100), et une sélectivité maximale de $S_{nHEX/22DMB}$ = 3 (MIL-100(Cr) – éthylamine). La fonctionnalisation provoque la diminution de la taille accessible de la fenêtre en gardant l'eau coordonnée au cation métallique ce qui permet d'augmenter de manière significative la sélectivité du MIL-100(Cr) mais il a une réduction de la capacité d'adsorption. Une alternative a été de greffer une monoamine (éthylamine) au cation métallique pour diminuer la taille des fenêtres d'accès aux mésopores, sans pour autant trop affecter la capacité d'adsorption. Pour le MIL-100(Cr)MEDA nous avons obtenu un total adsorbé de 24 pds% à 343 K et 10 kPa alors que le MIL-100(Cr) – éthylamine à une quantité adsorbée de 18 pds% à 343 K et 6 kPa. La sélectivité est supérieure pour le MIL-100(Cr) – éthylamine, où il a obtenu un maximum de 2 pour le ratio 23DMB/22DMB, de 2,5 pour le ratio 3MP/22DMB et de 3 pour le ratio

*n*HEX/22DMB. Les sélectivités expérimentales étaient similaires à celles obtenues avec les BETA zéolites (3 pour le ratio *n*HEX/22DMB et 1,4 pour le ratio de 23DMB/22DMB).

Le solide microporeux MIL-127(Fe) présente affinité pour l'isomère *n*HEX linéaire par rapport aux autres isomères avec une sélectivité maximale de 18 pour le ratio *n*HEX/22DMB, un effet similaire à celui observé dans la zéolite 5A mais avec une adsorption moindre (7 pds%). Une autre caractéristique intéressante de ce MOF est que le *n*HEX montre une approche lente à l'équilibre qui semble être lié à une forte résistance au transfert de masse. Cet effet est probablement dû aux dimensions similaires du *n*HEX et du pore de la structure qui entrave l'accès à celle-ci.

Le composé microporeux MIL-125–NH_2 présente un maximum d'absorption de 15 pds% avec une sélectivité maximale de 2,6 pour le ratio *n*HEX/22DMB. Dans ce MOF, un phénomène de *roll-up* est évident et caractéristique de l'adsorption compétitive des molécules dans la structure. Les fenêtres d'accès à la structure du MIL-125-NH_2 ont une ouverture libre entre 5 et 7 A, ce qui pourrait donc limiter l'accessibilité des isomères de l'hexane plus volumineux (diamètres cinétiques de *n*HEX, 3MP, et 23DMB 22DMB = 4,3 Å, 5,0 Å, 5,6 Å et 6,2 Å respectivement). Donc, si la *n*HEX peut facilement migrer dans les deux cages, 3MP, 22DMB et 23DMB pourraient être préférentiellement adsorbés dans la grande cage, ce qui pourrait expliquer la meilleure adsorption de *n*HEX relativement aux autres composants.

Conclusion

Ce travail a été accompli afin d'explorer le potentiel de MOFs poreux à adsorber et séparer des mélanges gazeux d'isomères de l'hexane. L'objectif principal été de rechercher des solides poreux avec une bonne capacité de séparation des isomères de l'hexane avec différents RON (*Research Octane Number*) afin d'améliorer l'indice d'octane de l'essence.

En général, en comparant les solides UiO-66(Zr) consignés et les solides fonctionnalisés, nous pouvons conclure que la sélectivité, en fonction de la quantité totale adsorbée, ne change pas significativement dans les échantillons fonctionnalisés, à l'exception d'UiO-66-NH_2; ce que ne montré la sélectivité inverse à des charges élevées. Tous les autres solides UiO-66(Zr) fonctionnalisés ont montré une sélectivité inverse 22DMB>23DMB>3MP>*n*HEX, caractéristique des UiO-66(Zr) consignés. La quantité adsorbée totale des composants dans toutes les matières solides fonctionnalisées est similaire (sur 15 pds%). En particulier, le solide UiO-66(Zr)-Br démontre une meilleure sélectivité aux faibles adsorptions 22DMB/*n*HEX (environ 3) que pour les hautes absorptions (environ 1,3).

Dans le cas du solide ZIF-8 étudié au chapitre 4, il a été démontré un grand potentiel pour séparer l'isomère linéaire *n*HEX, dû aux charges élevées de cet isomère (environ 25 pds% à 313 K et 10 kPa), relativement aux autres isomères (pratiquement zéro). Cette forte adsorption de *n*HEX peut s'expliquer par le volume important de pores accessibles du solide ZIF-8. Les expériences binaires avec les isomères 3MP et 22DMB montrent une séparation pauvre avec une sorption pratiquement négligeable. Par conséquent, nous pouvons considérer le ZIF-8 un adsorbant efficace pour séparer l'isomère linéaire des isomères ramifiés. Cette effet est similaire avec la zéolite 5A mais avec une quantité adsorbée supérieure, ce qui confère à ce matériau un comportement remarquable.

Les MOFs flexibles MIL-53(Fe) fonctionnalisés (–$2CH_3$ and –$(CF_3)_2$) et MIL-88B(Fe)–$2CF_3$ ont été étudiés dans le chapitre 5 et ont montré une quantité adsorbée entre 1 (pour le MIL-53(Fe)–$2CH_3$) et environ 6 pds% pour les structures MIL-53(Fe)–$(CF_3)_2$ and MIL-88B(Fe)–$2CF_3$. MIL-53(Fe)–$2CH_3$ n'adsorbe pas les isomères de l'hexane dans les conditions expérimentales testées. Par contre, le solide MIL-53(Fe)–$(CF3)_2$ permet non seulement d'adsorber près de 6,5 pds% mais il s'avère capable de séparer le 2,2 DMB des autres isomères. Ce comportement est particulièrement vrai à basse température et disparaît lorsque

l'on se rapproche des 423 K. Finalement, son polymorphe MIL88B-2CF_3 présente aussi une capacité d'adsorption maximale (6 wt%) similaire à celle du MIL-53(Fe)–$(CF_3)_2$, mais avec des sélectivités beaucoup plus faibles ($S_{n\text{HEX/22DMB}}$ = 4 ; $S_{\text{3MP/22DMB}}$ = 1,3). Du point de vue industriel le MIL-53(Fe)–$(CF_3)_2$ a un ordre de sélectivité idéal parce que l'isomère ramifié 22DMB (isomère avec un indice supérieur d'octane) n'est pas adsorbé et est totalement libéré de la colonne. En fonction de nos objectifs, ce résultat montre que le MIL-53(Fe)–$(CF_3)_2$ est un candidat prometteur pour l'amélioration de l'indice d'octane des procédés actuels TIP.

Les études pour les MOFs rigides sont présentées dans le chapitre 6 et montrent que les isomères de l'hexane sont tous adsorbés dans les matériaux avec un ordre de sélectivité similaire à celui des points d'ébullition normaux: *n*HEX > 3MP > 23DMB > 22DMB, excepté pour le MOF MIL-127(Fe). Dans cette exception, seulement le *n*HEX est capable d'entrer dans la structure donnant lieu à un effet de tamis moléculaire similaire à celui observé dans le ZIF–8 mais avec une capacité inférieure. Les quantités adsorbées par la classe des MOFs MIL-100(Cr) sont considérablement élevées (> 20 pds%) ; ce qui est une caractéristique de ces MOFs par rapport aux adsorbants classiques tels que le carbone activé ou les zéolites. Le MIL-100(Cr) non fonctionnalisé a une capacité d'environ 27 pds% à 343 K et 10 kPa. Cette valeur est pratiquement le double de celle constatée dans la zéolite 5A. Par contre, la sélectivité de ces MOFs n'est pas remarquable.

Finalement, nous pouvons conclure que les MOFs peuvent être efficaces dans la séparation des isomères de l'hexane. Les MOFs flexibles tels que le MIL-53 (Fe)-$(CF_3)_2$ et le ZIF-8 et le MIL-127(Fe) rigide ont démontré des effets de tamis moléculaires. L'UIO-66(Zr) fonctionnalisé maintient l'effet de sélectivité inverse comme déjà démontré dans une coopération antérieure entre le LSRE et l'ILV. Les grands cadres rigides de pores comme le MIL-100(Cr) montrent un ordre normal de sélectivité mais il peut adsorber de grandes quantités de masse (plus de 20 pds%); ce qui confère une bonne caractéristique. Le MOF ZIF-8 peut séparer le *n*HEX des isomères ramifiés avec un effet de tamis moléculaire très avantageux pour les stratégies d'amélioration de l'indice d'octane dans les industries pétrochimiques (TIP). Le MIL-53(Fe)-$(CF_3)_2$ a la capacité de séparer le 22DMB des autres isomères mono ramifiés et linéaires avec l'effet de tamis moléculaire. Donc, la combinaison des solides ZIF-8 et MIL-53 (Fe)-$(CF_3)_2$ dans un système d'adsorption peut donner un fractionnement complet du mélange d'isomères de l'hexane par adsorption, ce qui est le premier résultat montré dans la littérature. L'inconvénient majeur est la séparation

3MP/22DMB dans le MIL-53(Fe)-$(CF_3)_2$ qui est obtenu à une basse température de 313 K et à de faibles pressions partielles. Cela signifie que ce système a besoin d'une amélioration pour augmenter la capacité de la séparation à des températures et des pressions partielles plus élevées.

Références

1. *D. Jones, An introduction to crude oil and its processing, in: Handbook of Petroleum Processing, Springer, USA, 2006.*

2. *P. Pujadó, Isomerization technologies for the upgrading of light naphtha and refinery light ends in: Handbook of Petroleum Processing, Springer, USA, 2006.*

3. P. S. Bárcia, J. A. C. Silva, and A. E. Rodrigues, *Octane Upgrading of C5/C6 Light Naphtha by Layered Pressure Swing Adsorption, Energy Fuels, 24 (2010) 5116–5130*

4. *G. Férey, The Long Story and the brilliant Future of Crystallized Porous, in: D. Braga , S. Bureekaew , N. Champness, F. Grepioni, P. Hubberstey, J. Jia, S. Kitagawa, L. Maini, M. Polito, M. Schröder, S. Shimomura et al, Molecular Networks, Springer, 2009.*

5. *J. Rowsell, O. Yhagi, Metal-Organic Frameworks: a new class of porous, Micropor. Mesopor. Mater., 73 (2004) 3-14.*

6. *F. Paz, J. Klinowski, Sérgio Vilela, J. Tomé, J. Cavaleiro, J. Rocha, Ligand design for functional metal–organic frameworks. Critical Review, Chem. Soc. Rev., 41 (2011) 1080-1110.*

7. *J. Perry, J. Perman and, M. Zaworotko, Design and synthesis of metal–organic frameworks using metal–organic polyhedra as supermolecular building blocks, Chem. Soc. Rev., 38 (2009) 1400-1417.*

8. *P. Bárcia, D. Guimarães, P. Mendes, J. Silva, V. Guillerm, H. Chevreau, C. Serre, A. Rodrigues, Reverse Shape Selectivity in the Adsorption of Hexane and Xylene Isomers in MOF UiO-66, Micropor. Mesopor. Mater., 139 (2011) 67-73.*

9. *K. Tanabe, Z. Wang, S. Cohen, Systematic Functionalization of a Metal-Organic Framework via a Postsynthetic Modification, J. Am. Chem. Soc., 130 (2008) 8508-8517.*

10. 20. *J. Rowsell, O. Yaghi, Effects of Functionalization, Catenation, and Variation of the Metal Oxide and Organic Linking Units on the Low-Pressure Hydrogen Adsorption Properties of Metal-Organic frameworks, J. Am. Chem. Soc., 128 (2006)1304-1315.*

11. *R. Kupplera, D. Timmonsb, Q. Fanga, J. Li, T. Makala, M. Younga, D. Yuana, D. Zhaoa,W. Zhuanga, H. Zhou, Potential applications of metal-organic frameworks, Coordination Chemistry Reviews, 253 (2009) 3042–3066.*

12. *H. Jiang, Q. Xu, Porous metal–organic frameworks as platforms for functional applications., Chem. Commun., 47 (2011) 3351-3370.*

13. *U. Mueller, M. Schubert, F. Teich, H. Puetter, K. Schierle-Arndt, J. Pastre, Metal–organic frameworks—prospective industrial applications, J. Mater. Chem., 16 (2006) 626-636.*

14. *J. Li, R. Kupple, H. Zhou, Selective gas adsorption and separation in metal–organic frameworks., Chem. Soc. Rev., 38 (2009) 1477-1504.*

15. *D. Britt, D. Tranchemontagne, O. Yaghi, Metal-organic frameworks with high capacity and selectivity for harmful gases, PNAS, 105 (2008) 11623-11627.*

16. P. Mendes, F. Ragon, A. Rodrigues, P. Horcajada, C. Serre, J. Silva, Hexane isomers sorption on a functionalized metal–organic framework, Microporous and Mesoporous Materials 170 (2013) 251–258.

17. *K. Park et al., Exceptional chemical and thermal stability of zeolitic imidazolate frameworks. The National Academy of Sciences of the USA, 103 (2006) 10186–1019.*

18. J. A. C. Silva, A. E. Rodrigues, Equilibrium and Kinetics of n-Hexane sorption in pellets of zeolite 5A, AIChE Journal, 43 (1997) 2524-253.

19. *T. R Whitfield, X Wang, L. Liu, A. J. Jacobson, Metal-organic frameworks based on iron oxide octahedral chains connected by benzenedicarboxylate dianions, Solid State Sci., 7 (2005) 1096 – 1103.*

20. *T. Devic, P. Horcajada, C. Serre, F. Salles, G. M., B. Moulin, D. Heurtaux, G. Clet, A. Vimont et al., Functionalization in Flexible Porous Solids: Effects on the Pore Opening and the Host-Guest Interactions, J. Am. Chem. Soc., 132 (2010) 1127–1136.*

21. *G. Férey, C. Serre, C. Mellot-Draznieks, F. Millange, S. Surblé, J. Dutour, I. Margiolaki, A Hybrid Solid with Giant Pores Prepared by a Combination of Targeted Chemistry, Simulation, and Powder Diffraction, Angew. Chem. Int. Ed., 43 (2004) 6296-630.*

22. *M. Dan-Hardi, C. Serre, T. Frot, L. Rozes, G. Maurin, C. Sanchez, and G. Férey; A New Photoactive Crystalline Highly Porous Titanium (IV) Dicarboxylate; J. AM. CHEM. SOC., 131 (2009) 10857–10859.*

Table of Contents

List of Figures

Chapter 1

Chapter 2

Chapter 3

Chapter 4

Chapter 5

Chapter 6

List of Tables

Chapter 1

Chapter 3

Chapter 4

Chapter 5

Chapter 6

List of Symbols

A_{ads} – Adsorption section area of the adsorbate (cm^2.$molecule^{-1}$)

A_{qo} – Adsorption area of the isotherm curves

C – BET constant

d – Interplanar distance (Å)

d_k – Kinetic diameter (m)

F – Molar gas flow rate of sorbate species i in the bulk gas phase ($mol.min^{-1}$)

F_0 – Molar gas flow rate at the inlet of the fixed bed ($mol.min^{-1}$)

Ø – Internal diameter (Å)

I_0 – Intensity of the incident x-ray beam

$I(2\theta)$ – Intensity of the diffracted secondary beam

K – Langmuir constant (atm^{-1})

K_0 – Affinity constant (atm^{-1})

L – Column length (m)

m_{ads} – Adsorbent mass packed into the column (g)

M_{comp} – Molecular mass for the component in study ($g.mol^{-1}$)

N – Avogadro number ($molecule.mol^{-1}$)

P – Pressure of sorbate

P – Total equilibrium pressure of adsorbates (atm)

P_0 – Saturation pressure of adsorbates (atm)

pp – Partial pressure (atm)

q – Loading ($g.100g_{ads}^{-1}$)

q_{max} – Maximum monolayer capacity ($g.100g_{ads}^{-1}$)

R – Gas constant (J. $mol^{-1}.K^{-1}$)

S_{BET} – BET specific surface area ($m^2.g^{-1}$)

S_{Lang} – Langmuir specific surface area ($m^2.g^{-1}$)

T – Temperature (K)

t – Time (min)

T_{eb} – Temperature boiling point (K)

t_r – Retention time (min)

u – Velocity of the components for to pass in the column ($m.s^{-1}$)

V – Volume of gas adsorbed ($cm^3(STP).g^{-1}$)

V_a – Volume of mono layer of gas adsorbed ($cm^3(STP).g^{-1}$)

V_m – Maximum volume of nitrogen adsorbed ($cm^3(STP).g^{-1}$)

V_{mp} – Micropore volume ($cm^3(STP).g^{-1}$)

V_p – Pore volume ($cm^3(STP).g^{-1}$)

V_w – Molar volume of the adsorbate gas ($cm^3(STP).mol^{-1}$).

z – Reflection order

Greek Letters

α – Selectivity

ΔH – Heat adsorption enthalpy ($J.mol^{-1}$)

θ – Reflexion planes angle (º)

λ – Wavelength of the x-rays diffraction (Å)

φ – Fractional coverage

Abbreviations

ADI – Anti-detonation index

BPC – Back Pressure Controller

Br – Brome

BTX – Benzene, Toluene and Xylenes

ca. – Around, from Latin “circa”

C5 – Pentane isomers

C6 – Hexane isomers

C7 – Heptane isomers

C8 – Octane isomers

C9 – Nonane isomers

C10 – Decane isomers

C11 – Undecane isomers

C12 – Dodecane isomers

C_2H_5-NH_2 – Ethylamine

Cr – Chromium

Cr^0 – Non-reacted Chromium

CRON – Clear Research Octane Number

DIP – Deisopentanizer

DLS – Dynamic Light Scattering

22DMB – 2,2-dimethylbutane

23DMB – 2,3-dimethylbutane

DMF – Dimethylformamide

e.g. – For example, from Latin “exempli gratia”

EPA – Environmental Protection Agency

EPC – Electronic Pressure Controller

EtA – Ethylamine

EtAaq – Ethylamine aqueous

EtAp – Ethylamine pure

ETBE – Ethyl Tert Butyl Ether

Fe – Iron

FID – Flame Ionization Detector

Fig. – Figure

FTIR – Fourier transform infrared spectroscopy

GC – Gas Chromatography

H_2-BDC $(NH_2)_2$ – Aminoterephthalic acid

H_3BTC – Benzene Tricarboxylic acid

HCl – Hydrochloric acid

HF – Hydrofluoric acid

HKUST – Hong-Kong University of Science and Technology frameworks

H-MeIM – Methylimidazole

iC_5 – Isopemtane

i.d. – Internal diameter

IDP – Isobaric Displacement Processes

i.e. – That is, from Latin “id est”

ILV – *Institute Lavoisier de Versailles*

IR – Infra-Red analysis

IRMOF – IsoReticular MOFs

LPG – Liquefied Petroleum Gases

LSRE – Laboratory of Separation and Reaction Engineering

MeOH – Methanol

MEDA – Methyl ethylene diamine

MFC – Mass Flow Controller

MIL – Materials of Institute Lavoisier

MOF – Metal Organic Frameworks

MON – Motor Octane Number

2MP – 2-Methylpentane

3MP – 3-Methylpentane

MTBE – Methyl Tert Butyl Ether

*n*HEX – *n*-Hexane

NH_2 – Amine

NO_2BDC – Nitroterephthalic acid

PSA – Pressure Swing Adsorption

PSM – Post Synthetic Modification

PTFE – Polytetrafluoroethylene

RON – Research Octane Number

SMB – Simulated Moving Bed

TAME – Tert Amyl methyl Ether

TEL – Tetra Ethyl Lead

TGA – Thermogravimetric Analysis

Ti – Titanium

TIP – Total Isomerization Processes

TMB – True Moving Bed

UiO – University of Oslo frameworks

VdW – Van de walls

XRPD – X-Ray Powder Diffraction

ZIF – Zeolitic Imidazole framework

Zr-MOFs – Zirconium-based MOFs

1.

Introduction

The purpose of this introductory chapter is to show the motivation for the work developed during this Ph.D. thesis, aiming to demonstrate that Metal-Organic Frameworks might be a good alternative for hexane isomers separation. It also introduces the basic measurements and parameters necessary for understanding some of the processes from the Petroleum industry, such as, Naftha Isomerization process and the isomer hexane separation processes, where two different separation methods; cryogenic distillation and adsorption phenomena, are briefly described.

1.1. Relevance and Motivation

In the petroleum industry, the separation of hexane isomers for the enrichment of octane number (RON) of the gasoline is an important process. For motor fuel applications, the octane number is an essential parameter of product quality; a higher octane number reduces the tendency of a rapid and inefficient detonation of the hydrocarbons in the combustion and eliminates the impact sound caused by the rapid detonation [1]. For the separation of hexane isomers the method of fractionated distillation is normally used; however, due to the close boiling points of the isomers, it is high energy consuming. So, it is crucial for efficient energy use to find alternatives for the separation process of alkane isomers. Technologies have been developed, such as Total Isomerization Process (TIP) [2]; however, they aren't sufficient since zeolite is not able to separate mono from di-branched isomers. The Metal-Organic Frameworks (MOFs) appear to be a good alternative for the separation of hexane isomers due to their easy way to modulate their physico-chemical properties by incorporating different functional groups on the organic linkers offering a highly adaptable system to solve specific separation problems.

1.1.1. Petroleum Refinery Industry

The current available data indicates that the Petroleum is formed from rests of dead plants and animals that were decomposed during millions of years [3]. These dead plants and animals were submerged in reservoirs under several thousand feet of silt, sand or mud in many places around the world, several of them is under the oceans [4]. This fossil energy is non-renewable due to the millions of years that need to be formed again [5, 6].

The chemical components of Petroleum are mainly carbon and hydrogen with also nitrogen and sulphur; it is formed by hydrocarbon and sulphur compounds and a minority of other substances, and its natural form is known as crude oil, and can be clear, green or black [4]. Depending of the location the crude oil composition is different. The amount of sulphur

present on the crude oil and its density are predominant for its classification. It is more or less dense if it contains a great proportion of long-chain hydrocarbons or short-chain hydrocarbons, respectively [4]. So, it is necessary the crude oil assay analysis for its basic classification as described on the table 1.1.

Table 1.1 - Classification of the Crude oil [4].

Crude classification	Characteristic
sour	high levels of sulphur
sweet	low levels of sulphur
heavy	high density (richer in naphthenes and aromatics)
light	low density (higher paraffin content)

This classification only indicates it the crude is useful for certain applications; for example higher yield refining of the gasoline is obtained from light crude instead of heavy crude and the sweet crude is also preferable than the sour crude due to environmental impact of the sulphur harmful emissions [4]. From the petroleum we can obtain various products like: Gasoline, Diesel, Jet Fuel, Liquefied Petroleum Gases (LPG), Heavy Fuel Oil (Residual) and other products and distillates. Fig. 1.1 shows the amount of various products obtained from a barrel of crude oil.

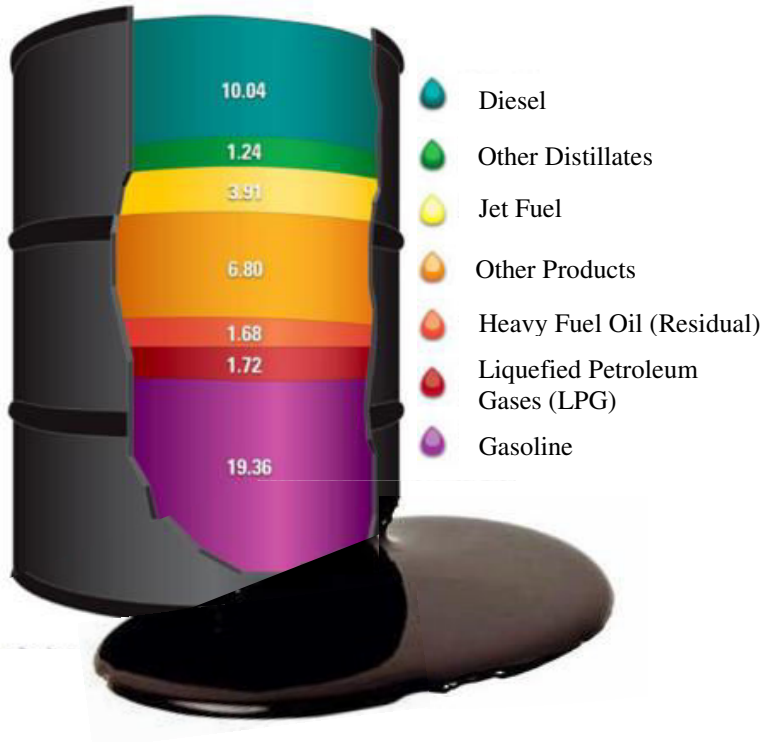

Figure 1.1 - Products obtained from a barrel of crude oil (L). Adapted from [6].

In a crude oil, there is a mixture of hundreds of hydrocarbon compounds; however, for its utilization it is necessary to refine the raw material in useful products [1]. The petroleum

refining consists on several processes that transform the crude oil onto final products as shown in the diagram of the Fig. 1.2.

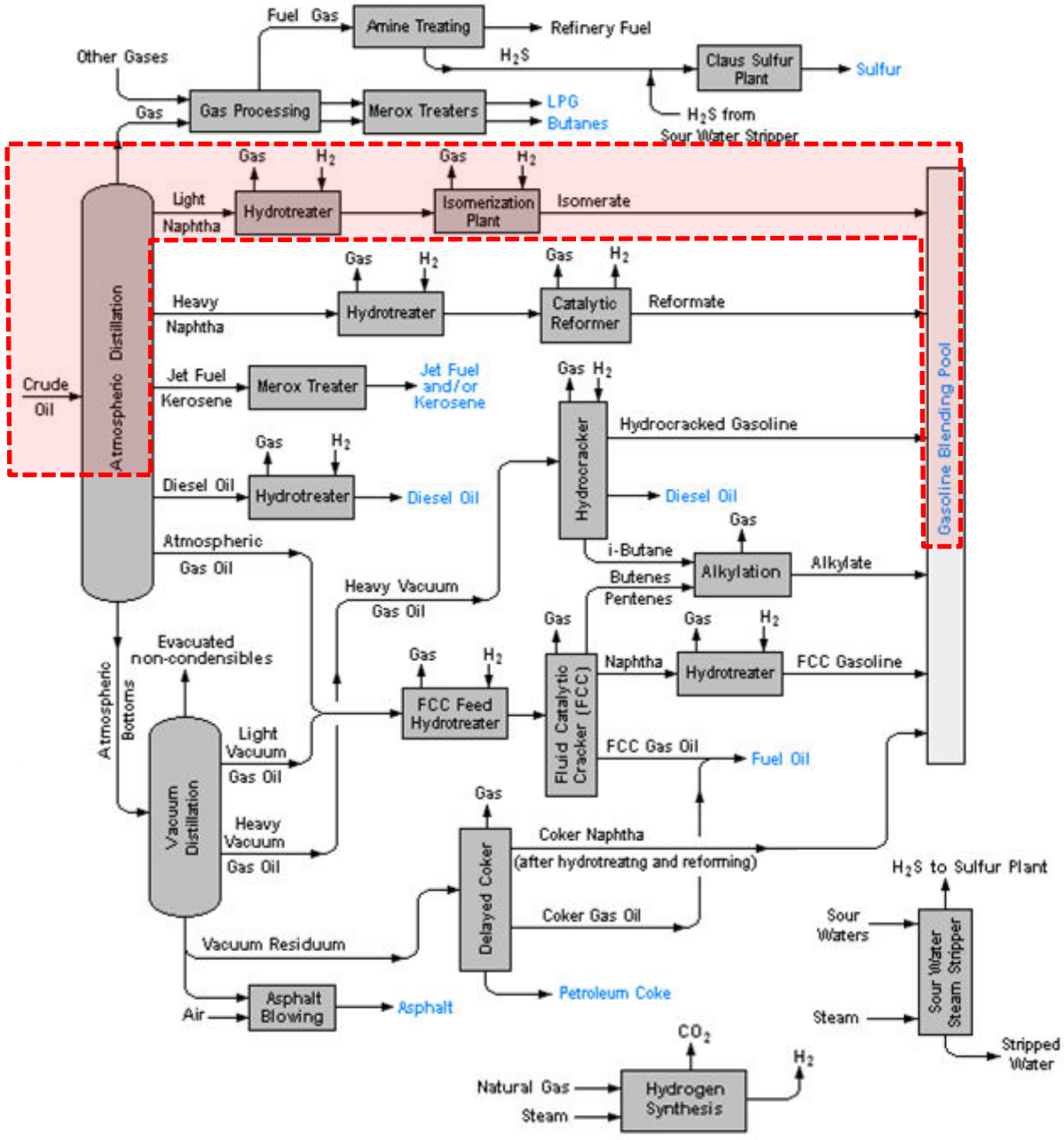

Figure 1.2 - Schematic flow diagram that represents a typical petroleum refinery [7]. Final products (blue), process of light naphtha (red).

There are different refinery intermediate products used in different applications. The refinery intermediate volatile and flammable constituted by hydrocarbons that origin the gasoline is designated by naphtha. Typical naphtha is constituted by paraffins or isomers of paraffins, but has also in its composition olefins, naphthenes and aromatics [1] as we can see in the table

1.2. The refining process of light naphtha (highlighted in Fig. 1.2 with red) gives the higher yield in gasoline, so, it is the main process for the gasoline production.

Table 1.2 - Concentration (w%) of each component in the typical composition of naphtha [1].

	Concentration (w%)		Concentration (w%)
Aromatics			
Benzene	1.45	Cyclohexane	3.26
Toluene	4.06	C7 Isoparaffins	4.55
Ethylbenzene	0.52	n-Heptane	4.65
p-Xylene	0.92	C7 Cyclopentanes	2.77
m-Xylene	2.75	Methylcyclohexane	7.57
o-Xylene	0.87	C8 Isoparaffins	4.24
C9+ Aromatics	3.31	n-Octane	3.43
Total Aromatics	13.88	C8 Cyclopentanes	1.52
Total Olefins	0.11	C8 Cyclohexanes	5.23
Paraffins and Naphthenes		C9 Naphthenes	3.63
Propane	0.79	C9 Paraffins	5.93
Isobutane	1.28	C10 Naphthenes	1.66
n-Butane	3.43	C10 Paraffins	3.41
Isopentane	5.62	C11 Naphthenes	1.04
n-Pentane	6.19	C11 Paraffins	0.53
Cyclopentane	0.64	C12 Paraffins+Naphthenes	0
C6 Isoparaffins	6	> 200 Paraffins +Naphthenes	0
n-Hexane	5.3	Total Paraffins	55.35
Methylcyclopentane	2.58	Total Naphthenes	30.7

In the typical process of crude oil refining (Fig. 1.2), it is necessary, first, the separation of the various components by distillation through their different boiling points, resulting on the separation of light and heavy naphtha, diesel oil and others. Subsequently, in the light naphtha case, sulphur and nitrogen are removed in the hydrotreater with a hydrogen feed [1] and after undergo the isomerization, which consists on the conversion of the hydrocarbons in their isomers with the objective of obtaining better quality parameters for the gasoline. The parameters that affect the engine performance and have major impact in the production and final treatments of the gasoline are: octane number, thermal efficiency, volatility of the gasoline and engine deposits [1]. The Octane number (RON) is the parameter that we want to improve.

1.1.2. Research Octane Number (RON)

The octane number is one of the most important parameters in the production of gasoline and is a measure of the gasoline resistance to "Knocking" [1]. After the almost complete combustion of the fuel, occurs a fast oxidation reaction of the unreacted residual fuel that creates a flame front from the spontaneous explosion that origins the "knock" or detonation [1]. The "knock" in a cylinder of a gasoline engine will be smaller for higher octane number. So, the great efficiency of the fuel is determined by its antiknock characteristic adequate to the motor. The percentage of isooctane (or 2,2,4 trimetylpentane) in the gasoline corresponds to the octane number.

The Research Octane Number (RON) is determined on low engine speeds (until 3000 rotation per minute, rpm) and the Motor Octane Number (MON) on high engine speeds. The difference of measurements between the RON and MON indicates the "sensibility of the gasoline" or "octane sensibility" [1]. Normally, the RON is higher than the MON. It is also usual the determination of the anti-detonation index (ADI) that corresponds to (MON + RON)/2.

In a fuel with hydrocarbon blend, the octane numbers are obtained by comparing the antiknock qualities of all hydrocarbons and is made a "blending of octanes". A fuel with isooctane or 2,2,4-trimethylpentane, (RON-100) and normal heptane (RON-0); therefore 90 octane gasoline blend that contains 90 % of isooctane and 10 % of n-heptane [1], as example. Table 1.3 shows some examples of pure hydrocarbons and their corresponding RON.

However, a blend of hydrocarbons corresponds to a blending of RONs that normally has the tendency to be low, due the big amount of hydrocarbons with low RON. There are various ways to enhance the octane number of the gasoline manufacture, for example, the addition of additives, that are substances rich in octanes, the catalytic reforming, the catalytic cracking, the conversion by alkylation and isomerization of the hydrocarbons in isomers with higher RON or also the exclusion from the gasoline blend of the hydrocarbons with low RON.

Table 1.3 - Research octane numbers of pure hydrocarbons [1].

Hydrocarbons	RON
Paraffins	
n-heptane	0
n-hexane	24.8
2-methylhexane	42.4
3-ethylpentane	65.0
2,4-dimethylpentane	83.1
isooctane	100
Aromatic	
Toluene	120.1
Ethylbenzene	107.4
Isopropylbenzene	113.0
1-methyl-3-ethylbenzene	112.1
1,3,5-trimethylbenzene	>120

The addition of substances as tetra ethyl lead (TEL) was used prior to 1990; however, the lead toxicity induced the environmental protection agency (EPA) to create the program of 'no lead' on the manufacturing gasoline [1]. The oxygenates as, methyl tert butyl ether (MTBE, RON 110–112), ethyl tert butyl ether (ETBE, RON 110–112), tert amyl methyl ether (TAME, RON 103–105) or ethanol (RON 112–115) were also used but are now being phased-out with limits for their use due to their volatility and facility to contaminate drinking water systems [1]. So, it was necessary to find alternatives to improve the enrichment of gasoline without using dangerous additives with environmental impact. To designate the octane number of a gasoline without additives the term clear research octane number (CRON) is also applied.

In order to increase the octane number it was further introduced the reformulated gasoline through the catalytic reforming and the catalytic cracking that are two process that convert paraffins in hydrocarbons with higher octane number. Through the catalytic reforming we convert cycloparaffin to light aromatics (majority in BTX compounds, benzene, toluene and xylenes), while in the catalytic cracking we convert paraffins to light olefins (majority ethylene, propylene and C4s) and both (light aromatics and olefins) have higher octane number than paraffins. Conversely, the aromatics are "Dirty Compounds" due to the harmful emissions to the air and the olefins are also considered a pollutant not as dangerous as the aromatics. So it is necessary to reduce the percentage of these products in the gasoline contents to reduce the harmful emissions to the air.

Alkylation and isomerization allow the increasing of the octane number without increasing the environmental impact. The alkylation consists on the conversion of unsaturated C4's to

high octane isobutanes, while the isomerization processes consist on the conversion of other low octane hydrocarbons to the high octane isomers [1].

1.1.3. Light Naphtha Isomerization process

An efficient technology to increase the octane number of light straight run naphtha streams is the Total Isomerization Processes (TIP) from UOP [8, 9, 10] and more recently, the Ipsorb and Hexorb processes [11, 12] from Axens [13]. In these processes, low Research Octane Number (RON) normal paraffins (e.g. *n*HEX (RON 24)) are converted in high RON branched hydrocarbons (e.g. 23DMB (RON-101.0), 22DMB (RON 91.8) or 3MP (RON 74.5), table 1.4) and after that it is necessary to separate the hydrocarbons with low RON from the higher RON to optimize the process of octane enrichment of the gasoline. So, the main objective of the isomerization is to increase the octane number of light naphtha streams and at the same time to substitute the BTX content with high RON. New catalysts and new process technologies are making light naphtha isomerization technology more economical and more effective for meeting the challenges of today's refinery [14]. Table 1.4 shows the differences between some hydrocarbon octane values of normal and isomer hydrocarbons.

Table 1.4 - Comparison between the hydrocarbon octane values of normal and isomer hydrocarbons [2].

Hydrocarbons	RON	MON	ADI
n-Butane	93.8	89.6	91.7
i-Butane	100.4	97.6	99.0
n-Pentane	61.7	62.6	62.2
i-Pentane	92.3	90.3	91.3
n-Hexane	24.8	26.0	25.4
2-Methylpentane (2MP)	73.4	73.5	73.4
3-Methylpentane (3MP)	74.5	74.3	74.4
2,2-Dimethylbutane (22DMB)	91.8	93.4	92.6
2,3-Dimethylbutane (23DMB)	101.0	94.3	97.6

UOP [2] has been developing catalytic systems for the isomerization process, with the objective of optimizing processes economically and operability; some of these are the aluminium chloride catalyst for alkane isomerization, the zeolitic isomerization catalysts, the sulphated metal oxide catalysts, the typical metal oxide catalyst, the UOP's LPI-100 catalyst and the newer I-80 catalyst that is a chloride alumina catalyst with higher and available usage

[2]. Among the UOP methods, the isomerization process that offers higher product octane number is the TIP unit (86–88 RON) [2]. However, more recently the Ipsorb and the Hexsorb processes from Axens (IFP group technologies) were developed enabling the RON of 89-90 and 91-92, respectively [13]. In these processes a combination of a chlorinated alumina catalyst and a molecular sieve to separate the normal paraffin [13] are used. Fig. 1.3 and 1.4 show the Hexsorb process and the Ipsorb process respectively.

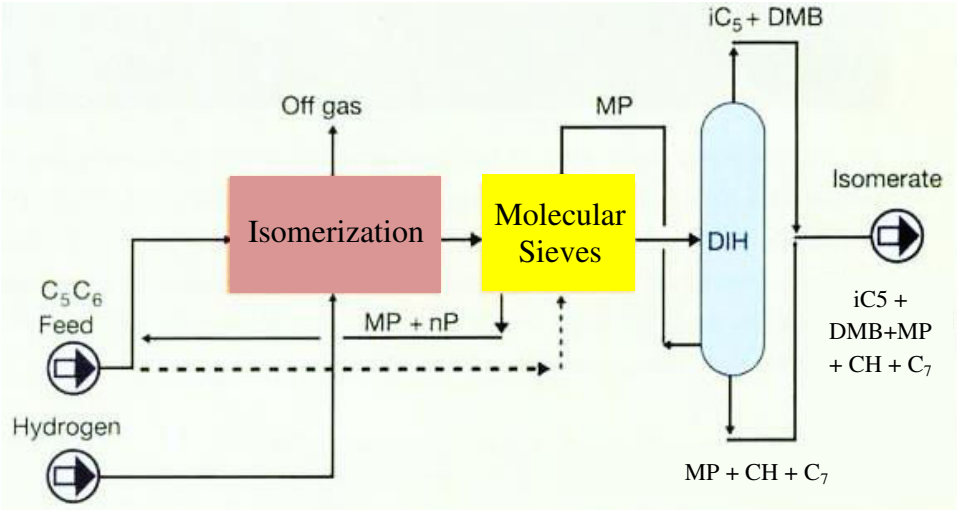

Figure 1.3 - Shematic diagram of the Hexsorb steps process [13].

In the Hexorb process (Fig. 1.3) the feed of C_5 and C_6 hydrocarbons goes to the isomerization and all the isomers flow through a bed of molecular sieve (to separate the isomer hydrocarbons by adsorption process) and its outlet stream is separated by a deisohexanizer split, in one stream rich in octane (isopentane, iC_5 and dimethylbutanes, DMB) and two streams with lower octane (methylpentane, MP; heptane, C_7 and others). In the Ipxorb process (Fig. 1.4) the feed of C_5 and C_6 hydrocarbons enters a deisopentanizer (DIP) that removes a isopentane-rich stream for the final stream that comes from the recycle of the adsorption unit (isopentane and normal paraffins). After the normal paraffins are isomerized and separated by the adsorption unit a final stream with high octane number (isopentanes and dimethylbutanes) is separated from other hydrocarbons with low octane number. The molecular sieve used for the cyclic adsorption (adsorption and desorption phases) is the zeolite 5A with high dynamic adsorption capacity [13]. So, another objective of this Ph. D. thesis is to research other molecular sieves to enrich the octane number of the final isomerate.

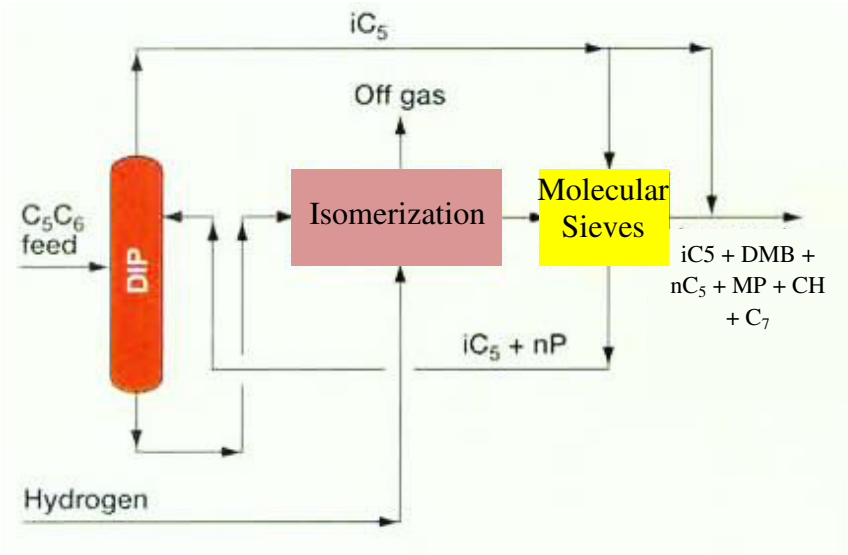

Figure 1.4 - Schematic diagram of the Ipsorb steps process [1].

1.1.4. Hexane isomers

The major components of the output of the Total Isomerization of Paraffin (TIP) are: linear *n*-hexane (*n*HEX), the mono-branched 3-methylpentane (3MP), the di-branched 2,2-dimethylbutane (22DMB) and 2,3-dimethylbutane (23DMB) [15]. It can be seen from Fig. 1.5 the conformation of the hexane isomers highlighting their linear (*n*HEX) and branched configurations, changing their connectivity and their physical and chemical properties [16]. The *n*HEX and their isomers are important due to their characteristics and high octane number of dimethylbutane (DMB).

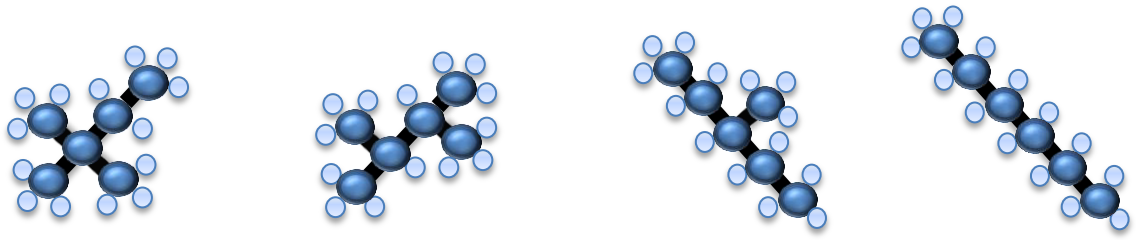

22DMB
RON-94.0
d_k-6.2 Å

23DMB
RON-101.1
d_k-5.6 Å

3MP
RON-74.5
d_k-5.0 Å

***n*HEX**
RON-24.8
d_k-4.3 Å

Figure 1.5 - The hexane isomers in study (22DMB, 23DMB, 3MP and *n*HEX) with their respective RON and d_k.

Table 1.5 indicates some of the more important parameters of the hexane isomers. We can observe that the di-branched isomers have higher RON than the mono-branched and the linear

isomer; therefore, it is necessary to eliminate from the final product the linear and mono-branched paraffins in order to increase the RON of the gasoline.

Table 1.5 - Values of the hexane isomers parameters relevant for this study.

Compounds	Abbreviation	d_k (Å)	Density ($g.cm^{-3}$)	T_{bp} (K)	RON
2,3-dimethylbutane	23DMB	5.6	0.6444	331	101.0
2,2-dimethylbutane	22DMB	6.2	0.6616	323	94.0
3-methylpentane	3MP	5.0	0.6598	337	74.5
n-hexane	*n*HEX	4.3	0.6606	342	24.8

It is interesting the relationship between their kinetic diameter (d_k) and the corresponding RON. For the low d_k we find the *n*HEX with the lower RON (24.8) and for the high d_k's we have the higher RON (94.0 and 101.1). In order to increase the RON number of petrochemical streams our goal is to separate linear *n*HEX from the branched isomers and it can be done based on the differences of the kinetic diameter of the compounds and the size of the windows of the molecular sieves as zeolites and MOFs.

1.1.5. Separation of Hexane isomers

1.1.5.1. Cryogenic Distillation

The cryogenic distillation or fractionated distillation is a technology of separation based on the boiling points of the components of the mixture. The distillation is divided in fractions along several plates [17]. Firstly the gaseous mixture is cooled, transformed in liquid and then the mixture is distilled [17]. To obtain a good efficiency and to produce high purity gases high energy investment (due to the heat exchangers involved and the amount of plates) is required [18]. As shown in the table 1.5, the difference between the boiling points of the hexane isomers is small. So, high number of plates on the experimental set-up is needed to separate the isomers completely [17]. All equipment and the separation or purification of components in a mixture using this traditional process of fractionated distillation leads to a high energy-consuming process. Accordingly, ecologic concerns are of great importance due to the decrease of energy resources that leads to the optimization of the processes. Non-cryogenic processes like pressure swing adsorption (PSA) allow separation reducing the economics and energy spent [19]. It is only necessary to use a molecular sieve (zeolite or metal-organic

framework) to satisfy the required purity by adsorption separation. The adsorbents generally used in these types of separations are zeolites, activated carbons and carbon molecular sieves. However, nowadays Metal-Organic-Frameworks (MOFs) are a very active domain of research since a significant number materials proved to be very competitive with already established adsorbents.

1.1.5.2. Adsorption separation Phenomena

The hexane isomers separation on adsorbents depends of the geometry of their internal cage and access window of the porous solid, as well as, of their different van der Waals (VdW) strengths, influencing the different selectivities of each isomer [20]. These interactions have influence on the molecules (gas or liquid) sticking on the surface of solids and this phenomenon is called adsorption [21]. The molecules with lower affinity with the solid will have higher diffusion rate through the pores and consequently low retention time (t_r) on the column. Fig. 1.6 illustrates a schematic molecular situation of an adsorption system, where are represented the adsorption/ desorption processes.

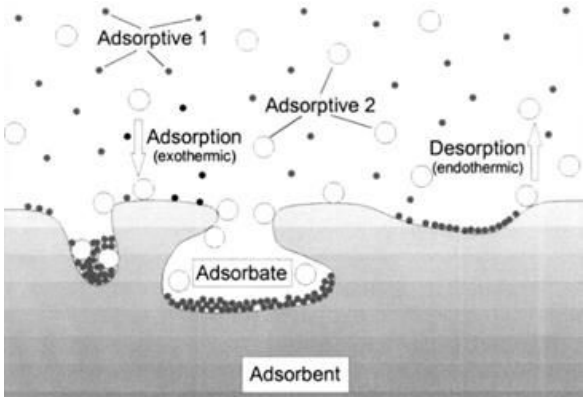

Figure 1.6 - Schematic situation of a molecular adsorption and desorption with two types of adsorptive molecules [21].

The adsorption corresponds to the stick of the adsorptive molecules of any fluid phase on the surface solid (adsorbent) while desorption corresponds to the return to mobile phase of the molecules placed on the surface phase (adsorbate molecules). When the molecules adsorb and desorb at equal rates adsorption equilibrium occurs [21]. The adsorption separation of the adsorptive molecules is based on three different mechanisms: steric, kinetic and equilibrium mechanisms [22]. The steric separation mechanism is based on the pores and windows dimension that exclude or allow the molecules to enter depending of their size, while the

kinetic mechanism is based on the separation through the affinity between the components and the porous structure [21]. The adsorption process reaches equilibrium depending of the adsorbate capacity. The component with the bigger rate of diffusion in the pores and with less affinity is firstly removed in a column. Several factors have influence on the interactions of the molecules with the surface area, such as size and properties. In this specific case of the hexane isomers separation, our goal is the separation preferentially of the di-branched relatively to the linear and mono-branched, so, it is interesting if the di-branched isomer is the more or the less adsorbed on the molecular sieves, because the more important aspect is the selectivity of the di-branched compared with the other components. If a molecular sieve has great adsorption capacity is good, but if the adsorption is equal for all components of the mixture is only important for storage application. For separation applications, the retention time of each component in the column is the more important parameter. The better separation corresponds to the bigger difference in the retention time. Normally we denote the order of adsorption as "normal hierarchy" for the tendency linear > mono-branched > dibranched and "reverse hierarchy" for the tendency dibranched>mono-branched>linear.

1.2. Metal-Organic Frameworks

Metal-Organic Frameworks (MOFs) emerged *ca.* 25 years ago as a simple concept, [23] becoming a major field of research with associated large number of potential applications. Currently, a strong effort has been focused to associate both academic and industrial researches with the aim of transforming these interesting solids in multifunctional materials [24]. Metal-Organic Frameworks (MOFs) are crystalline porous solids built up from inorganic unit (atoms, clusters, layers, etc.; Fig. 1.7a) and organic polycomplexant ligands (carboxylate, phosphate, azote, etc.; Fig. 1.7b) associated by exclusively strong interactions (ionocovalent) [25-28]. The three-dimensional arrangement of MOFs delimits an important porosity based on cages and/or pores with divers size, shape and interconnectivity (Fig. 1.7c) [26]. MOFs offer a highly versatile composition (inorganic and organic) and structure, with an adaptable porosity in terms of pore size and geometry [25, 26].

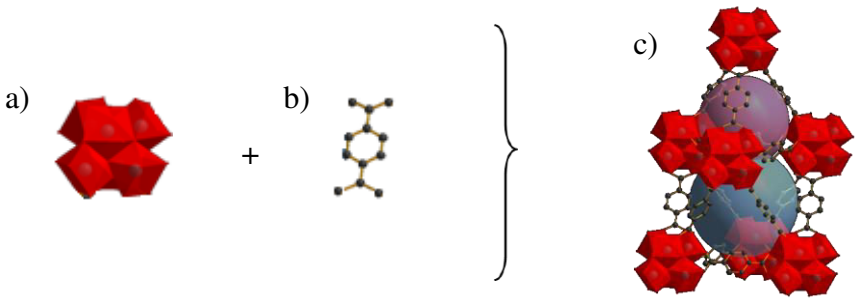

Figure 1.7 - The combination of (a) inorganic and (b) organic unit forms a structure (c) of UiO-66(Zr) with eight inorganic bricks and two types of cages, a super octahedron (blue sphere) and a super tetrahedron cage (purple sphere) [24].

The almost infinite choice of metal and ligands leads to a great MOF diversity [29-31]. Their three-dimensional framework can be also classified according with the dimensionality of the inorganic network in one-, two-, or three-dimensional porous solids (Fig. 1.8).

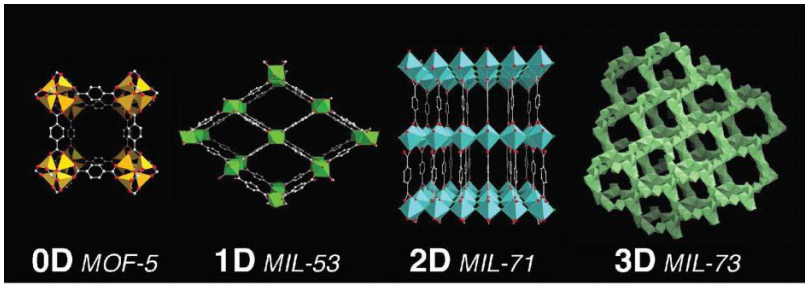

Figure 1.8 - Examples of MOFs (MOF-5, MIL-53, MIL-71 and MIL-73) in four dimensionalities of the inorganic sub network [23].

The first porous materials were reported by the group of Robson [25] and later, the groups of Yaghi, Férey, Kitagawa and Rosseinsky made important contributions on the MOFs development [26]. MOFs terminologies often refer to the network properties or to the name of the institute/university of the group that synthesized them. There are several used nomenclatures. Following is shown the most extended, where *n* is an integer in chronological order:

- MOF-*n*, the more general term [32].
- MIL-*n* (Materials of Institute Lavoisier) reported by Férey group [33, 34].
- UiO-*n* (University of Oslo) [35].
- ZIF-*n* (Zeolitic Imidazolate Frameworks) based on imidazolate linkers [36].
- IRMOF-*n* (IsoReticular MOFs) series of isoreticular compounds (based on a usually periodic and tailoring net), reported first by Yaghi's group [32].
- HKUST (Hong-Kong University of Science and Technology).

1.2.1. Different MOFs classes: Rigid and Flexible

MOF porosity can be classified in two different types: rigid and flexible. Rigid frameworks correspond to constant and robust structures, exhibiting permanent porosity [26]. Some examples of rigid MOFs are MIL-100 [37], MIL-125 [38] and UiO-66 [35]. Flexible frameworks correspond to adaptive structures that can reversibly 'breath' in response to an external stimulus such as temperature, pressure or guest adsorption. This stimulus cause either an expansion or shrinkage (Fig. 1.9) of the structure with strong dynamic movements (from 2 to 10 Å) of the atoms associated to unit cell volume increases (up to 300 %) without a loss of crystallinity [23].

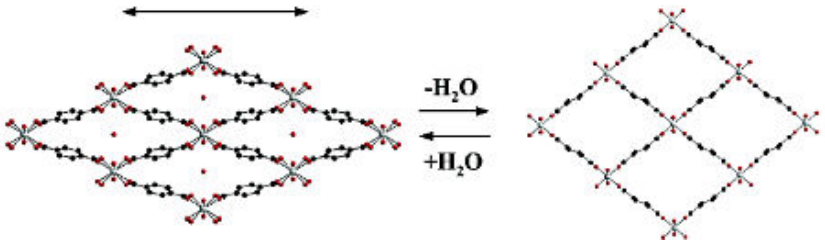

Figure 1.9 - Water effect in the MIL-53(Cr, Al) structure in their form: close (left) or open (right) [33].

Some of the most studied examples of flexible MOFs concerns the MIL-53(Fe, Al, Cr, Ga…) [39] and MIL-88(Cr, Fe) family [33]. The flexibility has a direct influence on the adsorption properties due to the modulation of their pore size and shape, which in addition can modify the interactions with an adsorbate. For instance, Fig. 1.9 shows the reversible breathing effect of MIL-53(Cr, Al) material, from its close hydrated form to its open dehydrated one.

1.2.2. Synthesis

MOFs are typically synthesized using the hydro/solvothermal method. However, other synthetic routes have been also applied to the MOF preparation, including microwave-assisted, ambient pressure, ionic liquids, mechanochemistry, ultrasound, electrochemistry, etc. [40].

1.2.2.1. Solvothermal method

MOFs are traditionally synthesized by hydro/solvothermal method, which basically consists on a mixture of the organic linker and the metal precursor into a solvent. The most common used solvents are water, alcohols, acetone, acetonitrile, pyridine, dimethyl or diethylformamide [41]. The mixture is heated in sealed vessels such as Teflon-lined vessels in stainless steel reactors (Fig. 1.10) or glass tubes, generating an autogenously pressure [31].

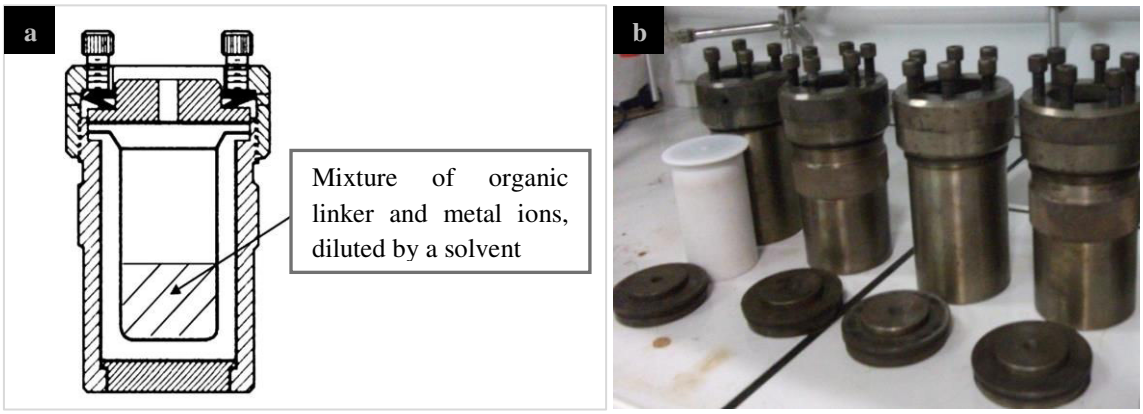

Figure 1.10 - (a) Schematic Teflon containers within stainless steel jackets closed [25] (b) A Teflon-lined container (white) and stainless steel rectors (the remainder). (Parr Instrument Co).

The stainless steel rectors are commercial autoclave assemblies, designed to prevent leakage from the Teflon-liner (PTFE resistant to the corrosion and temperature) and to burst safely if the pressure increases above expected limits [25]. Water is one the most relevant solvent because safety and cheap (specifically named hydrothermal method) [40]. These fundamental processes are influenced by a large number of synthetic parameters including the gel composition (inorganic/ organic components and solvent), pH of the reaction, temperature, time and stirring, among others [41].

1.2.2.2. Microwave-assisted hydro/solvothermal method

Microwave assisted hydro/solvothermal synthesis is another interesting method, recently applied for the synthesis of nanoporous organic-inorganic materials [42] due to short crystallization times needed in comparison with the solvothermal method. The use of irradiation for the reaction synthesis instead of the conventional heating has shown significant

reduction of reaction times (faster kinetics), reproducibility, selectivity of phase, increase of the product yields or improvement on product purities [43, 44]. Fig. 1.11 presents the microwave Mars equipment HP-500 (a), Teflon-lined vessels that contains the synthesis reaction mixture (b) and the vessel supports module HP-500 plus with the Teflon-lined vessels inside the microwave CEM, where the temperature and pressure are controlled.

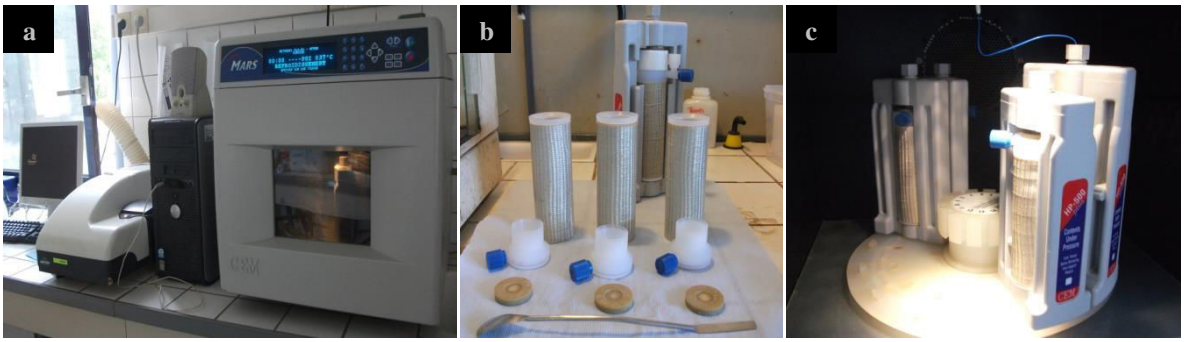

Figure 1.11 - (a) Microwave Mars equipment HP-500, manufactured by CEM Corporation. (b) A Teflon-lined vessel with the thermal covering and the respective lids with the blue thread that allow the aperture for pressure decrease. (c) Vessel supports module HP-500 plus with the Teflon-lined vessels inside the microwave CEM.

In the microwave method, the microwave irradiation acts on the activation of the dipole or ionic molecules, that is, the energy is transferred in less than a nanosecond (10^{-9} s), the molecules reaching an instantaneous equilibrium (unable to completely relax, ~ 10^{-5} s) that origins a high and instantaneous increase of the temperature, leading to a better control of the kinetics of the reaction [45].

1.2.2.3. Bottom- flask synthesis

Metal-Organic synthesis in a stirred round-bottom flask is applied for the synthesis of nanoporous materials due their constant stirring during the synthesis that limit the crystal grow. In this synthesis at room pressure, the round-bottom flask is placed in a heat source (heating plate, heating oil…) equipped with a thermometer for temperature control, a reflux condenser for cooler the vapours resulting of the synthesis mixture heating and a mechanical stirrer to keep a constant stirring (Fig. 1.12).

Figure 1.12 - Experimental set-up for the bottom flask synthesis.

The Fig. 1.12 shows the experimental set-up used for the bottom flask synthesis (at room pressure. Comparatively with the usual solvothermal method, the Bottom-flask synthesis is more reproducible, safety and cheaper route. Due to the room pressure used against the high pressures of the solvothermal method, the syntheses are more safety and reproducible. It was also obtained more yields through the Bottom-flask synthesis so, industrially, where it is necessary a scale-up in the production, this route suggest more interest due to their yields and safety synthesis conditions.

1.2.2.4. Functionalization of MOFs

Besides the large variety of combinations of the organic and inorganic parts to originate a vast number of topologies [46], MOFs also allow the possibility of easily modulate their physic-chemical properties by introducing different functional groups on either the organic or inorganic fraction of isostructural frameworks [47]. MOF functionalization can be realized either during the synthesis (starting from the functionalized ligand) or postsynthetically (on the preformed MOF), which is named as post synthetic modification (PSM) [39]. For the first, the synthesis conditions needs to be optimized in order to obtain the isostructural/isoreticular phase. For the PSM route, a sufficient chemical stability is required to avoid the MOF degradation during the chemical transformation [48]. Recently, the series of functionalized MIL-53(Fe)–X*n* (X*n*= –Cl, –Br, $–CH_3$, $–(CF_3)_2$, $–NH_2$, $–OH_2$,$–CO_2H$, etc), has been reported using the modified terephthalate linkers of the Fig. 1.13 [39].

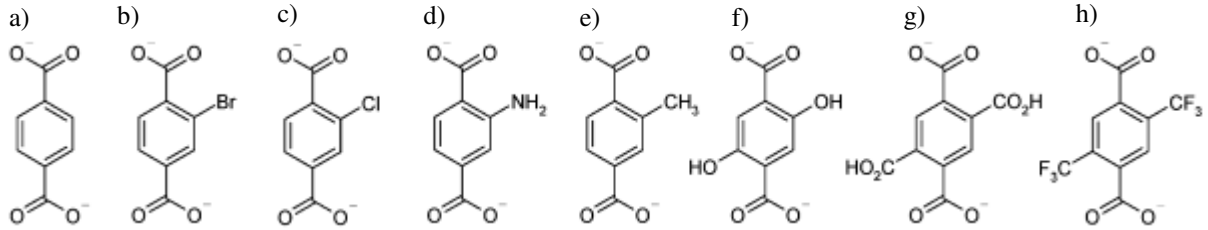

Figure 1.13 - Modified terephthalate linkers from (a) BDC linker and originating BDC–X_n with X_n=(b) Br, (c) Cl, (d) NH_2, (e) CH_3, (f) OH, (g) CO_2H or (h) CF_3 [39].

The functionalized structure allows easily tailoring the storage /separation properties with improvements on sorption and selectivity. To date, functionalization of MOFs has been more investigated using rigid than for the flexible MOFs. In both cases, their adsorption/ separation features are strongly affected; however, in flexible MOFs, functionalization can also modify their flexible behaviour [39]. Fig. 1.14 shows the MIL-53 structure with the functionalized linkers and the different breathing according with each functional group [39]. Concerning the rigid MOFs, we can mention here the case of the mesoporous chromium (III) trimesate MIL-100(Cr).

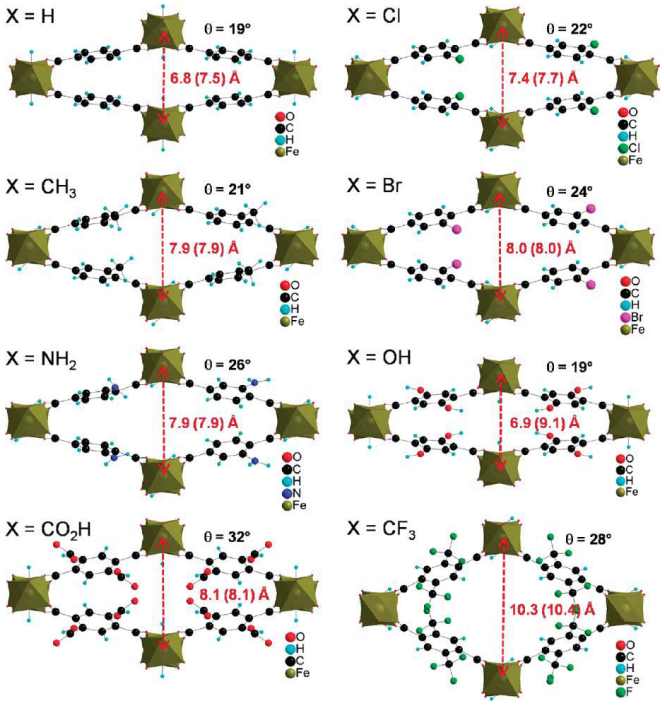

Figure 1.14 - Structures of MIL-53(Fe)–Xn functionalized with the pore internal diameter on their form dry and hydrated (parentheses) [39].

Several functional groups including $–H_2O$, $–CD_3OH$, $–CF_3CH_2OH$, $–(CF_3)_2CHOH$ have been introduced by post-synthetic grafting [49] or by direct synthesis (i.e. –OH) [50]. Similarly, a series of functionalized UiO-66(Zr) solid has been obtained by either post synthetic or direct method [46]. Finally, IRMOF–3 and IRMOF-1 have been modified by using the functionalized terephthalate linkers [51, 52], among others.

1.2.3. Characterization

The full characterization of MOFs includes several techniques like X-ray Powder Diffraction analysis, Infra-red analysis, Thermogravimetric analysis, surface area measurement through

nitrogen adsorption measurements among others. Fig. 1.15 illustrates a general procedure that could be applied for the characterization of most of MOFs.

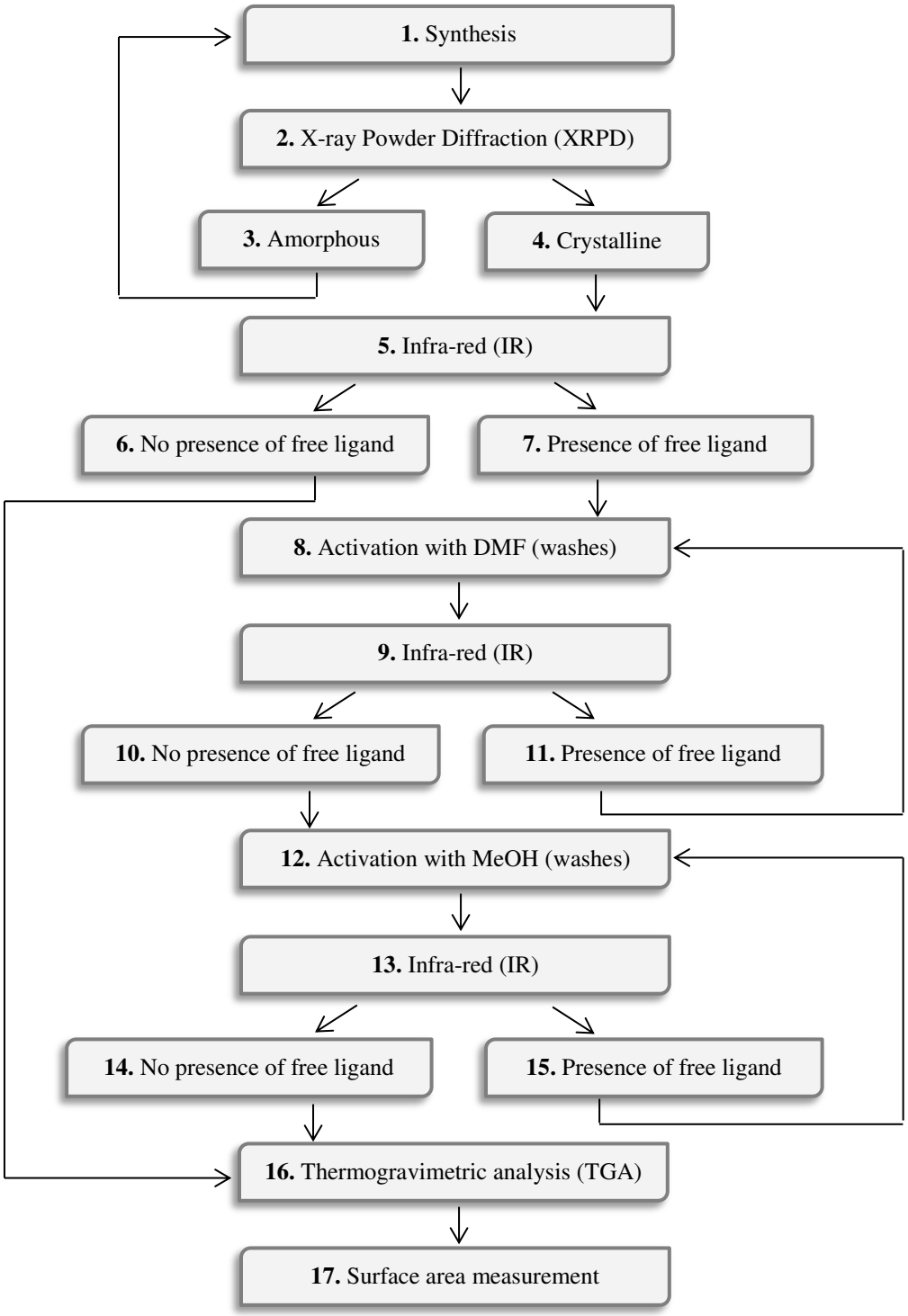

Figure 1.15 - Schematic representation of the ordered steps on the crystalline structures characterization.

Following, these main principles of each technique will be briefly described and an example of each one was also presented.

1.2.3.1. X-Ray Powder Diffraction (XRPD) analyses

X-Ray Powder Diffraction is an analytical technique used for characterization of materials, applied in several areas such as: geology, materials, chemistry, pharmaceutical and forensic, among others through three main forms: radiography; crystallography and fluorescence spectrometry [28]. For the characterization of MOFs, we used the crystallography based on the incidence of a X ray beam (I_0) on the crystal and the diffraction of secondary beam ($I(2\theta)$) (see Fig. 1.16).

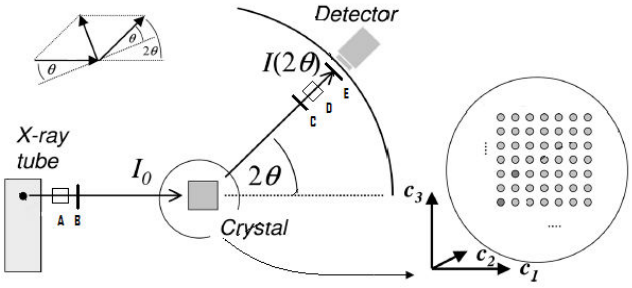

Figure 1.16 - X-rays scatter scheme on a cubic structure crystalline [53]. A–Soller slit; B–divergent slit; C–convergent slit; D–Soller slit; E–scatter slit; I–Intensity.

The beams path is described by the Bragg's law (Equation 1.1), that makes a relation between the x-ray wavelength and the spatial site of each atom [53].

$$n\lambda = 2d\ sin\Theta \qquad (1.1)$$

where, n is the order of reflection; λ (Å) is the wavelength of the X-rays; d (Å) is the interplanar distance, between the reflexion planes; θ (º) is the diffraction angle of the incident and diffracted beam.

The intensity and periodicity of the beams depend of the electrons number existing in the organized space of the crystal [53]. The crystalline solid consists of an ordered arrangement of structural units, while the amorphous solid has a disordered structure. Then, this technique allows the phase identification of the material (crystalline or amorphous) depending of the structure arrangement. The diffraction angle of the incident and diffracted beam is called θ y Theta and can be specified on the analysis (2θ normally). This angle allows an analysis closer or more distant if this value is bigger or smaller, respectively. Fig. 1.17 shows the Equipment Siemens, D5000 and an example of XRPD where the comparison of the original ZIF-8 [36] pattern (black) and other five samples synthesized it is shown. The diffraction diffractogram

allow the characterization of crystalline materials since their phase identification, unknown materials determination and synthesis confirmation by the comparison with typical pattern diffractions.

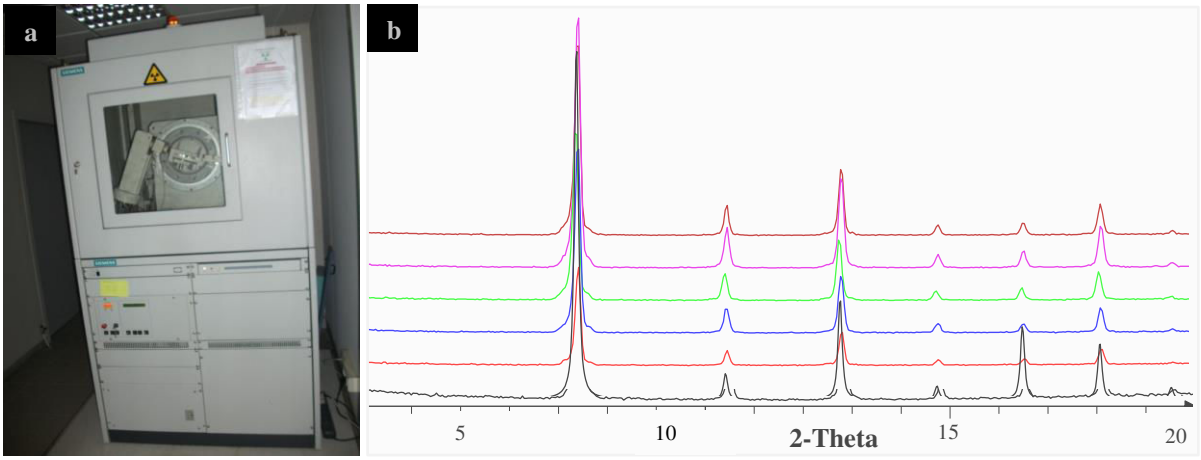

Figure 1.17 - (a) Equipment Siemens, D5000. (b) X-Ray powder diffractions example of the ZIF-8 structure.

This technique permits also to identify same structure alteration after same treatment of the MOF. Other crucial information obtained is the crystallography data of the structure unit cell. The crystallography data provide the unit cell parameters such as, space-group, cell dimensions (Volume and corner lengths [a, b, c]), atoms parameters, etc.

1.2.3.2. Infra-Red (IR) spectroscopy analyses

Infra-Red analysis (IR) is a vibrational spectroscopy that provides characteristic fundamental vibrations for interpretation of the molecular structures applied on the study of the nature of the forces between the atoms of a molecule or molecular structure determination for calculation of thermodynamic quantities [54]. The methods of Infrared diffractogram are based on molecular emission or absorption; however, the latter is the more common. For the molecule to show an infrared absorption it is necessary an electric dipole moment that change during the vibrations/ rotations and these movements depend of the internal degrees of freedom typical of each molecule [55]. There are groups with characteristic frequencies of vibrations (Wavenumbers [cm^{-1}]) subject to the atoms mass, geometric arrangement and the strength of their chemical bonds, represented by a band on a vibrational spectrum [54]. Therefore, this technique offers the possibility to detect the presence or not of some functional group and to understand better the molecular structure. Fig. 1.18 shows an example of Infra-red diffractogram of the sample UiO-66 (Br) as-synthesized (red) and after activation (black).

In the spectrum we can see the bands of the principal connections of the molecules on the synthesis and the peaks of the guest molecules on the pores of the framework. Then, this technique is very useful to both check the formation of metal-linker interactions and follow the presence of residual solvent and/or ligand.

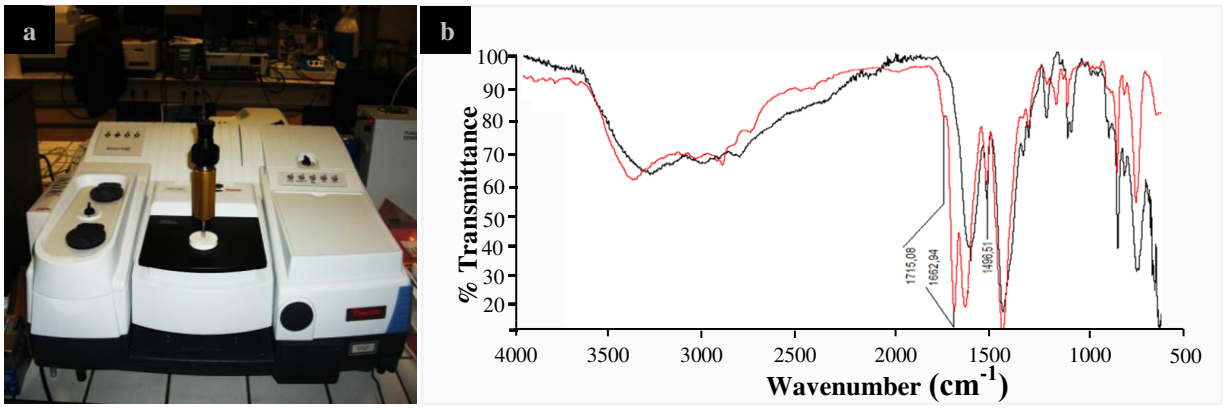

Figure 1.18 - (a) Equipment Nicollet, 6700 Thermo scientific. (b) Infra-Red comparison of the sample UiO-66(Zr)–Br as-synthesized (red) and after activation (black).

1.2.3.3. Thermogravimetric Analysis (TGA)

Thermal analyses are based on the control of a chemical or physical property of one substance as function of time and temperature upon a specific atmosphere that can involve variations of mass, energy or size deformations, depending of the objective under study [56]. The technique used for the characterization of MOF structures is the Thermogravimetric Analysis (TGA) that consists on a weight measurement of the material as a function of the temperature. The crystalline material exposed to the gradual rises in temperature along the time loses main first by vaporization of solvents and afterwards by degradation. Fig. 1.19 shows an example of TGA of the MOF MIL-100(Cr) [37] after synthesis. TGA analysis provides information concerning composition of the solid.

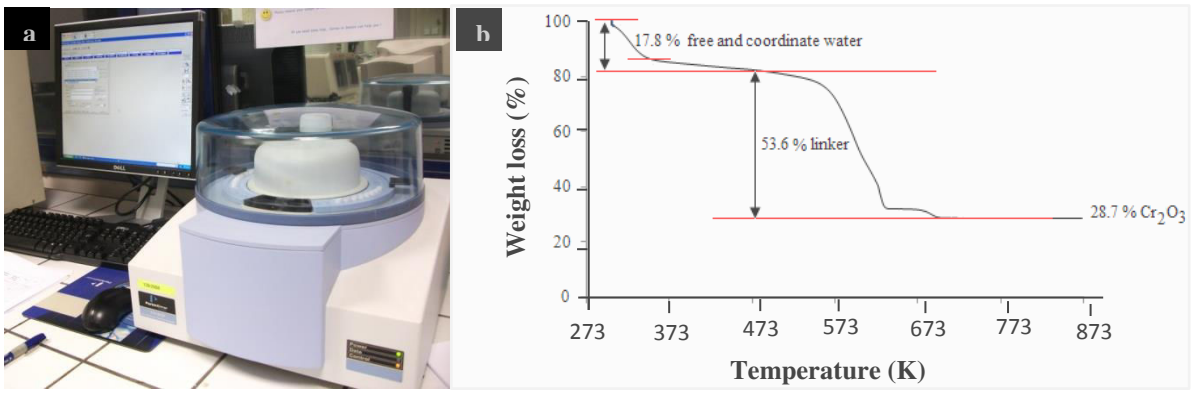

Figure 1.19 - (a) Equipment PerkinElmer, STA 6000 (b) Thermogravimetric Analysis of MIL-100(Cr) activated under air atmosphere (Heating rate of 275 K.min^{-1}; 4.198 mg of solid).

According to the temperature of the weight loss, a quantification of the solvent, organic and inorganic part can be carried out. Also, we can estimate the thermal stability of the solid (temperature at which occurs the weight loss of linker).

1.2.3.4. Nitrogen sorption measurements

Nitrogen sorption porosimetry consists on the sorption of nitrogen gas on the material surface at 77 K and provides important information about the material porosity, including pore size and distribution, surface area and pore volume.

Pore dimensions can limit the access of guest molecules, determining the adsorption on the internal surface. It can be classified as: micropore (0-20 Å); mesopore (20-500 Å); macropores (0.05-7.5 µm) and megapores (>7.5 µm) [57]. The pore size distribution is also important.

In addition, we can estimate the surface area of the material by nitrogen sorption measurements. Considering a monolayer adsorption, the surface is described by Langmuir isotherm, while the multilayer adsorption is described by BET theory. The BET theory is most used; however it cannot be applicable in all cases. The equation 1.2 allows the calculation using the BET theory [58].

$$V = \frac{V_a C P}{(P - P_0)\left[1 + (C - 1)\left(\frac{P}{P_0}\right)\right]} \qquad (1.2)$$

where, V ($cm^3(STP).g^{-1}$) is the volume of gas adsorbed, V_a ($cm^3(STP).g^{-1}$) is the volume of mono layer of gas adsorbed, P/P_0 is the relative pressure, P (atm) is the total equilibrium pressure of adsorbates, P_0 (atm) is the saturation pressure of adsorbates and C is the BET constant.

As a consequence of the BET equation simplification, a linear plot of $1/[(V(P_0/P)-1)]$ versus P/P_0 of the BET equation is obtained (equation 1.3). The value of the slope $[(C-1)/(V_aC)]$ and the Intercept $(1/V_aC)$ obtained by the linear plot is used to determine the values of C and V_a.

$$\frac{1}{V\left(\frac{P_0}{P}\right)-1} = \frac{1}{V_a C} + \frac{C-1}{V_a C}\left(\frac{P}{P_0}\right) \qquad (1.3)$$

The specific BET surface area of the adsorbent is calculated through the equation 1.4,

$$S_{BET} = \left(\frac{V_a N A_{ads}}{V_w}\right) \qquad (1.4)$$

where, S_{BET} ($cm^2.g^{-1}$) is the BET specific surface area, N ($molecule.mol^{-1}$) is the Avogadro number, A_{ads} ($cm^2.molecule^{-1}$) is the adsorption section area of adsorbate and V_w ($cm^3(STP).mol^{-1}$) is the molar volume of the adsorbate gas.

The equation 1.5 allows the calculation of the surface area using the Langmuir theory [58].

$$V = V_a \frac{KP}{1+KP} \qquad (1.5)$$

where K is the Langmuir constant.

As a consequence of the Langmuir equation simplification, a linear plot of P/V versus P of the Langmuir equation is obtained (equation 1.6). The value of the slope $1/V_a$ and the Intercept ($1/KV_a$) obtained by the linear plot is used to determine the values of K and V_a.

$$\frac{P}{V} = \frac{P}{V_a} + \frac{1}{KV_a} \qquad (1.6)$$

The specific Langmuir surface area of the adsorbent is calculated through the equation 1.7,

$$S_{Lang} = \frac{V_a N A_{ads}}{V_w} \qquad (1.7)$$

where S_{Lang} is the Langmuir specific surface area ($cm^2.g^{-1}$).

In the nitrogen adsorption isotherms, the saturation of active adsorption sites or the equilibrium among adsorption/desorption processes corresponds to the constant part of the isotherms. So, the maximum volume of nitrogen adsorbed [V_m ($cm^3(STP).g^{-1}$)], is the nitrogen volume that corresponds to the beginning of the constant part of the isotherm. It is also calculated the total pore volume [V_p($cm^3(STP).g^{-1}$)] and micropore volume [V_{mp}($cm^3(STP).g^{-}$

[1])] that is obtained from the amount of vapour adsorbed in all pores and in micropores, respectively.

Fig. 1.20 shows the equipment for samples degasification under vacuum (a), Equipment BEL Japan, BELSORP Mini (b) and the measurement of the N_2 adsorption isotherms (c) for MIL-100(Cr) samples.

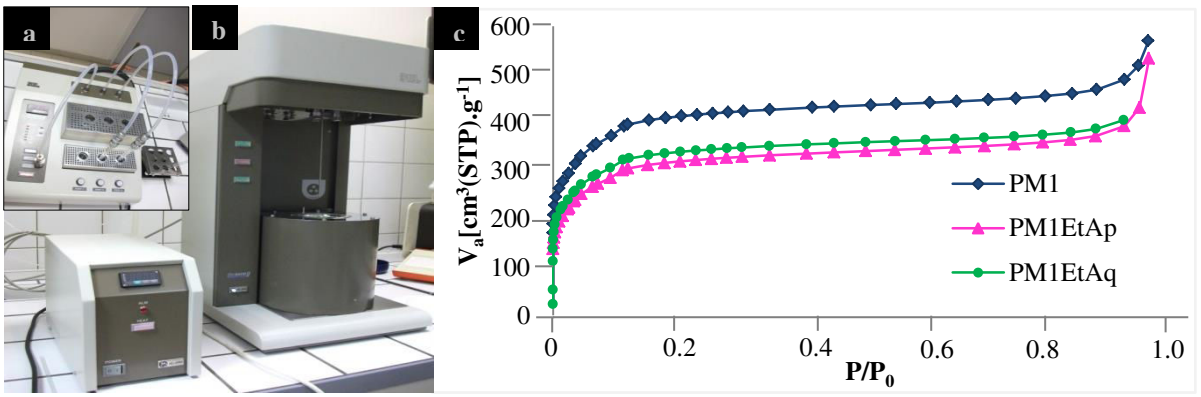

Figure 1.20 - (a) Equipment for outgas the samples under vacuum (b) Equipment BEL Japan, BELSORP Mini. (c) Nitrogen adsorption isotherm of MIL-100(Cr) (PM1) at 77K, the sample graft with ethylamine pure (PM1EtAp) and with ethylamine aqueous (PM1EtAaq) at T=77 K (Po=1 atm).

Prior to the analysis, samples are outgassed in order to remove all the entities present within the MOF porosity, allowing the nitrogen adsorption. Then, nitrogen adsorption-desorption isotherms are measured at 77 K. The isotherms obtained from the surface measurement (Fig. 2.14c) indicate for a specific partial pressure and amount adsorbed the micro and mesopores saturation.

From the initial curve of the isotherms to the constant part (from P/P_0 ~ 0 and ads ~ 0 V_a[cm^3(STP).g^{-1}] to P/P_0 ~ 0.15 to ads ~ 300-400 V_a[cm^3(STP).g^{-1}] corresponds to the micropores saturation. The final of the constant part (P/P_0 ~ 9 and ads ~ 350-450 V_a[cm^3(STP).g^{-1}] corresponds to the mesopores saturation.

1.2.4. Applications of MOFs in hexane isomers separation

The large variety of MOF skeleton composition confers them various properties such as, magnetic, electrical, optical, adsorptive and catalytic ones, which originate several potential applications in these strategic fields [58]. The hybrid skeleton is important due to their physical properties like magnetism, conductivity or luminescence, among others. The internal surface area is important for adsorption and/or catalysis feature. Finally, the different surface areas and pore volumes, together with a large variety of pore size and shape are of interest on selective adsorption (separation) of fluids or in storage [26]. Thus, some potential applications of MOFs in relevant processes for the industry include gas storage (H_2, CO_2, CH_4, NO_x, SO_x, C_2H_2 etc.), separation and purification by adsorption (industrial gas drying, H_2O removal; paraffins separation; CO_2 removal from blast-furnace gas and capture from flue gas; production of O_2 and N_2 enriched air; medical use (air separation, mainly N_2/O_2 separation), etc...) [51]. Despite their interesting performances, MOFs aren't applied yet in industry since an important effort might be done for large production and shaping of the synthesized particles [52, 59, 60].

Important applications involve potential adsorption capacities, advantageous for separation of components either for bulk separation or purification [61]. The purification process consists normally on the capture of harmful components or humidity of the mixtures, while the bulk separation provides the component separation from a mixture that normally is difficult through the normal techniques of separation [62]. The great performances of some MOFs reported by Yaghi [62] (MOF-5, IRMOF-3, MOF-74, MOF-177, MOF-199 and IRMOF-62) demonstrate good selectivities for eight harmful gases: sulphur dioxide, ammonia, chlorine, tetrahydrothiophene, benzene, dichloromethane, ethylene oxide, and carbon monoxide. Table 1.6 shows some Metal Organic Frameworks and the different components of separation associated [59, 61, 63].

Table 1.6 - Separation studies in MOFs [21].

MOF	Adsorbate
MOF-508	2-methylbutane, n-pentane, 2,2-dimethylbutane, 2-methylpentane, *n*-hexane
Zn-MOF	*n*-hexane, 3-methylpentane, 2,2-dimethylbutane
CUK-1	H_2, O_2, N_2, CH_4, CO_2
MIL-47	linear and branched alkanes; *o*-, *m*-, *p*-xylene, ethylbenzene;
MIL-53	linear and branched alkanes; xylenes, ethylbenzene, ethyltoluenes, cymenes
HKUST-1, MIL-47, MIL-53(Al)	olefins, alkylnaphthalenes, dichlorobenzenes
MIL-47, MIL-53(Al)	ethylbenzene, styrene
MIL-96	C5-hydrocarbons (isoprene, trans- and cis-piperylene)
SiO2-HKUST-1	ethylbenzene, styrene
MIL-53(Al)	*p*-, *m*-, *o*-xylene, ethylbenzene, linear and branched alkanes
MIL-101	*p*-, *m*-, *o*-xylene, ethylbenzene, *p*-, *m*-, *o*-chlorotoluene, 1,3,5-trimethylbenzene, n-propylbenzene, isopropylbenzene, *n*-alkanes
ZIF-8	linear and branched alkanes, CO_2/CO, H_2 and CH_4
MOF-177, MOF-5, HKUST-1, MOF-505, UMCM-150	dibenzothiophene and 4,6-dimethyldibenzothiophene in diesel fuel
HKUST-1, MOF-5	benzene, ethylbenzene, styrene, naphthalene, phenanthrene, pyrene, 1,3,5-triphenylbenzene,anthracene, 1,3,5-tris(4-bromophenyl)benzene

The separation of alkane isomers is very important in the industry and the MOFs are potential materials with promising results. A good example is the MOF-508, which is selective to the linear alkanes in contrast of the branched alkanes [64]. IRMOFs were tested for separation of branched and linear hexanes, but did not show significant selectivities [65]. A recent study [66] showed the separation of hexane isomers with uncommon reverse shape affinity: 22DM>23DMB>3MP>*n*HEX through the UiO-66(Zr). The MIL-100 shows a normal hierarchy trend *n*HEX>3MP>23DMB>22DM (by their ebullition points) with high affinity for the n-hexane, adsorbing larger amounts comparatively to the 0.282 $mL.g^{-1}$ of the NaY zeolite [67]. In spite of these results, it is necessary the development of novel structures that satisfy the industrial requirements and optimize the results with existing MOFs.

The separation of alkane isomers with MOFs might be an alternative due to the wide number of structures, compositions, pore volumes or pore sizes and their easy functionalization. Particular emphasis is made actually on the synthesis of more chemically stable MOFs based on high valence (+III or +IV) and non-toxic metals (Fe, Ti, Zr) or linkers that can be easily scaled for potential large scale in industrial applications. ILV (*Institut Lavoisier de Versailles*) has a world-wide renowned expertise in the synthesis, structure determination and applications of porous MOFs. Within the ILV, these porous materials are denoted MIL (for Material Institute Lavoisier), and might be good candidates to solve several separation

problems in chemical industry [2]. Fig. 1.21 shows some of the MILs evaluated for hexane isomers separation within this thesis. MIL-53(Fe) and MIL-88 have a flexible structure with adaptable pores to the guest molecules and specific experimental conditions, while MIL-100(Cr) and MIL-125 are rigid materials with fixed pore sizes. These materials were studied and the corresponding results are described in chapters 5 and 6. MIL-100(Cr) demonstrates high adsorption capacities, adsorbing larger amounts comparatively to the NaY zeolite [68].

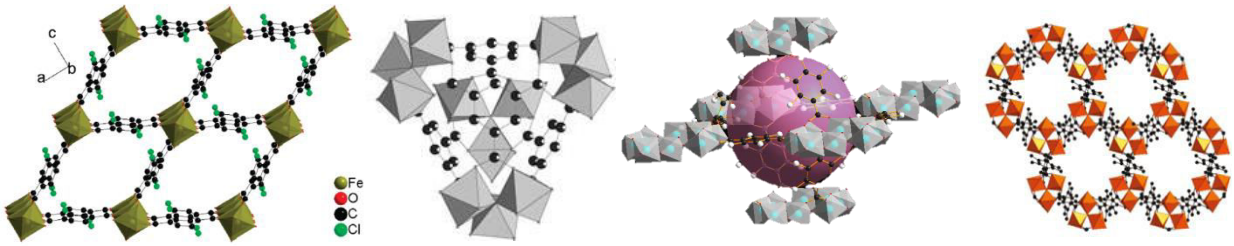

MIL-53 (Fe) MIL-100 (Cr) MIL-125 MIL-88

Figure 1.21 - Examples of MILs frameworks (MIL-53(Fe) [33, 39], MIL-100(Cr) [34], MIL-125 [69] and MIL-88) [70].

Prior to this work, interesting results were reported by Barcia *et al.* [19] for *n*HEX, 3-methylpentane and 2,2-dimethylbutane separation by fixed bed adsorption using the Zn_2(1,4-bdc)$_2$(dabco) MOF, where binary experiments showed selectivities of 9.9 and 2.2 for the ratios *n*HEX/3MP and 3MP/22DMB at 313 K and 4.8 kPa, respectively. Another recent study [71] shows that the MOF UiO-66(Zr) can be also a potential candidate for the separation of hexane isomers with uncommon reverse shape affinity: 22DM>23DMB>3MP>*n*HEX. This material showed similar values of selectivity with a maximum of 6.5 for the ratios 22DMB/*n*HEX and 23DMB/*n*HEX at 0.6 kPa and 420 K and a maximum selectivity value of 1.5 at 473 K and 6.3 kPa was obtained for the ratio di/mono branched 22DMB/3MP. In order to improve the adsorption and selectivity properties, this material was synthesized and studied their separation properties but the structure was functionalized with three different groups, which is described on chapter 3. Another interesting material is the ZIF-8 based on imidazolate type linkers, which demonstrate good results in terms of hexane isomers separation and a recent comparative study with the zeolite 5A [72] shows that it can be a competitive material in the separation of the linear *n*HEX from the branched isomers.

1.2.5. MOFs vs Zeolites

Inside each class of porous solids (Inorganic and Hybrid), Zeolites and MOFs as respectively inorganic and hybrid highly porous materials have outstanding properties. Zeolites are microporous aluminosilicates based on corner-sharing of SiO_4 and AlO_4 tetrahedral, pentahedral and octahedral coordinations for the metal with an important thermal and chemical stability [23, 26]. Zeolites are currently been applied in several processes such as gas separation/storage, catalysis and as ion-exchanger in detergents and water softeners [73]. In comparison to zeolites, MOFs exhibit higher porosities, with larger pore sizes and surface and volumes. In addition, they possess a wider variety of structures and compositions, based on their hybrid character. [31]. However, MOFs exhibit a much lower thermal stability than zeolites [26].

Recently, it has been shown that zeolite BETA can be used to upgrade actual Total Isomerization Processes [74]. In that work, it is demonstrated that an optimal layered bed of zeolite 5A-to-zeolite BETA can improve the product average RON up to 1.0 point compared to actual existing TIP processes using zeolite 5A only. Moreover, process simulations demonstrated that increasing the operating temperature from 523 K to 543 K results in an octane gain of 0.2 RON.

Today metal-organic frameworks represent a new class of porous materials proving to be a competitive alternative to zeolites since they combine an important regular porosity (up to pore volumes ~ 4 $cm^3.g^{-1}$, BET surface areas up to 6500 $m^2.g^{-1}$ and pore diameters~ 3-60 Å) with an easily tuneable hybrid crystalline framework [75].

1.3. Objectives and Organization

The main objective of this thesis was the adsorption and separation studies of hexane isomers using topical Metal-Organic Frameworks (MOFs), with the aim of discovering MOFs able to better adsorb and separate branched and linear isomers. Metal-Organic Frameworks (MOFs)

are interesting crystalline hybrid solids with an important porosity, which can be rigid (or permanent) or flexible (their porous structure can be modified according with an external stimuli). Their high versatile structure and composition confer to each MOF different physicochemical and textural properties. MOFs are often synthesized under hydro/solvothermal conditions, starting from an inorganic and organic precursor in a polar solvent. Some of the most used synthetic methods include the conventional heating hydro/solvothermal, microwave-assisted hydro/solvothermal conditions or room pressure route. MOFs are typically characterized using different techniques, such as e X-Ray Powder Diffraction (XRPD), Infra-Red spectroscopy (IR), Thermogravimetric Analysis (TGA), elemental analysis and nitrogen adsorption porosimetry providing important information about their crystalline structure, composition and textural properties. Synthesis and characterization of a selected number of MOFs was carried out at *Institut Lavoisier de Versailles* (ILV-UVSQ, France) at the hundred milligrams and multi-grams scale. In addition to the different structures and compositions, the functionalization of the MOFs by direct synthesis using functionalized linkers or by post synthetic modification (PSM) was carried out to modulate the pore size of the materials and the selectivity.

Thereafter the MOFs synthesized at ILV were characterized in LSRE through screening studies to attain their capability to separate hexane isomers. This thesis comprises seven chapters: one describing the motivation, one chapter containing the material and methods, four chapters dealing with the experimental results and another one with the conclusions. Fig. 1.22 illustrates the contents.

In Chapter 1 the relevance and motivation to find alternatives for the hexane isomers separation are discussed.

Chapter 2 presents the different classes of MOFs, synthesis and characterization. The set-up for the breakthrough experiments of the hexane isomers separation using the MOFs is also introduced.

Chapter 3 deals with the experimental section and the multicomponent hexane isomers sorption experiments on a functionalized UiO-66 MOF with functional groups –Br, $–NH_2$ and $–NO_2$. Their synthesis and characterization are also detailed.

Chapter 4 details the single, binary and multicomponent experiments of the hexane isomers sorption in the zeolitic imidazole framework ZIF-8 and its synthesis and characterization.

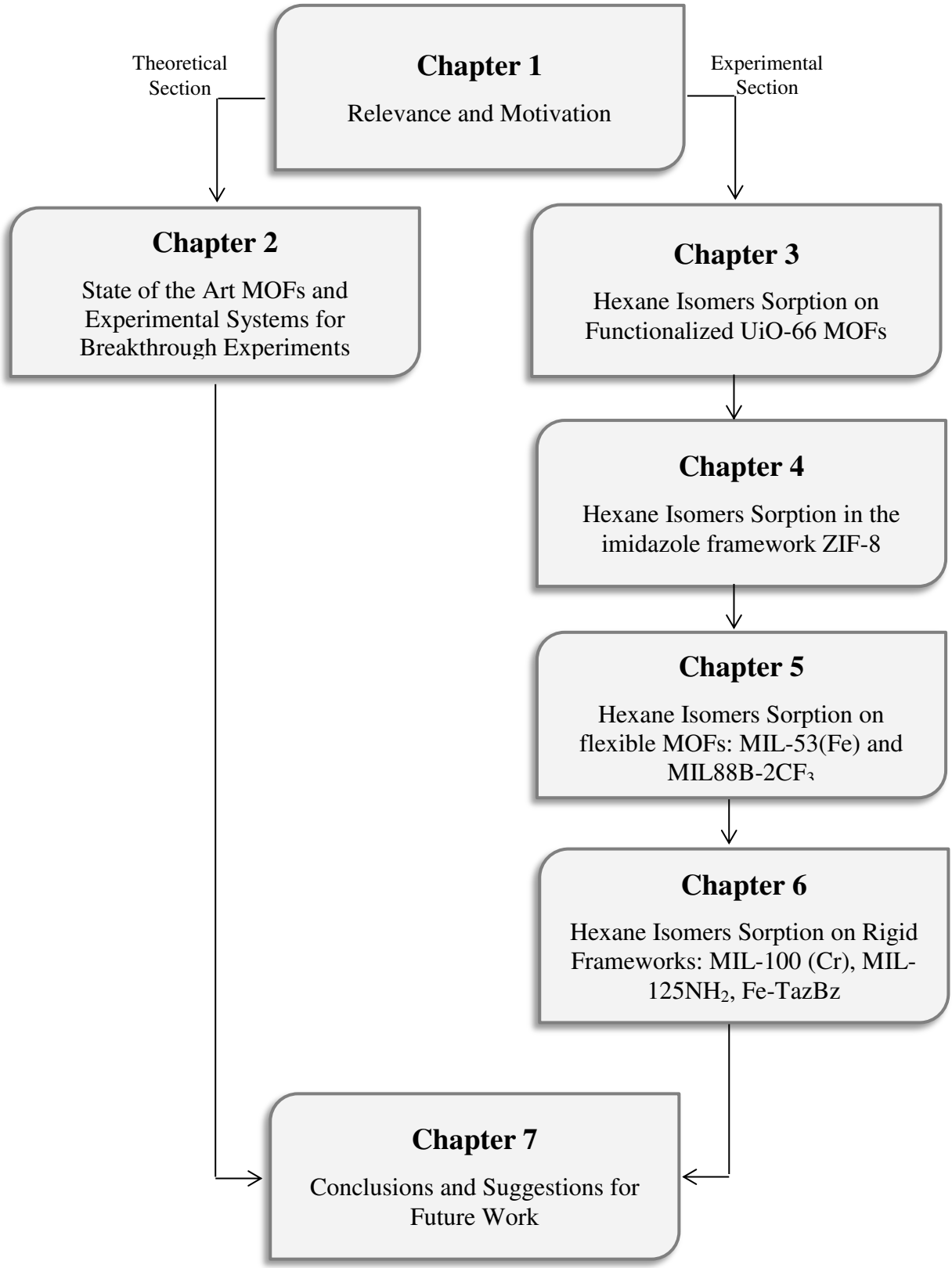

Figure 1.22 - Schematic representation of the thesis organization.

Chapter 5 displays the hexane isomers sorption on some flexible MOFs: MIL-53(Fe)–$2CH_3$, MIL-53(Fe)–$(CF_3)_2$ and MIL88B–$2CF_3$ with focus on the synthesis and characterization of the MIL-53(Fe)–$2CH_3$ and MIL88B-$2CF_3$.

Chapter 6 exhibits the breakthrough experiments of the hexane isomers sorption on some rigid frameworks as MIL-100 (Cr), MIL-125-NH_2 and MIL-127(Fe). The synthesis and characterization of MIL-100 (Cr) and its functionalization with ethylamine was detailed.

Finally, Chapter 7 presents the main conclusions and some suggestions for future work.

1.4. References

1. *D, Jones, An introduction to crude oil and its processing, in: Handbook of Petroleum Processing, Springer, USA, 2006.*

2. *P. Pujadó, Isomerization technologies for the upgrading of light naphtha and refinery light ends in: Handbook of Petroleum Processing, Springer, USA, 2006.*

3. *T. Brooks, The Origin of Petroleum in the Light of Recent,The Ohio Journal of Science, 48 (1948) 129-145.*

4. *http://www.petroleum.co.uk/; An introduction to Petroleum, Copyright © 2013 Petroleum.co.uk.*

5. *The NEED Project, Petroleum, Secondary Energy Infobook, (2012) 32-35.*

6. *http://energy.gov/articles/hows-and-whys-replacing-whole-barrel, Copyright © 2011 energy.gov.*

7. M. Beychok, *http://www.eoearth.org/article/Petroleum_refining_processes?topic=74180, Copyright © 2011 eoearth.org.*

8. *N. Cusher, UOP TIP and Once-Through Zeolitic Isomerization Processes. In Handbook of Petroleum Refining Processes, R. Meyers, Ed.; 3rd Edition, McGraw Hill: New York, 2004.*

9. *T. Holcombe, n-Paraffins - Isoparaffins Separation Process. U.S. Patent (1979) 4,176,053.*

10. *T. Holcombe, Total Isomerization Process. U.S. Patent (1980) 4, 210,771.*

11. *A. Minkkinen, L. Mank, S. Jullian, Process for the Isomerization of C5/C6 Normal Paraffins with Recycling of Normal of Multicomponent Adsorption Beds. U.S. Patent (1993) 5,233,120.*

12. *A. Deschamps, S. Jullian, Adsorption in the Oil and Gas Industry. In Petroleum Refining: Separation Processes, Volume 2; Wauquier, J.P., Ed.; Editions Technip: Paris, 2000.*

13. *B. Domergue, L. Watripont, Paraffins Isomerization Options, Axens, PTQ Q2, 2005, Axens.*

14. *V. Deak, R. Rosin and D. Sullivan, Tutorial:Light Naphtha Isomerization, 2008, UOP LLC.*

15. *P. Bárcia, J. Silva, A. E. Rodrigues, Separation of Branched Hexane Isomers on Zeolite BETA, Adsorption Science & Technology, 25 (2007)169-183.*

16. *D. Reger, S. Goode, E. Mercer et al., Química: Principios e Aplicações, Ed:Fundação Calouste Gulbenkian, 1997.*

17. *C. J. Calzon-McConville, M. B. Rosales-Zamora, J. G. Segovia-Hernández, S.Hernández et al, Design and Optimization of Thermally Coupled Distillation Schemes for the Separation of Multicomponent Mixtures, Ind. Eng. Chem. Res., 45 (2006) 724-732.*

18. *G. Dünnebier and C. C. Pantelides, Optimal Design of Thermally Coupled Distillation Columns, Ind. Eng. Chem. Res., 38 (1999) 162-176.*

19. *P. Bárcia, F. Zapata, J. Silva, A. E. Rodrigues and B. Chen, Kinetic Separation of Hexane Isomers by Fixed-Bed Adsorption with a Microporous Metal-Organic Frameworks., J. Phys. Chem., 111 (2007) 6101-6103.*

20. *B. Chen, C. Liang, J. Yang, D. Contreras, Y. Clancy, E. Lobkovsky, O. Yaghi, S. Dai, A Microporous Metal–Organic Framework for Gas-Chromatographic Separation of Alkanes, Angew. Chem. Int. Ed., 45 (2006) 1390-1393.*

21. *J. Keller, R. Staudt, Gas Adsorption Equilibria Experimental methods and Adsorption Isotherms, Springer , Germany, 2005.*

22. *D. Do, Adsorption analysis: Equilibria and Kinetics, ICP, Australia, 1998.*

23. *G., Férey, Some suggested perspectives for multifunctional hybrid porous solids, Chem. Soc. Rev., Dalton Trans, (2009) 4400-4415.*

24. *P. Bárcia, D. Guimarães, P. Mendes, J. Silva, V. Guillerm, H. Chevreau, C. Serre, A. Rodrigues, Reverse Shape Selectivity in the Adsorption of Hexane and Xylene Isomers in MOF UiO-66, Micropor. Mesopor. Mater., 139 (2011) 67-73.*

25. *B. F. Hoskins , R. Robson, Design and construction of a new class of scaffolding-like materials comprising infinite polymeric frameworks of 3D-linked molecular rods. A reappraisal of the zinc cyanide and cadmium cyanide structures and the synthesis and structure of the diamond-related frameworks* $[N(CH_3)_4][CuIZnII(CN)_4]$ *and CuI[4,4',4'',4'''-tetracyanotetraphenylmethane]*$BF_4.xC_6H_5NO_2$, *J. Am. Chem. Soc.*, 112 (1990) 1546–1554.

26. *G. Férey, The Long Story and the brilliant Future of Crystallized Porous, in: D. Braga , S. Bureekaew , N. Champness, F. Grepioni, P. Hubberstey, J. Jia, S. Kitagawa, L. Maini, M. Polito, M. Schröder, S. Shimomura et al, Molecular Networks, Springer, 2009.*

27. *D. Ebbing, S. Gammom, General Chemistry. 8th ed., Houghton Mifflin Company, 2006.*

28. *C. Suryanarayana, M. Grant Norton., X-Ray diffraction: a practical approach, Springer, 1998.*

29. *F. Paz, J. Klinowski, Sérgio Vilela, J. Tomé, J. Cavaleiro, J. Rocha, Ligand design for functional metal–organic frameworks. Critical Review, Chem. Soc. Rev., 41 (2011) 1080-1110.*

30. *J. Perry, J. Perman and, M. Zaworotko, Design and synthesis of metal–organic frameworks using metal–organic polyhedra as supermolecular building blocks, Chem. Soc. Rev., 38 (2009) 1400-1417.*

31. *J. Rowsell, O. Yhagi, Metal-Organic Frameworks: a new class of porous, Micropor. Mesopor. Mater., 73 (2004) 3-14.*

32. *O. Yaghi, M. O'Keeffe, N. Ockwig, H. Chae, M. Eddaoudi, J. Kim, Reticular synthesis and the design of new materials, Nature, 423 (2003) 705-714.*

33. *C. Serre, F. Millange, C. Thouvenot, M. Noguès, G. Marsolier et al, Very Large Breathing Effect in the First Nanoporous Chromium(III)-Based Solids: MIL-53 or CrIII(OH).{O2C-C6H4-CO2}.{HO2C-C6H4-CO2H}x.H2Oy. J. Am. Chem. Soc., 124 (2002)13519-13526.*

34. *C. Volkringer, D. Popov, T. Loiseau, G. Férey, M. Burghammer, C. Riekel et al., Synthesis, Single-Crystal X-ray Microdiffraction,and NMR Characterizations of the Giant PoreMetal-Organic Framework Aluminum Trimesate MIL-100. Chem. Mater.,21 (2009) 5695-5697.*

35. *J. Hafizovic Cavka, S. Jakobsen, U. Olsbye, N. Guillou, C. Lamberti, S. Bordiga, K. Lillerud, A new zirconium inorganic building brick forming metal organic frameworks with exceptional stability, J. Am. Chem. Soc., 130 (2008) 13850-13851.*

36. *K. Park, Z. Ni, A. Côté, J. Choi, R. Huang, F. Uribe-Romo, H. Chae, M. O'Keeffe, O. Yaghi, Exceptional chemical and thermal stability of zeolitic imidazolate frameworks, PNAS, 103 (2006) 10186-10191.*

37. *G. Férey, C. Serre, C. Mellot-Draznieks, F. Millange, S. Surblé, J. Dutour, I. Margiolaki, A Hybrid Solid with Giant Pores Prepared by a Combination of Targeted Chemistry Simulation and Powder Diffraction, Angew. Chem. Int. Ed., 43 (2004) 6296-6301.*

38. *M. Dan-Hardi, C. Serre, T.Frot, L. Rozes, G. Maurin, C. Sanchez, G. Férey, A New Photoactive Crystalline Highly Porous Titanium(IV) Dicarboxylate, J. Am. Chem. Soc., 131 (2009) 10857-10859.*

39. *T. Devic, P. Horcajada, C. Serre, F. Salles, G. Maurin, B. Moulin, D. Heurtaux, G. Clet, A. Vimont, et al., Functionalization in Flexible Porous Solids: Effects on the Pore Opening and the Host-Guest Interactions, J. Am. Chem. Soc., 132 (2010) 1127-1136.*

40. *R. Morris, Ionothermal synthesis—ionic liquids as functional solvents in the preparation of crystalline materials, Chem. Commun., (2009) 2990-2998.*

41. *D. Tranchemontagne, J. Hunt , O. Yaghi, Room temperature synthesis of metal-organic frameworks: MOF-5, MOF-74,MOF-177, MOF-199, and IRMOF-0, Tetrahedron, 64 (2008)8553-8557.*

42. *G. Blãnitã, O. Ardelean, D. Lupu, G. Borodi, M. Mihet, M. Coros et al, Microwave Assisted Synthesis Of MOF-5 at Atmospheric Pressure, Rev. Roum. Chim., 56 (2011) 583-588.*

43. *C. O. Kappe, D. Dallinger, and S. S. Murphree, Microwave Synthesis – An Introduction, In: Practical Microwave Synthesis for Organic Chemists: Strategies, Instruments and Protocols, WILEY-VCH Verlag GmbH & Co. KGaA, Weinheim, (2009) 1-9.*

44. *S. B. Mohan et al, Microwave Irradiation Versus Conventional Method: Synthesis of Benzimidazolyl Chalcone Derivatives, Int.J. ChemTech Res., 2 (2010) 1634-1637.*

45. *B. L. Hayes,CEM Corporation, Recent Advances in Microwave-Assisted Synthesis, Aldrichimica Acta 37 (2004) 66-76.*

46. *S. Garibay, S. Cohen, Isoreticular synthesis and modification of frameworks with the UiO-66 topologys, Chem. Commun, 46 (2010) 7700-7702.*

47. *S. Chavan,J. Vitillo,M. Uddin, F. Bonino, C. Lamberti, E. Groppo et al.,Functionalization of UiO-66 Metal-Organic Framework and Highly Cross-Linked Polystyrene with Cr(CO)3: In Situ Formation, Stability, and Photoreactivity. Chem. Mater, 22 (2010) 4602-4611.*

48. *S. Cohen, Modifying MOFs: new chemistry, new materials, Chem. Sci., 1 (2010) 32-36.*

49. *A. Vimont, H. Leclerc, F. Maugé, M. Daturi, J. Lavalley, S. Surblé, et al., Creation of Controlled Brønsted Acidity on a Zeotypic Mesoporous Chromium (III) Carboxylate by Grafting Water and Alcohol Molecules, J. Phys. Chem. C., 111 (2007) 383-388.*

50. *A. Vimont, J.Goupil, J. Lavalley, M. Daturi, S. Surblé, C. Serre, F. Millange, G. Fé rey, N. Audebrand, J. Am. Chem. SOC., 128 (2006) 3218-3227.*

51. *K.Tanabe, Z. Wang, S. Cohen, Systematic Functionalization of a Metal-Organic Framework via a Postsynthetic Modification, J. Am. Chem. Soc., 130 (2008) 8508-8517.*

52. *J. Rowsell, O. Yaghi, Effects of Functionalization, Catenation, and Variation of the Metal Oxide and Organic Linking Units on the Low-Pressure Hydrogen Adsorption Properties of Metal-Organic frameworks, J. Am. Chem. Soc., 128 (2006)1304-1315.*

53. *M. Birkholz, Thin Film Analysis by X-Ray Scattering, WILEY-VCH, Weinheim, 2006.*

54. *P. Larking, Raman Spectroscopy: Principles and spectral interpretation, Elsevier, USA, 2011.*

55. *S. Barbara, Infrared Spectroscopy: Fundamentals and applications, Australia, Wiley, 2004.*

56. *C. Brebbia, A. Mammoli, et al., Computational methods and experiments in materials Characterization II, Wit Press, USA,UK, 2005.* 47. *R. Malherbe, Adsorption and diffusion in nanoporous materials. CRC, USA, 2007.*

57. *S. Lowell , Surface Area Analysis from the Langmuir and BET Theories in: S. Lowell, J. E. Shields, M. A. Thomas, M. Thommes, Characterization of Porous Solids and Powders: Surface Area, Pore Size and Density, Springer Sience, 2004.*

58. *R. Kupplera, D. Timmonsb, Q. Fanga, J. Li, T. Makala, M. Younga, D. Yuana, D. Zhaoa,W. Zhuanga, H. Zhou, Potential applications of metal-organic frameworks, Coordination Chemistry Reviews, 253 (2009) 3042–3066.*

59. *H. Jiang, Q. Xu, Porous metal–organic frameworks as platforms for functional applications., Chem. Commun., 47 (2011) 3351-3370.*

60. *U. Mueller, M. Schubert, F. Teich, H. Puetter, K. Schierle-Arndt, J. Pastre, Metal–organic frameworks—prospective industrial applications, J. Mater. Chem., 16 (2006) 626-636.*

61. *J. Li, R. Kupple, H. Zhou, Selective gas adsorption and separation in metal–organic frameworks., Chem. Soc. Rev., 38 (2009) 1477-1504.*

62. *D. Britt, D. Tranchemontagne, O. Yaghi, Metal-organic frameworks with high capacity and selectivity for harmful gases, PNAS, 105 (2008) 11623-11627.*

63. *D. Fairen-Jimenez, S. Moggach, M. Wharmby, P. Wright, S. Parsons, T. Düren, Opening the Gate: Framework Flexibility in ZIF-8 Explored by Experiments and Simulations, J. Am. Chem. Soc., 133 (2011) 8900-8902.*

64. *B. Chen, C. Liang, J. Yang, D. Contreras, Y. Clancy, E. Lobkovsky, O. Yaghi, S. Dai, A Microporous Metal–Organic Framework for Gas-Chromatographic Separation of Alkanes, Angew. Chem. Int. Ed., 45 (2006) 1390-1393.*

65. *D. Dubbeldam, C. Galvin, K. Walton, D. Ellis, R. Snurr, Separation and Molecular-Level Segregation of Complex Alkane Mixtures in Metal-Organic Frameworks, J. Am. Chem. Soc., 130 (2008) 10884-10885.*

66. *P. Bárcia, D. Guimarães, P. Mendes, J. Silva, V. Guillerm, H. Chevreau, C.Serre, A. Rodrigues, Reverse Shape Selectivity in the Adsorption of Hexane and Xylene Isomers in MOF UiO-66, Micropor. Mesopor. Mater, 139 (2011) 67-73.*

67. *T. Trung, N. Ramsahye, P. Trens, N. Tanchoux, C.Serre, F. Fajula, G. Férey, Adsorption of C5–C9 hydrocarbons in microporous MOFs MIL-100(Cr) and MIL-101(Cr): A manometric study, Micropor. Mesopor. Mater., 134 (2010) 134-140.*

68. *T. Trung, N. Ramsahye, P. Trens, N. Tanchoux, C.Serre, F. Fajula, G. Férey, Adsorption of C5–C9 hydrocarbons in microporous MOFs MIL-100(Cr) and MIL-101(Cr): A manometric study, Micropor. Mesopor. Mater., 134 (2010) 134-140.*

69. *S. Kim, J. Kim, H. Kim, H. Cho, W. Ahn, Adsorption/catalytic properties of MIL-125 and NH2-MIL-125, Catalysis Today, 204 (2013) 85– 93.*

70. *P. Horcajada, F. Salles, S. Wuttke, T. Devic, D. Heurtaux, G. Maurin, A. Vimont, M. Daturi, O. David et al., How Linker's Modification Controls Swelling Properties of Highly Flexible Iron(III) Dicarboxylates MIL-88,J. Am. Chem. Soc., 133(2011)17839–17847.*

71. *P. Bárcia, D. Guimarães, P. Mendes, J. Silva, V. Guillerm, H. Chevreau, C. Serre, A. Rodrigues, Reverse Shape Selectivity in the Adsorption of Hexane and Xylene Isomers in MOF UiO-66, Micropor. Mesopor. Mater., 139 (2011) 67-73*

72. *D. Peralta, G. Chaplais, A. Simon-Masseron, K. Barthelet, and G. D. Pirngruber, Separation of C6 Paraffins Using Zeolitic Imidazolate Frameworks: Comparison with Zeolite 5A, Ind. Eng. Chem. Res., 51 (2012) 4692–4702.*

73. *J. Stuart, Metal-organic frameworks., Chem. Soc. Rev., 32 (2003) 276–288.*

74. *P. Bárcia, J. Silva, A. E. Rodrigues, Multicomponent Sorption of Hexane Isomers in Zeolite BETA, AIChE Journal, 53(2007)1970-1981.*

75. *P. Mendes, F. Ragon, A. E. Rodrigues, P. Horcajada, C. Serre, J. Silva, Hexane isomers sorption on a functionalized metal–organic framework, Microporous and Mesoporous Materials, 170 (2013) 251–258.*

2.

Breakthrough experiments for screening studies

In this chapter it is described the experimental breakthrough apparatus used to perform screening studies in MOFs, highlighting the methodology applied to measure the breakthrough curves and also how adsorbed amounts and selectivities are calculated. It is also briefly described the principles to model adsorption equilibrium data (when possible) with the simple Langmuir model.

2.1. Gas Chromatography (GC)

Gas Chromatography (GC) is one of the most important techniques for the separation of compounds. It consists on a separation method in which components of a flow stream are split into two phases: one of these phases is a stationary bed with an adsorbent and the other is a mobile phase (an inert carrier gas) which percolates through the stationary bed [1]. In a typical GC analysis, a single or multicomponent mixture is being vaporized and continuously carried by the mobile phase through the column packed with an adsorbent. If a frontal chromatography technique is used we can measure breakthrough curves to determine sorption capacities as well as selectivities for a certain sorbate-sorbent interactions.

There are several chromatographic techniques. Each one supports some specific characteristics that can be classified with a different terminology [1- 3]:

- Chromatographic system: Plan or Column Chromatography;
- Chromatographic bed: Fixed bed, True Moving Bed (TMB);
- Physical state of mobile phase: Gas Chromatography (GC),
- Mobile Phase composition: Isocratic (constant composition) or Gradient (variable composition);
- Physical state of stationary phase: Solid, liquid or chemically linked
- Separation Mechanisms: Adsorption (gas-solid), ion exchange, size-exclusion or affinity;
- Operation mode: Frontal analysis displacement or elution;
- Separation objective: Analytical or Preparative (production/purification).

The technique used for the hexane isomers separation consists more specifically on analytical gas chromatography through frontal analyses by adsorption separation in a fixed bed.

2.1.1. Frontal Analysis

In frontal analysis, the mixture to be separated is continuously injected to the column for the separation of components. The output of the column after a time t corresponds to a front of concentration represented by so called breakthrough curve as exemplified on the Fig. 2.1.

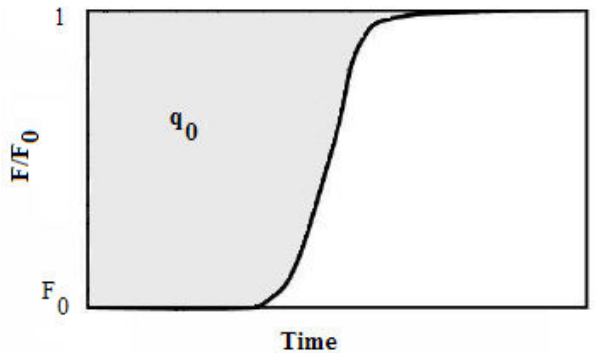

Figure 2.1 - Frontal breakthrough curve.

This chromatographic technic for separation is based in the different affinity between the adsorbent and each component to be separated [4-7]. Depending of the affinity of each component with the adsorbent, the retention time of the components in the column is different [4]. The equation 2.1 displays the relation among the retention time (t_r) in the column and the velocity (u) of the components for to pass in the column with a certain length (L) [6].

$$u = \frac{L}{t_r} \qquad (2.1)$$

The Fig 2.2 shows an example of the mobile phase mass transfer in a packed column, where $t_{r3} > t_{r\,2} > t_{r\,1}$, so, the $u_3 < u_2 < u_1$. The flow rate of the equimolar mixture (1, 2, 3) and carrier gas is constant, so, they arrive to the outlet of the column at different times depending to their affinity [7].

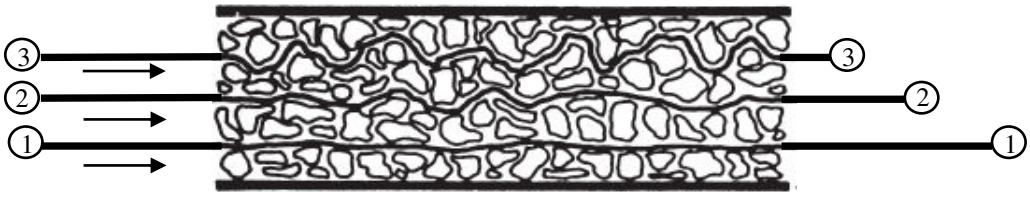

Figure 2.2 - Mobile phase mass transfer in packed columns; $t_{r1} > t_{r\,2} > t_{r\,3}$ [4].

Only the component that goes out first from the column will be isolated from the others due to the mixture of concentrations after the output of the second component resulting of the constant flow rate. Ideally, an excellent separation corresponds to a smaller retention time of the component that needs to be isolated. After that, a mixture of the components is expelled with a different component amount on the composition to the saturation [7]. On the saturation, the composition of each component on the output column is same of the amount injected. This process is described through a chromatogram, designated by breakthrough.

2.2. Experimental Set-up

The single and multicomponent breakthrough experiments were performed in a Gas Chromatograph (GC) SRI model 8610c (Fig. 2.3a) which was adapted specifically for this specific experiments. The mixture to be analysed is introduced by a syringe pump (Fig. 2.3b) in the carrier gas before entering in the column. A heating chamber (evaporator) vaporizes completely the liquid mixture. The adsorption column consists in a 4.6 mm *i.d.* stainless steel column with 100 mm in length containing the adsorbent and placed in the ventilated chromatographic oven (Fig 2.4a), as well as a heated collector with 10 loops (Fig 2.4b) to collect samples at the outlet of the column.

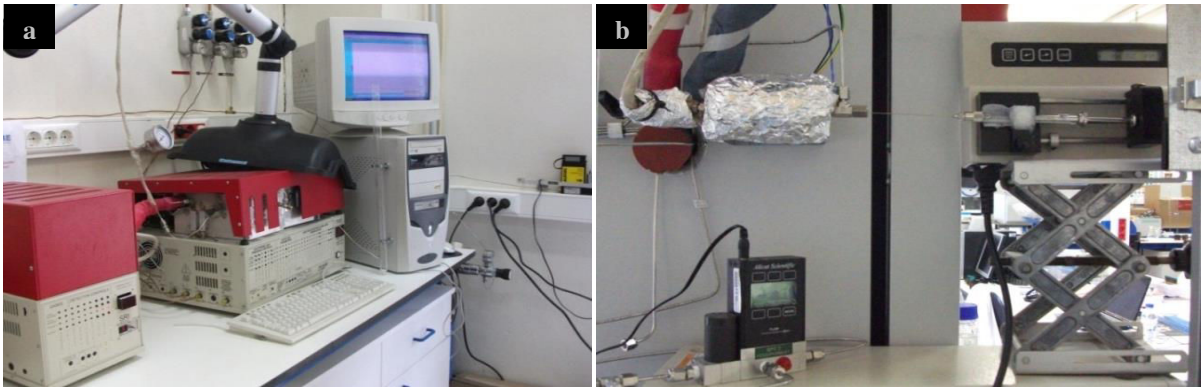

Figure 2.3 - Experimental Gas Chromatography (GC) set-ups for the breakthrough experiments, where is showed the (a) GC equipment [left: SRI model 110, centre: SRI model 8610c with exhaustion of vapours, right: computer] and mass flow controller (MFC), most to the right. (b) Injection and control pressure part [Top left: Injector port connected to the evaporator, Top right: syringe pump; Bottom left: Back Pressure control (BPC)].

The analytical section is composed by a chromatographic column and a flame ionization detector (FID) (Fig 2.4c). Complete information about the experimental setup is reported elsewhere Bárcia *et al.* [8].

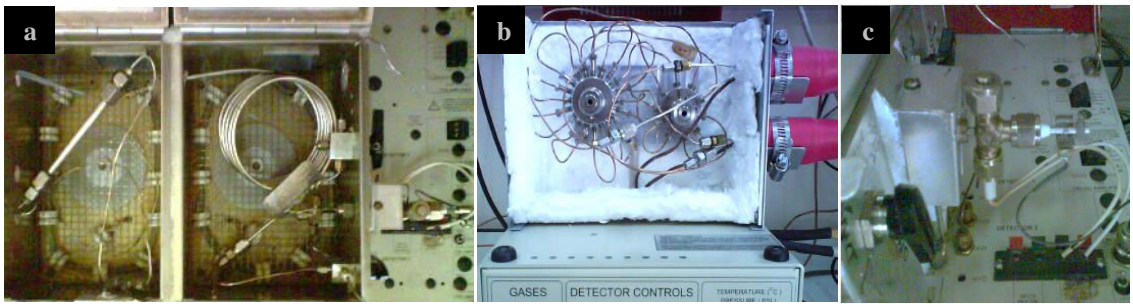

Figure 2.4 - Visualization of the (a) collector with 10 loops, from the equipment SRI model 110; (b) ovens, from the equipment SRI model 8610c [left: stain-less column packed with the MOF, sending the effluent for the sample collector, right: Chromatograph column that receives the samples from the sample collector sending the effluent for the FID detector] (c) Flame ionization detector (FID).

2.3. Adsorption Equilibrium Isotherms

Single and multicomponent adsorption equilibrium isotherms were obtained from breakthrough curves experiments. The breakthrough curves describe the progressive adsorption of the sample on the crystalline material [9, 11]. The adsorption column packed with the MOF under study was operated by introducing continuously a C_6 isomers mixture with known composition in a helium stream at a fixed total pressure. In the case of multicomponent feed mixture, the concentration is continuously measured at the outlet of the packed bed in order to collect samples during the most important part of the breakthrough curve. When the saturation is reached, the composition of each sample loop is evaluated by chromatography in a proper separate column. The FID detects the solute concentration in the column outlet and sends the signal to the computer [12]. In these type of experiments it is necessary to make a relation between the signal (mV) detected by the FID and the physical concentration. The equilibrium loading is the adsorbed amount that is obtained by the integration of the breakthrough curves in each experiment. An example of the procedure is exemplified in Fig. 2.5a for a single component experiment and in Fig. 2.5b for a binary one. The breakthrough signal increases with the increasing of the concentration detected and stabilizes at a constant value on the saturation of the crystal pores.

In the saturation, the pores are totally filled and the composition at the inlet and outlet of the column is the same concentration, so the molar flow introduced (F_0) is the same as the outlet molar flow (F), then F/F_0 =1. In the single component experiment the number of moles retained in the bed is simply the *Area A*.

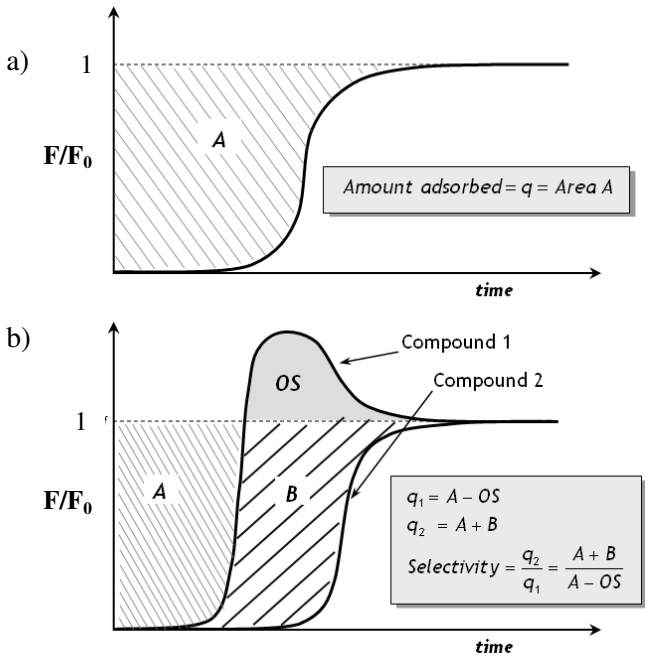

Figure 2.5 - Schematic representation of experimental breakthroughs (a) mono component and (b) multicomponent [8].

For a binary experiment the number of moles of compound 1 retained in the bed is equal to the *Area A* minus the roll-up *Area OS*. For the compound 2, the number of moles retained in the bed is equal to *Area A* plus *Area B*. The amount adsorbed of each compound is then calculated by the following relations:

$$q_1 = Area\ A - Area\ OS \qquad (2.2)$$

$$q_2 = Area\ A + Area\ B \qquad (2.3)$$

Through the subtraction of the area under the curves to the total area (Fn.tn) is obtained the adsorption area (A, OS and B). The area under the curve is calculated using of the trapezoidal rule. The equation 2.4 shows the mathematical procedure for the calculation of the amount adsorbed of each component from the trapezoidal rule,

$$A_{q_0} = F_n\ x\ t_n - \sum_{i=0}^{n} \left(\frac{(F_{i+1} + F_i) \times (t_{i+1} - t_i)}{2} \right) \qquad i = 0, n \qquad (2.4)$$

where A_{qo} (mol) is the amount adsorbed, F_i (mol.min^{-1}) is the molar flow rate; t (min) is the time, i is the increment that determine the time position from t_0 until t_n.

The amount adsorbed per unit mass of adsorbent q_0 (g.100g$_{ads}^{-1}$) can be calculated from the following equation:

$$q_0\left(\frac{g}{100g_{ads}}\right) = \frac{A_{q_0} \times M_{comp}}{m_{ads} \times 100} \qquad (2.5)$$

where M_{comp} (g.mol^{-1}) is the molecular mass for the component under study; m_{ads} (g) is the adsorbent mass packed into the column.

In the case of an equimolar mixture the selectivity (α), is given by the ratio between the amounts adsorbed of the two species as follows:

$$\alpha = \frac{q_2}{q_1} = \frac{Area\ A + Area\ B}{Area\ A - Area\ OS} \qquad (2.6)$$

where component 1 is the less adsorbed component.

2.3.1. Modelling adsorption equilibrium

2.3.1.1. Pure component isotherms

To represent a Type I isotherm the simplest model is the Langmuir isotherm [7, 9, 10]. It is based on localized adsorption in a homogeneous surface. The adsorption isotherm is:

$$\varphi = \frac{q}{q_{\max}} = \frac{Kp}{1 + Kp} \qquad (2.7)$$

where φ is the fractional loading coverage, q (g.100g^{-1}) is the loading, p (atm) is the pressure of sorbate, K (atm^{-1}) is the adsorption equilibrium constant and q_{max} (g.100g^{-1}) is the maximum monolayer capacity.

The best way to examine the validity of Langmuir isotherm is to plot $\varphi/(1-\varphi)p$ versus φ. If the model is valid a horizontal line is found. To give thermodynamic consistency the parameter q_{max} is supposed to be a constant independent of temperature. The adsorption equilibrium constant K should also follow a Van't Hoff equation [9]:

$$K = K_0 \cdot e^{\left(\frac{-\Delta H}{RT}\right)} \qquad (2.8)$$

where K_0 (atm^{-1}) is the factor of affinity constant, ΔH ($J.mol^{-1}$) is the enthalpy of sorption, R ($J.\ mol^{-1}.K^{-1}$.) is the universal gas constant and T (K) is the temperature.

2.3.1.2. Multicomponent adsorption isotherms

Using the parameters given by the single component adsorption equilibrium fitting, the mixture sorption data can be predicted by an extended Langmuir model [9]. Accordingly, the amount adsorbed of component i, q_i, in a mixture is given by,

$$q_i = q_{\max\, i} \cdot \frac{K_i p_i}{1 + \sum_{k=1}^{n} K_k \cdot p_k} \qquad (2.9)$$

where n is the number of components in the mixture.

The selectivity for an equimolar system with the same q_{max} described by the extended Langmuir model is simply the ratio of the adsorption equilibrium constants,

$$\alpha_{1,2} = \frac{K_1}{K_2} \qquad (2.10)$$

where $\alpha_{1,2}$ is the selectivity between components 1 and 2.

The selectivity can also be expressed through the ratio of the adsorbed amount of the components,

$$\alpha_{1,2} = \frac{q_1}{q_2} \qquad (2.11)$$

where 2 is the component less adsorbed.

2.4. Conclusions

The main potential applications of MOFs are catalysis, gas storage and streams purification/separation. An important example of separation in the petrochemical industry is the separation of hexane isomers, which is the main objective of this Ph. D. thesis. For the screening studies of hexane isomers in the new synthesized MOFs Gas Breakthrough curves are measured to determinate the selectivity between the compounds and respective adsorbed amounts. This analytical technique uses Frontal analysis by adsorption separation in a fixed bed with a hybrid adsorbent. A constant flow of an equimolar mixture of hexane isomers is fed in the system that passes in the fixed bed for adsorption separation. Breakthrough curves are measured and the adsorbed amount of each component obtained by the curves integration. An important parameter is the MOF selectivity that indicates their capacity of separation between components.

2.5. References

1. *H. McNair, J. Miller, Basic Gas Chromatography, 2nd ed., Wiley, USA, 2009.*

2. *E. Heftmann, Cromatography, fundamentals and applications of chromatography and related differential migration methods, 6th ed, Elsevier, 2004.*

3. *W. M. A. Niessen, Current Practise of Gas Chromatography- Mass Spectrometry, Marcel Dekker, Inc., 2001.*

4. *J. Keller, R. Staudt, Gas Adsorption Equilibria Experimental methods and Adsorption Isotherms, Springer , Germany, 2005.*

5. *R . P.W. Scott, Introduction to Analytical Gas Chromatography, 2nd ed, ;Marcel Dekker, Inc., 1998.*

6. S. Ahuja, Chromatography and Separation Science, Elsevier Science, 2003

7. R. M.A. Roque-Malherbe, Adsorption and Diffusion in Nanoporous Material, Taylor & Francis Group, 2007.

8. *P. Bárcia, J. Silva, A. E. Rodrigues, Separation by Fixed-Bed Adsorption of Hexane Isomers in Zeolite BETA Pellets, Ind. Eng. Chem. Res, 45 (2006), 4316-4328.*

9. *D. Do, Adsorption analysis: Equilibria and Kinetics, ICP, Australia, 1998.*

10. D. M. Ruthven, Principles of Adsorption & Adsorption Processes, Jonh Wiley & Sons, 1984.

11. S. G. Greg, K. S. W. Sing, Adsorption, Surface Area and Porosity, Academic Press Inc, 1982.

12. J. Cazes, Analytical Instrumentation Handbook, 3rd Ed, 2004.

3.

Hexane Isomers Sorption on Functionalized UiO-66(Zr) MOFs

This chapter shows a series of microporous Zr-MOFs with the UiO-66(Zr) structure type based on terephthalate ligands bearing Br, NH_2 or NO_2 groups. These functionalized solids UiO-66(Zr) have been synthesized at the multi-gram scale *via* a simple atmospheric pressure route with the final aim of investigating the influence of functionalization on the separation of hexane isomers (22DMB, 23DMB, 3MP and *n*HEX). The separation studies were performed in a fixed bed adsorption column with a quaternary equimolar mixture at temperatures between 343 and 423 K and partial pressures up to 10 kPa. Interestingly, UiO-66 Br, NO_2 and NH_2 forms exhibit an important uptake reaching 15 wt%, being the sorption selectivity hierarchy comparable to the bared UiO-66(Zr) solid: 22DMB > 23DMB > 3MP > *n*HEX. This chapter is based on the publications with the references [1, 2].

3.1. Introduction

Design of specific porous structures with improved performances in adsorption separation processes and catalysis is a challenging goal of current solid state chemistry. Another interesting feature of MOFs concerns the easy way to modulate their physic-chemical properties by incorporating different functional groups on the organic linkers [3-7], offering a highly adaptable system to solve specific separation problems [8, 9]. The effect of the functionalization on the adsorption process has been recently evaluated through i) the adsorption of linear alkanes on a series of functionalized flexible microporous iron(III) terephthalates MIL-53(Fe)–X (MIL stands for Material of Institut Lavoisier; X = CH_3, Cl, Br, NH_2) [9], and ii) the natural and biogas upgrading using the mesoporous aluminium amino-terephthalate MIL-101(Al) [10]. Furthermore, a quantitative structure–activity relationship (QSAR) has evidenced the strong impact of the functionalization of a series of functionalized flexible iron(III) terephthalates MIL-88(Fe) on the adsorption of a therapeutic molecule (caffeine), paving the way for the prediction of adsorption processes as a function of the functionalization of a given MOF [11]. Concerning hexane isomers porous MOFs have been also proposed to improve the separation of hexane isomers and thus, increase the RON number. In this sense, we have reported the use of the highly thermally and mechanically stable (T ~ 623–673 K or P ~ 10.000 $kg.cm^{-2}$) porous cubic zirconium terephthalate UiO-66 (UiO for University of Oslo; Zr_6O_4 $(OH)_4(C_6H_4(CO_2)_2)_6.nH_2O$) [12] for the separation of hexane isomers mixtures:*n*-hexane (*n*HEX), 3-methylpentane (3MP), 2,3-dimethylbutane (23DMB), 2,2dimethylbutane (22DMB). The crystalline cubic structure of UiO-66 possesses an important porosity (S_{BET} > 1100 $m^2.g^{-1}$) associated to tetrahedral (~8 Å) and octahedral cavities (~11 Å) accessible through microporous triangular windows (5–7 Å).

Remarkably, UiO-66 exhibited an opposite sorption hierarchy (22DMB > 23DMB > 3MP > *n*HEX) to the one observed in conventional adsorbents [1], with selectivity values reaching 4 for the ratio 22DMB/*n*HEX. This reverse shape selectivity might be attributed to the rotational freedom of the molecules within the small cages [1]. Hexane isomers adsorption might be modified by adjusting the dimensions of the windows through the introduction of different functional groups in substitution to one of the protons of the aromatic ring of the

terephthalate linker, as already reported for the CO_2 adsorption over gases such as CH_4 and N_2 [13]. In this latter case, a selectivity increase was observed, being tentatively attributed to both the steric hindrance of the functional group and the significant reduction of the ability to rotate of the aromatic ring as a consequence of the interaction between the functional group and the metal (*i.e.* NH_2 group) [14].

Therefore, we report in this chapter the effect of the functionalization of the UiO-66 architecture on the separation of hexane isomers by adsorption. To that purpose, three porous UiO-66 materials built up from terephthalate linkers bearing –Br, $–NH_2$, or $–NO_2$ groups were synthesized at the multi-gram lab-scale under atmospheric pressure. These functionalized UiO-66(Zr) solids were fully characterized by X-ray powder diffraction (XRPD), Fourier transform infrared spectroscopy (FTIR), Thermogravimetric Analysis (TGA), Dynamic Light Scattering (DLS) and nitrogen adsorption measurement. The potential of separation of the hexane isomers has been then assessed on the UiO-66(–Br, $–NH_2$, $–NO_2$) materials by performing several screening studies in a breakthrough apparatus, investigating the effect of temperature and partial pressure.

3.2. Structure of UiO-66(Zr)

The zirconium (IV) terephthalate UiO-66(Zr) (UiO for University of Oslo) [12] is a three-dimensional cubic close packed structure (Fm-3m (225); a = 20.7004 Å, V= 8870.3 A^3) built up from $Zr_6(O)_4(OH)_4$ oxoclusters linked together by twelve terephthalate linkers (Fig. 3.1).

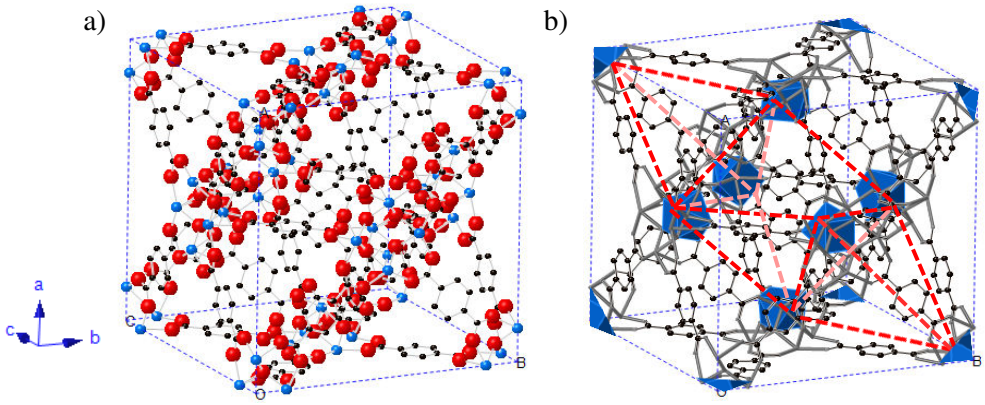

Figure 3.1 - Unit cell of the UiO-66(Zr) on the set view direction [-0.472, 0.747, 1.49] in their form: (a) ball & stick and (b) polyhedral. Zirconium (blue), oxygen (red), carbon (black); hydrogen atoms have been omitted for clarity.

The UiO-66(Zr) solid exhibits tetrahedral and octahedral cages of 6 Å and 11 Å, respectively, accessible through microporous windows (5-7 Å) (Fig. 3.2), leading to a high porosity (BET surface area ~ 1200 $m^2.g^{-1}$, pore volume ~ 0.47 $cm^3.g^{-1}$) combined with a high thermal (up to 723 K under air), chemical (hydrothermal, organic solvents, acidic conditions) and mechanical stability (up to 10000 $kg.cm^{-2}$) [12, 15, 16]. Due to these interesting properties, the UiO-66(Zr) solid has been proposed as a promising candidate in adsorption [17].

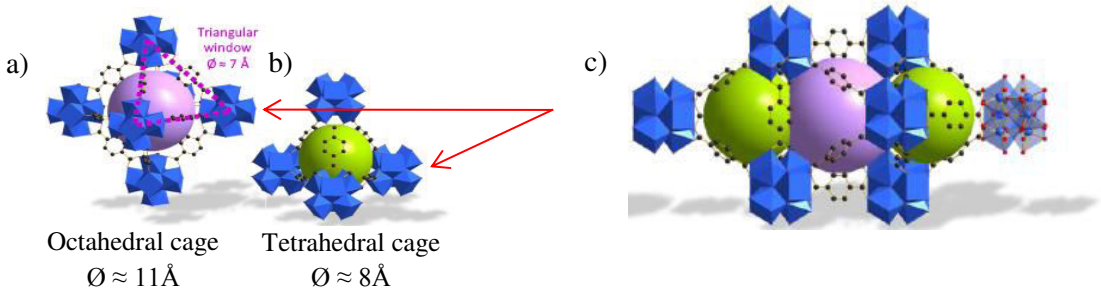

Figure 3.2 - (a) The super octahedron cage; (b) The super tetrahedron cage; (c) The combination of the octahedron and two tetrahedron cages that represent the UiO-66(Zr) structure [1]. Different spaces of molecules adsorption is represented through purple and green spheres, respectively. Zirconium (blue), oxygen (red), carbon (black); hydrogen atoms have been omitted for clarity.

The textural and physicochemical properties of the UiO-66(Zr) solid can be easily tuned by using either functionalized terephthalate linkers (NH_2, Br, NO_2, *etc.*) or extended organic polycarboxylate ligands [6, 18]. As mentioned previously, the adsorption might be modified through the introduction of different functional groups on the aromatic ring of the terephthalate linker due to both the steric hindrance of the functional group and the reduction of the rotation ability of the aromatic ring [14]. Furthermore, the size of the UiO-66(Zr) crystals can be synthetically controlled by simply changing the zirconium precursor ($ZrCl_4$ *vs.* $ZrOC_{l2}.8H_2O$) from the micro to nanometric scale, respectively. The effect of the functionalization as well as the particle size of the UiO-66(Zr) on the separation of hexane isomers by adsorption have been evaluated and deeply described on the section 3.3.

3.3. Previous Studies

3.3.1. Micrometric UiO-66(Zr)

Elaborated separation studies was previously developed by Dr. Patrick Bárcia [1] using UiO-66(Zr) microparticles at LSRE/IPB through a quaternary equimolar mixture of n-hexane

(*n*HEX), 3-methylpentane (3MP), 2,2-dimethylbutane (22DMB) and 2,3-dimethylbutane (23DMB) [1]. The breakthrough experiments of hexane isomers adsorption on the UiO-66(Zr) indicated that the branched C_6 are more adsorbed compared to their linear isomers, showing reverse shape selectivity: 22DMB > 23DMB > 3MP > *n*HEX. Note that this behaviour totally differs from the conventional adsorbents, in which the linear isomers are more retained than the branched ones. Thus, hexane isomers with higher branching degree (22DMB and 23DMB) were more adsorbed on the UiO-66 solid, being this performance very interesting for the hexane isomers separation and then, for the enrichment of the gasoline.

The less retained molecule is the *n*HEX whatever the ranges of studied temperature and pressure. This performance was attributed to shape selectivity [1]; similarly to the MCM-22 material, in which the inverse shapes selectivity, is due to differences in rotational freedom in the pockets of the super cage. For the rotational freedom, it is important to consider the reported molecular lengths of the *n*HEX (9.1 Å), 3MP (8.6 Å) and 22DMB (6.7 Å) [17]. Linear and mono branched isomers exhibit larger molecular lengths than the internal diameter of the tetrahedral cages, so, these isomers are exclusively adsorbed within the large octahedral cage, being the less retained molecules [1].

In contrast, the lengths of the bulkier di-branched hexane isomers are short enough to allow their free rotation inside the small cages, supporting their preferential adsorption. Regarding the separation of mono-/di-branched isomers, the general trend is that the selectivity slightly increases with the temperature partial pressure. In addition, UiO-66(Zr) shows selectivity between SMP/22DMB ($S_{3MP/22DMB}$) significantly lower than zeolite beta [19]. For instance, at 473 K and a partial pressure of 6.3 kPa, the 22DMB/3MP selectivity was 1.5 and 2.7 for respectively UiO-66 and zeolite beta. Thus, unlike zeolite beta, the UiO-66 does not made a significant discrimination between di-branched C_6 isomers However, the adsorbed amount in the UiO-66(Zr) at 343 K and 6.2 kPa are around 11 %wt, while for the zeolite Beta the maximum value for quaternary experiences was around 2.5 %wt at 423 K and 6 kPa.

3.3.2. Nanometric UiO-66(Zr) (FR55)

UiO-66(Zr) (FR55) was synthesized at the nanoscale by Dr. Florence Ragon at the ILV whereas the screening studies were performed at the LSRE- IPB. Prior to the separation tests,

the solid was activated by heating at 473 K under vacuum (10 kPa) for 15 hours. 363 mg of the powder nanometric UiO-66(Zr) was packed in a stainless steel column (diameter = 4.3 mm, length = 80 mm). The screening studies were performed with a quaternary equimolar mixture (*n*HEX, 3MP, 23DMB, 22DMB) at two temperatures (343 and 423 K) and two partial pressures: low (0.6 kPa) and high pressure (6 kPa). The experimental conditions and the amounts adsorbed for each run are displayed in Table 3.1.

Table 3.1 - Experimental conditions and amounts adsorbed of the hexane isomers in UiO-66(Zr) nano.

Run	*T* (K)	Helium flow rate (ml(STP).min^{-1})	Mixture pressure (kPa)	m_{ads} (mg)	Partial loading (g.100g$_{ads}^{-1}$)				Total loading (g.100g$_{ads}^{-1}$)
					22DMB	23DMB	3MP	*n*HEX	
Uio66nano_a1	343	46.3	0.6	363	1.36	1.13	1.21	0.99	4.69
Uio66nano_a2	423				0.25	0.23	0.11	0.04	0.64
Uio66nano_b1	343	13.9	6		1.63	1.32	1.60	1.56	6.10
Uio66nano_b2	423				1.25	1.15	1.13	1.12	4.66

Some significant differences can be observed concerning the total adsorbed amount between the UiO-66(Zr) micro and nanoparticles. Under similar conditions (at 342K and P_{mix} = 6 kPa) the maximum adsorbed amount in the micrometric UiO-66(Zr) is 11 wt% against 6 wt% in the nanometric UiO-66(Zr). This difference can be related with the slightly lower porosity of the nanometric UiO-66(Zr).

The Table 3.2 shows the hexane isomers selectivity of each run for the UiO-66(Zr) nanoparticles. Good selectivities are found at 423 K and 0.6 kPa for the hexane isomers 22DMB, 23DMB and 3MP relatively to the less adsorbed hexane isomer, *n*HEX.

Table 3.2 - Sorption hexane isomers selectivity on the MOF UiO-66(Zr) nano.

Run	*T* (K)	Mixture pressure (kPa)	Selectivities		
			22DMB/ *n*HEX	23DMB/ *n*HEX	3MP/ *n*HEX
Uio66nano_a1	343	0.6	1.4	1.1	1.2
Uio66nano_a2	423		6.3	5.8	2.7
Uio66nano_b1	343	6	1.1	0.9	1.0
Uio66nano_b2	423		1.1	1.0	1.0

The maximum selectivity value *n*HEX/di-branched isomers obtained using the nanometric UiO-66(Zr) at low pressure and 423 K was higher than that reported for the UiO-66(Zr) microparticles at low pressure and 373 K (6.3 vs. 5.2, respectively). Although the values of

adsorption and selectivity are quite similar for both nano and micrometric UiO-66(Zr), the nanometric version seems to offer slightly better results.

3.3.3. Breakthroughs comparison of nano and micrometric UiO-66(Zr)

In order to compare the separation performances of UiO-66(Zr) nano and microparticles, a similar study of the previously done by Dr. Patrick Barcia *et al.* [1] was carried out at LSRE using two different temperatures and pressures: 343 K or 423 K and 6 kPa or 0.6 kPa. As shown in Fig. 3.3, the breakthroughs obtained for both nano and micrometric versions are similar for the same temperature and partial pressure conditions.

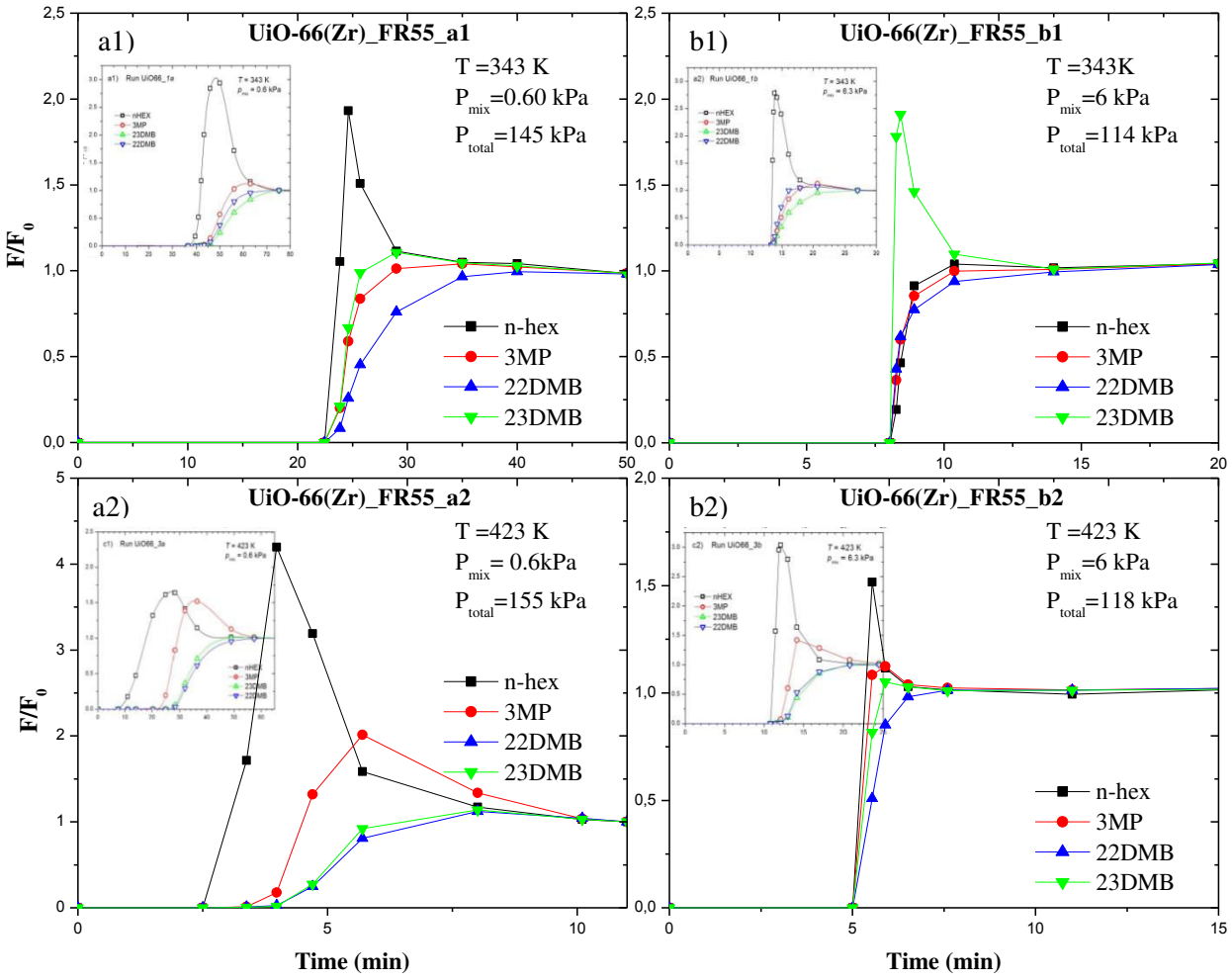

Figure 3.3 - Experimental breakthrough curves for sorption of hexane isomers in bigger form (UiO-66(Zr) nano, FR55) and the litle form (UiO-66(Zr) micro, experimental data Barcia *et al.* [1]; where (a1) pp = 0.6 kPa, T = 343 K; (b1) pp = 6 kPa, T = 343 K; (a2) pp = 0.6 kPa, T = 423 K (b2) pp = 6 kPa, T = 423 K.

The sorption hierarchy is predominantly 22DMB > 23DMB > 3MP > *n*HEX (see Fig. 3.3 a2 and b2). An important overshoot of the *n*HEX adsorption was evidenced in almost all the breakthrough curves, indicating a significant difference in the sorption affinity compared to its branched isomers. A slight change is remarked on the sorption hierarchy of exclusively the UiO-66(Zr) nano at high pressure (6 kPa) and lower temperature (343 K): 22DMB > 23DMB > 3MP > *n*HEX (Fig. 3.3b1).

3.4. Experimental Section

3.4.1. Synthesis of functionalized UiO-66 (Zr) nanoparticles

As mentioned in the introduction part, our main goal is to adjust the dimensions of the accessible windows of the UiO-66(Zr) to the hexane isomers *via* the introduction of different functional groups on the aromatic ring. The UiO-66(Zr) functionalization was previously reported by *in situ* methods using functionalized linkers during the synthesis [6] or by post-synthetic modification [18] using the preformed UiO-66(Zr). Kandiah *et al.* has reported the direct synthesis of modified UiO-66 solids based on the terephthalate derivatives bearing –NH_2, –NO_2 and –Br groups, using the $ZrCl_4$ as metal precursor and the solvothermal route [6].

Considering the interesting results obtained with the UiO-66(Zr) nano or microparticles, three functionalized nanometric UiO-66(Zr) solids based on the –Br, –NH_2, –NO_2 terephthalate derivatives were prepared using the cheaper and safer gram-scale route at ambient pressure starting from the $ZrOCl_2.8H_2O$ precursor (UiO-66(Zr)–NH_2, UiO-66(Zr)–NO_2 and UiO-66(Zr)–Br). Fig. 3.4 represents the three-dimensional schematic view of one octahedral and one tetrahedral cage, as well as the possible position of the grafted functional group [2].

Thus, the substitution of one of the protons of the aromatic ring of the terephthalate ligands can clearly modify the windows accessibility, leading to different adsorptive performances. These materials were synthesized at the multi-gram scale and fully characterized at the ILV.

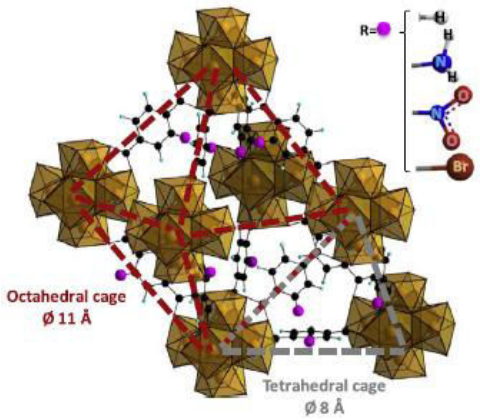

Figure 3.4 - Schematic illustration of one octahedral (red dotted line) and one tetrahedral cage (grew dotted line) of the modified UiO-66(Zr) structure. The purple sphere represents the possible position of the grafted functional group on the benzene ring. Zirconium polyhedral (brownish-yellow), oxygen (red), carbon (black) and hydrogen (light green).

3.4.1.1. UiO-66(Zr)–Br

Zirconium 2-bromoterephthalate or UiO-66(Zr)–Br ($Zr_6O_4(OH)_4(C_6H_3Br(CO_2)_2)_6 \cdot nH_2O$) was synthesized starting from a solution of 6.10 g of 2- bromoterephthalic acid (Br-BDC; 24.89 mmol; Aldrich, 99 %) and 8.15 g of zirconium oxychloride octahydrate ($ZrOCl_2.8H_2O$; 25.29 mmol; Alfa Aesar, 98 %) in 63 mL of N,N dimethylformamide (DMF; 814.11 mmol; Carlo Erba, 99.7 %) in a round bottom flask. Then, 4 mL of 12 M hydrochloric acid solution (HCl; 48 mmol) were added to the previous solution. The final solution was stirred for 15 min and heated under reflux for 24 h (Fig. 3.5a). The final product was filtered and dried at room temperature resulting in a white viscous solid. The amount of obtained as-synthesized solid was 7.90 g.

For their activation, the previously obtained solid was first suspended overnight in 500 mL of DMF (Carlo Erba, 99.7 %) under vigorous stirring in order to remove the free remaining 2-bromoterephthalic acid (this procedure was repeated five times). A second exchange was carried out in 500 mL of methanol (MeOH, Aldrich, 99 %) in order to replace the DMF within the pores (this step was repeated three times). Fig. 3.5 shows the as-synthetized (b) and after activation product (c). The obtained weight of activated UiO-66(Zr)–Br solid was 6.50 g, corresponding to a yield of 92 %.

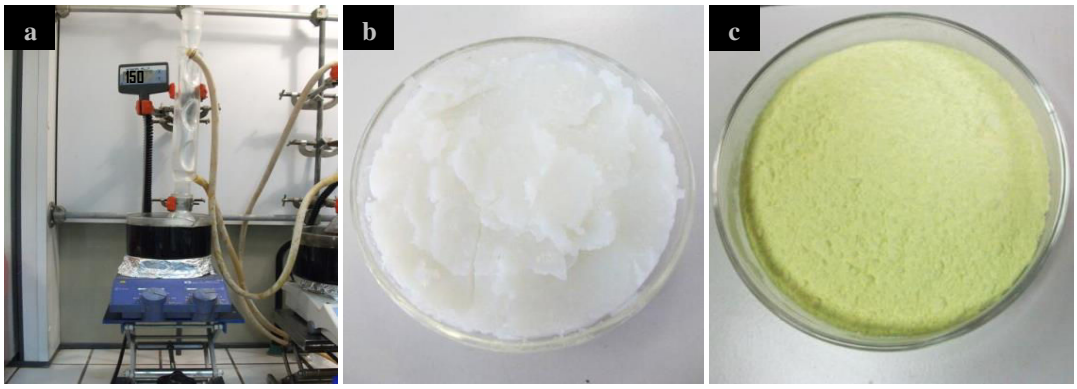

Figure 3.5 - (a) Experimental set-up used for UiO-66(Zr)–Br synthesis; (b) Viscous sample of UiO-66(Zr)–Br as-synthesized (c) Final product after activation.

3.4.1.2. UiO-66(Zr)–NO_2

Zirconium 2-nitroterephthalate or UiO-66(Zr)–NO_2 ($Zr_6O_4(OH)_4(C_6H_3NO_2(CO_2)_2)_6$ $n H_2O$) was also synthesized at room pressure using a round bottom flask. After the complete dissolution of 1.69 g of 2-nitroterephthalic acid (NO_2-BDC; 8 mmol; Aldrich, 99 %) in 8.67 mL of DMF (112 mmol; Carlo Erba, 99.7 %), 1.69 g of $ZrOCl_2.{}_8H_2O$ (8 mmol; Alfa Aesar, 98%) and 1.33 mL of 12 M HCl (15.96 mmol) were added. The mixture was stirred in a round bottom flask under reflux for 24 h (Fig. 3.6a). After filtration, 2.50 g of material were recovered (Fig. 3.6b).

Figure 3.6 - (a) Experimental set-up used for UiO-66(Zr)–NO_2 synthesis; (b) Sample of UiO-66(Zr)–NO_2 as-synthesized (c) Final product after activation.

A similar washing procedure than for the UiO-66(Zr)–Br was applied to UiO-66(Zr)–NO_2. In this case, washing three times with 500 mL of DMF (Carlo Erba, 99.7 %) and three times in 500 mL of MeOH (Aldrich, 99 %). The obtained amount of activated UiO-66(Zr)–NO_2 was 1.50 g, which corresponds to a yield of 58 % (Fig. 3.6c).

3.4.1.3. UiO-66(Zr)–NH_2

Zirconium 2-aminoterephthalate or UiO-66(Zr)–NH_2 ($Zr_6O_4(OH)_4(C_6H_3NH_2(CO_2)_2)_6.nH_2O$) was synthesized at atmospheric pressure, similar to the Br or NO_2 analogues. After the dissolution of 7.24 g of 2-aminoterephthalic acid (NH_2-BDC; 40.2 mmol; Alfa Aesar, 98 %) in 100 mL of DMF (1.29 mol; Carlo Erba, 99.7 %), 12.9 g of $ZrOCl_2.8H_2O$ (40 mmol; Alfa Aesar, 98%) and 6.4 mL of 12 M HCl (76 mmol) were added. The mixture was placed in a round bottom flask under mechanical stirring and reflux for 24 h (Fig. 3.7a).

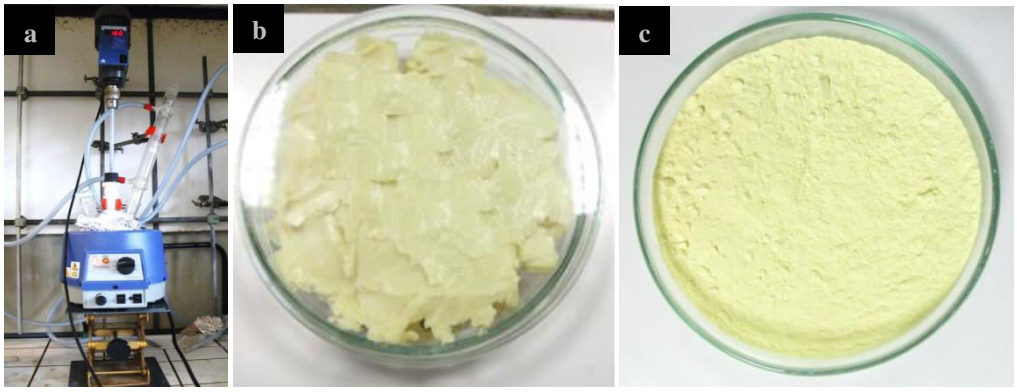

Figure 3.7 - (a) Experimental set-up for the synthesis of UIO-66(Zr)–NH_2 with mechanical stirring and heating (≈ 150 °C) with reflux; (b) Viscous and yellow final product as-synthesized; (c) Yellow final powder, after activation.

Thereafter, the final product was filtered resulting in a yellow viscous material. The amount of obtained solid was 11.6 g (Fig 3.7b).Similar washing procedure to the previous one used to UiO-66(Zr)–NO_2 was carried out for activating the UiO-66(Zr)–NH_2 solid. Thus, two washes with 500 mL of DMF followed by three washes with MeOH were required. 10.2 g of the activated UiO-66(Zr)–NH_2 were obtained, corresponding to a yield of 73% (Fig 3.7c).

3.4.2. Characterization of the functionalized UiO-66(Zr)

UiO-66(Zr) solids were fully characterized by X-Ray Powder Diffraction (XRPD), N_2 adsorption porosimetry, Dynamic Light Scattering (DLS) Infrared Spectroscopy (IR) and Thermogravimetric Analysis (TGA).

3.4.2.1. X-Ray Powder Diffraction (XRPD) analyses

UiO-66(Zr)–Br

Fig. 3.8 shows the x-ray powder diffraction patterns of the as-synthesized (red) and activated (blue) UiO-66(Zr)–Br and the reported theoretical UiO-66 pattern (black). It is clear from the figure that the sample synthesized corresponds to UiO-66(Zr). The peak broadening of UiO-66 (Zr)–Br synthesized from the atmospheric pressure conditions in comparison to the one synthesized by the solvothermal route are in agreement with a small crystal size (see Table 3.3, section 3.4.2.3).

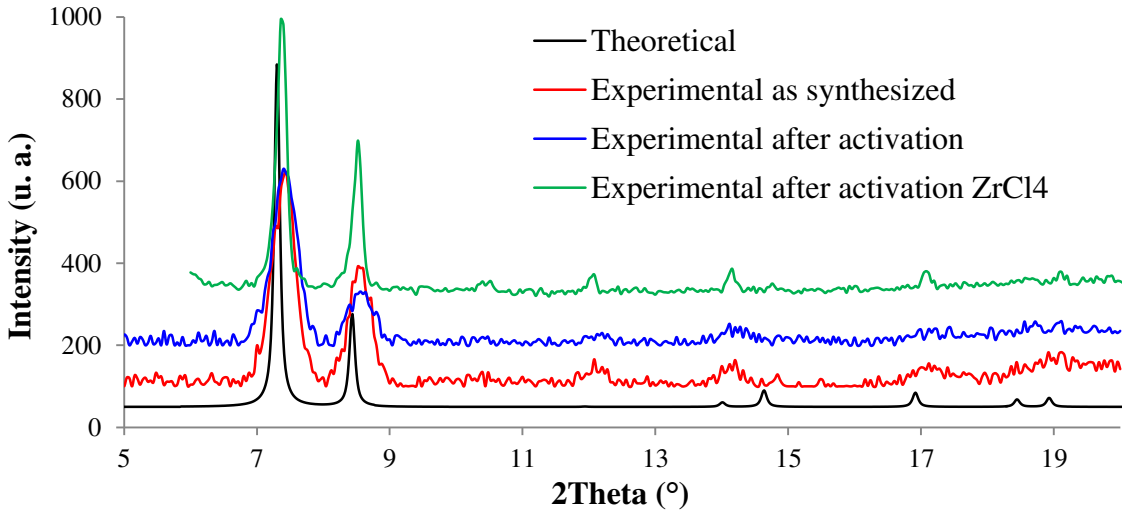

Figure 3.8 - XRPD of the reported theoretical UiO-66 pattern (black) and the as-synthesized (red) and activated (blue) UiO-66(Zr)–Br using a Siemens diffractometer D5000 (Cu Kalpha1 radiation λ= 1.54056 Å). XRPD pattern of the UiO-66(Zr)–Br (green) solvothermally synthesized from the $ZrCl_4$ precursor has been included with comparative purposes.

UiO-66(Zr)–NO_2

XRPD patterns of the sample of the as-synthesized (red) and after activation (blue) UiO-66(Zr)–NO_2 are shown on the Fig. 3.9 in comparison with the reported theoretical UiO-66(Zr) pattern (black). The peak broadening of UiO-66(Zr)–NO_2 synthesized from the atmospheric pressure conditions in comparison to the one synthesized using the solvothermal route are in agreement with the smaller crystal size (see Table 3.3, section 3.4.2.3).

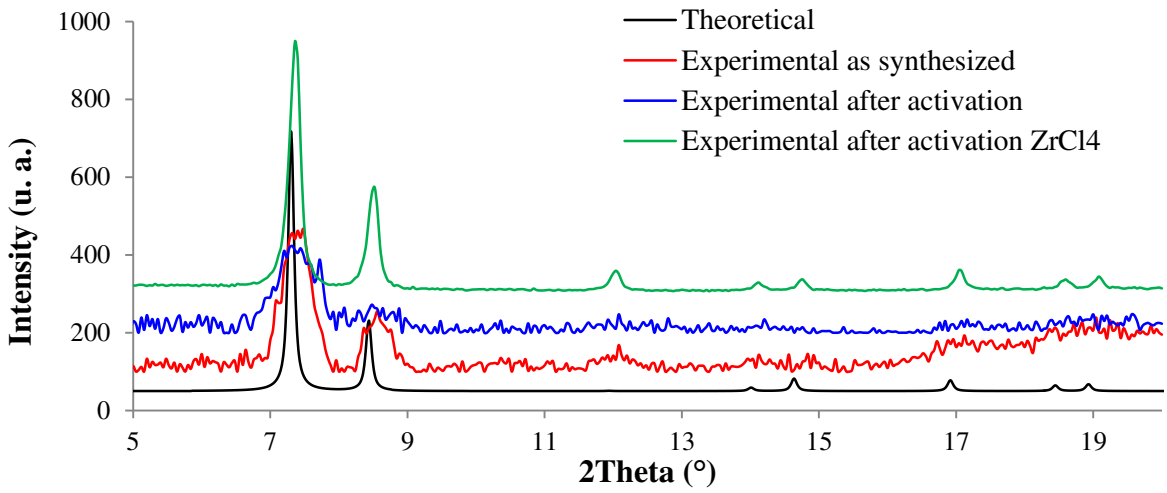

Figure 3.9 - XRPD of the reported theoretical UiO-66(Zr) pattern (black) and the as-synthesized (red) and activated (blue) UiO-66(Zr)–NO_2 using a Siemens diffractometer D5000 (Cu Kalpha1 radiation λ = 1.54056 Å). XRPD pattern of the UiO-66(Zr)–NO_2 (green) solvothermally synthesized from the $ZrCl_4$ precursor has been included with comparative purposes.

UiO-66(Zr)–NH_2

Fig. 3.10 shows the XRPD patterns of the as-synthesized (red) and after activation UiO-66(Zr)–NH_2 (blue) in comparison with the reported theoretical UiO-66(Zr) (black). The UiO-66(Zr)–NH_2 synthesized from the atmospheric pressure conditions shows a peak broadening more important than the one synthesized by the solvothermal route, indicating a smaller particle size (see Table 3.3, section 3.4.2.3).

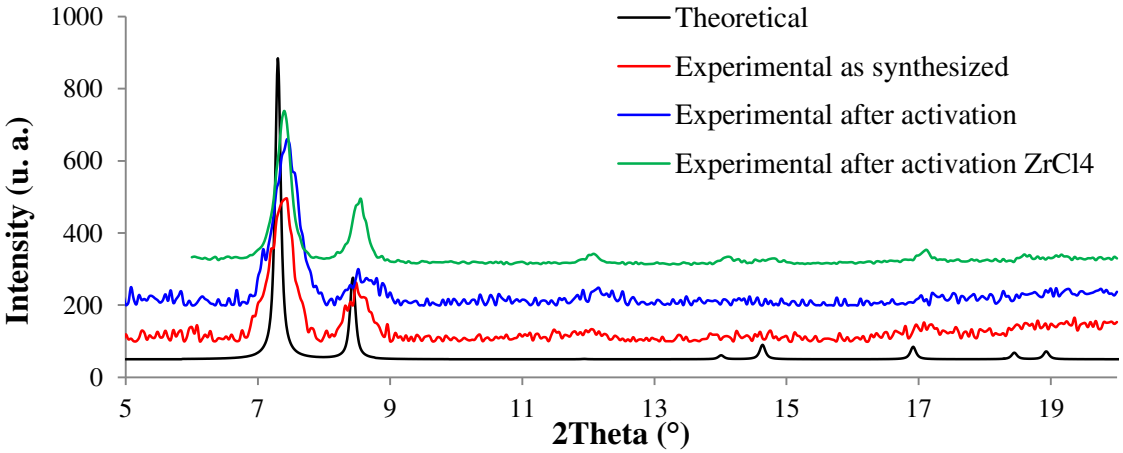

Figure 3.10 - XRPD of the reported theoretical UiO-66 pattern (black) and the as-synthesized (red) and activated (blue) UiO-66(Zr)–NH_2 using a Siemens diffractometer D5000 (Cu Kalpha1 radiation λ= 1.54056 Å). XRPD pattern of the UiO-66(Zr)–NH_2 (green) solvothermally synthesized from the $ZrCl_4$ precursor has been included with comparative purposes.

3.4.2.2. Infra-Red (IR) spectroscopy analyses

UiO-66(Zr)–Br

Fig. 3.11 displays the IR diffractogram of the as-synthesized (red) and after activation UiO-66(Zr)–Br (black). Vibrational bands around 1662 and 1715 cm^{-1} in the as-synthesized solid indicate the presence of remaining DMF and free ligand, respectively. After activation, both bands disappear, indicating the complete activation of the solid. Characteristic bands of carboxylates are visible at around 1450 and 1550 cm^{-1}.

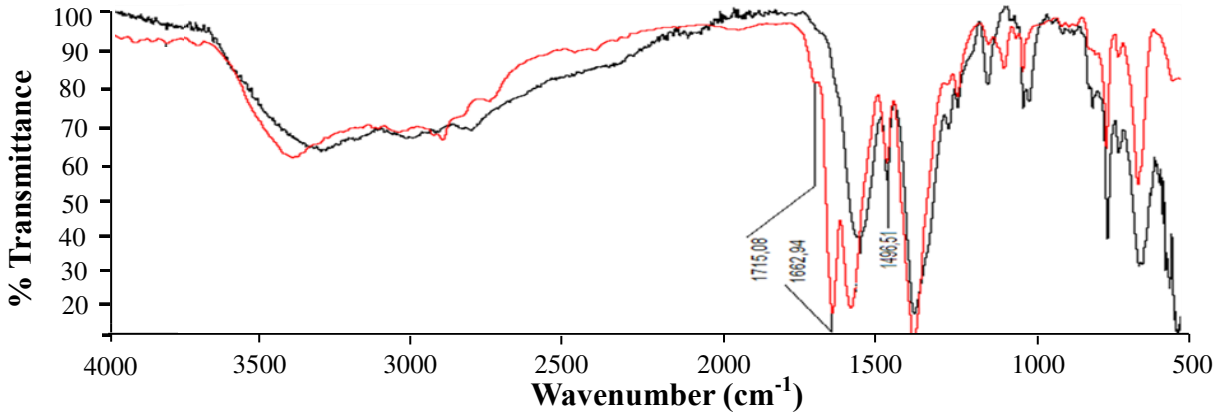

Figure 3.11 - IR diffractogram of the as-synthesized (red) and after activation (black) sample UiO-66(Zr)–Br, performed in a Nicollet 6700 spectrometer, Thermo scientific.

UiO-66(Zr)–NO_2

IR spectrum of the activated UiO-66(Zr)–Br (Fig. 3.12) shows the absence of bands at 1664 and 1718 cm^{-1}, indicating the complete removal of remaining DMF and free ligand, respectively. Characteristic bands of carboxylates are visible at around 1450 and 1550 cm^{-1}.

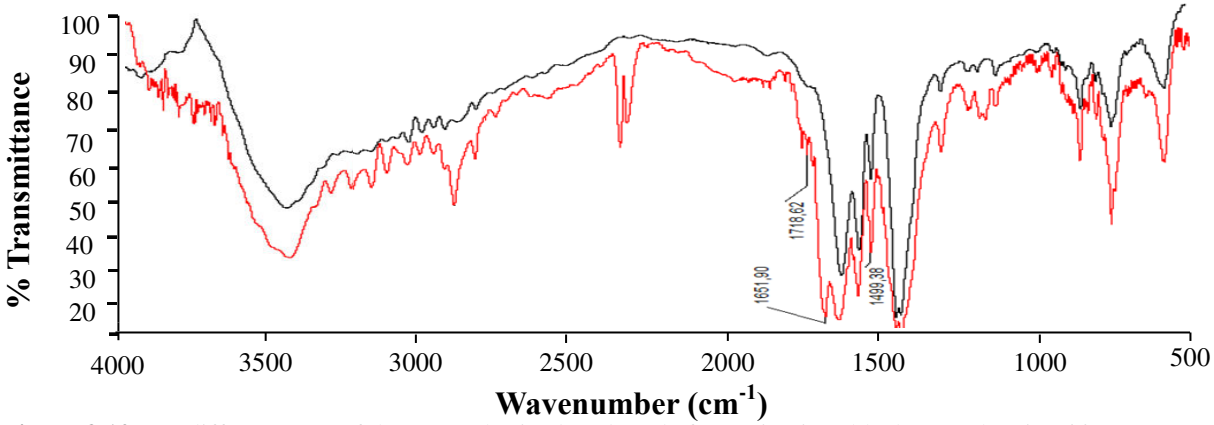

Figure 3.12 - IR diffractogram of the as-synthesized (red) and after activation (black) sample UiO-66–NO_2, performed in a Nicollet 6700 spectrometer, Thermo scientific.

UiO-66(Zr)–NH_2

Fig. 3.13 shows the IR diffractogram of the as-synthesized (red) and after activation (black) UiO-66–NH_2. After activation, bands at 1662 and 1715 cm^{-1}, corresponding to DMF and free carboxylic ligand, are not visible, confirming the correct activation of the solid. Characteristic bands of carboxylates are visible at around 1450 and 1550 cm^{-1}. In addition, the band at 886 cm^{-1} is consistent with the presence of the NH_2 group of the linker (ν(C-N).

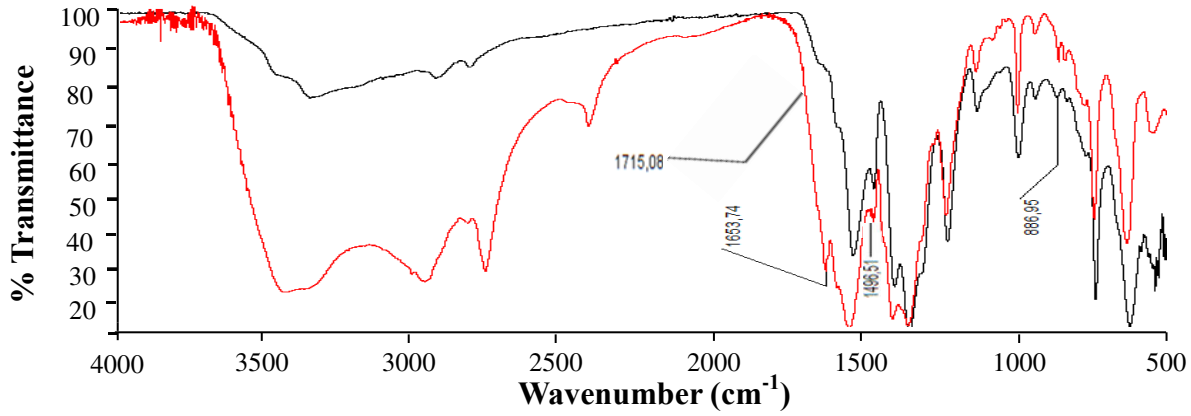

Figure 3.13 - IR diffractogram of the as-synthesized (red) and after activation (black) sample UiO-66–NH_2, performed in a Nicollet 6700 spectrometer, Thermo scientific.

3.4.2.3. Thermogravimetric Analysis (TGA)

UiO-66(Zr)–Br

TGA of UiO-66(Zr)–Br (Fig. 3.14) shows a first weight loss corresponding to the removal of 15.8 wt% of water and/or some residual MeOH. Around 50 wt% is loss at around 623 K, corresponding to the combustion of the organic linker.

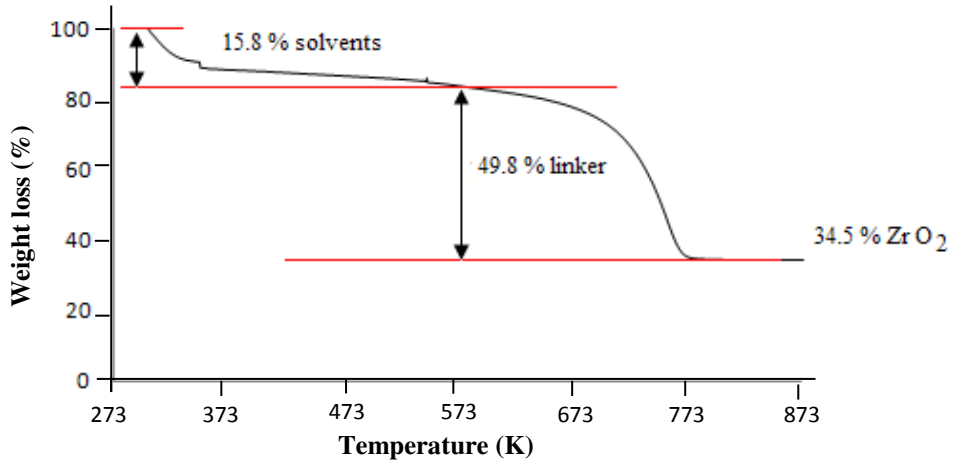

Figure 3.14 - TGA of activated UiO-66–Br (275 $K.min^{-1}$ under atmospheric pressure; 10.58 mg of solid) using a STA 6000 simultaneous thermal analyser, PerkinElmer.

UiO-66(Zr)–NO_2

TGA of UiO-66(Zr)–Br (Fig. 3.15) exhibit a first weight loss attributed to the solvent removal at around 353 K (8.9 wt%), then the linker is removed at around 623 K (40.1 wt%).

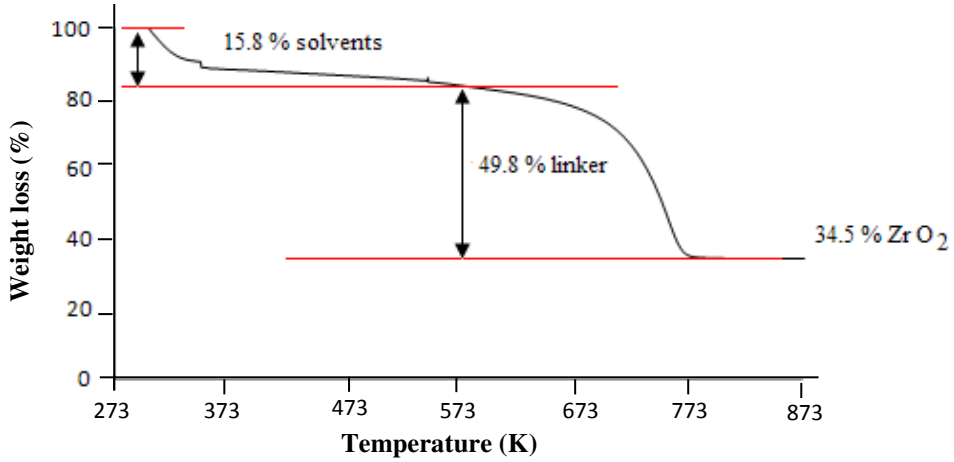

Figure 3.15 - TGA of activated UiO-66(Zr)–NO_2 (275 K.min^{-1} under atmospheric pressure; 4.010 mg of solid) using a STA 6000 simultaneous thermal analyser, PerkinElmer.

Table 3.3 disclosed the comparison between experimental and theoretical weight losses. The important difference between the experimental and calculated weight loss can be explained by the presence of some zirconium oxide in the activated sample.

UiO-66(Zr)–NH_2

TGA of the UiO-66(Zr)–NH_2, displayed in Fig. 3.16, shows two main weight losses. The first weight loss of around 7.6 wt% is attributed to the solvent evaporation.

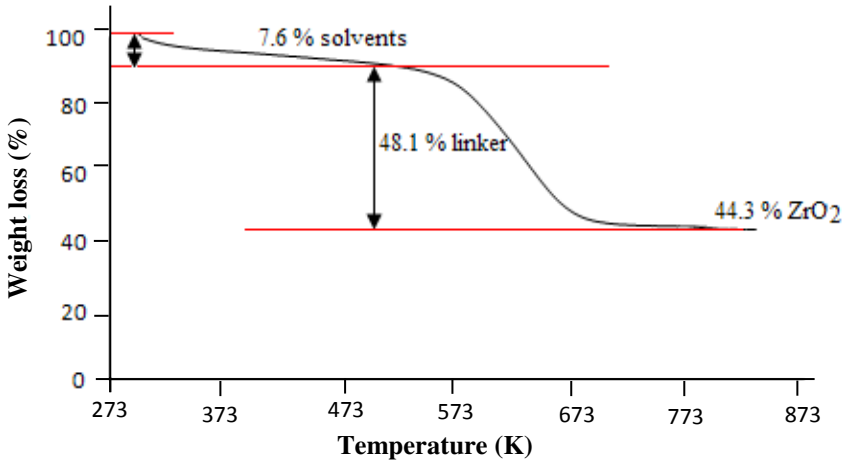

Figure 3.16 - TGA of activated UiO-66–NH_2 (275 K.min^{-1} under atmospheric pressure; 7.186 mg of solid) using a STA 6000 simultaneous thermal analyser, PerkinElmer.

The second, at around 523 K, corresponds to the organic linker combustion (48.1 wt%) The slight difference in the experimental and theoretical weight loss values is probably due to the presence of some oxide in the activated sample (Table 3.3).

Table 3.3 - Crystal size and theoretical and experimental weight loss of functionalized UiO-66 solids.

	Particle size (nm)		Theoretical (wt%)		Experimental (wt%)	
	$ZrCl_4$*	$ZrOCl_2$	ligand	ZrO_2	ligand	ZrO_2
UiO-66–Br	1400	850	55.1	29.1	49.8	34.5
UiO-66–NH_2	910	630	53.5	38.9	48.1	44.3
UiO-66–NO_2	900	760	55.4	27.3	40.1	49.2

*for comparison purposes

3.4.2.4. Nitrogen sorption measurements

UiO-66(Zr)–Br

Fig. 3.17 shows the N_2 adsorption isotherms measured at 77 K on the UiO-66(Zr)–Br. First, the sample was outgassed at 423 K under primary vacuum overnight (Belsorp Belsprep, BEL Japan). The BET (S_{BET}) and Langmuir (S_{Lang}) specific surface areas were estimated to 600 and 640 $m^2.g^{-1}$, respectively. The pore volume was 0.7 $cm^3.g^{-1}$, which will be used as a good capacity reference for the following adsorptive studies with hexane isomers. Both the progressive adsorption at relative pressures higher than 0.2 and the important nitrogen adsorption observed at high relative pressures close to 1, are in agreement with the presence of important inter-nanoparticle porosity.

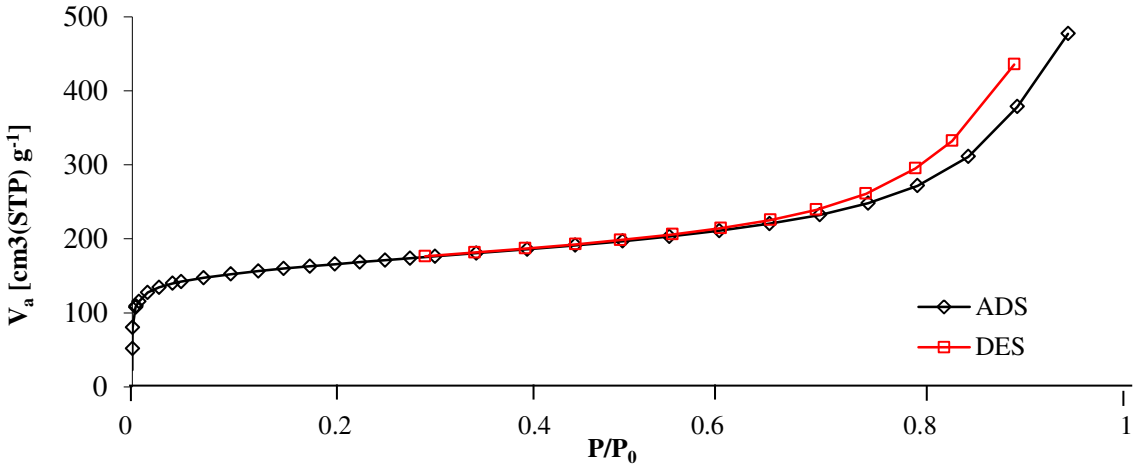

Figure 3.17 - Nitrogen adsorption isotherm at 77K (P_0 =1atm) of UiO-66–Br using a BEL Japan equipment, BELSORP Mini.

UiO-66(Zr)–NO_2

Fig. 3.18 shows the N_2 adsorption isotherms measured on the UiO66–NO_2. Prior to the analysis, the sample was outgassed at 150 °C under primary vacuum overnight (Belsorp Belprep, BEL Japan. Estimated pore volume, BET (S_{BET}) and Langmuir (S_{Lang}) surface areas were 1.0 $cm^3.g^{-1}$, 670 and 710 $m^2.g^{-1}$, respectively (Table 3.10). Both the progressive adsorption at relative pressures higher than 0.2 and the important nitrogen adsorption observed at high relative pressures close to 1, are in agreement with the presence of important inter-nanoparticle porosity.

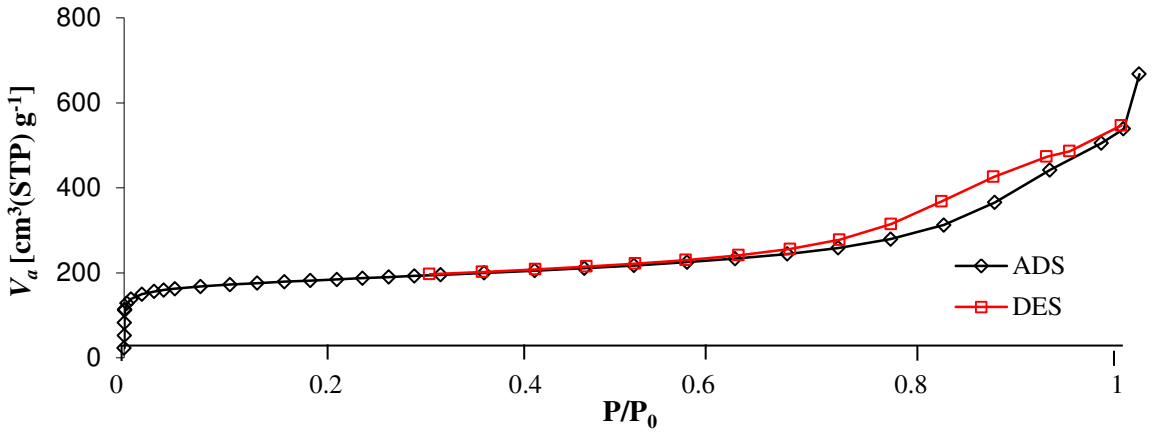

Figure 3.18 - Nitrogen adsorption and desorption isotherms at 77 K (P_0 = 1 atm) of UiO-66(Zr)–NO_2 sample using a BEL Japan equipment, BELSORP Mini.

UiO-66(Zr)–NH_2

Fig. 3.19 shows the N_2 adsorption isotherms measured on the UiO-66(Zr)–NH_2. First, the sample was outgassed at 423 K under primary vacuum overnight (Belsorp Belprep, BEL Japan).

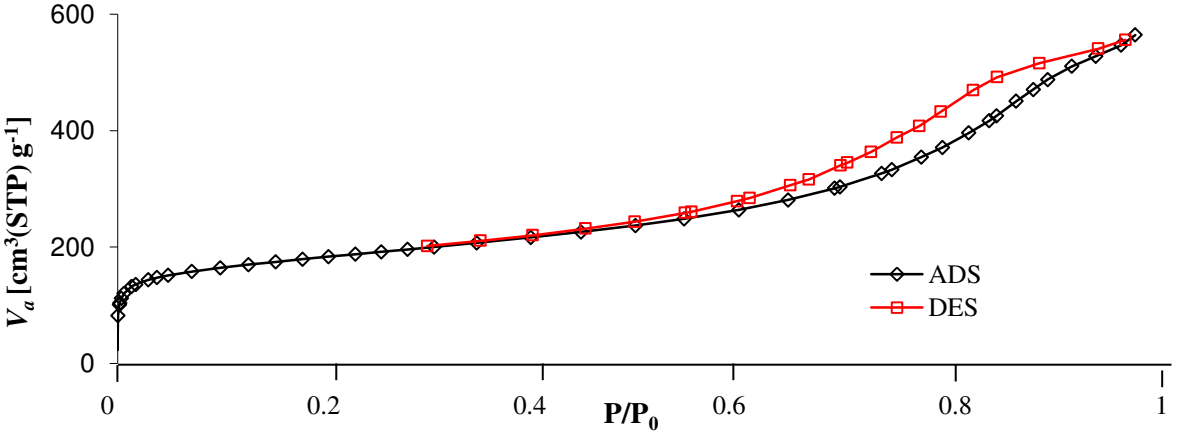

Figure 3.19 - Nitrogen adsorption and desorption isotherms at 77 K (P_0 = 1 atm) of UiO-66(Zr)–NH_2 sample using a BEL Japan equipment, BELSORP Mini.

The estimated pore volume, BET (S_{BET}) and Langmuir (S_{Lang}) specific surface areas were 0.9 $cm^3.g^{-1}$, 650 and 900 $m^2.g^{-1}$, respectively. Both the progressive adsorption at relative pressures higher than 0.2 and the important nitrogen adsorption observed at high relative pressures close to 1, are in agreement with the presence of important inter-nanoparticle porosity.

Table 3.4 displays the comparison of the micropore volume and BET surface area for the functionalized UiO-66(Zr) solids synthesized under both solvothermal route and atmospheric pressure method. Thus, except for the UiO-66(Zr)–NH_2, totally comparable porosities are observed for both methods. However, UiO-66(Zr)–NH_2 synthesized from $ZrCl_4$ solvothermal method exhibited a higher surface area (930 *vs*. 650 $m^2.g^{-1}$) with however similar pore volume (0.37 $cm^3.g^{-1}$) (Table 3.10).

Table 3.4 - BET surface area and microporous volume of the functionalized UiO-66 solids synthesized from the $ZrCl_4$ (solvothermal) or $ZrOCl_2.8H_2O$ (atmospheric pressure) route.

	S_{BET} ($m^2.g^{-1}$)	V_{mp} ($cm^3.g^{-1}$)	S_{BET} ($m^2.g^{-1}$)	V_{mp} ($cm^3.g^{-1}$)
Zr precursor	$ZrCl_4$		$ZrOCl_2.8H_2O$	
UiO-66(Zr)–Br	665	0.27	600	0.19
UiO-66(Zr)–NO_2	660	0.38	670	0.34
UiO-66(Zr)–NH_2	930	0.37	650	0.36
UiO-66(Zr)	1050		1024	0.40

3.4.2.5. Particle size determination

Particle size was analysed using the UiO-66(Zr) solids dispersed in an aqueous solution by DLS measurements (Table 3.3). The particle size of the functionalized UiO-66(Zr) solids synthesized from $ZrCl_4$ using the previously reported solvothermal method was also determine for comparative purposes. Thus, the resulting particles sizes for the $ZrCl_4$ solvothermal method were 900, 910 and 1400 nm for respectively UiO-66(Zr)–NO_2, –NH_2 and –Br. In contrast, UiO-66(Zr)–NO_2, –NH_2 and –Br synthesized from the atmospheric pressure route starting from the $ZrOCl_2$ precursor exhibit a smaller crystal size of 760, 630 and 850 nm, respectively. The smaller particle size is in agreement with XRPD and nitrogen sorption characterization.

3.4.3. Results and discussion

The potential of separation of the hexane isomers on the functionalized UiO-66(Zr) materials was tested by performing several screening studies in the LSRE-IPB. Prior to the separation studies, the solid was activated by heating at 473 K for the UiO-66(Zr)–Br or 423 K for UiO-66(Zr)–NO_2 and UiO-66(Zr)–NH_2 under vacuum (10 kPa) for 15 hours. This activation step by calcination is a crucial point since the pore content is removed, leading to accessible porosities for the hexane isomers. For the screening studies, each solid was packed in a stainless steel column (diameter = 4.3 mm, length = 80 mm).

3.4.3.1. Breakthrough curves of UiO-66(Zr)–Br

The stationary phase was package using 391 mg of the activated UiO-66(Zr)–Br. The solute for analysis was a quaternary equimolar mixture of *n*HEX, 3MP, 23DMB and 22DMB. The screening studies were performed at two different temperatures (343 and 423 K) and three partial pressures: low (0.3 kPa), moderate (0.8 kPa) and high pressure (10 kPa). The experimental conditions and adsorbed amounts of the hexane isomers in each run, calculated from the breakthrough experiments (see chapter 1) are reported in Table 3.5.

Table 3.5 - Experimental conditions and adsorbed amounts of hexane isomers in MOF UiO-66(Zr)-Br.

Run	*T* (K)	Helium flow rate (ml(STP).min^{-1})	Mixture pressure (kPa)	m_{ads} (mg)	Partial loading (g.100g$_{ads}^{-1}$)				Total loading (g.100g$_{ads}^{-1}$)
					22DMB	23DMB	3MP	*n*HEX	
Br_a1	343	37.3	0.3	391	2.6	2.8	2.3	1.7	9.4
Br_b1	423				1.3	1.3	1.3	0.5	4.4
Br_a2	343	28.0	0.8		3.3	3.5	3.2	2.6	12.6
Br_b2	423				2.8	2.8	2.7	2.3	10.6
Br_a3	343	14.0	10		3.5	4.1	3.9	3.7	15.2
Br_b3	423				3.5	3.7	3.2	3.1	13.5

The total adsorbed amount range from 4.4 wt% at 423 K and 0.3 kPa to 15.2 wt% at 343 K and 10 kPa, which can be considered as important capacities when compared to zeolites. For instance, the maximum adsorbed amount regardless the temperature in pellets of zeolite Beta (with a binder ranging from 20 to 30 wt%) reaches 9 wt% [19]. The selectivity, measured by

the ratio of the adsorbed amount of the isomers (relatively to the less adsorbed component *n*HEX), are given in Table 3.6.

Table 3.6 - Selectivities of hexane isomers in UiO-66(Zr)-Br.

Run	*T* (K)	Mixture pressure (kPa)	Selectivities		
			22DMB/ *n*HEX	23DMB/ *n*HEX	3MP/ *n*HEX
Br_a1	343	0.3	1.5	1.6	1.4
Br_a2	423		2.6	2.6	2.6
Br_b1	343	0.8	1.3	1.3	1.2
Br_b2	423		1.2	1.2	1.2
Br_c1	343	10	0.9	1.1	1.1
Br_c2	423		1.1	1.2	1.0

The highest selectivity value, observed at 423 K and 0.3 kPa, achieves almost 2.6 for the ratio 22DMB/*n*HEX. Moreover, the lowest total adsorbed amount (4.4 wt%) is reached under these conditions (see Table 3.5). This means that low uptake improves the host–guest interactions, which could play a role in the selectivity increasing between *n*HEX and the rest of the isomers. This effect can be rationalized if one considers a porous solid exhibiting heterogeneous active sites on its surface where the guest molecules can adsorb. Thus, the guest adsorption could be energetically heterogeneous. In gas mixtures, there will be competition for sorption in the active sites, being rational to propose that at low partial pressure the highest energetic sites are first occupied with the preferential molecules. This effect results in a higher selectivity. When the adsorbed amount increases, guests continue to be trapped within the structure but with different type of interactions, which leads to a decrease in the selectivity. Accordingly, the selectivity decrease when the coverage increases. This effect has also been observed by Couck *et al.* [20] in the separation of CO_2 from light gases in a functionalized NH_2-MIL–53(Al) MOF. The sorption hierarchy is the following in most of the experiments: 23DMB > 22DMB > 3MP > *n*HEX. This unusual reverse shape selectivity (*n*HEX is the less adsorbed component), previously reported by Barcia *et al.* for the bared UiO-66(Zr) [1], is once again observed, evidencing that the functionalization of the ligand does not impact the sorption hierarchy of the hexane isomers. As explained before, the reverse shape selectivity seems to be related with the linear long nature of *n*HEX (1.03×0.49 nm), which might be too long to be accommodated into the small tetrahedral cages (~8 Å; See Fig. 3.1). Accordingly, the adsorbed amounts of *n*HEX are lower than for the other isomers since the tetrahedral cavities of the framework would be inaccessible for *n*HEX molecules. Although the selectivity values of the branched paraffins related to *n*HEX reach 2.6

(Run_Br_a2), the major drawback for the UiO-66(Zr)–Br solid is its lower selectivity between the mono and di-branched paraffins (~ 1.1) which is, in addition, practically independent of the uptake. Further considerations dealing with the influence of the uptake on the selectivities of hexane isomers in the different solids are given in the Section 3.6. Fig. 3.20 shows the breakthrough curves of the hexane isomers for all runs.

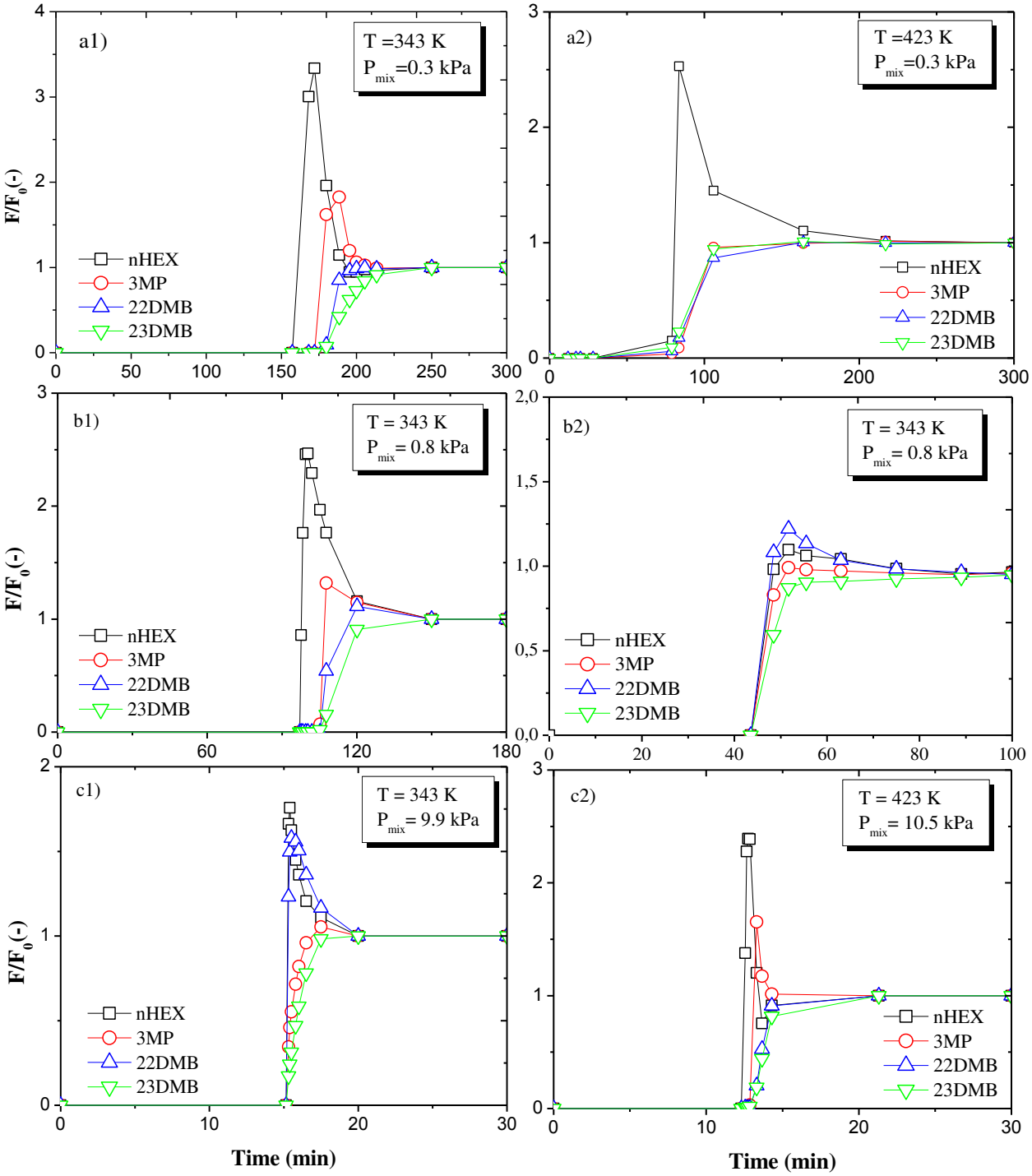

Figure 3.20 - Breakthrough curves of the hexane isomers in UiO-66(Zr)–Br. (a1) pp = 0.58 kPa, T = 343 K; (a2) pp = 0.7 kPa, T = 423 K; (b1) pp = 0.95 kPa, T = 343 K; (b2) pp = 1 kPa, T = 423 K; (c1) pp = 9.9 kPa, T = 343 K; (c2) pp = 10.5 kPa, T = 423 K.

It is clear the reverse shape selectivity in all experiments. *n*HEX is clearly the first component to break the column followed by 3MP, 22DMB and 23DMB, respectively. The roll-up for *n*HEX is very significant reaching a value around 3.5 for Run_Br_a1 (Fig. 3.20a1), suggesting a strong sorption competition between *n*HEX and the other hexane isomers on the framework.

3.4.3.2. Breakthrough curves of UiO-66(Zr)–NO_2

In this set of experiments, the fixed bed column was packed with 395 mg of UiO-66–NO_2. The studies covered two temperatures (343 and 423 K) and three partial pressures (0.3, 0.8 and 10 kPa). The experimental conditions and adsorbed amounts in each run of the multicomponent experiments (22DMB, 23DMB, 3MP and *n*HEX) are listed in Table 3.7.

Table 3.7 - Experimental conditions and amount adsorbed of hexane isomers on UiO-66(Zr)–NO_2.

Run	*T* (K)	Helium flow rate (mL(STP).min^{-1})	Mixture pressure (kPa)	m_{ads} (mg)	Partial loading (g.100g$_{ads}^{-1}$)				Total loading (g.100g$_{ads}^{-1}$)
					22DMB	23DMB	3MP	*n*HEX	
NO_2_a1	343	37.0	0.3	395	2.2	2.3	2.1	1.2	7.8
NO_2_a2	423				1.8	1.7	1.6	1.3	6.4
NO_2_b1	343	27.8	0.8		2.8	2.8	2.4	1.5	9.5
NO_2_b2	423				2.6	2.4	2.1	1.6	7.0
NO_2_c1	343	13.9	10		3.8	4.0	3.8	3.5	15.1
NO_2_c2	423				4.0	4.0	3.8	3.3	15.1

Looking at the Table 3.7, we can conclude that the adsorbed amounts are very similar to the ones obtained when using UiO-66–Br as adsorbent (Table 3.5), with an uptake reaching 15.1 wt% (Run_NO_2_a3). The sorption hierarchy on most of the runs is once again: 22DMB > 23DMB > 3MP > *n*HEX, also with the usual reverse shape selectivity. Table 3.8 displays the estimated selectivity related to *n*HEX.

Contrary to UiO-66(Zr)–Br at low uptake (Runs_NO_2_b1, b2, a2), the UiO-66–NO_2 solid shows a certain degree of separation between 3MP and the di-branched isomers, which is clearly an interesting advantage. Fig. 3.21 shows the breakthrough curves for all the experiments performed.

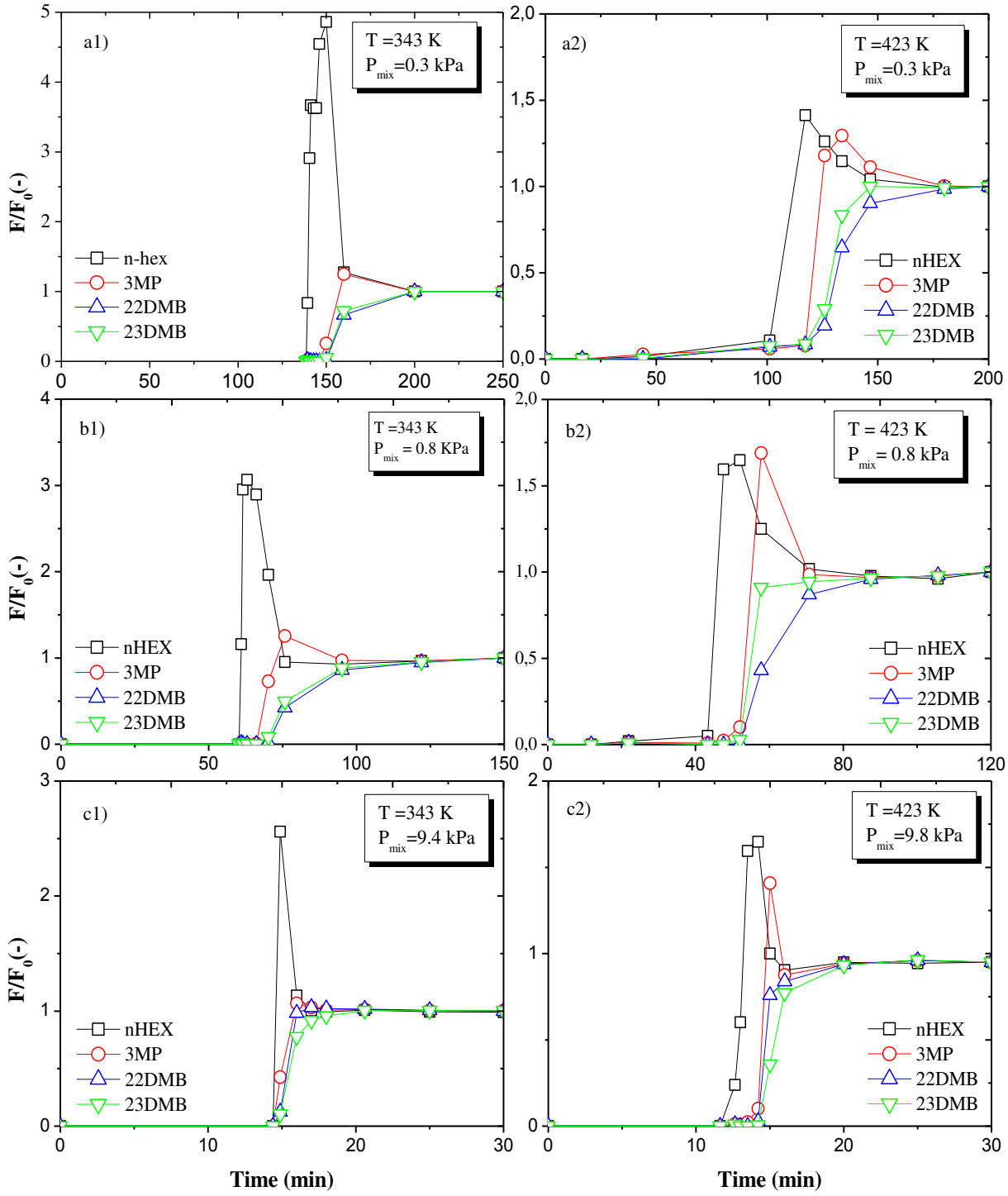

Figure 3.21 - Breakthrough curves of the hexane isomers in UiO-66(Zr)-NO_2. (a1) pp = 0.3 kPa, T = 343 K; (a2) pp = 0.3 kPa, T = 423 K; (b1) pp = 0.8 kPa, T = 343 K; (b2) pp = 0.8 kPa, T = 423 K;(c1) pp = 9.4 kPa, T = 343 K;(c2) pp = 9.8 kPa, T = 423 K.

Once more, a significant roll-up of *n*HEX is observed in most of the runs (nearly 5 for Run_NO_2_a1). For practical purposes UiO-66(Zr)–NO_2 at 343 K and 0.8 kPa (Run_NO_2_a2, Fig. 3.21a2) is the most promising system since the separation between *n*HEX and 3MP from the di-branched isomers 23DMB and 22DMB is evidenced.

Table 3.8 - Adsorption selectivities of hexane isomers for the experiments in UiO-66(Zr)–NO_2.

Run	*T* (K)	Mixture pressure (kPa)	Selectivities		
			22DMB/ *n*HEX	23DMB/ *n*HEX	3MP/ *n*HEX
NO_2_a1	343	0.3	1.8	1.9	1.8
NO_2_a2	423		1.4	1.3	1.2
NO_2_b1	343	0.8	1.9	1.9	1.6
NO_2_b2	423		1.6	1.5	1.3
NO_2_c1	343	10	1.1	1.1	1.1
NO_2_c2	423		1.2	1.2	1.2

3.4.3.3. Breakthrough curves of UiO-66(Zr)–NH_2

452 mg of UiO-66–NH_2 solid activated at 423 K under vacuum (10 Kpa) for 15 hours were packed in a stainless column. The experiments covered two temperatures (343 and 423K) and two partial pressures: 0.3 and 6 kPa. The experimental conditions and adsorbed amounts of each run are summarized in Table 3.9.

Table 3.9 - Experimental conditions and amounts adsorbed of the hexane isomers in MOF UiO-66–NH_2.

Run	*T* (K)	Helium Flow rate (mL(STP).min^{-1})	Mixture pressure (kPa)	m_{ads} (mg)	Partial loading (g.100.g_{ads}^{-1})				Total loading (g.100g_{ads}^{-1})
					22DMB	23DMB	3MP	*n*HEX	
NH_2_a1	343	32.1	0.3	452	1.6	1.9	1.8	1.7	4.9
NH_2_a2	423				1.0	1.0	0.9	0.8	3.7
NH_2_b1	343	18.4	6		2.0	3.2	3.4	3.4	12
NH_2_b2	423				1.2	1.4	1.0	0.8	4.4

The adsorbed amount of the components in each run is very similar, except at low temperature (343K) and high partial-pressure (6 kPa; Run_NH_2_b1), where the adsorbed amount of 22DMB is 2 wt%, a value considerably smaller than for the other isomers (3.4 wt%). The sorption hierarchy exhibits here a little change in the following tendency, where is more evident for the Run_ NH_2_b1:

Run_ NH_2_a1: 23DMB > 3MP > *n*HEX > 22DMB

Run_ NH_2_a2: 22DMB ≈ 23DMB > 3MP > *n*HEX

Run_ NH_2_b1: *n*HEX ≈ 3MP >23DMB > 22DMB

Run_ NH_2_b2: 23DMB >22DMB > 3MP > *n*HEX

These results show that the di-branched isomers are more retained than the linear/mono branched isomers, so, the reverse shape selectivity observed by Barcia *et al.* [1] is once again observed in almost all of the experiments. However, the Run_NH_2_a2 shows a tendency for the normal hierarchy, which means that this functionalization introduces some differences on the isomers retention. Table 3.10 discloses the selectivities for each run measured again relatively to *n*HEX.

In order to separate 22DMB (high RON) from the other low RON isomers, the normal selectivity for 22DMB (Run_NH_2_a2) around 0.6 obtained with UiO-66–NH_2 at 343 K and 6 kPa, is the most convenient for industrial purposes. Breakthrough curves (Fig. 3.22) show a small degree of separation between the isomers, except for Run_NH_2_b1 (343 K and 6 kPa) which lead to an uptake of 12 wt%.

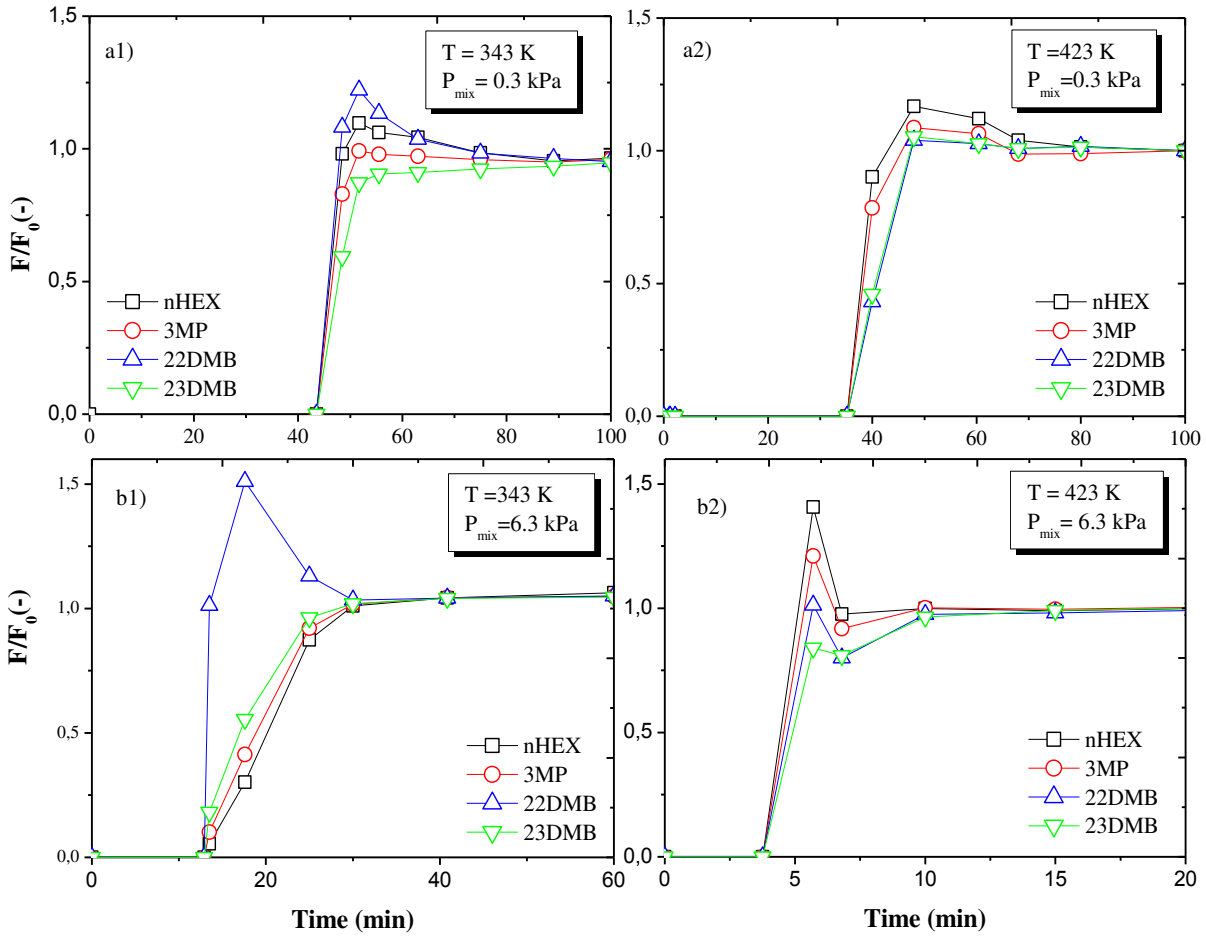

Figure 3.22 - Experimental breakthrough curves for sorption of hexane isomers in UiO-66(Zr)–NH_2. (a1) pp = 0.3 kPa, T = 343 K; (a2) pp = 0.3 kPa; T = 423 K; (b1) pp = 6.3 kPa, T = 343 K; (b2) pp = 6.3 kPa, T = 423 K.

Table 3.10 - Selectivities of hexane isomers in UiO-66–NH_2.

Run	T (K)	Mixture pressure (kPa)	Selectivities		
			22DMB/ *n*HEX	23DMB/ *n*HEX	3MP/ *n*HEX
UiO-66(Zr)-NH_2_a1	343	0.6	0.9	1.1	1.1
UiO-66(Zr)-NH_2_a2	423		1.2	1.2	1.1
UiO-66(Zr)-NH_2_b1	343	6	0.6	0.9	1.0
UiO-66(Zr)-NH_2_b2	423		1.5	1.8	1.3

3.4.3.4. Comparison of functionalized UiO-66(Zr) solids

The Fig. 3.23 represents the sorption selectivities between 22DMB and *n*HEX (Fig. 3.23a) and between 22DMB and 3MP (Fig. 3.23b) as a function of total mixture loading for the functionalized MOFs on the different materials. In a general overview of Fig. 3.23a and b, selectivity seems to decrease when the total adsorbed amount increases. A possible explanation for this behaviour comes from the fact that UiO-66 solid exhibits entropy effects due to rotational limitations of linear molecules in the smaller tetrahedral cages (leading to their exclusion), which seems to be responsible for the observed reverse shape selectivity [1].

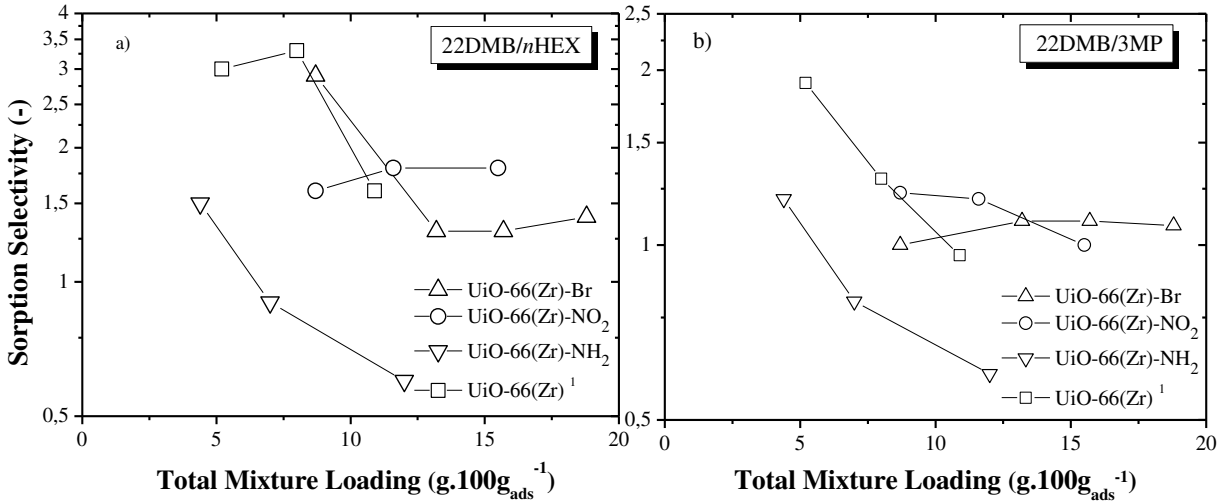

Figure 3.23 - Sorption selectivity as a function of total mixture loading for the functionalized MOFs and bared samples. (a) Between 22DMB and *n*HEX; and (b) between 22DMB and 3MP. [1]Data from reference [1].

Regarding the UiO-66–Br solid (Fig. 3.23a), lower uptakes favour the separation between 22DMB and *n*HEX with a selectivity close to 3.0. For higher uptakes, the selectivity values decrease to reach a plateau with a value nearly to 1.3. The 22DMB/3MP selectivity (Fig. 23b) shows small and constant values around 1.0.

Concerning the UiO-66–NO_2, 22DMB/*n*HEX selectivity is ranging between 1.5 and 1.8 (Fig. 3.23a). The major difference relatively to the UiO-66–Br is found at low uptake where the selectivity 22DMB/3MP (Fig. 3.23b) is the highest, reaching the value of 1.3. Finally, when uptake increases, the UiO-66–NH_2 leads to 22DMB/*n*HEX and 22DMB/3MP ratios around 0.6 (Fig. 3.23a and 3.23b).

3.5. Conclusions

At low loadings, selectivity is higher between branched and linear paraffins since branched molecules can access to both tetra and octahedral cages of UiO-66. Thermodynamically, smaller tetrahedral cages will be first filled. Accordingly, at high partial pressures (high loadings); only the octahedral cages continue adsorbing molecules [2].

However, in this case linear molecules are preferably adsorbed over branched ones (conventional effect) due to the higher Henry´s constants. This selectivity is governed by an equilibrium effect, therefore, the decrease of the branched/linear sorption selectivity suggests an equilibrium effect but with different interactions between the molecules due to the existence of different active sites at higher uptakes.

In a global comparison between bared and functionalized solids UiO-66(Zr), we can conclude that the selectivity as a function of the total adsorbed amount does not significantly change in the functionalized samples, with the exception of UiO-66–NH_2, in which reversal selectivity is observed for 22DMB at high loadings. In addition, the adsorbed amount of each component in all functionalized solids is similar. Apparently, the functionalization with NH_2 groups does not improve the separation, when compared with its Br analogue.

3.6. References

1. *P.S. Bárcia, D. Guimarães, P.A. Mendes, J.A.C. Silva, V. Guillerm, H. Chevreau, C. Serre, A.E. Rodrigues, Reverse Shape Selectivity in the Adsorption of Hexane and Xylene Isomers in MOF UiO-66, Micropor. Mesopor. Mater., 139 (2011) 67-73.*

2. *P. Mendes, F. Ragon, A. Rodrigues, P. Horcajada, C. Serre, J. Silva, Hexane isomers sorption on a functionalized metal–organic framework, Microporous and Mesoporous Materials 170 (2013) 251–258.*

3. H. Zhou, J. R. Long, O. M. Yaghi *et al., Introduction to Metal–organic frameworks, Chem. Soc. Rev., in Chemical Review, 112 (2012) 673–1268.*

4. *M. Kim, S.M. Cohen, Discovery, development, and functionalization of Zr(IV)-based metal–organic frameworks, Cryst. Eng. Com. 14 (2012) 4096-410.*

5. *H. Deng, C. Doonan, H. Furukawa, R. Ferreira, J. Towne, C. Knobler, B. Wang, O. Yaghi, Multiple Functional Groups of Varying Ratios in Metal-Organic Frameworks, Science 327 (2010) 846–850.*

6. *M. Kandiah, M.H. Nilsen, S. Usselgio, S. Jakobsen, U. Olsbye, M. Tiset, C. Laraby, E.A. Quadrelli, F. Bonino, K.P. Lillerud, Synthesis and Stability of Tagged UiO-66 Zr-MOFs, Chem. Mater. 22 (2010) 6632–6640.*

7. *S. Horike, S. Bureekaew, S. Kitagawa, Functional groups can be added post- synthetically, Chem. Commun. (2008) 471–473.*

8. *G. Férey, C. Serre, T. Devic, G. Maurin, H. Jobic, P. Llewellin, G. Weireld, A. Vimont, M. Daturi, J. Chang, Why hybrid solids capture greenhouse gases?, Chem. Soc. Rev. 40 (2011) 550–562.*

9. *N. A. Ramsahye, T. K. Trung, S. Bourrelly, Q. Yang, T. Devic, G. Maurin, P.Horcajada, P. L. Llewellyn, P. Yot, C. Serre, Y. Filinchuk, F. Fajula, G. Férey, P. Trens, Influence of the Organic Ligand Functionalization on the Breathing of the Porous Iron Terephthalate Metal Organic Framework Type Material upon Hydrocarbon Adsorption, J. Am. Chem. Soc. 115 (2011) 18683–18695.*

10. *P.S. Crespo, E.V.R. Fernandez, J. Gascon, F. Kapteijn, Synthesis and Characterization of an Amino Functionalized MIL-101(Al): Separation and Catalytic Properties, Chem. Mater. 23 (2011) 2565–2572.*

11. *C. Gaudin, D. Cunha, E. Ivanoff, P. Horcajada, C. Chevé, A. Yasri, O. Loget, C.Serre, G. Maurin, Micropor. Mesopor. Mater. A quantitative structure activity relationship approach to*

probe the influence of the functionalization on the drug encapsulation of porous metal-organic frameworks, 157 (2012) 124–130.

12. *J. H. Cavka, S. Jakobsen, U. Olsbye, N. Guillou, C. Lamberti, S. Bordiga, K. P.Lillerud, A New Zirconium Inorganic Building Brick Forming Metal Organic Frameworks with Exceptional Stability, J. Am. Chem. Soc. 130 (2008) 13850–13851.*

13. *Q. Yang, A. Wiersum, P. Llewellyn, V. Guillerm, C. Serre, G. Maurin, Functionalizing porous zirconium terephthalate UiO-66(Zr) for natural gas upgrading: a computational exploration, Chem. Commun. 47 (2011) 9603–9605.*

14. *S.D. Vinot, G. Maurin, C. Serre, P. Horcajada, D.P. Cunha, V. Guillerm, E.S. Costa, F. Taulelle, C. Martineau, Structure and Dynamics of the Functionalized MOF Type UiO-66(Zr): NMR and Dielectric Relaxation Spectroscopies Coupled with DFT Calculations, Chem. Mater. 24 (2012) 2168–2177.*

15. *A. D. Wiersum, E. Soubeyrand-Lenoir, Q. Yang; B. Moulin, V. Guillerm, M. B. Yahia, S. Bourelly; A. Vimont, S. Miller, C. Vagner, M. Daturi, G. Clet, C. Serre, G. Maurin, P. L. Llewellyn, An Evaluation of UiO-66 for Gas-Based Applications, Chem. Asian J., 6 (2011) 3270-3280.*

16. M. Kim and S. M. Cohen, Discovery, development, and functionalization of Zr(IV)-based metal–organic frameworks, CrystEngComm, 14(2012)4096-4104.

17. *Y. Traa, S. Sealy, J. Weitkamp, Characterization of the Pore Size of Molecular Sieves Using Molecular Probes, in: Characterization II, H.G. Karge, J. Weitkamp (Eds.), Molecular Sieves –Science and Technology, Vol. 5, Springer, Berlin, Heidelberg, New York, 2007, p. 103-154.*

18. *S.J. Garibay, S.M. Cohen, Isoreticular synthesis and modification of frameworks with the UiO-66 topology, Chem. Commun. 46 (2010) 7700–7702.*

19. *P.S. Bárcia, J. Silva and A. Rodrigues, Separation of Branched Hexane Isomers on Zeolite BETA, Adsorption Science & Technology,*25(*2007)*169-183.

20. *S. Couck, E. Gobechiya, C.E.A. Kirschhock, P.S. Crespo, J.J. Alcañiz, A.M. Joaristi,E. Stavitski, J. Gascon, F. Kapteijn, G.V. Baron, J.F.M. Denayer, Adsorption and separation of light gases on an amino-functionalized metal-organic framework: an adsorption and in situ XRD study, ChemSusChem. 5 (2012) 740–750.*

4.

Hexane Isomers Sorption in the imidazolate framework ZIF-8

Another porous hybrid framework that shows interesting features is the microporous zinc methyl-imidazolate ZIF-8. This chapter reports the single, binary and ternary breakthrough experiments of hexane (C_6) isomers, *n*-hexane (*n*HEX), 3-methylpentane (3MP), and 2,2-dimethylbutane (22DMB) that were performed using ZIF-8, covering the temperature range between 313 and 423 K and partial pressures up to 0.2 atm. Adsorption equilibrium isotherms were obtained from breakthrough curves experiments and showed that the sorption behaviour of linear *n*HEX is totally different from the one of the branched isomers, leading to an efficient separation of linear *n*HEX from branched paraffins through a molecular sieve effect with a remarkable working capacity (25 wt%) at 313 K and partial pressure 0.1 atm. Langmuir isotherm is found to reasonably describe the sorption data of *n*HEX while the heat of sorption reaches 33 $kJ.mol^{-1}$ with Langmuir equilibrium affinity constants ranging from 174 to 6.4 atm^{-1} for 313 and 423 K, respectively. Finally, from the ternary experiments (*n*HEX/3MP/22DMB), a complete separation between linear *n*HEX and the branched isomers is observed together with an adsorbed amount of *n*HEX similar to the one found in single component experiments. In the binary experiments (3MP/22DMB) the separation and sorption capacity is negligible. This chapter is based on the submitted paper entitled "Single and Multicomponent Adsorption of Hexane Isomers in the microporous ZIF-8".

4.1. Introduction

Today, the new class of crystalline hybrid porous materials metal-organic frameworks (MOFs) are revealed as a competitive alternative or complementary to zeolites for separation processes since they combine an important regular porosity (pore volumes ~0.1 - 4 $cm^3.g^{-1}$, BET surface areas from 100 to 6500 $m^2.g^{-1}$ and pore diameters ~ 3 - 60 Å) with an easily tuneable hybrid crystalline framework based on inorganic units (or Secondary Building Units – SBU) and organic polycomplexant linkers (carboxylates, phosphates, imidazolates, etc) [1]. Among the large number of topologies and compositions, Zeolitic Imidazolate Frameworks (ZIFs) [2] are of particular interest due to their chemical and thermal robustness. In particular, the zinc 2-methyl-imidazolate ZIF-8 with the sodalite (SOD) topology, which possesses an important porosity (S_{BET} ~ 1800 $m^2.g^{-1}$; V_p ~ 0.66 $cm^3.g^{-1}$) can be compared with the zeolite 5A that consists of a LTA type framework with sodalite composite building.

The discovery of the synthesis of molecular sieve zeolite 5A in the laboratories of Linde Air Products in 1956 [3], which has the ability to completely separate *n*-paraffins from other hydrocarbons, is a major success even today in the petrochemical industry with application in the TIP process from UOP [4, 5]. A recent study [6] has shown a comparative screening study of the sorption capabilities of hexane isomers on ZIF-8 and zeolite 5A, proving that ZIF-8 is indeed a competitive material for the separation of linear *n*HEX from their respective branched isomers with a remarkable molecular sieve effect. In addition, ZIF-8 coated capillary columns have previously shown a strong ability to sieve branched alkanes from linear alkane isomers [7, 8].

In view of a design and optimization of cyclic adsorption processes, the present work aims to better understand the adsorption of hexane isomers on ZIF-8 through fixed bed adsorption experiments (dynamic system), measuring simultaneously the adsorption equilibrium isotherms of single, binary and ternary breakthrough curves with hexane isomers *n*HEX, 3MP and 22DMB. Then, the influence of partial pressure and temperature on the single and multicomponent breakthrough curves and adsorption isotherms will be analysed. Finally, the thermodynamic data will be further analysed with the corresponding validation of the

thermodynamic model and the calculation of the thermodynamic parameters (Henry´s constants, equilibrium affinity constants, heats of sorption and saturation loading).

4.2. Structure of ZIF-8

Based on divalent cations (Zn, Co…) and imidazolate type linkers under solvothermal conditions, one can prepare the so called ZIFs [2], or Zeolitic Imidazolate Frameworks that lead to series of known of new zeotype hybrid architectures. One of the most topical ZIFs is ZIF-8 whose crystalline porous structure is obtained from a mixture of zinc nitrate hexahydrate and 2-methylimidazole (H-MeIM). Its chemical composition is of $Zn(MeIM)_2.(DMF).(H_2O)_3$, and it crystallizes in the cubic space group I43m with a cell parameter of 16.9910(1) Å, cell volume of 4905.2(6) $Å^3$ [2]**.** The unit cell consists in a cubic arrangement with 8 sodalite cages in the corners. Fig. 4.1 highlights the framework structures of ZIF-8 and zeolite 5A, while the Table 4.1 shows the physical properties of both molecular sieves for complement of the comparison.

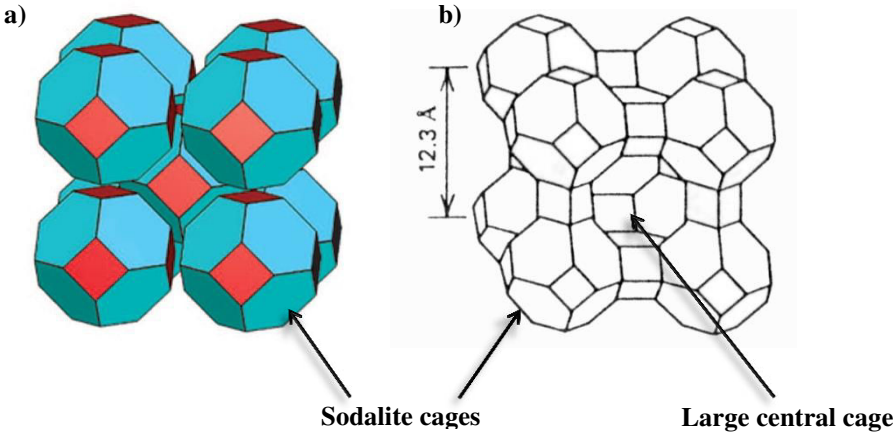

Figure 4.1 - Unit cell framework structures and physical properties of: (a) MOF ZIF-8 and (b) zeolite 5A [2].

ZIF-8 consists in a sodalite type framework with sodalite composite building units having large pore diameter (11.6 Å) accessible by a flexible six ring pore diameter aperture of 3.4 Å. The ZIF-8 framework has a surface area of 1950 $m^2.g^{-1}$ and a pore volume of 0.66 $cm^3.g^{-1}$. For comparison, zeolite 5A consists in a LTA type framework with sodalite composite building units having a smaller pore diameter (6.6 Å) accessible through a six ring rigid pore diameter aperture (2.2 Å). The unit cell consists in a cubic arrangement with 8 sodalite cages at the corners resulting in a large cavity in the centre of the cube (11.4 Å) accessible through

eight ring rigid windows (4.3 Å). This arrangement in zeolite 5A results in a significant lower power volume (0.27 $cm^3.g^{-1}$). Adsorption in ZIF-8 occurs in the sodalite cages while in zeolite 5A adsorption exclusively occurs in the large cavity.

Table 4.1 - Physical properties of MOF ZIF-8 and Zeolite 5A [2].

Physical properties of unit cell ZIF-8	
Framework type	SOD
SOD units	8
Pore diameter SOD unit [a]	11.6 Å
SOD window aperture diameter (6-ring)	3.4 Å
Small central cage diameter	negligible
Small central cage window aperture diameter (4-ring)	negligible
Pore volume	0.66 $cm^3.g^{-1}$
Physical properties of unit cell 5A	
Framework type	LTA
SOD units	8
Pore diameter SOD unit	6.6 Å
SOD window aperture diameter (6-ring)	2.2 Å
Large central cage diameter [b]	11.4 Å
Large cage window aperture diameter (8-ring)	4.3 Å
Pore volume large cage	0.27 $cm^3.g^{-1}$

[a.] Adsorption of hydrocarbons in ZIF-8 is in the SOD cages
[b.] Adsorption of hydrocarbons in 5A is in the large central cage

Furthermore, it has also been demonstrated previously that ZIF-8 exhibits a structure flexibility, associated with a rotation of the organic spacer delimiting the windows, under high pressure (1.47 GPa), as shown Fig. 4.2. The slight increase in accessibility of the windows associated with the change in orientation of the imidazolate groups allows an easier adsorption of the guests [9]. This fact indicates the flexibility of the pore access of the structure ZIF-8.

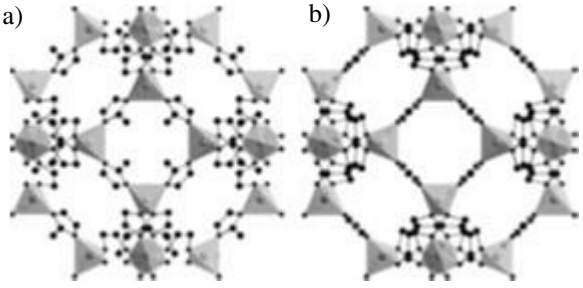

Figure 4.2 - Packing arrangement of ZIF-8 (a) at normal pressure and (b) at 1.47 GPa (ZIF-8-II). ZnN_4 tetrahedra are drawn as rigid polyhedra [9].

4.3. Experimental Section

4.3.1. ZIF-8 Synthesis

The material ZIF-8, [Zn(MeIM)2.(DMF).(H_2O)$_3$], albeit yet commercialized (BASF), was synthesized at the multi-gram scale and characterized in the ILV under hydrothermal conditions. A mixture of 5.00 g of 2-methylimidazole (H-MeIM; 60.9 mmol; Alfa Aesar, 97 %) in 25 mL of methanol (615 mmol; VWR, 99.9 %) was poured into a solution of 2.30 g of zinc nitrate hexahydrate, ($Zn(NO_3)_2.6H_2O$; 7.5 mmol; Aldrich, 99 %) in 25 mL methanol (615 mmol, VWR, 99.9 %). The mixture was placed in a 125mL autoclave Teflon liner and then put into a metallic PAAR digestion bomb at 373 K during 16 h. The resulting white powder was filtered and washed with ethanol. This procedure was repeated five times to finally obtain enough ZIF-8 for the fixed bed experiments (~ 2 g). The crystallinity of each batch was checked by XRPD before mixing all of them.

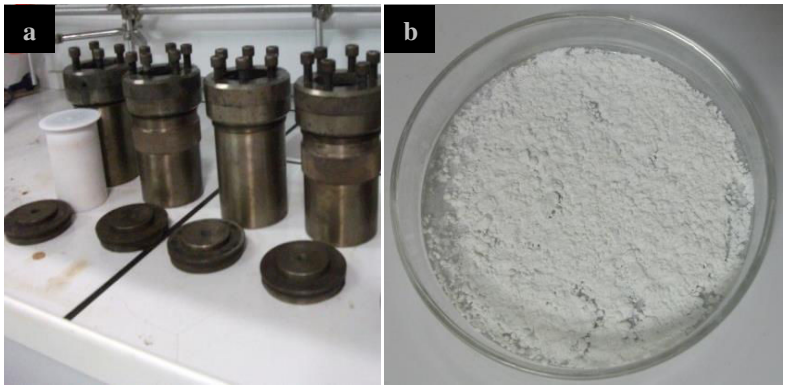

Figure 4.3 - (a) Teflon lined steel autoclave of 125 mL for ZIF-8 synthesis; (b) Sample of ZIF-8 as-synthesized.

To remove the excess of unreacted acid and zinc nitrate species, ZIF-8 was suspended in 40 mL of dimethylformamide (DMF) under stirring for 1 h at room temperature. The solid was collected by centrifugation (10500 rpm during 15 min) and then readily dispersed in 40 mL of methanol, repeating this process three times for a complete ZIF-8 purification.

4.3.2. Characterization

4.3.2.1. X-Ray Powder Diffraction (XRPD) analyses

It was necessary to check the purity of each sample synthesized at the gram scale by XRPD and compare it to the theoretical pattern of ZIF-8. Patterns were collected using a SIEMENS D5000 diffractometer (θ - 2θ) using Cu Kα1 radiation (λ ~ 1.54056 Å) from 3 to 20º (2θ) using a step size of 0.04 and 4 s per step in continuous mode. Fig. 4.4 shows the comparison between the patterns of the five ZIF-8 syntheses (color) which correspond to the Bragg peaks of ZIF-8 (black).

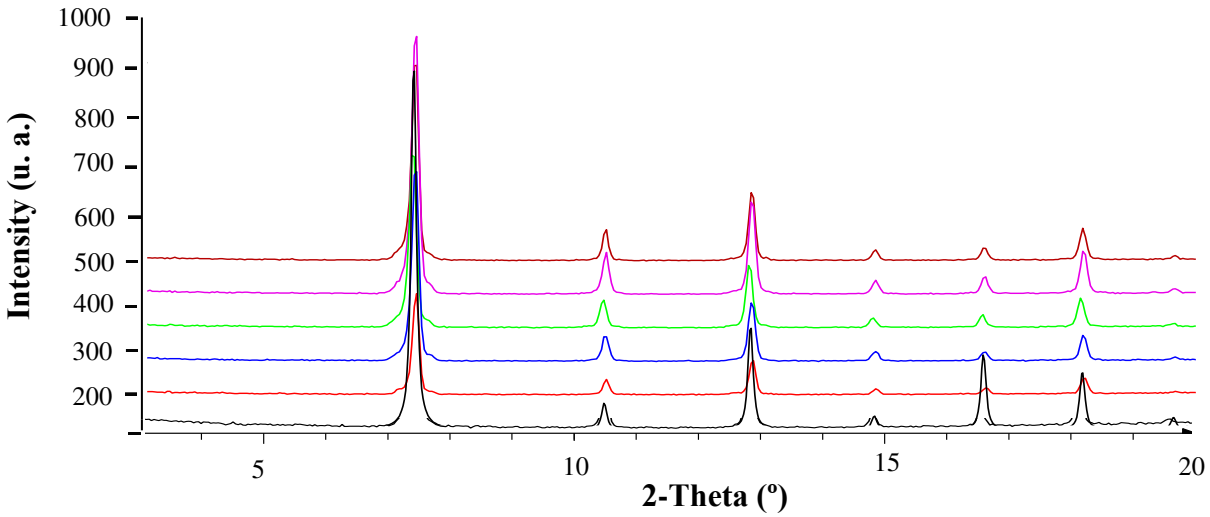

Figure 4.4 - XRPD of the theoretical ZIF-8 pattern (black), and the synthesized samples of ZIF-8 (Siemens diffractometer D5000 (Cu Kalpha1 radiation λ = 1.54056 Å).

4.3.2.2. Infra-Red (IR) spectroscopy analyses

Infrared diffractogram of the synthesized ZIF-8 were collected using a Thermo Nicolet spectrometer (Thermo, USA). Fig. 4.5 shows the diffractogram of ZIF-8 under its as-synthesized (red) and activated forms (black). The band of free imidazole (≈ 3606 cm^{-1}) is not observed as expected. DMF is still present within the pores as shown by the presence of the band at 1671 cm^{-1}. Further washing steps were not carried out due to the degradation of the

framework. The remaining DMF will be further removed after the activation treatment prior to the separation studies at 423 K under vacuum (10 kPa) for 15 hours.

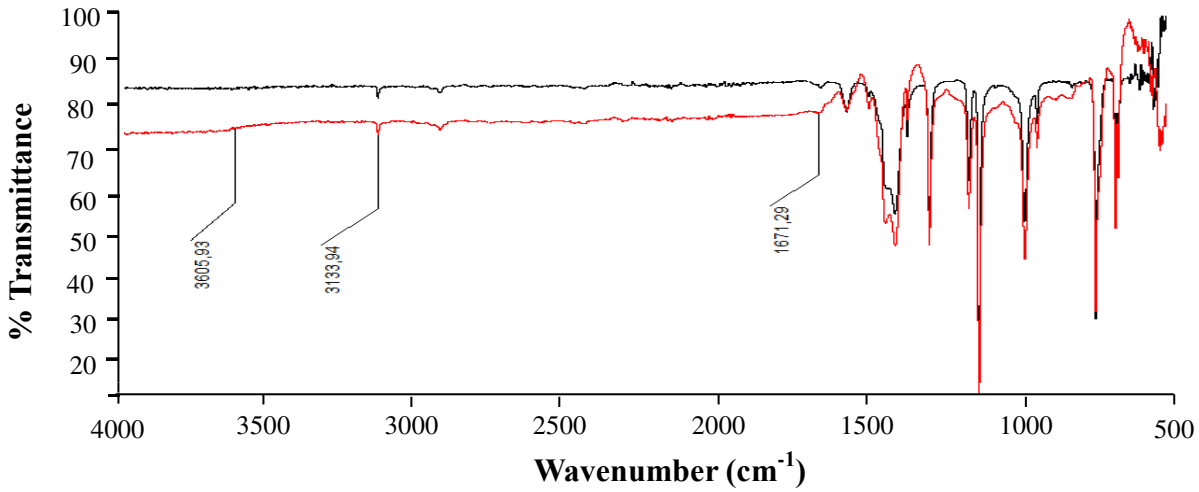

Figure 4.5 - Infra-Red diffractogram of ZIF-8 as-synthesized (red) and activated (black). (Nicollet, 6700 Thermo scientific).

4.3.2.3. Thermogravimetric Analysis (TGA)

Thermogravimetric analysis was performed on the activated ZIF-8 (≈ 6 mg) under an oxygen flow (20 mL.min^{-1}) using a Perkin Elmer Diamond TGA/DTA STA 6000 from room temperature to 873 K with a scan rate of 275 K.min^{-1}. Fig. 4.6 shows the rather good thermal stability of ZIF-8. The degradation of the sample corresponds to the 56.2 wt% loss (linker) that begins at 573 K. The first 4.1 % loss (373 K– 573 K) corresponds to residual DMF impurities.

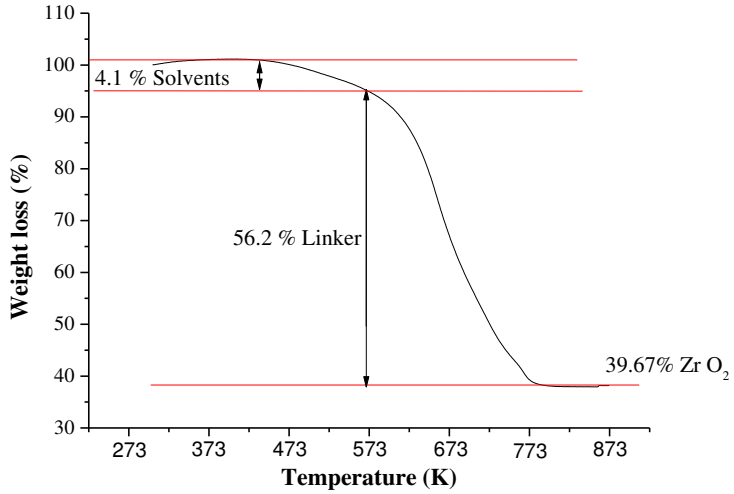

Figure 4.6 - Thermogravimetric analysis of ZIF-8 activated under atmospheric pressure (Heating rate of 275 K.min^{-1}; 5.6360 mg of solid). (PerkinElmer, STA 6000).

4.3.2.4. Nitrogen adsorption measurement

N_2 isotherms were obtained at 77 K using a Belsorp Mini (Bel, Japan). Prior to the analysis, approximately 40-60 mg of activated ZIF-8 was evacuated for 16 h at 423 K under vacuum. Fig. 4.7 shows the N_2 adsorption and desorption isotherms.

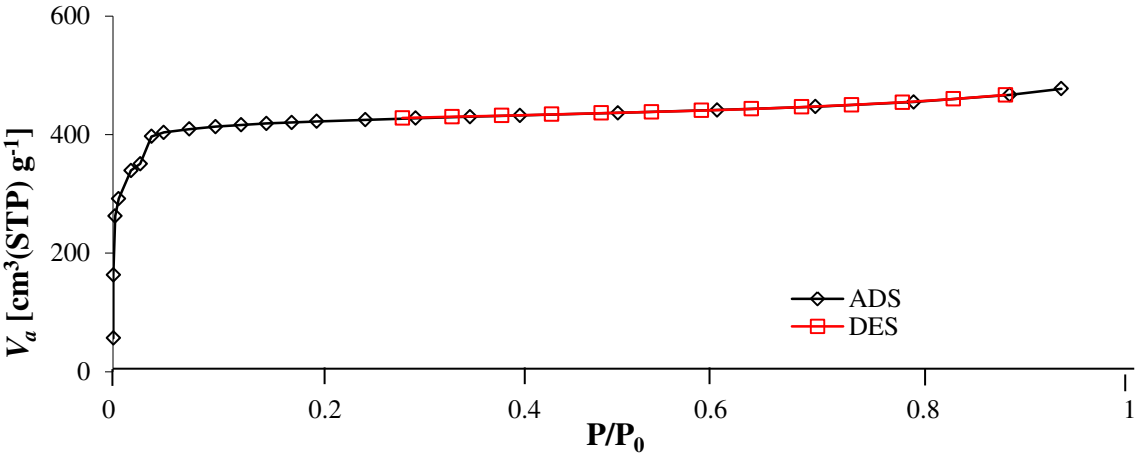

Figure 4.7 - Nitrogen adsorption isotherm of ZIF-8 at 77 K (P_0 = 1 atm) using a BEL Japan equipment, BELSORP Mini.

Surface area and micropore volume were estimated at a relative pressure lower than 0.25. The BET (S_{BET}) and Langmuir (S_{Lang}) surface area were 1400 $m^2.g^{-1}$ and 1915 $m^2.g^{-1}$, with a total micropore volume (V_{mp}) around 0.68 $cm^3.g^{-1}$, in agreement with an optimal ZIF-8 porosity.

4.3.3. Results and Discussion

With the purpose of testing the adsorption capacity of ZIF-8, several screening studies were performed at LSRE-IPB. Prior to the screening studies, the sample in its powdered form (particles with diameter until 0.03 mm) was activated by heating under vacuum (10 kPa) at 423 K for 15 hours. Following this, 313 mg of the activated sample was packed in a stainless steel column (diameter = 4.3 mm, length = 80 mm) for the breakthroughs determination. Table 4.2 summarizes the experimental conditions and amounts adsorbed in each run.

Table 4.2 - Experimental conditions and loading for single, binary and ternary breakthrough runs of *n*HEX in ZIF-8.

Run	T (K)	Helium flow rate (mL(STP).min^{-1})	C_6 flowrate, F_{C6} (μmol.min^{-1})			Mixture Pressure (atm)	Loading, q (g.100g^{-1})
			*n*HEX	3MP	22DMP		*n*HEX
m_1	313	27.0	3.6	-	-	0.005	14.2
m_2		27.9	16.8	-	-	0.020	21.0
m_3		27.9	34.3	-	-	0.040	23.8
m_4		27.9	59.8	-	-	0.069	24.6
m_5		27.9	87.2	-	-	0.100	25.3
m_6	373	27.9	3.8	-	-	0.005	3.6
m_7		27.9	15.6	-	-	0.017	9.4
m_8		27.9	31.1	-	-	0.036	13.6
m_9		27.9	56.1	-	-	0.062	17.1
m_10		27.9	81.0	-	-	0.088	18.7
m_11	423	27.9	3.7	-	-	0.005	0.8
m_12		27.9	15.6	-	-	0.018	2.8
m_13		27.9	31.0	-	-	0.038	5.0
m_14		27.9	55.8	-	-	0.066	8.0
m_15		27.9	85.0	-	-	0.095	10.2
b_1	313	30.7	-	6.4	6.4	0.013	-
b_2		11.2	-	42.8	42.8	0.170	
b_3	373	27.9	-	6.4	6.4	0.015	-
b_4		11.2	-	42.2	42.1	0.170	
b_5	423	26.1	-	5.8	5.8	0.015	-
b_6		9.3	-	40.9	40.9	0.200	
t_1	313	27.9	4.6	4.7	4.7	0.018	15.3
t_2		11.2	27.8	28.5	28.5	0.170	25.2
t_3	373	27.9	4.2	4.3	4.3	0.015	4.0
t_4		9.3	27.4	28.1	28.1	0.200	19.0
t_5	423	22.4	3.7	3.8	3.8	0.018	0.9
t_6		9.3	26.6	27.2	27.2	0.200	8.4

The screening studies were conducted at three temperatures (313, 373 and 423 K) with partial pressures between 0.005 atm and 0.2 atm for mono, binary or ternary equimolar mixture of the hexane isomers (*n*HEX, 22DMB and 3MP). Accordingly to Table 4.2, ZIF-8 exhibits approximately a 2.5 times larger accessible pore volume to accommodate linear paraffins than zeolite 5A.

Thus, it was of interest to further investigate this sample. Another interesting feature is the strong impact of the temperature on the *n*HEX loading, being of 25 and 10 wt% at respectively 313 and 423 K at similar partial pressures (0.1 atm). At low partial pressure (0.005 atm) the impact of temperature is even more pronounced, being 14 wt% at 313 K and

only 0.8 wt% at 423 K. This is probably associated with the gate opening flexible character of ZIF-8. In the following sections the mono, binary and ternary breakthrough curves are given.

4.3.3.1. Pure component sorption

Sorption isotherms

Fig. 4.8 shows the single component adsorption equilibrium isotherms for *n*HEX plotted in terms of the loading in wt% as a function of the partial pressure in atm. The isotherms were measured from breakthrough experiments where the sorbates are diluted in a helium stream (inert carrier gas; see experimental section).

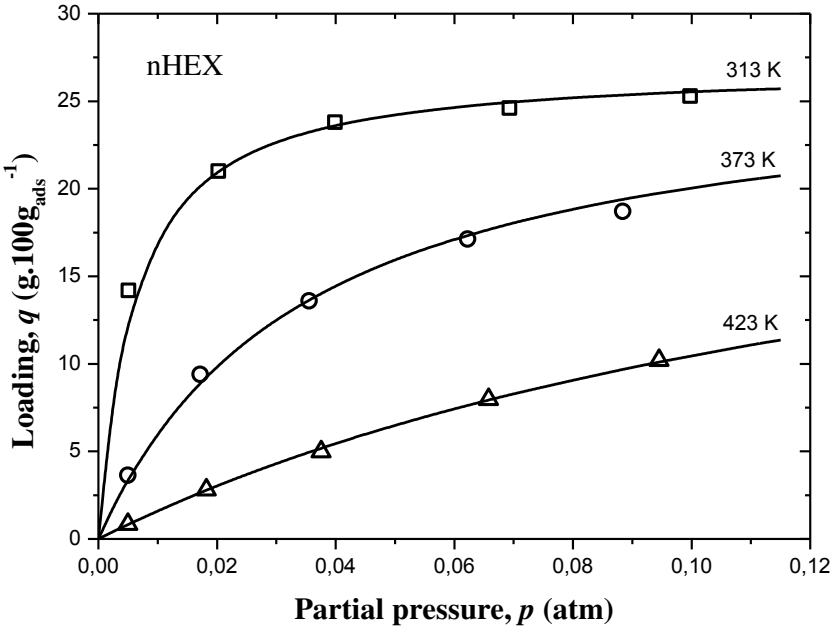

Figure 4.8 - Isotherm of *n*HEX in ZIF-8 at 313, 373 and 423 K. The continuous lines represent the estimated values with the Langmuir model with parameters given in Table 4.3.

Note that one experiment means one adsorption equilibrium point. The experimental conditions and results obtained at three different temperatures (313, 373 and 423 K) and partial pressures up to 0.10 atm are summarized Table 4.2. From Fig. 4.8 one can point out the very large loading capacity of *n*HEX in ZIF-8, close to 25 wt% at 313 K and a partial pressure equal to 0.1 atm. For comparison, the maximum loading capacity of *n*HEX in zeolite 5A is around 13 wt% [10, 11] which means that the capacity of ZIF-8 is twice higher. As stated previously in the introduction, this difference can be explained (i) by the larger pore diameter of the sodalite cage in ZIF-8 compared with 5A (11.6 *vs.* 6.6 Å; see Table 4.1), (ii) a lower packing efficiency of *n*HEX in 5A due to the adsorption occurring only within the large

cavity [6]. Fig. 4.9 gathers the single component breakthrough curves of *n*HEX in ZIF-8 from where the adsorption equilibrium isotherms were collected.

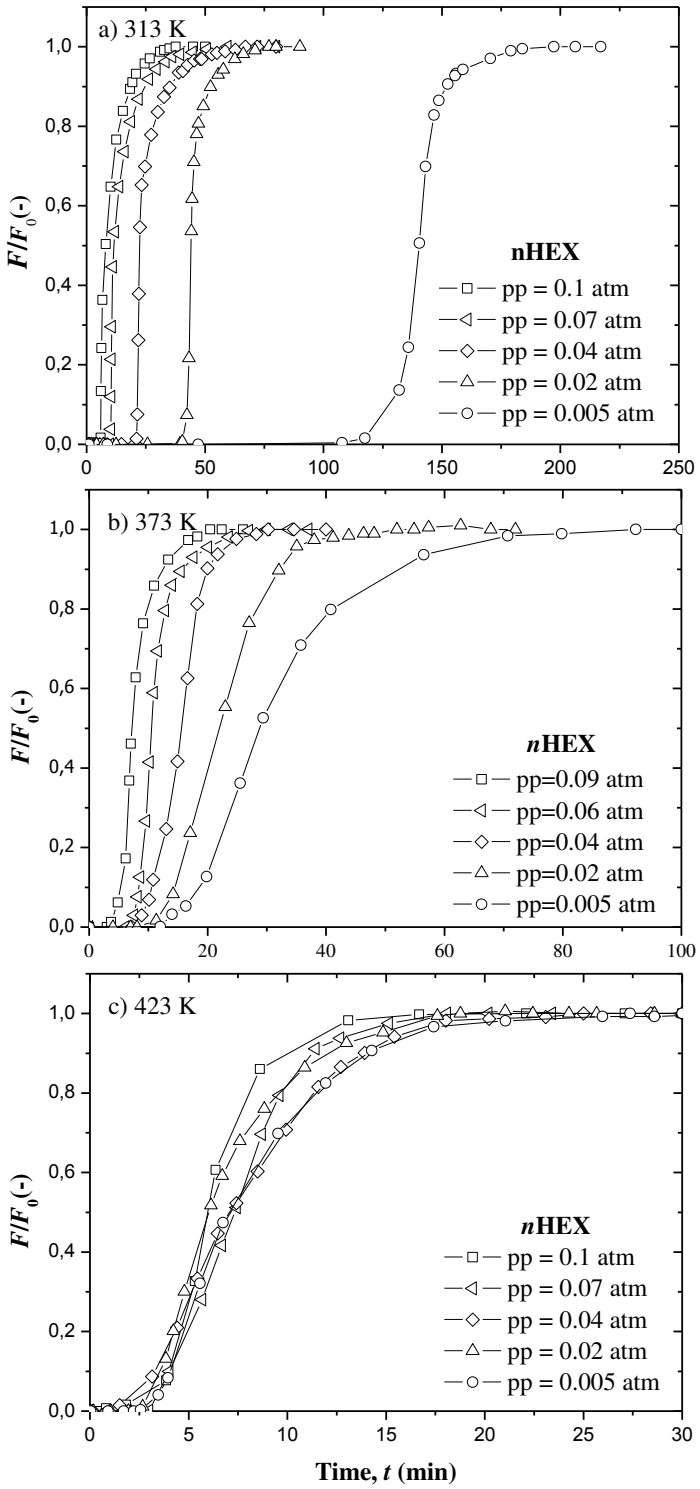

Figure 4.9 - Experimental breakthrough curves for sorption of nHEX in ZIF-8 performed at several partial pressures. (a) T = 313 K; (b) T = 373 K and (c) T = 423 K. Experimental conditions are given in Table 4.2.

The experimental conditions are given in Table 4.2. At low temperature (Fig. 4.9a), the breakthrough curves are sharp, indicating a highly favourable adsorption isotherm. However,

looking at the last part of the curve, a slow approach to saturation is noted, which could be explained by heat effects influencing the last part of the profiles of the breakthrough curves. At higher temperature (423 K), the breakthrough curves spread along the time due to the fact that the isotherm approaches a linear shape at this temperature (see Fig. 4.8).

Finally, similar single component sorption studies were carried out with the mono-branched 3MP and di-branched 22DMB, with no evidence of any adsorption in the fixed bed. In addition, the elution time of these compounds were totally comparable with the ones of blank experiments (without sorbent in the column). This is due to the fact that despite a gate opening character of ZIF-8, the size of the expanded windows is not large enough to accommodate these isomers ($d_{k\ 3MP}$ = 5.0 Å and $d_{k\ 22DMB}$ = 5.6 Å). The absence of adsorption of the pure mono- and di-branched isomers indicates a high adsorption selectivity of the hexane isomers on ZIF-8 material.

Modelling sorption isotherms

For the development of an adsorption process, it is of importance to model adsorption equilibrium data. Accordingly, the validity of Langmuir isotherm model was tested to represent equilibrium data of nHEX by plotting φ/(1-φ)/p against φ (Fig. 4.10).

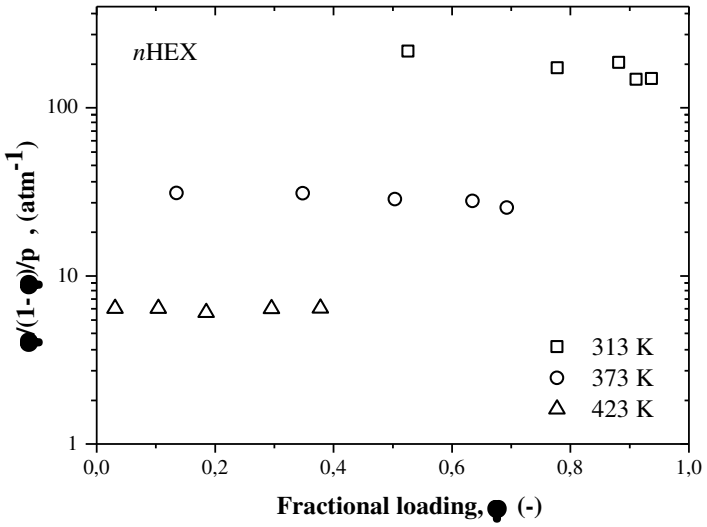

Figure 4.10 - Plots of φ/p(1-φ) against φ for analysis of Langmuir isotherm for data of *n*HEX.

For the plotting, a maximum loading capacity q_{max} of *n*HEX in ZIF-8 equal to 27 wt% was assumed (regardless the temperature). This value is very close to the one experimentally observed here for *n*HEX at 313 K at a high partial pressure of 0.12 atm. In addition, the choice of this value could be also justified by the ratio of the pore volume between ZIF-8 and

zeolite 5A, close to 2.5. Note that the q_{max} parameter must be kept constant in the fitting in order to obtain consistent thermodynamic models. The plot of $\varphi/(1-\varphi)/p$ against φ is illustrated in Fig. 4.10, evolving almost in parallel to the fractional coverage φ axis in a considerably range of φ, which means that the Langmuir isotherm is reasonably valid for fitting the data of *n*HEX in ZIF-8.

Therefore, one can propose the Langmuir model to predict the *n*HEX adsorption. In the *n*HEX isotherms that are represented in Fig. 4.8, the Langmuir model predictions with parameters given in Table 4.3, was used. A very good agreement between the experimental and simulated adsorption equilibrium data of *n*HEX in ZIF-8 is observed (Fig. 4.8). From the Langmuir model parameters (Table 4.3), the Langmuir constant K for *n*HEX is found to range from 175 to 6.3 atm^{-1} between 313 and 423 K. In addition, Henry´s constants $H=q_{max}.K$ and its temperature dependence were also estimated (Table 4.3). The heat of sorption calculated from a Van't Hoff dependence of Henry´s constants with temperature is around 32.8 $kJ.mol^{-1}$, indicating a strong impact of the temperature on the sorption of *n*HEX in ZIF-8.

Table 4.3 - Langmuir model parameters used on the Langmuir model predictions.

Parameter	Unit	*n*HEX
q_{max}	$(g.100g_{ads}^{-1})$	27
K (313 K)	(atm^{-1})	175
K (373 K)	(atm^{-1})	28.8
K (423 K)	(atm^{-1})	6.32
H (313 K)	$(g.g_{ads}^{-1}.atm^{-1})$	47.2
H (373 K)	$(g.g_{ads}^{-1}.atm^{-1})$	7.78
H (423 K)	$(g.g_{ads}^{-1}.atm^{-1})$	1.71
$-\Delta H$	$(kJ.mol^{-1})$	32.8

H (Henry Constant) = $q_{max}.K$

4.3.3.2. Multicomponent sorption

A set of breakthrough experiments with equimolar ternary mixtures of *n*HEX/3MP/22DMB and equimolar binary mixtures of 3MP/22DMB was performed to evaluate the sorption behaviour of hexane isomers mixtures in ZIF-8.

Ternary experiments (nHEX/3MP/22DMB)

Two different sets of experiments (Fig. 4.11) were carried out: i) at a low partial pressure to study the influence of the temperature; and ii) at a high partial pressure to evaluate the isomers separation in more industrially relevant conditions.

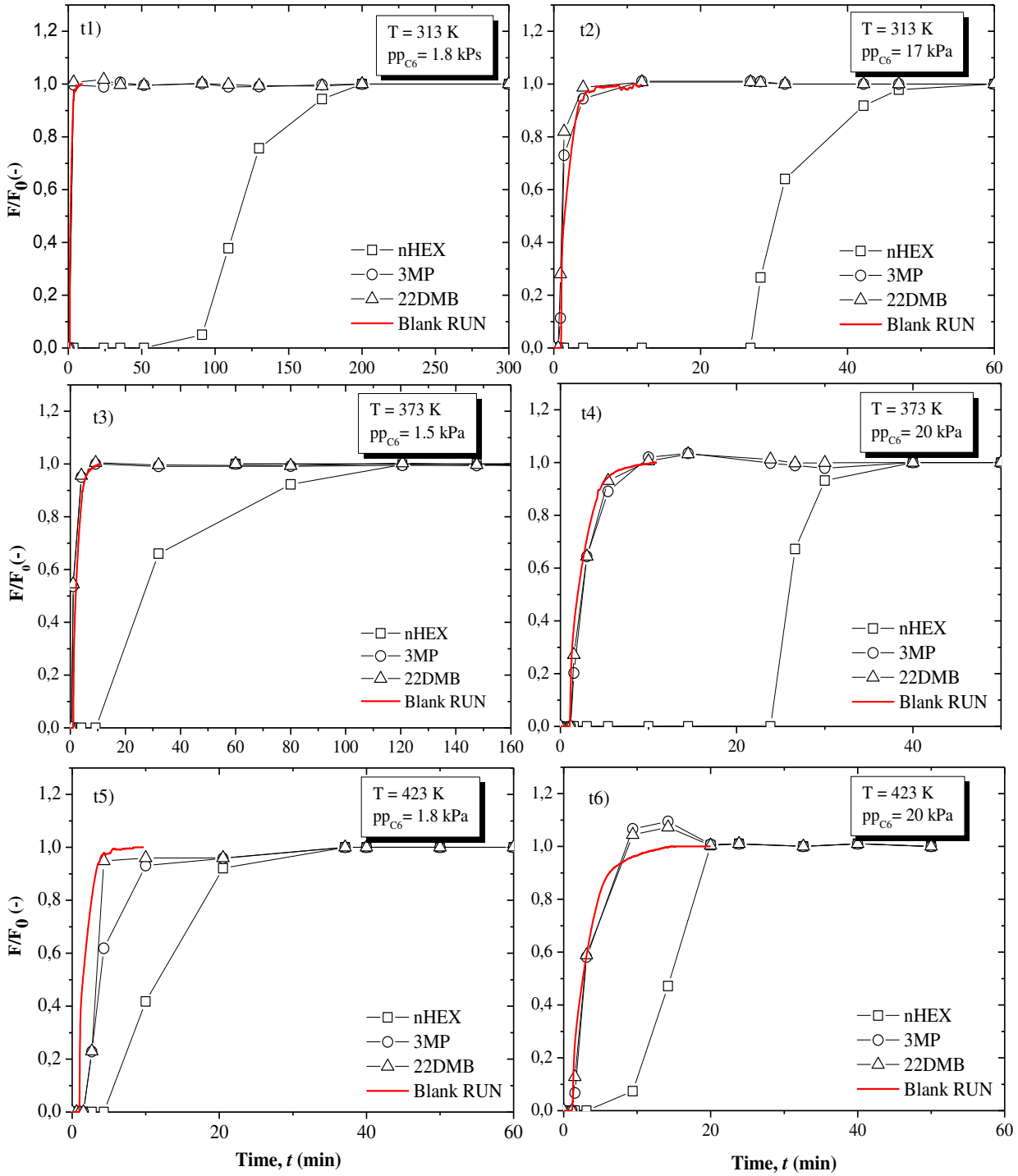

Figure 4.11 - A comparison of experimental breakthrough curves relatively to the sorption of ternary mixtures *n*HEX/3MP/22DMB in ZIF-8. (t1) pp = 1.8 kPa, T = 313 K; (t2) pp = 17 kPa, T = 313 K; (t3) pp = 1.5 kPa; T = 373 K; (t4) pp = 20 kPa, T = 373 K; (t5) pp = 1.8 kPa, T = 423 K; (t6) pp = 20 kPa, T = 423K. Experimental conditions are given in Table 4.2. Red lines in the Figure represent blank runs at the same experimental conditions with the column filled with glass spheres.

Fig. 4.11 (t1, t3 and t5) discloses breakthrough curves for ternary equimolar mixtures (*n*HEX/3MP/22DMB) at a low total isomers partial pressure around 1.8 kPa as a function of the temperature. Similarly, Fig. 4.11 (t2, t4 and t6) shows the same temperature effect at a high total isomers partial pressure of around 20 kPa. The breakthrough curves were plotted in terms of normalized flux of sorbates F/F_0 as a function of time. The experimental conditions are given in Table 4.2, as well as the isomers loadings. For comparison, the blank runs experiments (red lines) at the same feed conditions of the real experiments (performed in the same column filled with glass spheres) were included in Fig. 4.11.

Thus, a complete separation between *n*HEX and the branched isomers is achieved in all experiments, in agreement with an elution of the branched isomers similar to the one obtained during the blank experiment. This confirms that the branched isomers are not adsorbed at all on ZIF-8 in a fixed bed flow dynamic system. Moreover, the loading of *n*HEX in all experiments is similar to that one found at a similar partial pressure and temperature in the single component studies, suggesting that ZIF-8 can be used as molecular sieve to separate linear *n*HEX from respective branched isomers with a two times higher sorption capacity than zeolite 5A.

Binary experiments (3MP/22DMB)

In light of previous results and in order to check if ZIF-8 is able to discriminate between the mono-branched 3MP and di-branched 22DMB without the presence of *n*HEX, a set of binary breakthrough experiments was carried out (Fig. 4.12). Figure 4.12 proves that the binary sorption of 3MP/22DMB in ZIF-8 is negligible, a result similar to the one found in the ternary experiments (Fig. 4.11).

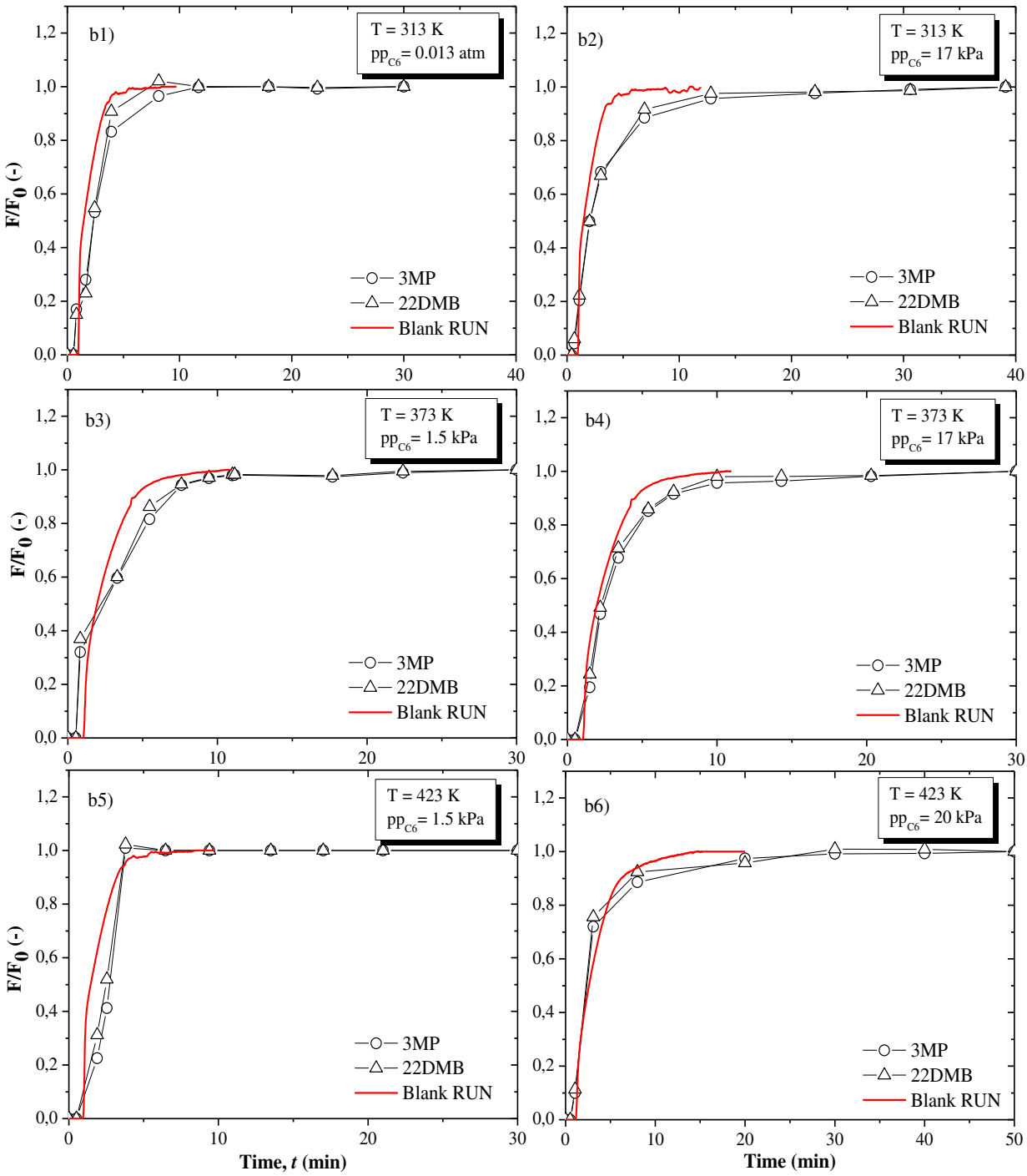

Figure 4.12 - A comparison of experimental breakthrough curves relatively to the sorption of binary mixtures 3MP/22DMB in ZIF-8. (b1) pp = 1.3 kPa, T = 313 K; (b2) pp = 17 kPa, T = 313 K; (b3) pp = 1.5 kPa; T = 373 K; (b4) pp = 17 kPa, T = 373 K; (b5) pp = 1.5 kPa, T = 423 K; (b6) pp = 20 kPa, T = 423 K. Experimental conditions are given in Table 4.2. Red lines in the Figure represent blank runs at the same experimental conditions with the column filled with glass spheres.

4.4. Conclusions

The systematic study of sorption of hexane isomers (linear *n*HEX, mono-branched 3MP and di-branched 22DMB) has been performed, including breakthrough curves for single, binary and ternary mixtures as a function of temperature and partial pressure, using ZIF-8 (also commercially named Basolite Z1200). It appears that this microporous zinc 2-methylimidazolate MOF is capable to separate the hexane isomers due to its structural similarity with the zeolite 5A, i.e. the presence of sodalite cages accessible through super microporous windows. Ternary *n*HEX/3MP/22DMB breakthrough experiments show a complete separation of linear *n*HEX from the branched paraffins with, moreover, a working capacity similar to that one found for the single component experiments. However, a poor separation with a practically negligible sorption was found for the binary experiments 3MP/22DMB.

Noteworthy, ZIF-8 also exhibits (i) a high loading of *n*HEX reaching 25 wt% at 313 K and partial pressure 0.1 atm, associated with its larger accessible pore volume, (ii) a more favourable adsorption of *n*HEX at low temperature and (iii) an estimated *n*HEX heat of sorption close to 32.8 $kJ.mol^{-1}$.

The adsorption equilibrium isotherms for *n*HEX were also set-up from these experiments as well as models of adsorption data using the simple Langmuir model, describing highly suitable Type I isotherms.

Finally, ZIF-8 can be considered as an efficient separator with a molecular sieve effect of linear *n*HEX from the branched isomers with a significant working capacity (25 wt%). This porous hybrid MOF is therefore a promising candidate exceeding the working capacity of other existing molecular sieves, such as zeolite 5A.

4.5. References

1. *See theme issues: Metal–organic frameworks, Chem. Soc. Rev. 1201 (2010) 112, Chem. Rev. (2012) 673–1268.*

2. *K. Park et al., Exceptional chemical and thermal stability of zeolitic imidazolate frameworks. The National Academy of Sciences of the USA, 103 (2006) 10186–10191*

3. *T.B. Reed and D.W. Breck, Crystalline zeolites. II. Crystal structures of synthetic zeolite, type A, J. Am. Chem. Soc., 78 (1956) 5972-5977 .*

4. *N. Cusher, UOP TIP and Once-Through Zeolitic Isomerization Processes. In Handbook of Petroleum Refining Processes, R. Meyers, Ed.; 3rd Edition, McGraw Hill: New York, (2004).*

5. *T. Holcombe, n-Paraffins - Isoparaffins Separation Process. U.S. Patent 4 (1979) 176,053.*

6. *D. Peralta, G. Chaplais, A. Simon-Masseron, K. Barthelet, and G. D. Pirngruber, Separation of C6 Paraffins Using Zeolitic Imidazolate Frameworks: Comparison with Zeolite 5A, Ind. Eng. Chem. Res., 51 (2012) 4692–4702.*

7. *N.Chang, Z. Y.Gu, X. P.Yan, Zeolitic Imidazolate Framework-8 Nanocrystal Coated Capillary for Molecular Sieving of Branched Alkanes from Linear Alkanes along with High-Resolution Chromatographic Separation of Linear Alkanes, J.Am.Chem.Soc.132(2010)13645.*

8. *M. T. Luebbers, T.Wu, L. Shen, R. I. Masel, Effects of molecular sieving and electrostatic enhancement in the adsorption of organic compounds on the zeolitic imidazolate framework ZIF-8. Langmuir, 26 (2010)15625.*

9. *S. Moggach, T. Bennett, A. Cheetham, The Effect of Pressure on ZIF-8: Increasing Pore Size with Pressure and the Formation of a High-Pressure Phase at 1.47 GPa, Chem., 121 (2009) 7221-7223.*

10. *J. A. C. Silva, A. E. Rodrigues, Sorption and Diffusion of n-Pentane in Pellets of 5A Zeolite, Ind. Eng. Chem. Res, 36 (1997) 493-500.*

11. *J. A. C. Silva, A. E. Rodrigues, Equilibrium and Kinetics of n-Hexane sorption in pellets of zeolite 5A, AIChE Journal, 43 (1997) 2524-2534.*

5.

Hexane Isomers Sorption in flexible MOFs: MIL-53(Fe) and -88B(Fe)

Highly flexible MOFs are attractive candidates for separation due the adaptability of their pores in the presence of various stimuli such as temperature, pressure or guest sorption (among others). We report here of the hexane isomers (22DMB/3MP/*n*HEX) sorption properties (pure components, binary or ternary mixtures, 313 - 423 K, partial pressures up to 20 kPa) of two types of highly flexible iron(III) dicarboxylate MOFs of the MIL-53(Fe) and MIL–88B(Fe) structure type, bearing or not CF_3 or CH_3 functional groups. If MIL-53(Fe) or the functionalized MIL-53(Fe)–2CH_3 and MIL-88B(Fe)–2CF_3 solids are not able to separate the isomers, the MIL-53(Fe)–2CF_3 MOF exhibits a molecular sieve effect between the di-branched isomer 22DMB and the mono-branched 3MP and linear *n*HEX. The separation is temperature dependent, being decreased at higher temperatures, together with sorption capacities for the 3MP and *n*HEX which do not exceed 5 wt% at 323 K, 3 wt% at 373 K and 1 wt% at 423 K, respectively.

5.1. Introduction

So far, the sorption properties of highly flexible MOF have not been investigated as much as those of the more traditional rigid MOFs [1-7]. Nevertheless, several studies have evidenced within the past decade the remarkable properties associated to their reversible breathing or swelling upon guest sorption [6, 8]. One of the most topical flexible MOF is the metal(III) dicarboxylate MIL-53 whose flexibility involves a reversible shift between the narrow or large pores forms, typically associated with an hysteresis [9]. Such behaviours have recently been evaluated in order to propose new applications in the field of gas storage or separation/purification [7, 10]. For instance, linear alkanes are adsorbed in MIL-53(Cr) with adsorption steps associated with a breathing of the structures together with large sorption capacities of 85 wt% and 60 wt% for *n*Hex and *n*-Nonane, respectively [10, 11], which exceeds by 50% those of zeolites [12, 13]. In this chapter, we will report the study of hexane isomers adsorption/separation using series of highly flexible iron(III) dicarboxylate frameworks of the MIL-53(Fe) and MIL-88 structure types, bearing or not functional apolar groups (CH_3, CF_3).

5.2. Structure of MIL-53(Fe)

MIL-53(Fe) materials exhibit a three dimensional flexible structure built up from chains of corner-sharing octahedral ($MO_4(OH)_2$; M= Cr, Al, Fe, Ga or In) related together through terephthalate linkers BDC-$(X)_n$ (X= Cl, Br, CH_3, NH_2, OH, CO_2H, CF_3) as shown Fig. 5.1.

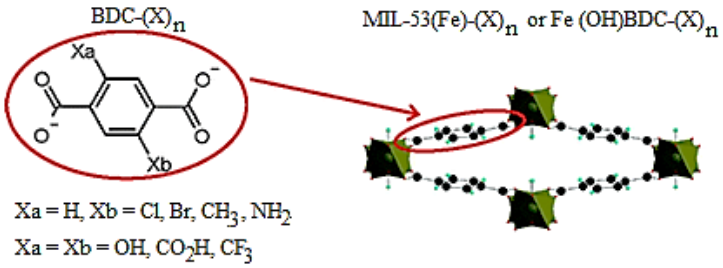

Figure 5.1 - Schematic structure of MIL-53(Fe) in its narrow pore form, as well as the different functionalized 1,4 BDC-linkers [6].

The general chemical formula is [Fe(OH)[O_2C-$C_6H_{4-n}X_n$-CO_2(n=1-4)] with X representing the functional group X_n and n the number of groups per spacer. As the iron MIL-53 structure exhibits a closure of its pores upon dehydration with no accessible porosity to nitrogen (77 K), one can use the grafting of functional groups on the aromatic linkers to tune the flexibility and the initial pore opening of the sample paving the way for an "à la carte" sorption behaviour.

The flexible character of MIL-53 has a very strong impact over the sorption properties due to the adaptation of the pore opening to the size of the guest molecule to optimize the host-guest interactions. Fig. 5.2 shows the hydrated and dehydrated forms of MIL-53(Cr) and the corresponding narrow and large pore forms.

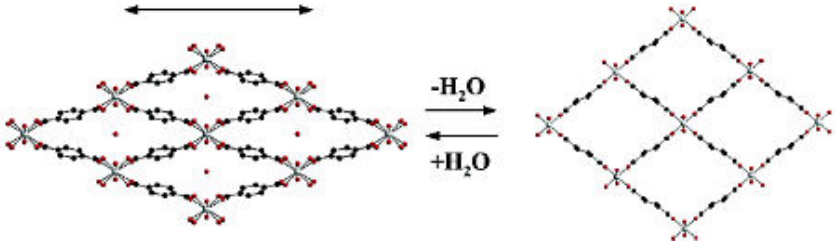

Figure 5.2 - Breathing of MIL-53(Cr) upon adsorption/desorption of water (left: narrow pores; right : large pores) [8].

Among the various functionalized MIL-53(Fe) solids reported to date, MIL-53(Fe)–$(CF_3)_2$ is an attractive framework due the functional group –CF_3 that limits the rotation of the aromatic linker, reducing the amplitude of flexibility and thus increase the initial pore opening of the solid once dried. MIL-53(Fe)–$(CF_3)_2$ or Fe(OH)BDC-$(CF_3)_2$.$6H_2O$ possesses a microporous lozenge types channels as shown Fig. 5.3.

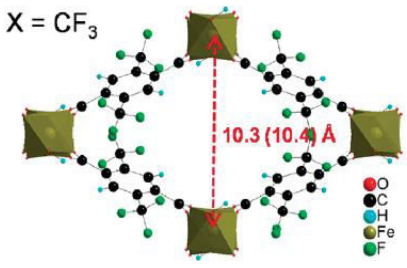

Figure 5.3 - Simulated crystal structure of the narrow pores form of MIL-53(Fe)–$(CF_3)_2$ [6].

MIL-53(Fe)–$(CF_3)_2$ crystallizes in the C_2/c space group with cell parameters a = 19.429 Å, b = 10.355 Å c = 6.911 Å and a unit cell volume of 1317.9 ($Å^3$) leading to a surface area of S_{BET} = 95 $m^2.g^{-1}$ and S_{Lang} = 140 $m^2.g^{-1}$ through the BET and Langmuir method respectively.

5.2.1. MIL-53(Fe)

5.2.1.1. Experimental Section

The MOF MIL-53(Fe) was synthesized in ILV (CH61A) and thereafter sent to LSRE–IPB for the breakthrough experiments.

5.2.1.2. Results and Discussion

The breakthrough experiments were performed with ternary equimolar mixture of *n*HEX, 3MP and 22DMB. The sample was first activated under vacuum (10 kPa) during 15 hours at 473 K (particles in their powdered form with diameter around 0.03 mm). Thereafter the solid was packed (289 mg) in a stainless steel column (diameter = 4.3 mm, length = 80 mm) for the screening studies. Table 5.1 shows the experiments performed at 313 K and at two partial pressures: low (1 k Pa) and high pressure (10 kPa).

Table 5.1 - Experimental conditions and adsorbed amounts of hexane isomers in MIL-53(Fe).

Run	T (K)	Helium flow rate ($mL(STP).min^{-1}$)	Mixture pressure (kPa)	m_{ads} (mg)	Partial loading ($g.100g_{ads}^{-1}$)			Total loading ($g.100g_{ads}^{-1}$)
					22DMB	3MP	*n*HEX	
MIL-53(Fe)_a1	313	37.2	1	289	1.2	1.1	1.1	3.4
MIL-53(Fe)_b1		14.0	10		2.9	3.1	3.2	9.2

Fig. 5.4 discloses the ternary breakthrough curves 22DMB/3MP/*n*HEX in the MIL-53(Fe) at 1 kPa and 10 kPa for 313 K. These breakthroughs demonstrate that the hexane isomers adsorb in the MOF with amounts 3.4 wt% at 1 kPa and 9 wt% at 10 kPa total mixture pressure, however the adsorbed amounts are practically the same for the three isomers and accordingly they are not separated. These results aim us to introduce new functional groups in the MIL-53(Fe) framework to change adsorption properties of the isomers.

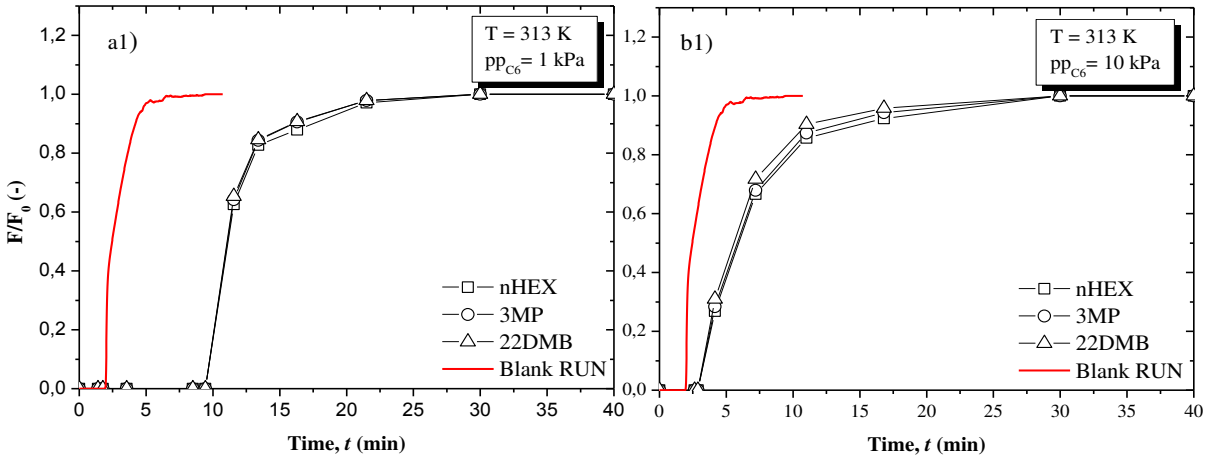

Figure 5.4 - Ternary breakthrough curves 22DMB/3MP/*n*HEX in MIL-53(Fe) (calcination of sample at 473 K). (a1) pp = 1 kPa, T = 313 K; (b1) pp = 10 kPa, T = 313 K. Red lines in the figure represent blank runs at the same experimental conditions with the column filled with glass spheres.

5.2.2. MIL-53(Fe)–$(CF_3)_2$

5.2.2.1. Experimental Section

Synthesis of MIL-53(Fe)–$(CF_3)_2$

MIL-53(Fe)–$(CF_3)_2$ was synthesized (Fig. 5.5) at ILV and outgassed in LSRE at 473 K under vacuum (10 kPa) overnight prior to the screening studies. The synthesis was performed as reported previously [6] by mixing 0.755 g (2.5 mmol) of 2,5-diperfluoroterephthalic acid, 0.675 g (2.5 mmol) of iron(III) chloride hexahydrate and 25 mL of deionized water in a 100 mL Teflon-lined reactor. The resulting mixture is thereafter, stirred for ten minutes and then introduced within a microwave assisted solvothermal Teflon lined reaction.

Figure 5.5 - Final product of the sample MIL-53(Fe)–$(CF_3)_2$ after calcination**.**

The reactor is then heated at 373 K for 20 min (heating rate 333 K.min^{-1}). The resulting light yellow crystalline solid can be recovered by centrifugation, and dried under air atmosphere, as reported.

X-Ray Powder Diffraction (XRPD) analysis

Fig. 5.6 shows the XRPD of MIL-53(Fe)–$(CF_3)_2$ after activation (black) and after calcination (red). Changes in the relative intensity of the main Bragg peaks are indicative of a structure modification and/or adsorption within the pores. After activation (under vacuum or high temperature) the relative proportion of the narrow or large pores forms varies.

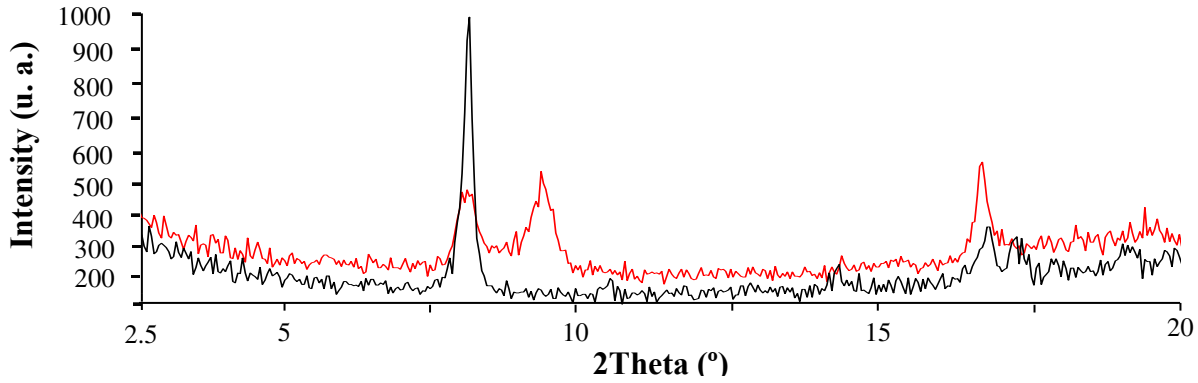

Figure 5.6 - X-Ray powder diffraction of the sample MIL-53(Fe)–$(CF_3)_2$ activated (black) and calcined (red), using a Siemens diffractometer D5000 (Cu Kalpha1 radiation λ= 1.54056 Å).

Infra-Red spectroscopy

Fig. 5.7 shows the IR diffractogram of MIL-53(Fe)–$(CF_3)_2$ activated (red) and after calcination (black). Note the vibrational band at 1730 cm^{-1} observed after activation.

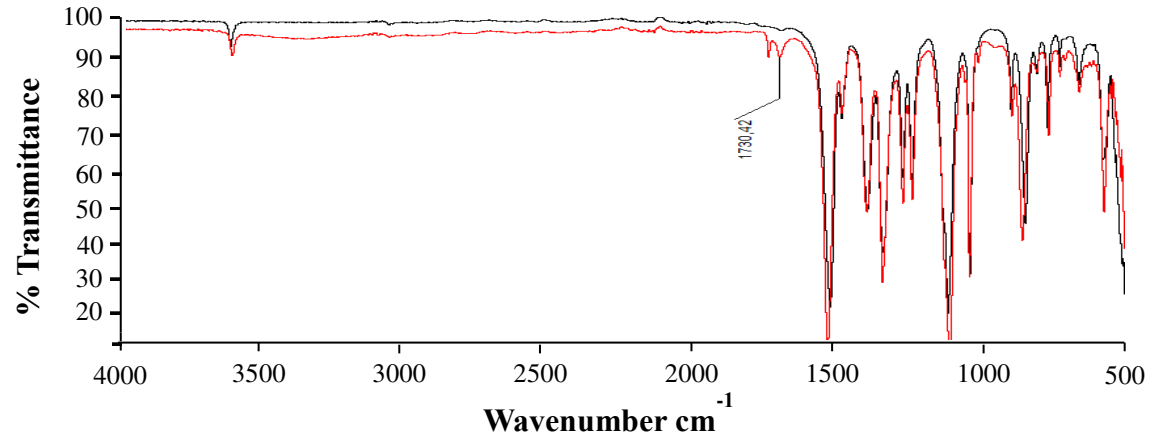

Figure 5.7 - IR diffractogram of the sample MIL-53(Fe)–$(CF_3)_2$ after activation (black) and after calcination (red), (Nicollet 6700 spectrometer), Thermo scientific.

Thermogravimetric Analysis (TGA)

Fig. 5.8 displays the thermogravimetric analysis of MIL-53(Fe)–$(CF_3)_2$. The weight loss is of 67.4 wt%) at ca. 573 K and is related to the combustion of the organic linker.

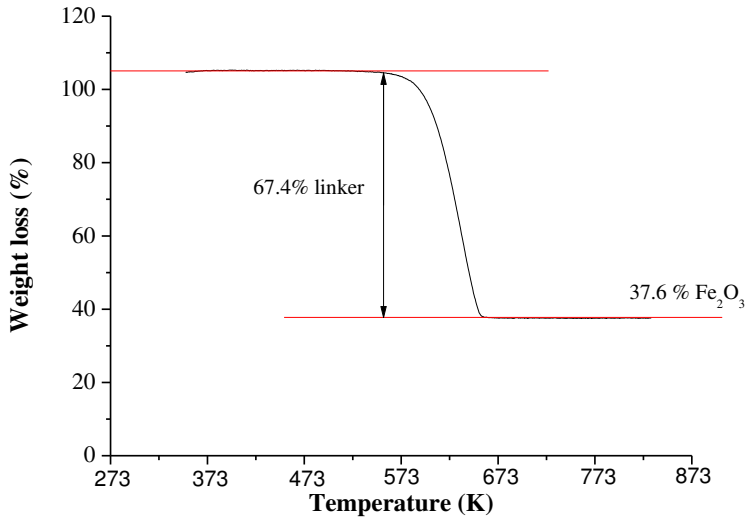

Figure 5.8 - Thermogravimetric analysis of MIL-53(Fe)–$(CF_3)_2$ activated under atmospheric pressure (Heating rate of 2 °C.min^{-1}; 2.615 mg of solid). Equipment PerkinElmer, STA 6000.

Experimental and theoretical values are on the whole in agreement (67. 4 % vs 75 %) despite a slight excess of inorganic species due probably to the presence of residual iron oxide. Note that the solid contains almost no water at room temperature due to its hydrophobic character.

5.2.2.2. Results and discussion

A set of breakthrough experiments with equimolar ternary mixtures of *n*HEX/3MP/22DMB and equimolar binary mixtures of 3MP/22DMB and 22DMB/*n*HEX was performed to evaluate the sorption behaviour of hexane isomers mixtures in MIL-53(Fe)–$(CF_3)_2$. After calcination (activation step under vacuum (10 kPa) during 15 hours at 473 K), 276 mg of sample was packed in a stainless steel column (diameter = 4.3 mm, length = 80 mm), connected to an experimental set-up for single and multicomponent experiments, as described on Chapter 2. The experiments were performed, covering the temperature range between 313 and 423 K and pressures between 0.5 kPa and 20 kPa. Blank runs were also performed (column without MOF).

Ternary Mixtures nHEX/3MP/22DMB

This set of experiments was performed with a ternary equimolar mixture of *n*HEX/3MP/22DMB. The experimental conditions together with the results of the partial loading of each isomer calculated by the integration of the breakthrough profiles are summarized in Table 5.2.

Table 5.2 - Experimental conditions and adsorbed amounts of ternary mixture in MIL-53(Fe)–$(CF_3)_2$.

Run	T (K)	Helium flow rate (mL(STP).min^{-1})	Mixture pressure (kPa)	m_{ads} (mg)	Partial loading (g100.g_{ads}^{-1})			Total loading (g.100g_{ads}^{-1})
					22DMB	3MP	*n*HEX	Total
MIL-53_a1	313	27.6	0.5	276	0.04	0.8	1.0	1.8
MIL-53_b1	313	36.8	1		0.1	0.8	1.2	2.1
MIL-53_b2	373				0.1	0.5	0.5	1.1
MIL-53_b3	423				0.07	0.07	0.05	0.2
MIL-53_c1	313	9.2	10		0.2	1.4	2.4	4.0
MIL-53_c2	373				0.5	1.1	1.3	2.9
MIL-53_c3	423				0.1	0.3	0.5	1
MIL-53_d1	313	9.2	20		0.8	1.9	3.7	6.5
MIL-53_d2	373				1.1	1.6	1.8	4.2
MIL-53_d3	423				0.2	0.4	0.6	1.1

Three different sets of experiments were carried out: i) at a low partial pressure of the isomers of 1 kPa; ii) at a medium partial pressure of the isomers of 10 kPa and iii) at a higher partial pressure of the isomers of 20 kPa. This set of experiments was repeated at three different temperatures: 313, 373 and 423 K. For the temperature of 313 K another run was performed at a very low partial pressure of 0.5 kPa. Fig. 5.9 (a1-d1) discloses the breakthrough curves for ternary equimolar mixtures (*n*HEX/3MP/22DMB) at 313 K. The breakthrough curves were plotted in terms of normalized flux of sorbates F/F_0 as a function of time. For comparison, the blank runs experiments (red lines) at the same feed conditions of the real experiments (performed in the same column filled with glass spheres) were included in Fig. 5.9. Noteworthy, a complete separation between 22DMB and mono branched 3MP and linear *n*HEX is achieved in all experiments, in agreement with an elution of the 22DMB practically similar as the one obtained during the blank experiments, except at very low pressure (0.5 kPa) where the mono-branched 3MP is also excluded from the framework (see Fig. 5.9a1).

This means that 22DMB is not adsorbed at all on MIL-53(Fe)–$(CF_3)_2$ in a fixed bed flow dynamic system in ternary experiments (22DMB/3MP/*n*HEX) at 313 K.

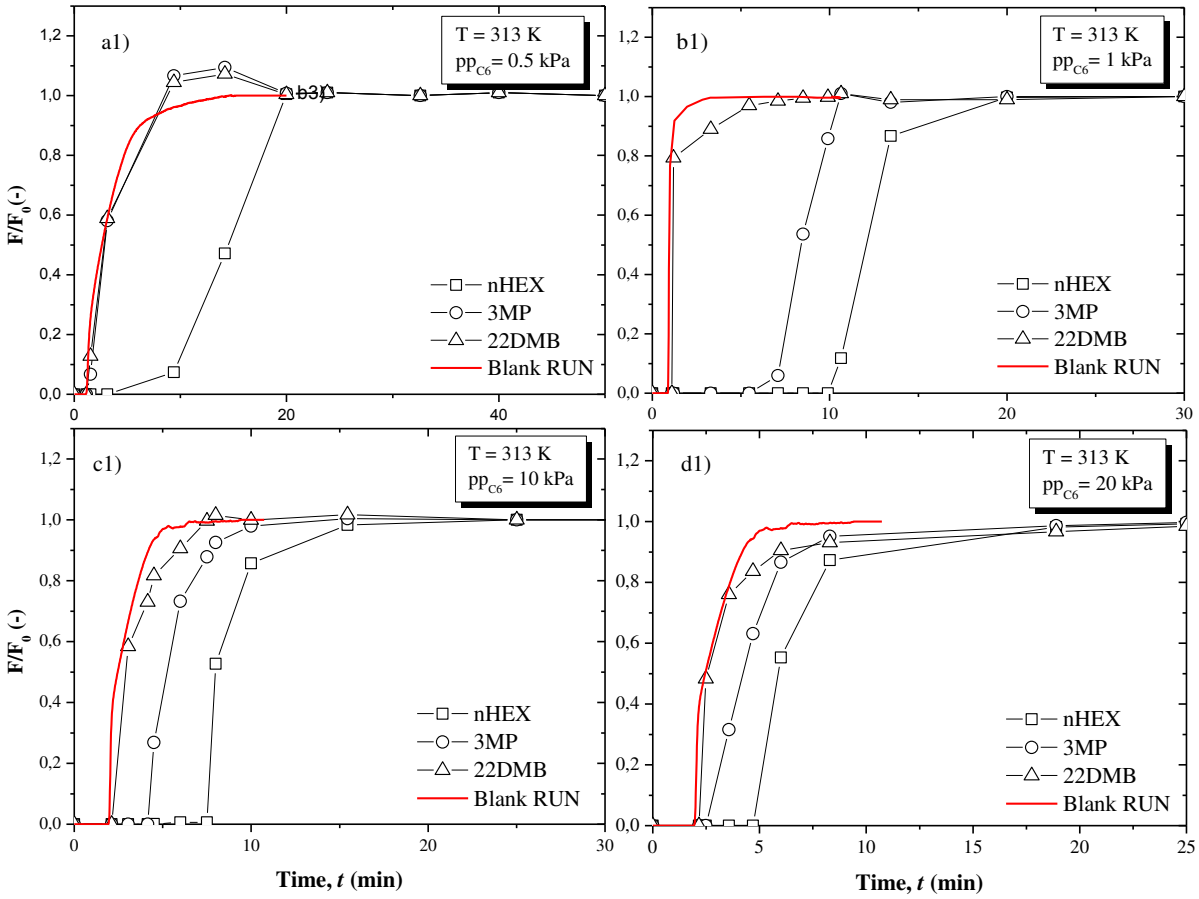

Figure 5.9 - Ternary breakthrough curves 22DMB/3MP/*n*HEX in MIL-53(Fe)–$(CF_3)_2$ at 313 K. (a1) pp = 0.5 kPa; (b1) pp =1 kPa; (c1) pp = 10 kPa and (d1) pp = 20 kPa.

Moreover, at a very low partial pressure the same occurs for 3MP. Table 5.1 shows that the amounts adsorbed of *n*HEX and 3MP are reasonable being in the order of 4 wt% for *n*HEX and around 3 wt% for 3MP. Fig. 5.10 shows the same data 373 K (Fig. 5.10b2 and c2) and 423 K (Fig. 5.10b3 and c3).

The ternary results at 313 K suggest that MIL-53(Fe)–$(CF_3)_2$ can be used as molecular sieve to separate linear *n*HEX and mono branched 3MP from the respective di-branched isomer 22DMB predominantly at partial pressures of 1 kPa at 313 K. This indicates that this solid exhibits a molecular sieve effect for 22DMB relatively to the other hexane isomers which has never been reported so far. From Fig. 5.10, one can point out that the increase of temperature decreases significantly the degree of separation between the compounds mainly because the material loses its capacity to adsorb the mono and linear hexane isomers considering their

concentration profiles that almost match the profile of the blank run experiments. This might be a major drawback for practical applications based on this hybrid solid.

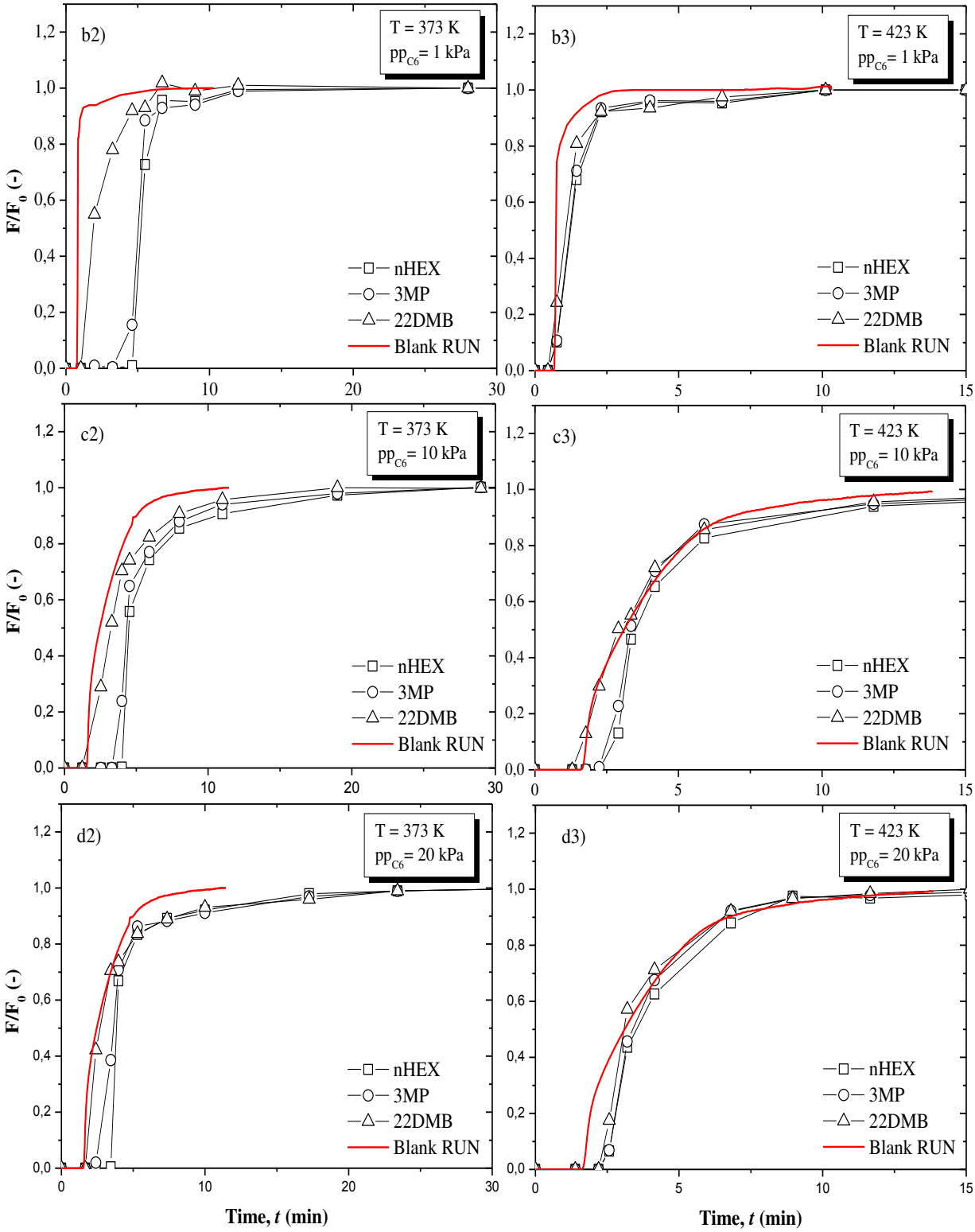

Figure 5.10 - Ternary breakthrough curves 22DMB/3MP/nHEX in MIL-53(Fe)–$(CF_3)_2$ at 373 and 423K. (b2) pp = 1 kPa, T = 373 K; (b3) pp = 1 kPa, T = 423 K; (c2) pp = 10 kPa, T = 373 K; (c3) pp = 10 kPa, T = 423 K; (d2) pp = 20 kPa, T = 373 K; (d3) pp = 20 kPa, T = 423 K;

Binary Mixtures 3MP/22DMB

In light of previous results and in order to check if material is also able to discriminate between di-branched 22DMB and mono-branched 3MP in a binary mixture, a set of breakthrough experiments with equimolar binary mixtures 22DMB/3MP was realized.
Two different sets of experiments were carried out: i) at a low partial pressure of the isomers of 1 kPa; ii) at a higher partial pressure of the isomers of 20 kPa. These set of experiments was repeated at three different temperatures: 313, 373 and 423 K. The experimental conditions are recorded in Table 5.3.

Table 5.3 - Experimental conditions and adsorbed amounts of binary mixture (3MP/22DMB) in MIL-53$(CF_3)_2$.

Run	T (K)	Helium flow rate (mL(STP).min^{-1})	Mixture pressure (kPa)	m_{ads} (mg)	Partial loading (g.100g$_{ads}^{-1}$)		Total loading (g.100g$_{ads}^{-1}$)
					22DMB	3MP	Total
MIL-53_a1	313	36.8	1	276	0.02	1.3	1.3
MIL-53_a2	373				0.07	0.8	0.9
MIL-53_a3	423				0.1	0.2	0.3
MIL-53_b1	313	9.2	20		1.6	3.8	5.4
MIL-53_b2	373				0.2	1.6	1.8
MIL-53_b3	423				0.2	1.5	1.7

The binary breakthrough curves (Fig. 5.11) show again a molecular sieve effect between the di-branched 22DMB and the mono-branched 3MP at 313 K. However this set of experiments shows that the molecular sieve effect (separation) is also clearly observed at 373 K with a difference of elution times of around 5 min at the low partial pressure of 1 kPa (Fig. 5.11a2). At 423 K, Fig. 5.11a3 and b3 show that the capacity of the material to adsorb 3MP is practically negligible, which is in accordance with the results from the previous ternary experiments.

These findings are the first in literature showing a molecular sieve effect between a di-branched (22DMB) and a mono-branched (3MP) paraffins and are of importance in octane enhancement technologies due to the differences in the octane number of 22DMB (RON 91.8) and 3MP (RON 74.5)

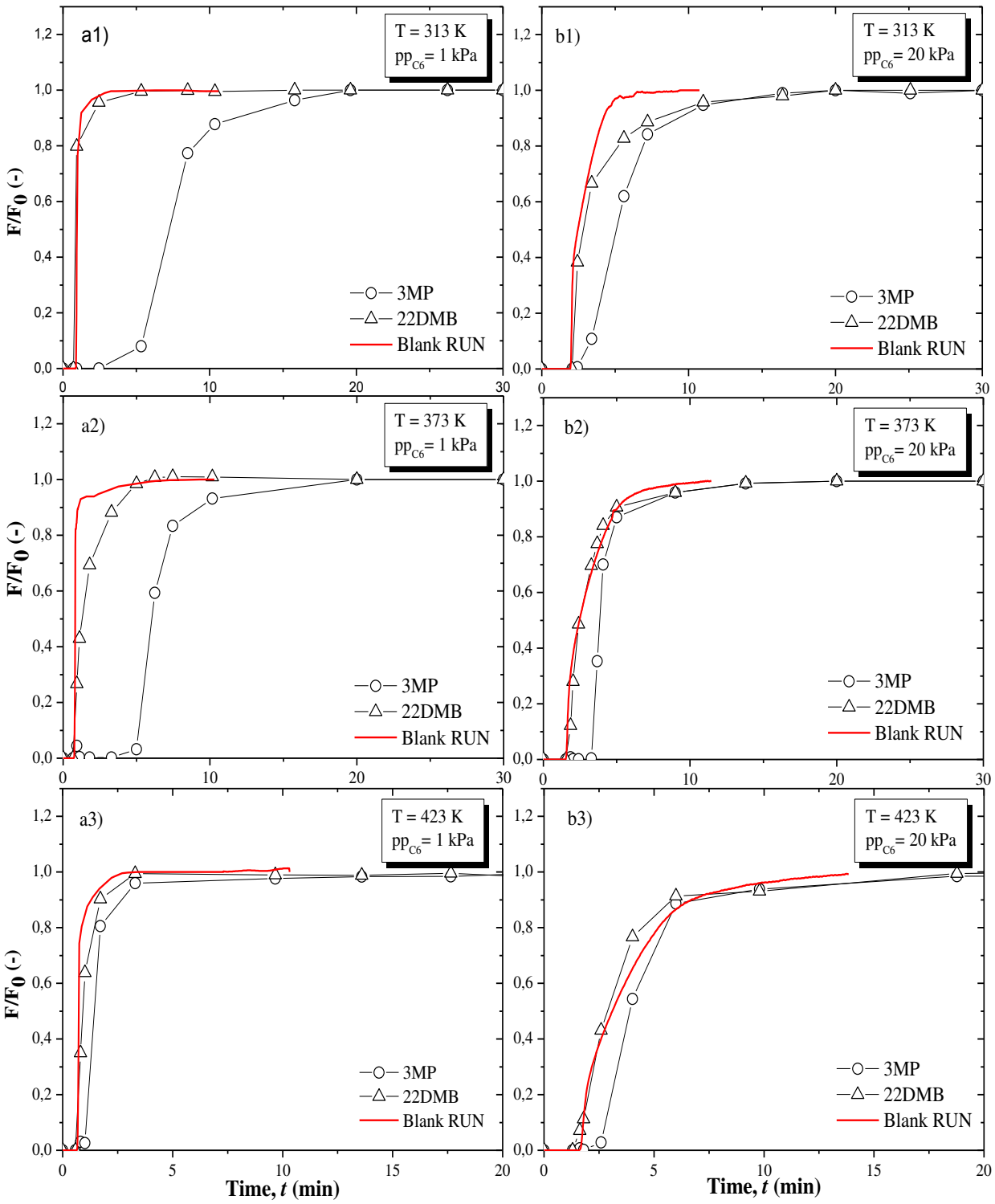

Figure 5.11 - Binary breakthrough curves of the hexane isomers (22DMB/3MP) in MIL-53(Fe)–$(CF_3)_2$ at 1 and 20kPa. (a1) pp = 1 kPa, T = 313K; (b1) pp = 20 kPa, T = 313 K; (a2) pp = 1 kPa, T = 373 K; (b2) pp = 20 kPa, T = 373 K, (a3) pp = 1 kPa, T = 423 K; (b3) pp = 20 kPa, T = 423 K.

Binary Mixtures nHEX/22DMB

A set of binary experiments with equimolar mixtures of 22DMB/*n*HEX at similar conditions of the ones performed for the binary mixture 22DMB/3MP was also performed. The

experimental conditions are recorded in Table 5.4. Fig. 5.12 shows the breakthrough curves where it can be seen also the complete separation between 22DMB and *n*HEX at the low temperature of 313 K (Fig. 5.12a1 and b1).

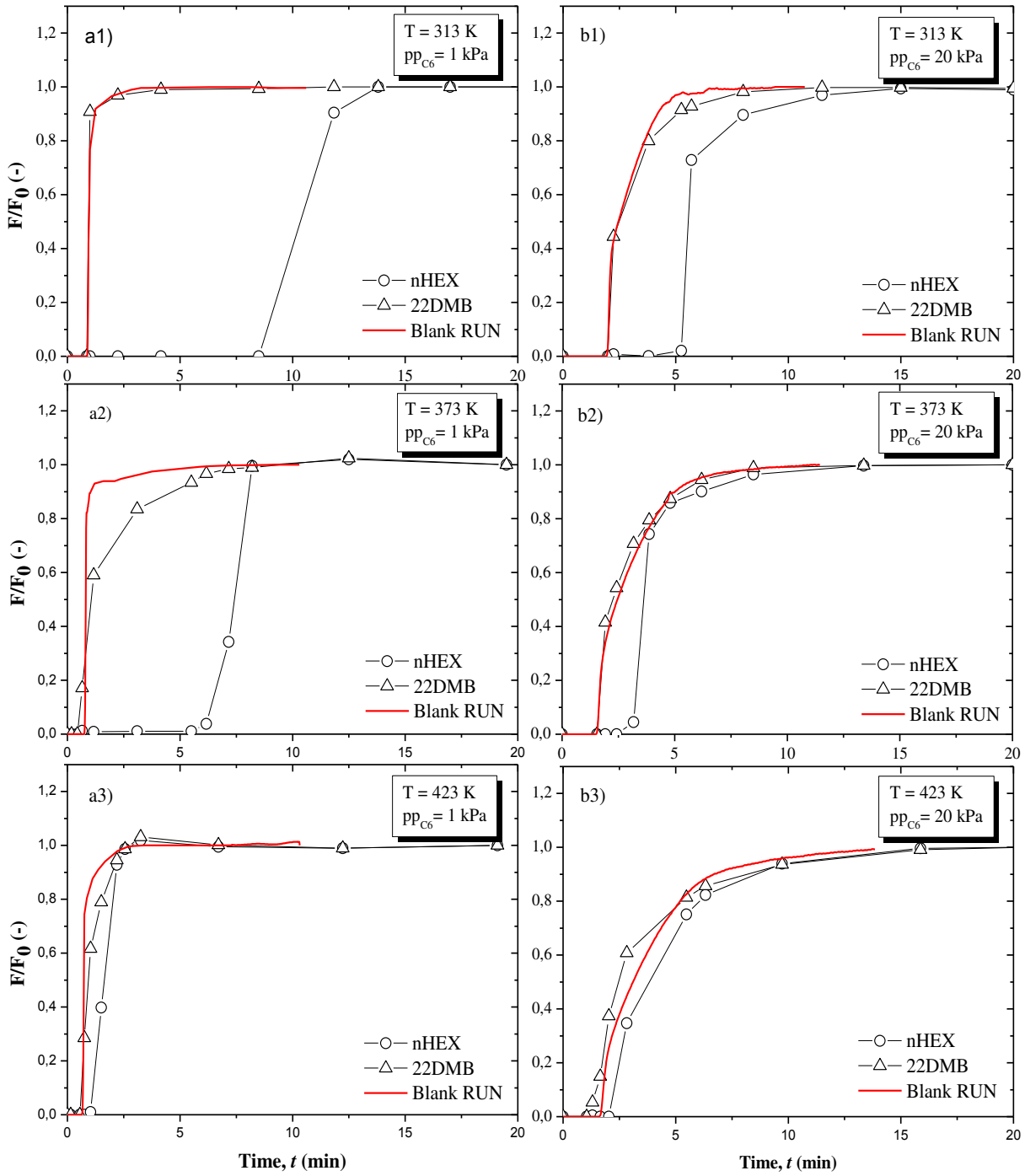

Figure 5.12 - Binary breakthrough curves of the hexane isomers (*n*HEX/22DMB) in MIL-53(Fe)-$(CF_3)_2$ at 1 and 20kPa. (a1) pp = 1 kPa, T = 313 K; (b1) pp = 20 kPa, T = 313 K; (a2) pp =1 kPa, T=373K; (b2) pp = 20 kPa, T = 373K, (a3) pp = 1 kPa, T = 423K, (b3) pp = 20 kPa, T = 423 K.

At higher temperature (373 K) Fig. 5.11a2 shows also a significant time difference in the elution times between 22DMB and *n*HEX. As the temperature further increases (Fig. 5.12),

the material loses again rapidly capacity in adsorbing *n*HEX since the elution time of the compounds is similar to the blank experiments (red line). This result is also interesting but for octane enhancement technologies, this is not so relevant since ZIF-8 does this task with great efficiency and independent of temperature.

Table 5.4 - Experimental conditions and adsorbed amounts of binary mixture (*n*HEX/22DMB) in MIL-53(CF_3)$_2$.

Run	T (K)	Helium flow rate (ml(STP)/min^{-1})	Mixture pressure (kPa)	m_{ads} (mg)	Partial loading (g.100g$_{ads}^{-1}$)		Total loading (g.100g$_{ads}^{-1}$)
					22DMB	*n*HEX	Total
MIL-53_a1	313	36.8	1	276	0.01	1.5	1.5
MIL-53_a2	373				0.1	0.8	0.9
MIL-53_a3	423				0.04	0.12	0.2
MIL-53_b1	313	9.2	20		0.4	4.4	4.8
MIL-53_b2	373				0.2	1.7	1.9
MIL-53_b3	423				0.2	1.0	1.2

5.2.3. MIL-53(Fe)–2CH_3

5.2.3.1. Experimental Section

Synthesis of MIL-53(Fe)–2CH_3

To assess the role of the CF_3 groups over the separation of hexane isomers, another functional solid bearing CH_3 groups instead of CF_3 ones was prepared. MIL-53(Fe)–2CH_3 or [$Fe(OH)C_6H_2(CH_3)_2(CO_2)_4$] was synthesized and characterized in the ILV. The synthesis consisted on the mix of 1.94 g of 2,5-dimethylterephthalic acid (1mmol, synthesized by Dr. Patricia Horcajada, ILV) and 3.54 g of iron(III) perchlorate hydrate (1mmol, Sigma-Aldrich, 99 %), diluted in 50 mL of N, N dimethylformamide, (DMF, Carlo Erba, 99.7 %). Finally, 1mL of hydrofluoric acid solution (HF, 5M) was added into the blend, placed in a 125 mL Teflon-lined steel autoclave (Fig. 5.13a), stirred for 15 min and heated at 423 K during 24 hours. The resulting product (Fig. 5.13b) was filtered at room temperature. The as-synthesized yellow material in their powdered form was of 1.54g.

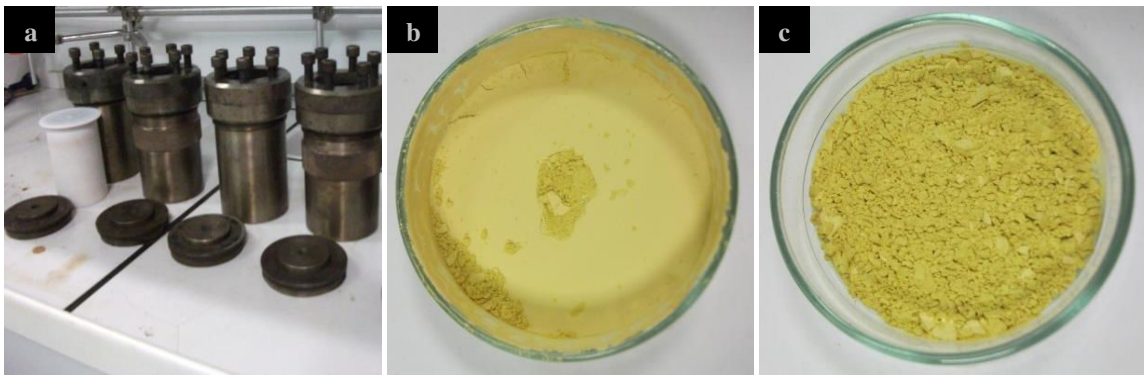

Figure 5.13 - (a) Teflonlined steel autoclave of 125 mL for MIL-53(Fe)–2CH3 synthesis; (b) Sample of UiO-66(Zr)–Br as-synthesized, (c) Final product after activation.

The as-synthesized solid was first washed overnight with around 200 mL of DMF (Carlo Erba, 99.7 %) under vigorous stirring in order to remove the free remaining 2-dimethylterephthalic acid and after filtrated. After that, it washed overnight with around 200 mL of methanol for to remove the DMF from the pores and after filtrated. Finally, the solid was kept overnight at 373 K to eliminate all methanol and finish the activation process. Between each wash it was made infra-red analyses for to evaluate the molecules removing. The final amount of MIL-53(Fe)–$2CH_3$ was of 1.46 g, which corresponds to a yield of 95 % (Fig. 5.13c).

X-Ray Powder Diffraction

With the aim to investigate the flexible character of the MIL-53(Fe)–$2CH_3$ material, its pore opening was first studied XRPD after the suspension of the dry solid in several solvents with different physicochemical properties. Fig. 5.14 shows the XRPD patterns of the solid after impregnation with dimethylformamide (DMF; red) or ethanol (green) in comparison with its anhydrous (black) or hydrated form (blue). The variation of the position of the main peaks of the patterns indicates the different pore opening (structure) MIL-53(Fe)–$2CH_3$, evidencing the breathing effect with important changes in the cell parameters. The unit cell parameters were determined by X-ray powder pattern indexing followed by a structure pattern profile refinement using respectively the DICVOL [14] and FULLPROF [15, 16], softwares from the WINPLOTR suite.

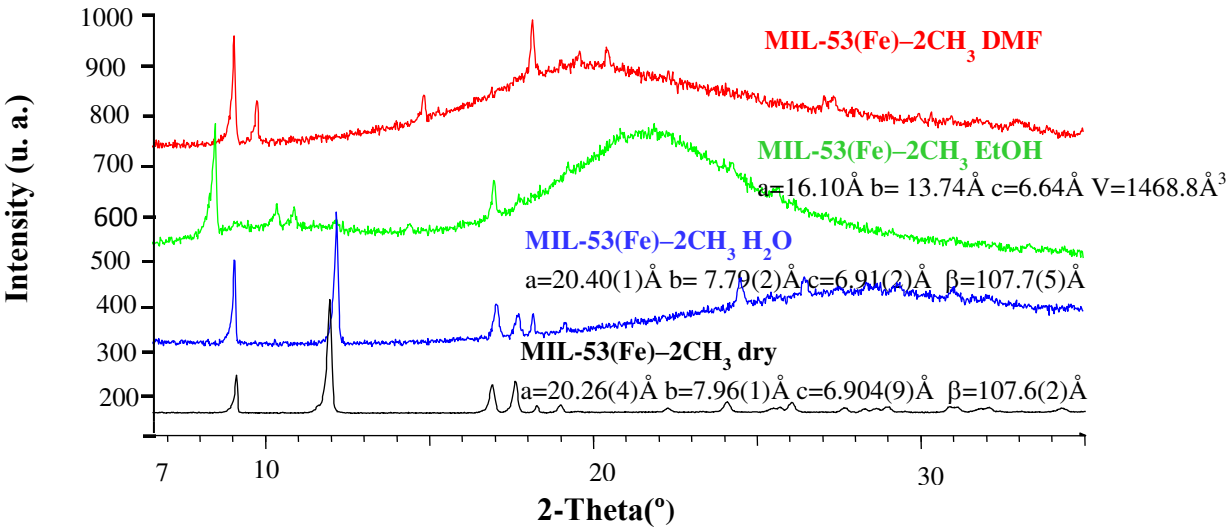

Figure 5.14 - X-Ray powder diffractions of the sample MIL-53(Fe)–$2CH_3$ after treatment with DMF (red), Methanol (green) and also in their dry (black) or hydrated form (blue). Equipment Siemens, D5000.

The anhydrous form (empty pores) corresponds to the more contracted form of the material, when the pores are totally closed. Noteworthy, the presence of two methyl groups on the aromatic ring of the organic ligand of MIL-53(Fe)–$2CH_3$ avoids the total contraction of the framework due to the steric hindrance of these voluminous functional groups. This is in agreement with the larger cell volume of the dry from of MIL-53(Fe)–$2CH_3$ (~1060 $Å^3$) in comparison with the non-functionalized MIL-53(Fe) solid (~ 900 $Å^3$). In contact with water (or at room temperature), the hydrated form of MIL-53(Fe)–$2CH_3$ shows a similar structure than the anhydrous form (~ 1055 $Å^3$). This is probably due to the presence of enough free volume in the contracted form where few water molecules (due to the hydrophobic character of this solid; see TGA) can be located without perturbing the structure in presence of ethanol, the pores completely open leading to the more open form with a cell volume of around 1470 $Å^3$, in agreement with the cell volume of open form of other functionalized MIL-53(Fe) [6].

Finally, it was not possible to refine the structure of the MIL-53(Fe)–$2CH_3$ containing DMF. However, if one takes into account the flexibility of other functionalized MIL-53(Fe), [6], the XRPD patterns are compatible with an intermediate opening between the contracted and the open structure. It was also of interest to study the behaviour of the material as function of the temperature through X-ray powder thermo diffraction. Fig. 5.15 shows the evolution of the X-ray powder thermo diffraction with an increase of temperature from the room temperature (~ 298 K) to 523 K and the reverse way for to test the stability of the MOF under high temperatures.

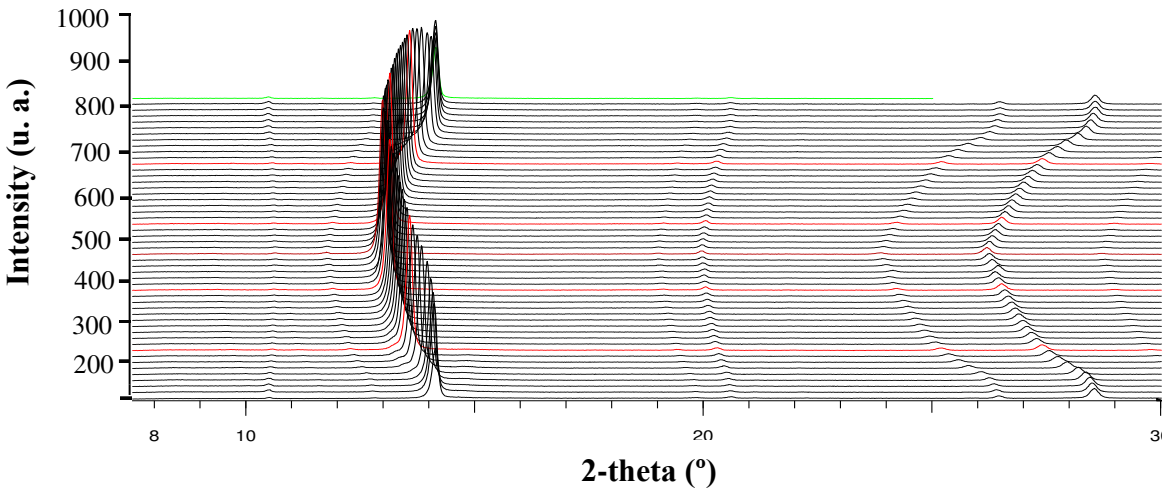

Figure 5.15 - X-Ray powder thermo diffraction rehid of the sample MIL-53(Fe)–2CH_3 in their hydrated form for 298 K- 573 K and after that 523 K - 298 K. Scale of temperature with the increment of 373 K (red). Equipment Siemens, D5000, X-ray diffractometer KV = 20, mA = 5.

Fig. 5.16 shows the evolution of the X-Ray powder thermo diffraction of the sample MIL-53(Fe)–2CH_3 in their form more open (with DMF) for 298 K - 673 K. These data demonstrate the flexible but reversible flexible character of this solid. This solid also possesses a satisfying thermal stability.

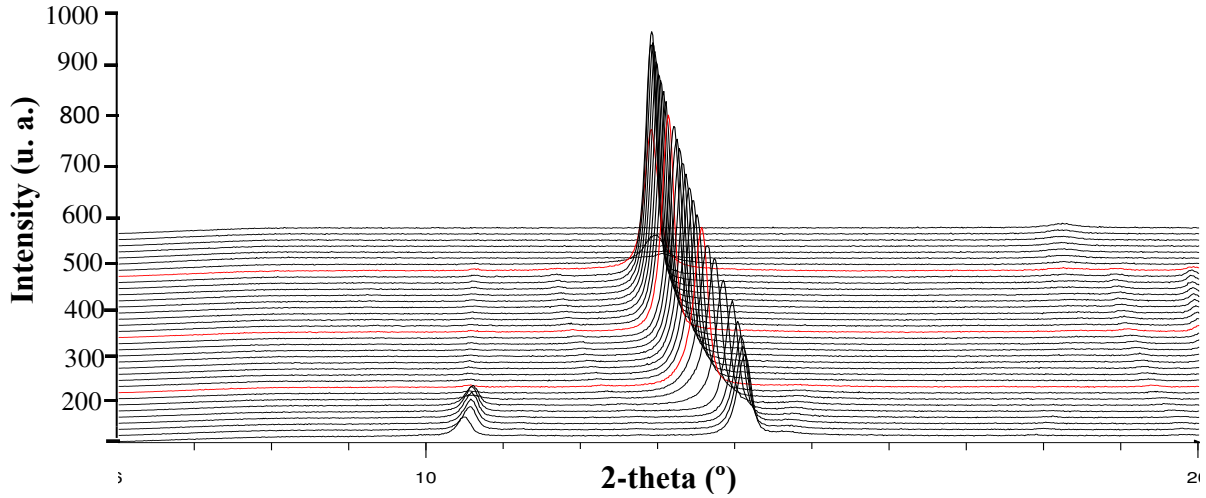

Figure 5.16 - X-Ray powder thermo diffraction of the MIL-53(Fe)–2CH_3 for 298 K –673K. Scale of temperature with the increment of 373 K (red). Equipment Siemens, D5000, X-ray diffractometer KV = 20, mA = 5.

Infra-Red (IR) spectroscopy analyses

Fig. 5.17 shows the infrared diffractogram of MIL-53(Fe)–2CH_3 after treatment with DMF (red), Methanol (green), in its dry (black) or hydrated form (blue). The disappearing of the vibrational band around the value 1714 cm^{-1} corresponds to a removal of the free acid. The

band around 1653 cm^{-1} that corresponds to DMF is reduced albeit still present despite the activation steps.

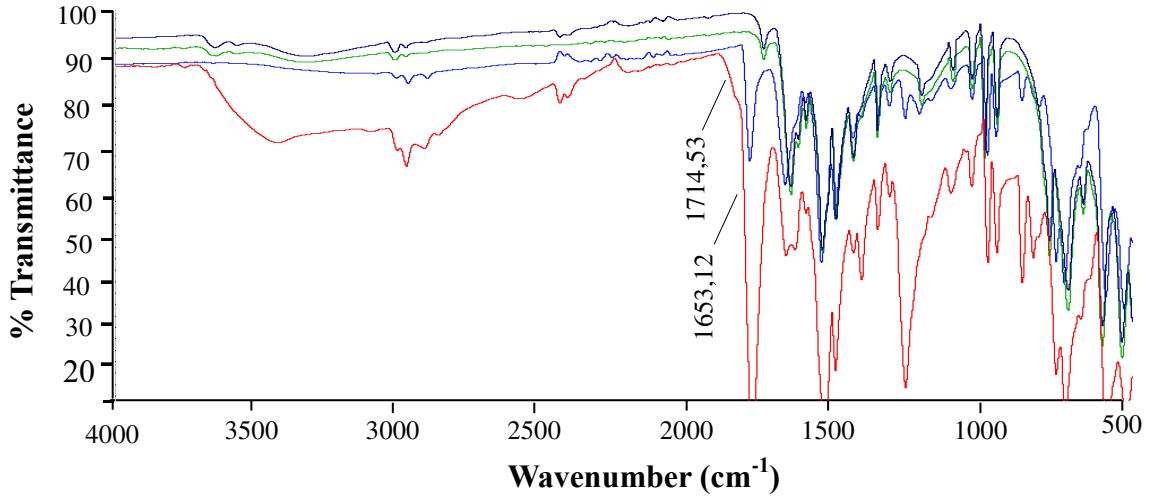

Figure 5.17 - Infra-Red analysis of the sample MIL-53(Fe)–$2CH_3$ after treatment with DMF (red), Methanol (green) and also in their dry (black) or hydrated form (blue). Equipment Nicollet spectrometer, KBr pellet.

Thermogravimetric Analysis (TGA)

In order to study its thermal stability, 6.086 mg of MIL-53(Fe)–$2CH_3$ was heated from 303 K to 873 K at 275 °K.min^{-1} (Oxygen at 20.0 ml.min^{-1}). Fig. 5.18 shows the TGA of MIL-53(Fe)-CH_3 with a first weight loss (9.26 wt%) at around 373 K which corresponds to the solvent departure and a second weight loss (60.6 wt%) at around 573 K related to the combustion of the organic linker. These losses are in agreement with the theoretical values.

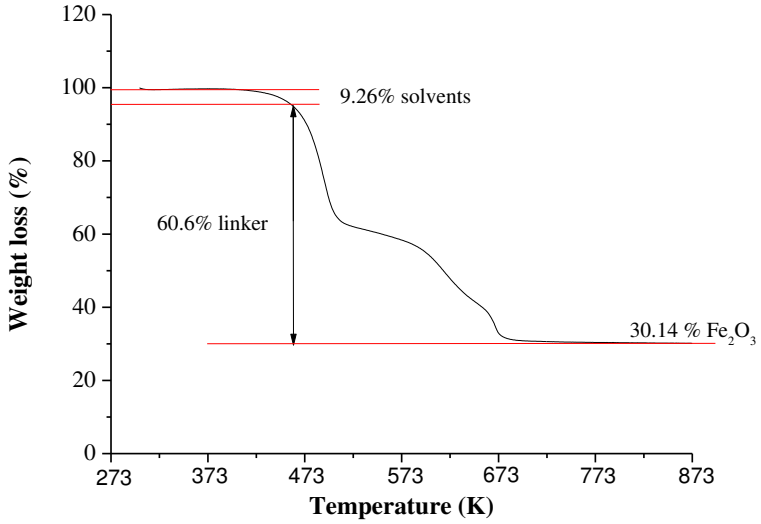

Figure 5.18 - Thermogravimetric analysis of MIL-53(Fe)–$2CH_3$ activated under atmospheric pressure (Heating rate of 275 K.min^{-1}; 6.086 mg of solid). (PerkinElmer, STA 6000).

Nitrogen adsorption measurement

It was determined the Nitrogen adsorption of the material at 77 K in order to obtain their surface area capable to adsorption. Before adsorption measurement, the solid was submitted to a calcination process (under vacuum at 423 K during 2 hours, Belsorp Belsprep, BEL Japan) for solvents elimination. So, the adsorption measurement corresponds to an approximation of the total surface area due their contracted form. Fig. 5.19 shows the N_2 adsorption isotherm of the MIL-53(Fe)–2CH_3. The BET (S_{BET}) and Langmuir (S_{Lang}) surface areas obtained were 12 and 14 $m^2.g^{-1}$, respectively.

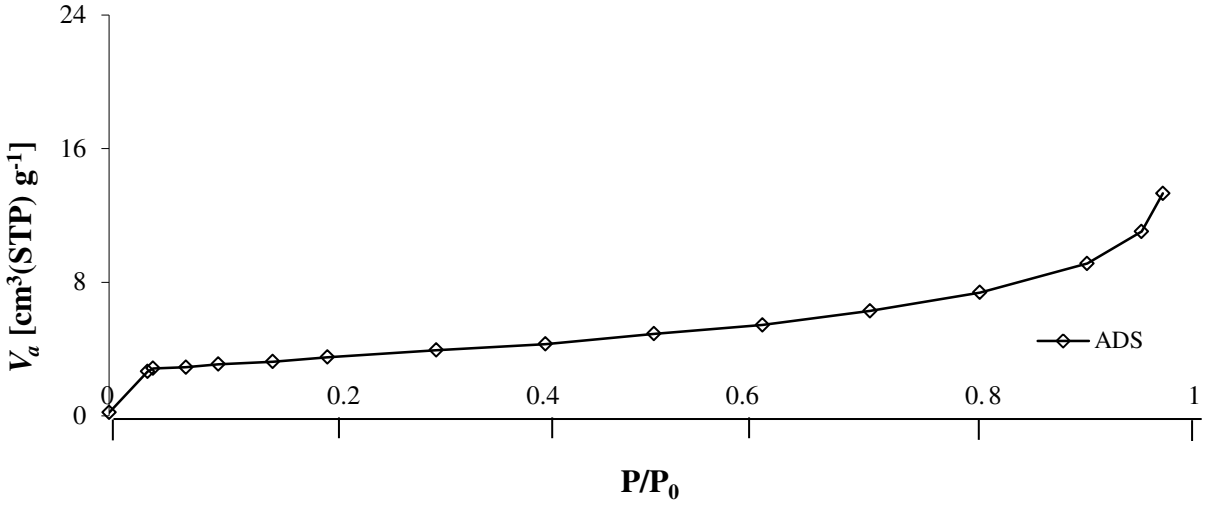

Figure 5.19 - Nitrogen adsorption isotherm of MIL-53(Fe)–2CH_3 at 77 K (P_0 = 1 atm) using a BEL Japan equipment, BELSORP Mini.

The pore volume was 0.021 $cm^3.g^{-1}$, which it is notable their few values due to their contracted form.

5.2.3.2. Results and Discussion

To test the MIL-53(Fe)–2CH_3 material, screening studies of hexane isomers were performed. The sample was first activated under vacuum (10 kPa) during 15 hours at 423 K (particles in their powdered form with diameter around 0.03 mm). Thereafter the solid was packed (540 mg) in a stainless steel column (diameter = 4.3 mm, length = 80 mm) for the screening studies. These were performed with a ternary equimolar mixture *n*HEX/3MP/22DMB, at a temperature of 313 K and at two partial pressures: low (0.5 kPa) and high pressure (10 kPa). The experimental conditions are reported in Table 5.5. As the loadings are negligible, they are not reported.

Table 5.5 - Experimental conditions and adsorbed amounts of hexane isomers in MIL-53 (Fe)–$2CH_3$.

Run	*T* (K)	Helium flow rate (mL(STP).min^{-1})	Mixture pressure (kPa)	m_{ads} (mg)	Partial loading (g.100g$_{ads}^{-1}$)			Total loading (g.100g$_{ads}^{-1}$)
					22DMB	3MP	*n*HEX	
2CH3_a1	313	37.3	0.5	540	-	-	-	-
2CH3_b1			10		-	-	-	-

Fig. 5.20 discloses the ternary breakthrough curves 22DMB/3MP/*n*HEX in the MIL-53(Fe)–$2CH_3$ at 0.5 kPa or 10 kPa for 313 K. These breakthroughs demonstrate that the hexane isomers are not adsorbed.

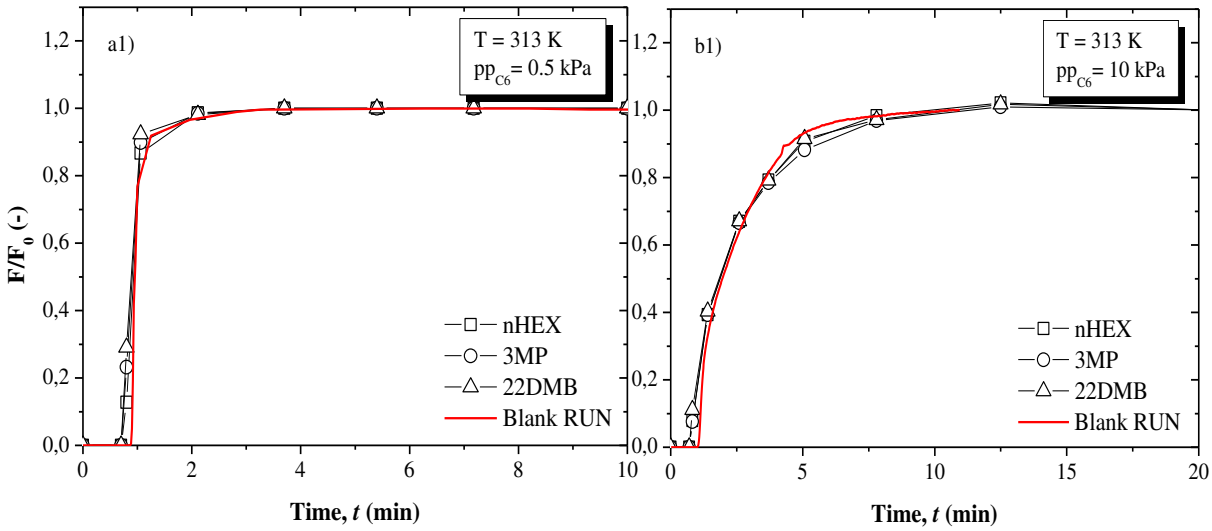

Figure 5.20 - Ternary breakthrough curves 22DMB/3MP/*n*HEX in MIL-53(Fe)–$2CH_3$ (calcination of sample at 423 K). (a1) pp = 0.5 kPa, T = 313 K; (b1) pp = 10 kPa, T = 313 K. Red lines in the figure represent blank runs at the same experimental conditions with the column filled with glass spheres.

In order to determine whether or not the absence of any sorption was due to a degradation of the sample during the activation process, a new sample was activated under milder conditions (353 K, mild vacuum (10 kPa)) during 15 hours and the breakthrough experiments repeated. XRPD and IR spectroscopy have been performed (not shown) using the sample before and after the sorption tests with no apparent degradation of the samples. Once again there is no significant adsorption of hexane isomers (Fig. 5.21).

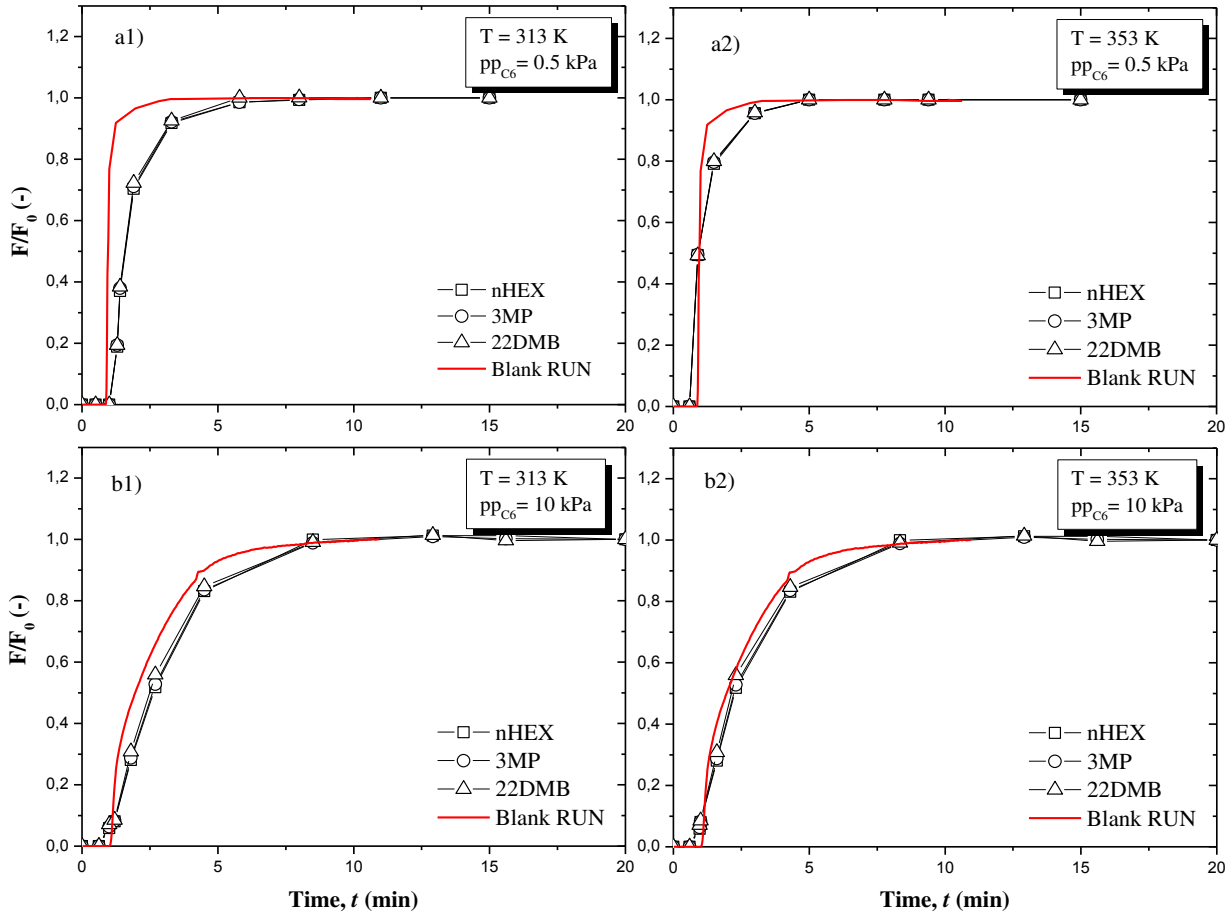

Figure 5.21 - Ternary breakthrough curves 22DMB/3MP/*n*HEX in MIL-53(Fe)–2CH_3 (calcination of sample at 353 K). (a1) pp = 0.5 kPa, T = 313 K; (a2) pp = 0.5 kPa, T = 353 K; (b1) pp = 10 kPa, T = 313 K, (b2) pp = 10 kPa, T = 353 K. Red lines in the figure represent blank runs at the same experimental conditions with the column filled with glass spheres.

Table 5.6 shows the experimental conditions used in the breakthrough experiments. Indeed, as the cell volume of the narrow form is rather low (1060 Å^3) compared to the one of the –2CF_3 form (> 1300 Å^3), the initial pore size is probably here not large enough to accommodate any of the alkane molecules under the conditions used here. In addition, we observed previously a pore reopening when dispersing the phase in polar liquids. However, we assume that due to rather strong intra-framework VdW interactions (CH_3 groups) within the narrow pores form, the dried MIL-53(Fe)–2CH_3 structure is slightly more difficult to reopen using apolar guests that bring host-guest interactions probably not sufficient to break the intra-framework VdW bonds that stabilize the narrow pore form.

Table 5.6 - Experimental conditions and adsorbed amounts of hexane isomers in MIL-53 (Fe)–$2CH_3$.

Run	*T* (K)	Helium flow rate (mL(STP).min^{-1})	Mixture pressure (kPa)	m_{ads} (mg)	Partial loading (g.100g_{ads}^{-1})			Total loading (g.100g_{ads}^{-1})
					22DMB	3MP	*n*HEX	
MIL53_2CH_3_a1	313	22.7	0.5	338	0.03	0.03	0.03	0.09
MIL53_2CH_3_a2	353				0.01	0.01	0.01	0.02
MIL53_2CH_3_b1	313		10		0.91	0.98	0.92	2.81
MIL53_2CH_3_b2	353				0.48	0.55	0.55	1.59

5.3. The case of the flexible MIL-88B(Fe)-2CF_3

MIL-88B series are another series of isoreticular highly flexible 3D MOFs. They exhibit a highly flexible character, in the presence of liquids or vapours, with a reversible swelling between 80 and 230 % in cell volume. These are metal(III) dicarboxylate solids (M=Fe, Cr) with a general formula of $M_3O(L)_3(H_2O)_2(X)$, with L=linear dicarboxylate and X=anion [17]. These samples are based on various organic spacers (fumarate: MIL-88A, muconate: MIL-89, terephthalate: MIL-88B, naphthalene dicarboxylate: MIL-88C, byphenyl dicarboxylate: MIL-88D....) [18]. In addition, as for the MIL-53 solids, these can be functionalized with several functional groups such as NH_2, Cl, Br and NO_2 or CH_3, CF_3 which allows to tune their polarity as well as a fine tuning of their flexible character. Fig. 5.22 shows a typical trimer of iron (III) octahedra and a typical functionalized MIL-88B structure type.

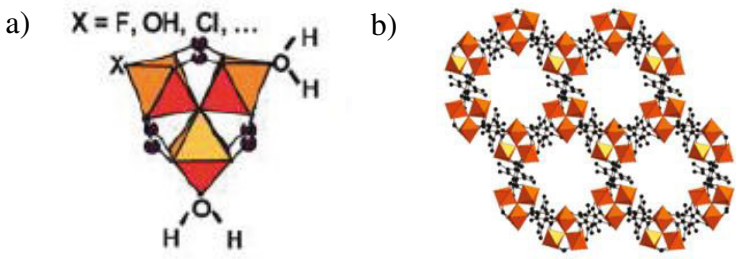

Figure 5.22 - (a) Oxocentered trimer of iron(III) octahedra and (b) view of the crystal structure of the open form of MIL-88B–2CF_3 [17].

Interestingly, the functionalized MIL-88B(Fe)–2CF_3 solid, based the modified organic linker terephthalic acid H_2BDC-$(CF_3)_2$ leads to a structure with moderate thermal stability (573 K) [17] but possessing a permanent porosity to nitrogen of 335 $m^2.g^{-1}$ (77 K) (Fig. 5.22b) due to the bulky functional groups (CF_3) that limit the contraction upon desolvation of the structure. As comparison, if the unit cell volumes of all the open form of MIL-88B(Fe)-X solids is close

to 3400 $Å^3$, the non-functionalized MIL-88B(Fe) solid exhibit a 1500 $Å^3$ volume in its dried state while the dried form of MIL-88B(Fe)–$2CF_3$ exhibit a cell volume of 2350$Å^3$ with cell parameters of a = 12.1 Å and c = 18.5 Å [17].

5.3.1. Experimental Section

5.3.1.1. Synthesis of MIL-88B(Fe)–$2CF_3$

MIL-88B-$2CF_3$ or $Fe_3O(OH)(H_2O).2[C_6H_2(CF_3)_2(CO_2)_2]_3$ was synthesized at the gram scale and characterized at ILV [16]. The synthesis consisted on the mixture of 755 mg of perfluorterephthalic acid (2.5 mmol, synthesized on ILV [17] and 675 mg of iron (III) chloride hexahydrate (2.5 mmol, Alfa Aesar, 98 %) diluted with 25 mL of ethanol (738.7 mmol, VWR, 99.9 %) and were placed in a Teflon-lined vessel and heated on the microwave (CEM) through a support module HP-500 plus under high pressure at 373 K for 5min (heating rate 276.33 $K.s^{-1}$) at 400W (Fig 5.23a and b). Finally, was recovered an orange solid by centrifugation (Fig. 5.23c). In each synthesis was obtained around 210 mg of solid. It was made six equal syntheses for to improve the scale originating 1.3 g of solid.

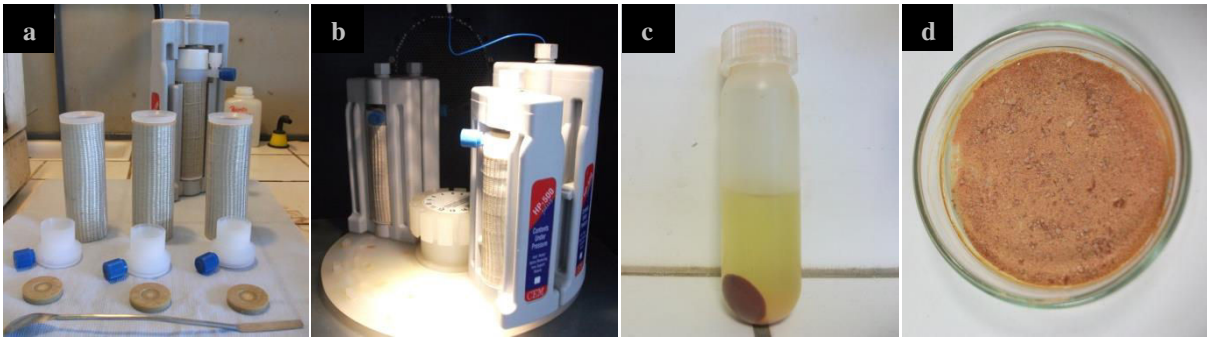

Figure 5.23 - (a) Teflonlined vessel. (b) Vessel supports module HP-500 plus with the Teflon-lined vessels inside the microwave CEM. (c) Solid recovers after centrifugation. (d) Final orange product of MIL-88(Fe–$2CF_3$.

The as-synthesized solid was first washed overnight with ca. 150 mL of acetone under vigorous stirring during 4h at ambient temperature in order to remove the free perfluorterephthalic acid by centrifugation. After infra-red analysis without perfluorterephthalic acid, it was complete the activation of solid and was kept overnight at 373 K to remove adsorbed acetone. The final amount of MIL-88B–$2CF_3$ solid was of 1.2 g, which corresponds to a yield of 92 % (Fig. 5.23d).

X-Ray Powder Diffraction (XRPD) analysis

Fig. 5.24 shows the XRPD of the sample MIL-88B(Fe)–2CF_3 as-synthesized (red), and the sample after activation (black). This comparison confirms the flexible character due to the change in Bragg peak positions with a shift towards high angle after drying in agreement with a cell volume contraction.

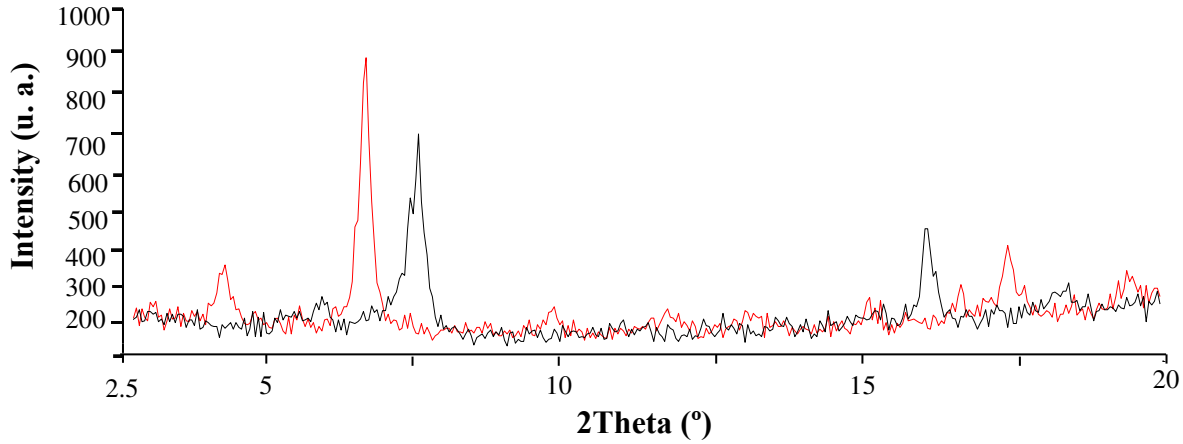

Figure 5.24 - XRPD of MIL-88B(Fe)-2CF_3 as-synthesized (red), after activation (black) (Siemens diffractometer D5000 (Cu Kalpha1 radiation λ= 1.54056 Å).

Infra-Red (IR) spectroscopy analyses

Fig. 5.25 shows the Infra-Red analyses of MIL-88B(Fe)–2CF_3 as-synthesized (red) and after activation (black). The band around 1707 cm^{-1} corresponds to the free acid but disappear after activation (blue). The band at around 1620 cm^{-1} corresponds to free water.

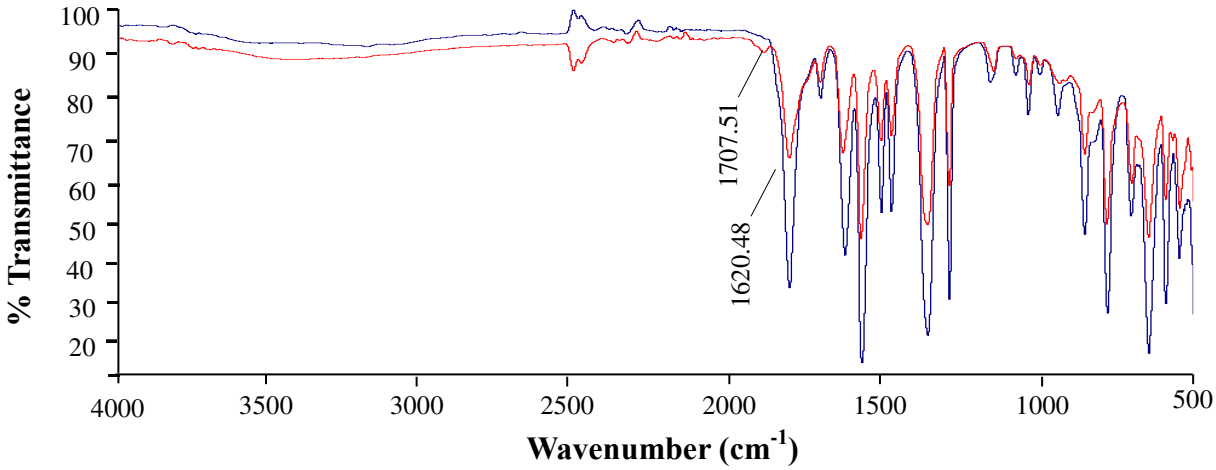

Figure 5.25 - Infra-Red diffractogram of MIL-88B(Fe)-2CF_3 as-synthesized (red) and after activation (black). Nicollet, 6700 Thermo scientific

Thermogravimetric Analysis (TGA)

Fig. 5.26 shows the TGA of MIL-88B-2CF_3. The first weight loss (6.4 wt%) corresponds to the removal of the free solvent and the 9.3 wt% of weight loss might correspond to the departure of coordinated water. The weight loss around 523 K (63.3 wt%) is related to the combustion of the organic linker. The overall experimental weight loss corresponds to the theoretical value (63.3 % vs 65 %).

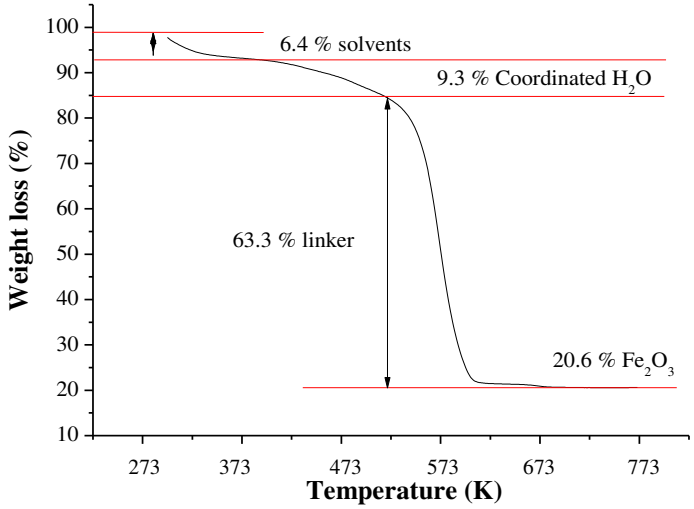

Figure 5.26 - Thermogravimetric analysis of MIL-88B-2CF_3 activated under atmospheric pressure (Heating rate of 275 $K.min^{-1}$; 6.021 mg of solid). (PerkinElmer, STA 6000).

Nitrogen adsorption measurement

Fig. 5.27 shows the N_2 adsorption isotherms of MIL-88B(Fe)–2CF_3. The sample outgassed at 423 K under vacuum during 2 hours shows a BET surface area of 335 $m^2.g^{-1}$.

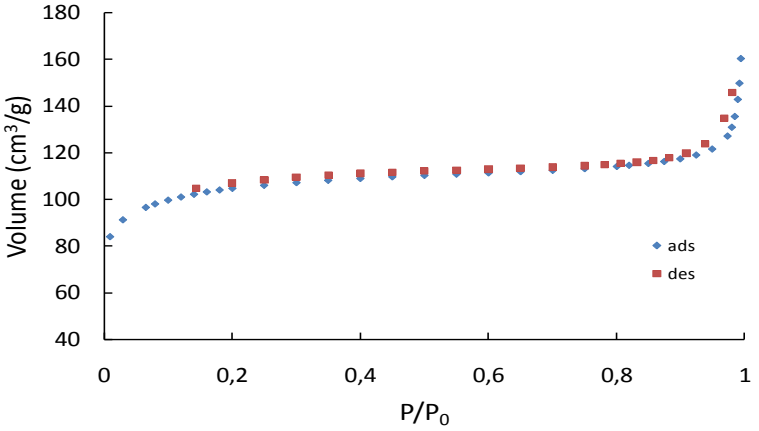

Figure 5.27 - Nitrogen adsorption isotherm of activated MIL-88B(Fe)–2CF_3 at 77 K (P_0 = 1 atm) (outgassed at 423 K during 5 h (note: if the outgassing time increases, the specific surface of this compound decrease). (Belsorp Belsprep, BEL Japan).

5.3.2. Results and Discussion

Again breakthrough experiments were performed to test this material with ternary mixtures: 22DMB/3MP/*n*HEX. Before the studies, the solid was activated under slight vacuum (10 kPa) during 15 hours at 393 K (particles in their powdered form with diameter around 0.03 mm). After activation, the solid was packed (404 mg) in a stainless steel column (diameter = 4.3 mm, length = 80 mm) for the breakthrough experiments.

The experiments were conducted at 313 and 393 K and at 0.5 kPa and 10 kPa. Table 5.7 shows the experimental conditions and adsorbed amounts of the hexane isomers in each run and we observe that for all isomers, the adsorbed amount increases as a function the pressure, with the highest total adsorbed amount being of 6 wt% at 313 K and 10 kPa.

Table 5.7 - Experimental conditions and adsorbed amounts of hexane isomers in MIL-88B–2CF_3.

Run	*T* (K)	Helium flow rate (mL(STP).min^{-1})	Mixture pressure (kPa)	m_{ads} (mg)	Partial loading (g.100g_{ads}^{-1})			Total loading (g.100g_{ads}^{-1})
					22DMB	3MP	*n*HEX	
MIL88_a1	313	23.4	0.5	404	0.1	0.1	0.4	0.6
MIL88_a2	393				-	-	-	-
MIL88_b1	313	9.3	1		1.0	1.3	1.3	3.6
MIL88_b2	393				0.3	0.4	0.4	1.1
MIL88_c1	313	9.3	10		0.8	1.0	4.2	6.0
MIL88_c2	393				0.9	1.1	1.1	3.1

Fig 5.28 compares the ternary breakthrough curves performed at 0.5, 1 and 10 kPa and 313 and 393 K. Blank runs were also performed (curve at red). It can be observed (Fig. 5.28) that all hexane isomers are adsorbed especially at low temperature (313 K) with however a poor degree of separation.

Only at low temperature 313 K and pressure 0.5 kPa, a significant separation between *n*HEX and the other isomers is present. Note also the broadening of the breakthrough profiles suggesting a strong resistance to mass transfer in the framework which could be attributed to a strong interaction of the compounds with the pore walls.

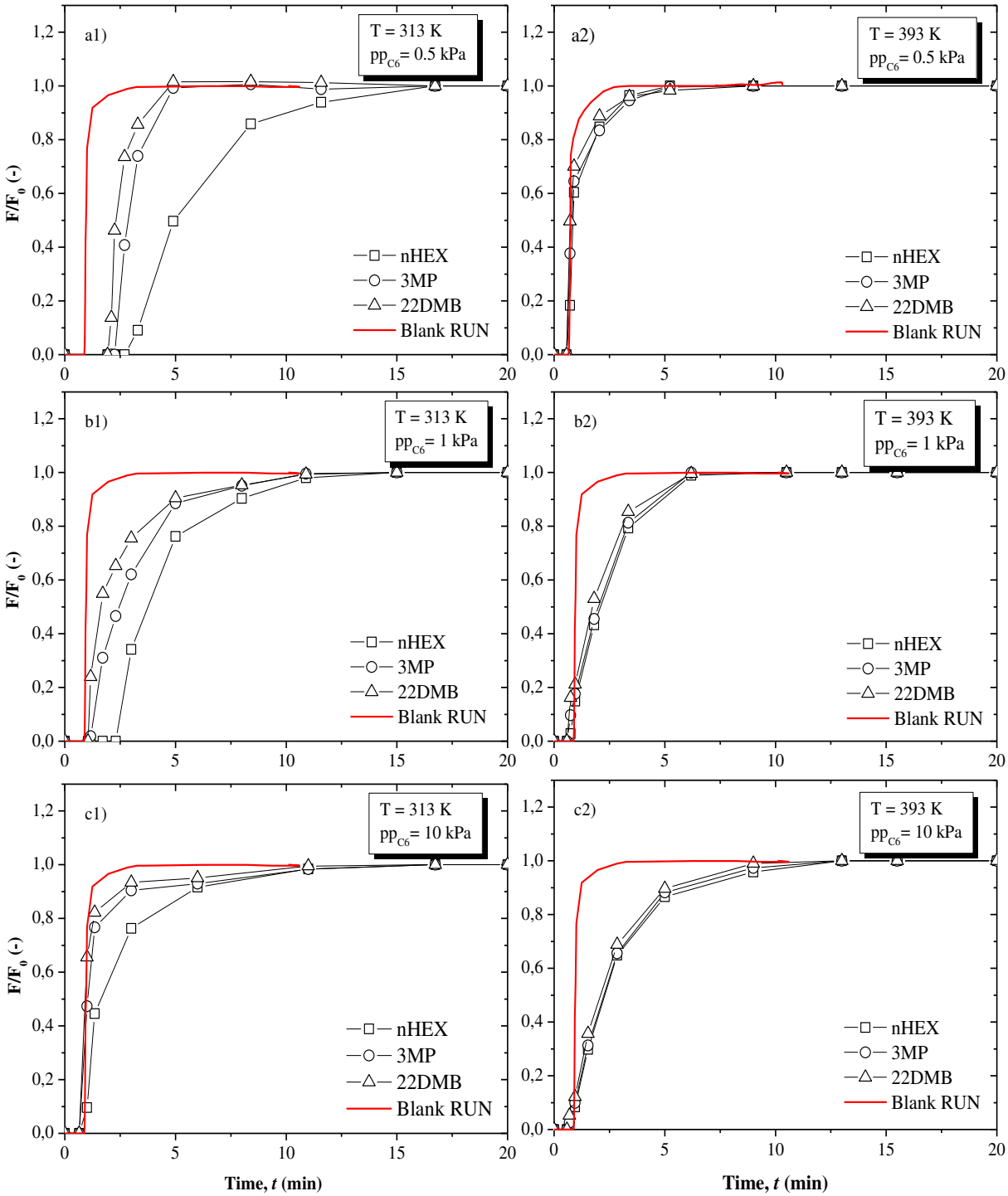

Figure 5.28 - A comparison of experimental breakthrough curves relatively to the sorption of ternary mixtures *n*HEX/3MP/22DMB in MIL-88B–CF_3. (a1) pp = 0.5 kPa, T = 313 K; (a2) pp = 0.5 kPa, T = 393 K. (b1) pp = 1 kPa, T = 313 K; (b2) pp = 1 kPa, T = 393 K, (c1) pp = 10 kPa, T = 313 K; (c2) pp = 10 kPa, T = 393 K. Red lines in the Figure represent blank runs at the same experimental conditions with the column filled with glass spheres.

5.4. Conclusion

Several flexible iron(III) dicarboxylate MOFs of the flexible MIL-53 or its polymorph MIL-88B, bearing or not functionalized groups were synthesized and characterized, such as MIL-53(Fe)-$(CF_3)_2$, MIL-53(Fe)-$2CH_3$ and MIL-88B-$2CF_3$. It was observed that hexane isomers adsorb in the MIL-53(Fe) with amounts around 9 wt% but with no separation.

However and for the first time in this field of research, was evidenced, through the case of the functionalized MIL-53$(CF_3)_2$ solid, a sorbent able to separate the di-branched 22DMB from the linear and mono branched isomers (*n*HEX and 3MP) in both binary and ternary experiments with a molecular sieve effect. The amount adsorbed of *n*HEX and 3MP for the MIL-53$(CF_3)_2$ solid can reach 6 wt%. The separation however becomes less efficient when the temperature increases. Other tests performed using different functionalized solids such as MIL-53(Fe)–$2CH_3$ did not allow any adsorption of hexane isomers while the polymorph MIL88B-$2CF_3$ led to a significant adsorption (6 wt%), similar to the one in MIL-53$(CF_3)_2$, but without any significant degree of separation. Considering the large number of available trivalent cations (Sc, Al, Ga, In, V…), functionalized linkers to build up flexible architectures (MIL-88, MIL-53…), these results pave the way for the use of flexible MOFs for an improved separation of alkane isomers.

5.5. References

1. *S. L. James, Metal-organic frameworks, Chem. Soc. Rev., 32 (2003) 276–288.*

2. *S. K.Ghosh, S. Bureekaew, S. Kitagawa, A Dynamic, Isocyanurate-Functionalized Porous Coordination Polymer, Angew. Chem., 47 (2008) 3403–3406.*

3. *J. Gascon, U. Aktay, D. H.-A. M., G. P. M. van Klink, F. J. Kaptejin, Amino-based metal-organic frameworks as stable, highly active basic catalyst, J. Catal., 261 (2009) 75–87.*

4. *K. Kasai, M. Fujita,* Guest-Dependent Flexible Coordination Networks with Fluorinated Ligands, *Chem.Eur. J., 13 (2007) 3089–3105.*

5. *C. Yang, X. Wang, M. A. Omary, Crystallographic observation of the dynamic gas adsorption sites and thermal expansion in a breathable fluorous metal-organic framework, Angew. Chem, 48 (2009) 2500–2505.*

6. *T. Devic, P. Horcajada, C. Serre, F. Salles, G. M., B. Moulin, D. Heurtaux, G. Clet, A. Vimont et al., Functionalization in Flexible Porous Solids: Effects on the Pore Opening and the Host-Guest Interactions, J. Am. Chem. Soc., 132 (2010) 1127–1136.*

7. *V. Finsy, L. Ma, L. Alaerts, D.E. De Vos, G.V. Baron, J.F.M. Denayer, Separation of CO2/CH4 mixtures with the MIL-53(Al) metal–organic framework, Microporous and Mesoporous Materials 120 (2009) 221–227.*

8. *C. Serre, F. Millange, C. Thouvenot, M. Noguès, G. Marsolier et al., Very Large Breathing Effect in the First Nanoporous Chromium(III)-Based Solids: MIL-53 or CrIII(OH)â{O2C-C6H4-CO2}â{HO2C-C6H4-CO2H}xâH2Oy, J. Am. Chem. Soc. 124 (2002) 13519-13526.*

9. *Y. Liu, J.-H. Her, A. Dailly, A. J. Ramirez-Cuesta, D. A. Neumann and C. M. Brown, Reversible Structural Transition in MIL-53 with Large Temperature Hysteresis, J. Am. Chem. Soc., 130 (2008) 11813–11818.*

10. *T. K. Trung. P. Trens, N. Tanchoux, S. Bourrelly, P.L. Llewellyn, S. Loera-Serna, C. Serre, T. Loiseau, F. Fajula and G. Férey, Hydrocarbon Adsorption in the Flexible Metal Organic Frameworks MIL-53(Al, Cr), J. Am. Chrm. Soc. 130 (2008) 16926–16932.*

11. *V. Finsy, S. De Bruyne, L. Alaerts, D. De Vos, P. A. Jacobs, G. V. Baron, J. F. M. Denayer, Shape selective adsorption of linear and branched alkanes in the $Cu_3(BTC)_2$ metal-organic framework, Stud. Surf. Sci. Catal. 170 (2007) 2048-2053.*

12. *P. Bárcia, J. Silva and A. Rodrigues, Separation by Fixed-Bed Adsorption of Hexane Isomers in Zeolite BETA Pellets, American Chemical Society, 45 (2006) 4316–4328.*

13. *P. Bárcia, J. Silva and A. E. Rodrigues, Separation of Branched Hexane Isomers on Zeolite BETA, Adsorption Science & Technology, 25 (2007) 169-183.*

14. *A. Boultif, D. Louer, Indexing of powder diffraction patterns for low-symmetry lattices by the successive dichotomy method, Journal of Applied Crystallography, 24 (1991) 987-993.*

15. *J. Rodriguez-Carvajal, A program for Rietveld refinement and pattern matching analysis. In Collected Abstracts of Powder Diffraction Meeting, (1990) 127-128.*

16. *T. Roisnel, J. Rodriguez-Carvajal, In Abstracts of the 7th European Powder Diffraction Conference, Barcelona, Spain, 2000, 71.*

17. *P. Horcajada, F. Salles, S. Wuttke, T. Devic, D. Heurtaux, G. Maurin, A. Vimont, M. Daturi, O. David et al., How Linker's Modification Controls Swelling Properties of Highly Flexible Iron(III) Dicarboxylates MIL-88,J. Am. Chem. Soc., 133(2011)17839–17847.*

18. *S. Surblé, C. Serre, C. Mellot-Draznieks,F. Millange and G. Férey, A new isoreticular class of metal-organic-frameworks with the MIL-88 topology, Chem. Commun., (2006) 284–286.*

6.

Hexane Isomers Sorption on Rigid Frameworks: MIL-100(Cr), -127(Fe) and -125(Ti)-NH_2

This Chapter describes the synthesis of the rigid materials MIL-100(Cr), MIL-125(Ti)-NH_2 and MIL-127(Fe) together with the respective screening studies performed with equimolar quaternary mixtures *n*HEX/3MP/22DMB/23DMB. A post synthetic modification (PSM) of the as-synthesized MIL-100(Cr) was also applied with the functional group ethylamine (EtA) to improve the *n*HEX separation thought the reduction of the pore opening. In all experiments *n*HEX is the most adsorbed isomer with the better selectivities obtained in the MIL-127(Fe) framework.

6.1. Introduction

There is a huge diversity of MOFs bearing different compositions, architectures, pore sizes and capacities. Depending of their structural and chemical features, the affinity between the adsorptive molecules and the framework will be modified and consequently cause a better or worse adsorption and separation capacity. A post synthetic method is a fast and easy alternative that can be used to adapt the pore size and host-guest by tuning the nature of the functional groups grafted [1].

The grafting consists on a post-synthesis substitution of a solvent molecule coordinated on the Lewis acid unsaturated metal sites of the MOF by an amine group. In the MIL-100(Cr) (Material from *Institut Lavoisier*), grafting with ethylamine occurs through a substitution of water by ethylamine molecules. The kinetic diameter of the hexane isomers is indeed between 4.3 and 6.2 Å and the free diameters of the pentagonal and hexagonal windows at the entrance of the two types of mesoporous cages of MIL-100(Cr) are close to 5.5 Å and 8.6 Å. Coordinated water molecules point at the centre of the windows. At this stage, only the pentagonal windows might lead to the isomers separation considering the larger dimension of the hexagonal ones. So, the objective was to graft with an amine to reduce the size of the windows to improve the adsorption and selectivity of the hexane isomers.

Two types of ethylamine precursors were used: pure ethylamine and an aqueous ethylamine solution (70 %; 1 mol MIL-100(Cr): 1 mol C_2H_5-NH_2 ratio). For the pure ethylamine, it is necessary to work at room temperature, due to low boiling point (288.8 K), but as the typical grafting conditions require higher temperatures, close to 423 K, we increased the reaction times. Although the aqueous solution of ethylamine can be heated at 423 K, this solution contains water, which might reduce the efficacy of the amine grafting. So, both experiments were not totally performed under ideal conditions. The characterizations of both syntheses are described during this chapter. Moreover, the synthesis of the rigid materials MIL-125(Ti)-NH_2 and MIL-127(Fe) are also addressed together with the respective screening studies

6.2. Structure of MIL-100(Cr)

MIL-100(Cr) or $[Cr_3F(H_2O)_2O[C_6H_3\text{-}(CO_2)_3]_2.nH_2O$, n ~ 28] exhibits a 3D cubic crystalline hybrid framework [2] based on trimmers of chromium(III) octahedral and trimesate linkers (Fig. 6.1), delimiting 2 types of mesoporous cages (25 and 29 Å) (Figure 6.2a and 6.2b, respectively), accessible by microporous windows (≈ 5 – 9 Å) (Figure 6.2c).

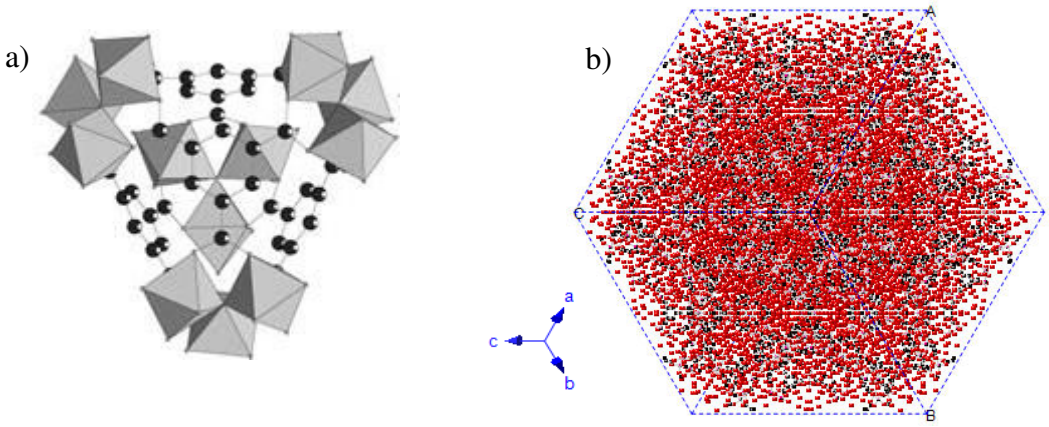

Figure 6.1 - (a) Structure of the MIL-100(Cr) [2] (b) Ball-and-stick view of a unit cell of MIL-100(Cr) on a set view direction (1, 1, 1).

It crystallizes in the cubic *Fd3m* space group (Fig. 6.1) with a cell parameter of 71.26 Å and a unit cell volume of 361.774 $Å^3$ [3]. Because of its hybrid structure, an important surface and pore volume is observed (S_{Lang} = 3100 $m^2.g^{-1}$; Vp = 1.6 $cm^3.g^{-1}$). Fig. 6.2 specifies the two types of mesoporous cages (small and large), as well the pentagonal and hexagonal microporous windows.

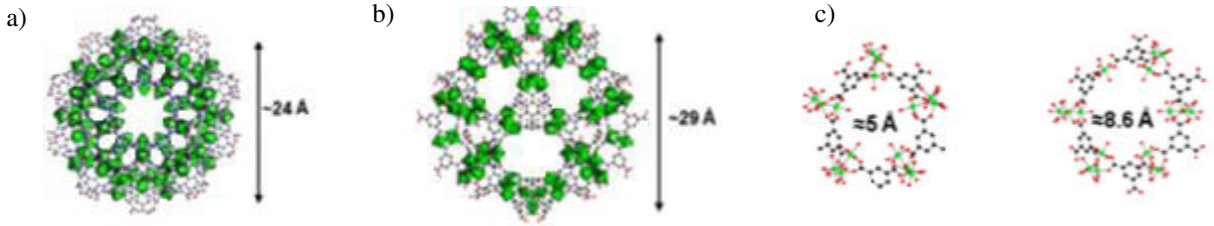

Figure 6.2 - MIL-100(Cr) mesoporous cages: (a) Small and (b) Large; (c) Hexagonal microporous windows [4].

6.2.1. MIL-100(Cr)

Three adsorption studies were developed at the LSRE-IPB concerning the MIL-100(Cr). The first study was related to the pattern MIL-100(Cr) solid, the second dealt with the MIL-100(Cr) grafted with EtAp (Ethylamine pure) and the third with MIL-100(Cr)MEDA (Methyl ethylene diamine). In this first set of experiments, the synthesis and characterization of MIL-100 (Cr) and MIL-100(Cr)EtAp were made. The MIL-100(Cr)MEDA was later synthesized and sent by *Institut Lavoisier* for the breakthrough experiments. The separation and adsorption capacity of each MOF were evaluated using an equimolar mixture of four hexane isomers: n-hexane (*n*HEX), 3-methylpentane (3MP), 2,3-dimethylbutane (23DMB) and 2,2-dimethylbutane (22DMB).

6.2.1.1. Experimental Section

Synthesis

MIL-100(Cr) was synthesized by the hydrothermal method. Metal chromium (520 mg, 10 mmol; ABCR, 99 %) and 1, 3, 5 benzene tricarboxylic acid, H_3BTC (1.4 g, 6.53 mmol; Aldrich, 99 %) were dissolved into distilled water (48 mL, 2.66 mol). Afterwards, a solution of hydrofluoric acid, HF (2 mL, 10 mmol; 5 M) was placed into the previous solution and stirred. The Teflon-lined containing the final solution was placed into a metallic Paar-type (Figure 6.3a). To obtain the enough amounts for the separation tests, a series of 5 syntheses were carried out.

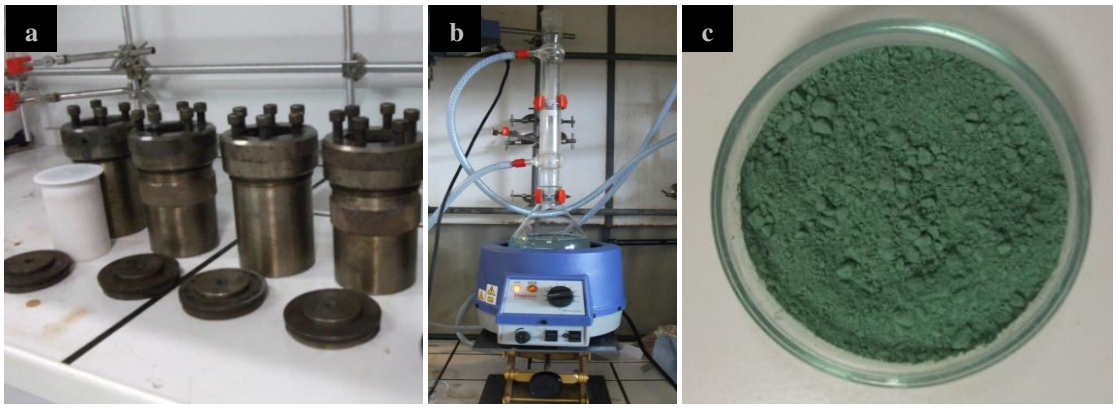

Figure 6.3 - (a) A Teflon vessel of 125 mL (white) and metallic rectors for the hydrothermal method. (b) Experimental set-up used for MIL-100(Cr) activation with mechanical stirring, reflux and heating (≈ 373 K). (c) Sample of the MIL-100(Cr) in its powdered form, after synthesis and activation.

All rectors were heated at rate of 289.25 $K.h^{-1}$ to 493 K (12 h), leaving this temperature during 96 h and then cooled at rate of 281.125 $K.h^{-1}$ (24 h). Thereafter, the green final product was filtered and decanted to remove the remaining non-reacted Cr^0 that lies at the bottom of the flask. The final product was filtered at room temperature resulting in a green powdered material, obtaining around 9.2 g of as-synthesized material (Fig. 6.3c).

The as-synthesized material was suspended in 700 mL of distilled water and heated under reflux during 3 h under stirring (Fig. 6.3b) with the objective to remove the unreacted species. The solid was recovered by filtration. This process was repeated twice until the disappearance of band corresponding to the free acid in the infrared spectrum. Finally, an additional activation step using ethanol (700 mL; Carlo Erba, 96 %) was performed at ambient temperature for 2 h to further purify the sample. Between consecutive washes, centrifugation was used to recover the powder. The weight of the final sample PM1 was 8.7 g.

X-Ray Powder Diffraction (XRPD) analysis

Fig. 6.4 shows the X-Ray powder diffraction of the five different batches as-synthesized products (red, blue, green, pink and brown) and the reference MIL-100(Cr) pattern (black) for comparison. We can see that the samples correspond all to MIL-100(Cr). Peaks are however broader then the reference pattern due to the presence of rather small particles.

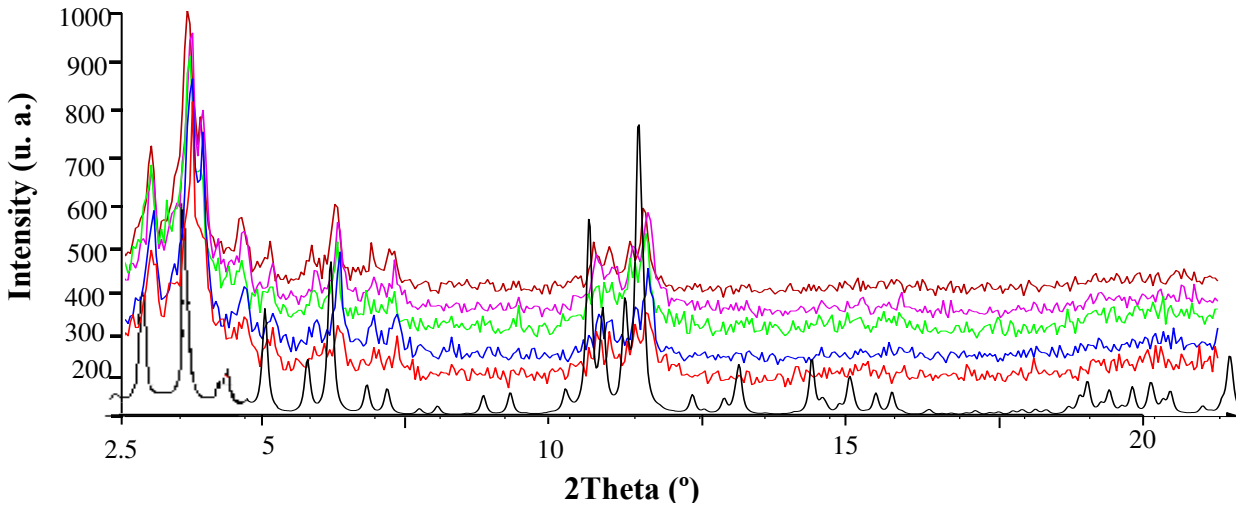

Figure 6.4 - XRPD of the MIL-100(Cr) pattern (black) and the as-synthesized samples (red, blue, green, pink and brown) using a Siemens diffractometer D5000 (Cu Kalpha1 radiation λ = 1.54056 Å).

Infra-Red (IR) spectroscopy analyses

Fig. 6.5 shows the IR diffractogram of MIL-100(Cr) before (red) and after the activation steps (black). Fig. 6.5a suggests the presence of the main free carboxylic acid peak (C=O ≈ 1700 cm^{-1}) while its intensity decreases throughout the different activation steps (from the red line to the black line). However, the peak can still be observed after the final activation, indicating the presence of a slight amount of residual free acid. Note that the presence of the carboxylate bands (COO$^-$ ≈ 1400 – 1550 cm^{-1}) is in agreement with the presence of the metal carboxylate bonds. The band (C–H ≈ 2900 cm^{-1}) is also indicative of the presence of aromatic C–H bands from the linker BTC.

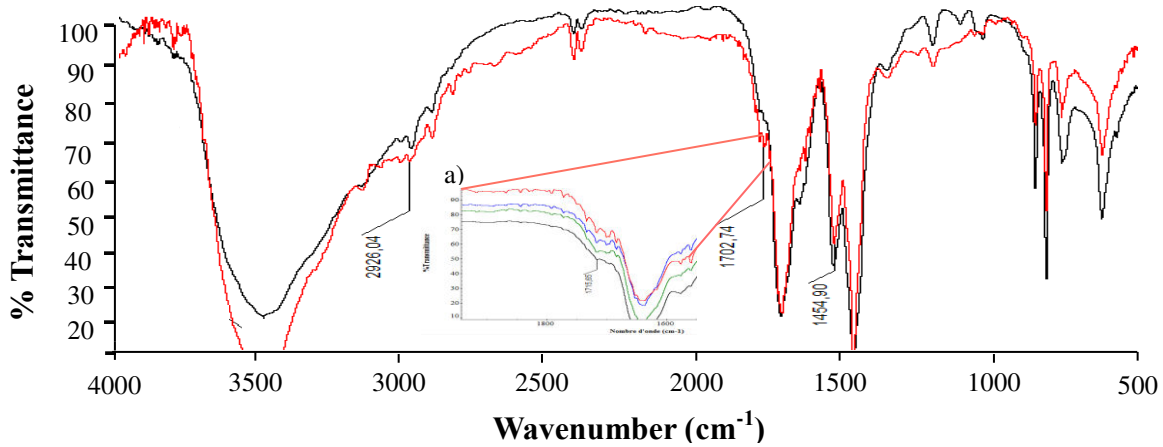

Figure 6.5 - Infra-Red diffractogram comparison between the sample MIL-100(Cr) as-synthesized (red) and the sample after activation (black). (a) Detailed peak disappearing between the sample as-synthesized (red), first activation (blue), second activation (green) and the last activation (black). Equipment Nicollet spectrometer, KBr pellet.

Thermogravimetric Analysis (TGA)

Fig. 6.6 shows the thermogravimetric analysis of MIL-100(Cr). The material degradation, which corresponds to the linker combustion (53.6 wt% of lost mass) begins at *ca*. 523 K.

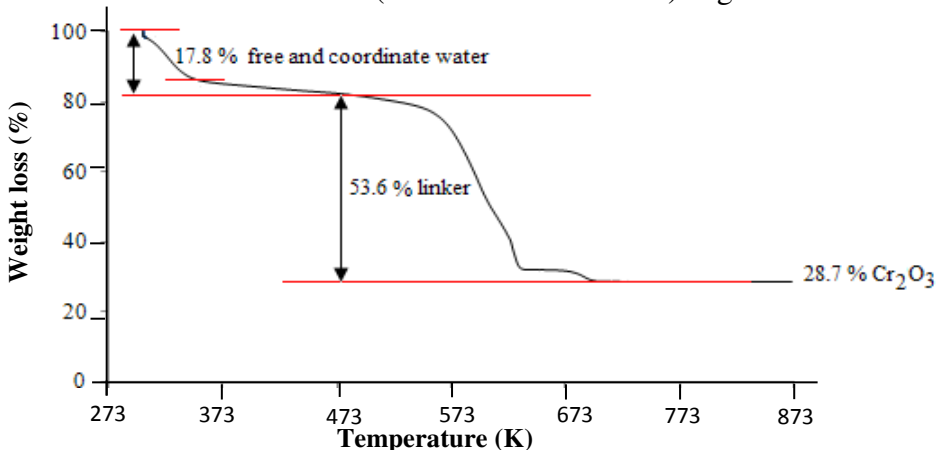

Figure 6.6 - Thermogravimetric analysis of MIL-100(Cr) activated under atmospheric pressure (Heating rate of 275 K.min^{-1}; 4.198 mg of solid). Equipment PerkinElmer, STA 6000.

The first weight loss (ambient temperature to ca. 100 °C) represents the departure of free water. The second mass loss (373 K – 523 K) indicates the departure of coordinated water. The total water loss corresponds to ~ 17.8 %. The experimental and theoretical weight losses are listed on Table 6.1. Both experimental and calculated values for both the organic ligand and the residual Cr_2O_3 are in well concordance. A slightly higher amount of ligand indicates the presence of remaining free acid, in agreement with the IR observations.

Table 6.1 - Theoretical and experimental percentage of mass lost and retained after thermal degradation.

	Theoretical	Experimental
% ligand	51.4	53.6
% Cr_2O_3	31.3	28.7

6.2.1.2. Results and Discussion

Prior to the breakthrough experiments, the MOF was outgassed in its powder form (particles with diameter around 0.03 mm), under vacuum (around 10 kPa) at 383 K, for 15 hours. 376 mg of sample was packed in a stainless steel column (diameter = 4.3 mm, length = 8 cm). Screening studies covered two partial pressures (1.6 kPa and an order of magnitude higher 10 kPa) at 343 K. Table 6.2 shows the experimental conditions and the adsorbed amounts calculated from the integration of the breakthrough profiles.

Table 6.2 - Experimental conditions and adsorbed amounts of breakthrough experiments performed on MIL-100(Cr).

Run	*T* (K)	Helium flow rate (mL(STP).min^{-1})	Mixture pressure (kPa)	m_{ads} (mg)	Partial loading (g.100g$_{ads}^{-1}$)				Total loading (g.100g$_{ads}^{-1}$)
					22DMB	23DMB	3MP	*n*HEX	
MIL100_a1	343	15.7	1.6	376	2.1	2.7	3.3	4.4	12.5
MIL100_b1		9.2	10		4.7	6.1	7.2	8.7	26.7

We can observe significant adsorbed amounts ranging from 27 wt% at 10 kPa to 12.5 wt% at 1.6 kPa. The sorption hierarchy is here *n*HEX>3MP>23DMB>22DMB with selectivities reported in Table 6.3. Between *n*HEX/22DMB the selectivity is 2.1 at 1.6 kPa and for 23DMB/22DMB one reaches 1.3. These values are reasonable and might be interesting for the separation of the compounds taking into account that adsorbed amounts are here considerable.

Table 6.3 - Selectivityies of hexane isomers in MIL-100(Cr) at 343 K.

Run	T (K)	Mixture pressure (kPa)	Selectivities		
			23DMB/22DMB	3MP/22DMB	*n*HEX/22DMB
MIL100_a1	343	1.6	1.3	1.6	2.1
MIL100_b1		10	1.3	1.5	1.9

Fig. 6.7 shows the quaternary breakthrough curves of the hexane isomers in MIL-100(Cr) under a partial pressure of 1.6 kPa and 10 kPa at 343 K from where the adsorbed amounts and selectivities are calculated. A roll-up phenomenon of the less adsorbed components is observed meaning that there is competition for sorption in MIL-100(Cr). The increase in mixture pressure has an influence on the degree of the roll-up phenomena since the amount adsorbed increases and consequently the competition effect is also higher.

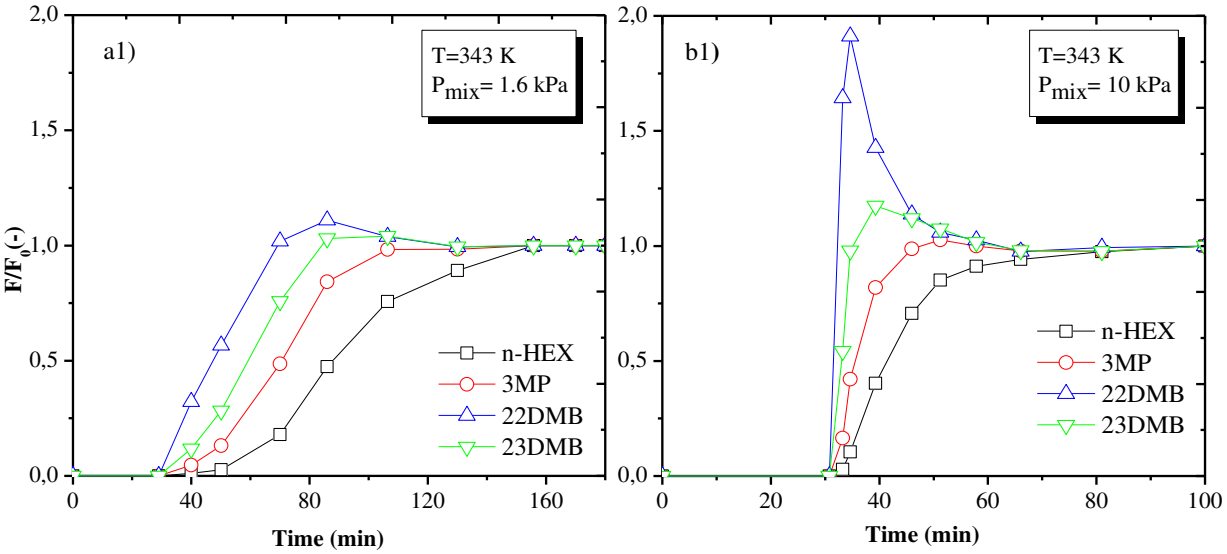

Figure 6.7 - Quaternary breakthrough curves of the hexane isomers in MIL-100(Cr) at 343 K. (a1) pp = 1.6 kPa and (b1) pp = 10 kPa.

6.2.2. MIL-100(Cr) Ethylamine

6.2.2.1. Experimental Section

Grafting procedure

Previously synthesized MIL-100(Cr) (sample PM1) was used for the PSM with ethylamine. Two PSM experiments were carried out either using pure ethylamine (EtAp) or an aqueous solution of ethylamine (EtAaq). In the first case, the sample PM1 (9.2 g) was left overnight at

423 K to remove the free water. The final weight was close to 7.0 g and its sharp decrease maybe is due the fast filtration which eliminated little quantity of water. Then, the dehydrated sample was divided in two parts for the two different PSM: one for the MIL-100(Cr)-EtAp ($m_{PM1EtAp}$ = 3.37 g) and another one for MIL-100(Cr)EtAaq ($m_{PM1EtAaq}$ = 3.80 g). In both cases, each sample was placed into different schlenk tubes and left under vacuum at 423 K for 12 h. The objective of this step was to remove the coordinated water from MIL-100(Cr). To prepare the MIL-100(Cr)EtAp, 2.92 g (4.8 mmol) of MIL-100(Cr) (sample PM1EtAp) were dispersed in 40 mL of dry toluene (0.376 mol; VWR, 99.99 %) and 0.33 mL of pure ethylamine (4.8 mmol, Aldrich, 99 %), under a N_2 flow. This blend was left at room temperature under stirring and N_2 flow for 48 h (Fig. 6.8a). Finally, the sample was recovered by filtration.

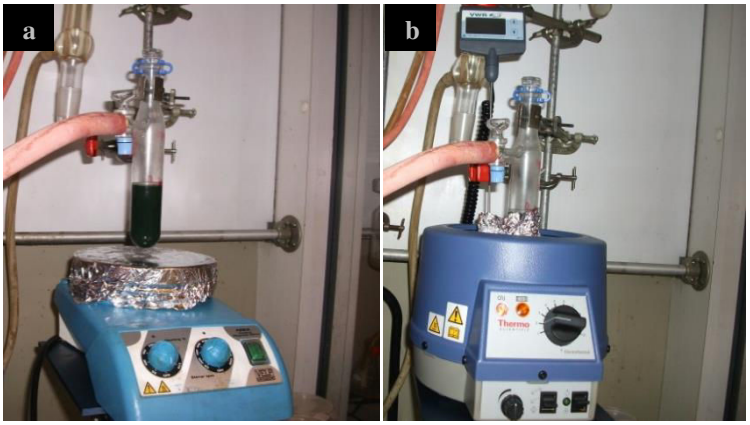

Figure 6.8 - Experimental set-up for (a) pure ethylamine grafted at room temperature and (b) aqueous ethylamine grafted at around 373 K.

MIL-100(Cr)EtAaq was obtained by dispersing quickly the sample PM1EtAaq (2.46 g, 4.05 mmol) into 40 mL of dry toluene (0.376 mol; vwr, 99.99 %) and 0.35 mL of aqueous ethylamine (4.05 mmol; Aldrich, 11.59 M), under a N_2 flow. This blend was left at 373 K under stirring overnight under a N_2 flow (Fig. 6.8b). Finally, the sample was recovered by filtration.

X-Ray powder diffraction (XRPD) analysis

Fig. 6.9 shows the X-Ray powder diffraction of the MIL-100(Cr) (black), MIL-100(Cr)EtAaq (blue) and MIL-100(Cr)EtAp (red), showing that crystallinity of both structures is maintained after the grafting.

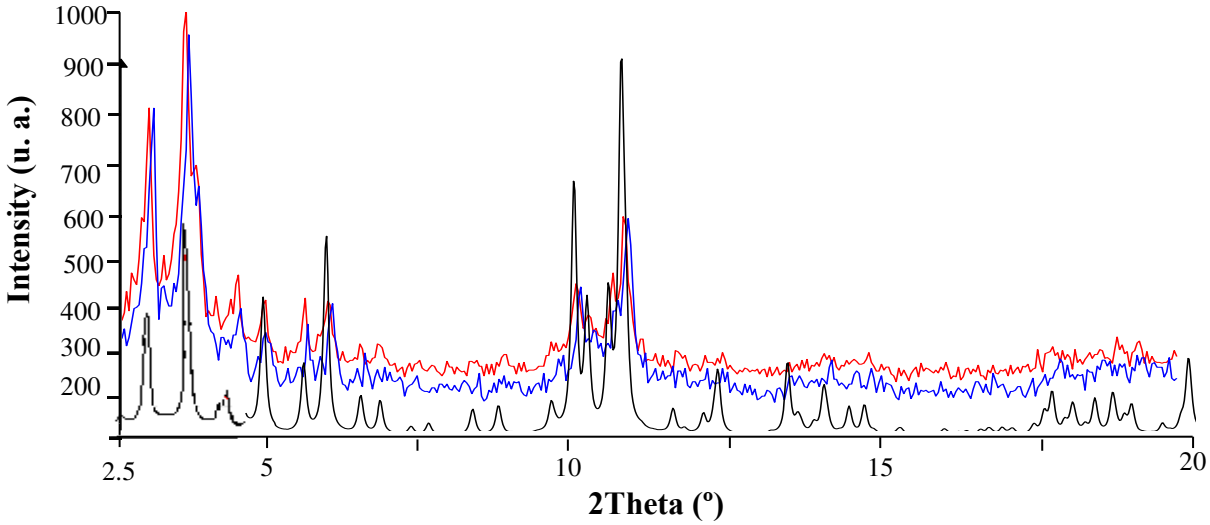

Figure 6.9 - XRPD of the MIL-100(Cr) pattern (black), the sample MIL-100(Cr)EtAaq (blue) and the sample MIL-100(Cr)EtAp (red) using a Siemens diffractometer D5000 (Cu Kalpha1 radiation λ = 1.54056 Å).

Infra-Red (IR) spectroscopy analyses

Fig. 6.10 shows the infra-red diffractogram of MIL-100(Cr) (black), MIL-100(Cr)EtAaq (red) and MIL-100(Cr)EtAp (green). One can point out the disappearance of the water band (3440 cm^{-1}) for the grafted samples, supporting the replacement of water by amine groups.

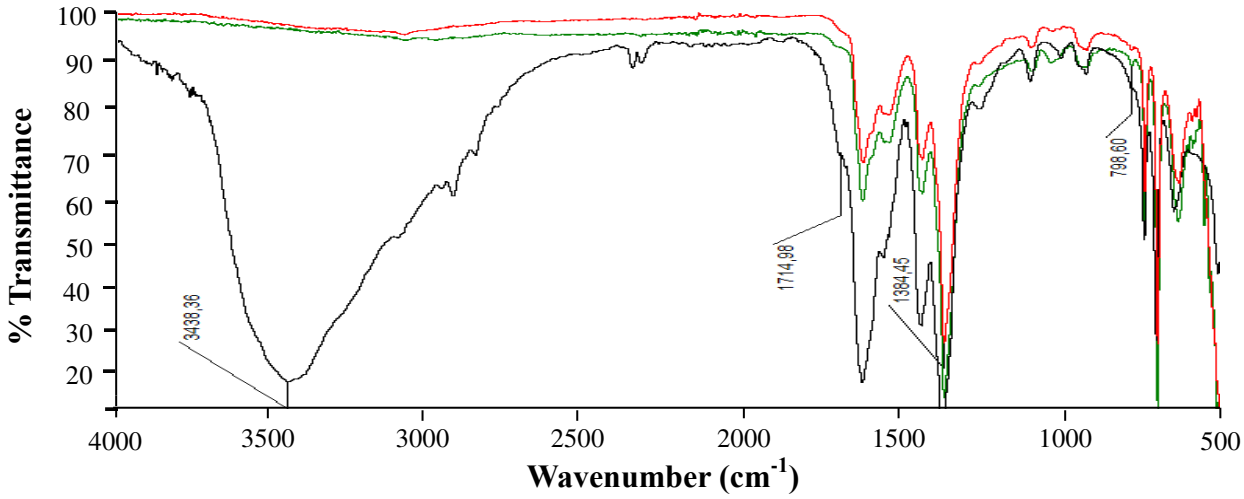

Figure 6.10 - Infra-Red diffractogram of PM1 after activation (black), MIL-100(Cr)EtAaq (red) and MIL100(Cr)EtAp (green). Equipment Nicollet, 6700 Thermo scientific.

The appearance of the band at ca. 800 cm^{-1} corresponds to the grafted amines and is in agreement with the presence of ethylamine (see also diffractogram of the pure ethylamine compound). Note that this is more obvious for the pure ethylamine grafted sample, indicating a higher grafting when using the pure ethylamine. This might be due to the presence of water in the aqueous ethylamine solution that makes harder the grafting of amines. As consequence, the breakthrough experiments were performed using the MIL-100(Cr)EtAp sample.

Thermogravimetric Analysis (TGA)

Fig. 6.11 shows the thermogravimetric analysis of MIL-100(Cr) (PM1) and MIL-100(Cr)EtAp (PM1EtAp). There are some differences between the samples. In the first decay, from ambient temperature to ca. 473 K, the weight losses are of only 5 % for PM1EtAp and 17.8 % for PM1, due to the dehydration of the samples. The weight loss associated with the degradation of the solid is slightly superior for PM1EtAp compared to PM1, indicating the presence of ethylamine within the sample.

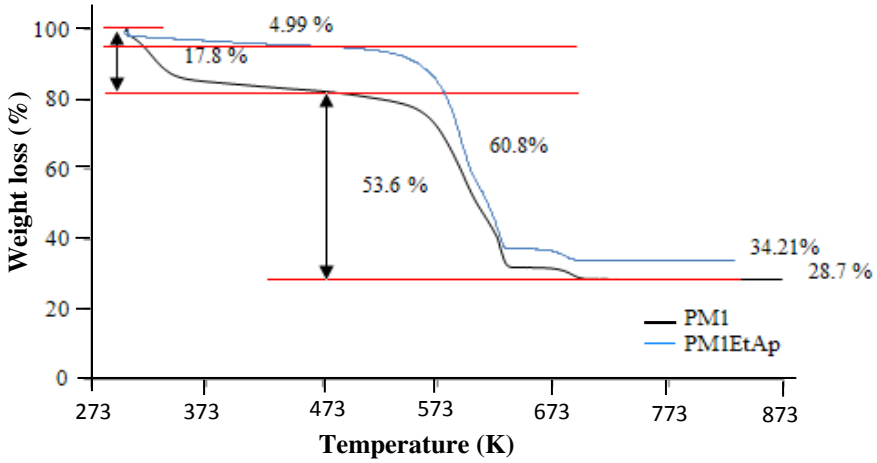

Figure 6.11 - Thermogravimetric analysis of MIL-100(Cr) (PM1) and MIL-100(Cr)EtAp (PM1EtAp) activated under atmospheric pressure (Heating rate of 275 $K.min^{-1}$; 4.198 and 7.649 mg of solid, respectively). Equipment PerkinElmer, STA 6000.

Nitrogen adsorption measurement

Fig. 6.12 shows the N_2 adsorption isotherms at 77 K of MIL-100(Cr) (PM1) and the grafted samples (PM1EtAp and PM1EtAaq). The samples were first outgassed at 423 K under vacuum overnight. The grafted samples demonstrate a diminution of sorption capacity compared with the sample PM1 due to the decrease of pore size after grafting. The maximum adsorption capacity of the sample PM1EtAp is also lower than the one of PM1EtAq which highlights the difference of grafting efficacy.

Table 6.4 indicates the pore volumes, maximum nitrogen uptake (micropores) and the surface area obtained by BET (S_{BET}) and Langmuir (S_{Lang}) theories. The experimental value of PM1 (S_{Lang} = 1930 $m^2.g^{-1}$) is lower than the previously reported value (S_{Lang} = 3100 $m^2.g^{-1}$).

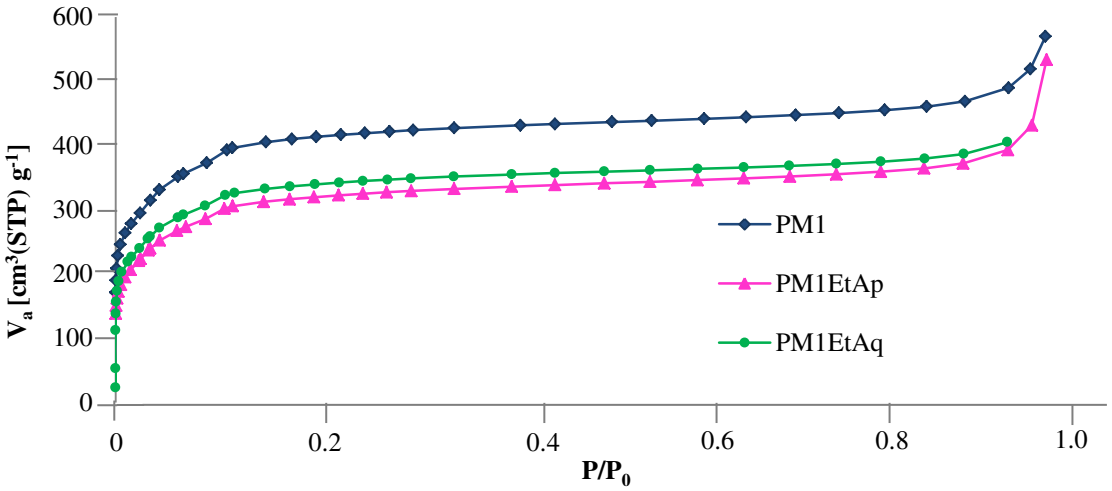

Figure 6.12 - Nitrogen adsorption isotherm of MIL-100(Cr) (PM1), the sample PM1EtAp and PM1EtAaq at T = 77K (P_o = 1 atm). Equipment BEL Japan, BELSORP Mini.

This is probably due to an excess of residual dense metal chromium and/or the presence of residual species within the pores. Grafting with pure ethylamine and aqueous also leads to a decrease of the surface areas ($S_{Lang\ EAp}$ = 1170 and $S_{Lang\ EAaq}$ = 1230 $m^2.g^{-1}$, respectively), in agreement with the presence of the coordinated ethylamine.

Table 6.4 - Principal parameters obtained from the Nitrogen adsorption measurement of the MIL-100(Cr) pattern comparatively to the samples PM1, PM1ETAp andPM1ETAaq.

	MIL-100(Cr) [8]	PM1	PM1EtAp	PM1EtAaq
S_{BET} [$m^2.g^{-1}$]	-	1490	1170	1230
S_{Lang} [$m^2.g^{-1}$]	3100	1930	1520	1300
V_m [cm^3(STP).g^{-1}]	-	440	350	300
V_p [$cm^3.g^{-1}$]	1.16	0.88	0.82	0.63
V_{mp} [$cm^3.g^{-1}$]	-	0.65	0.50	0.54

- Not available data

6.2.2.2. Results and Discussion

A set of breakthrough experiments with a quaternary equimolar mixture *n*HEX/3MP/23DMB/22DMB in the MIL-100(Cr)EtAp (PM1EtAp) was performed. Previously the sample was placed in its powdered form in an oven under vacuum (10 kPa) overnight at 383K for the dehydration. Table 6.5 discloses the experimental conditions and the amount adsorbed of each experiment. Again, within this rigid MOF the isomer less adsorbed is the 22DMB and the more adsorbed the *n*HEX. This result shows that the MOF follow the general tendency of the linear isomer to be the most adsorbed component with the

affinity order *n*HEX>3MP>23DMB>22DMB. It can be noticed a adsorbed maximum amount around 18 wt% at 343 K and 6 kPa of mixture pressure, but very small values (around 3 wt%) at 383 K. The temperature demonstrates a strong influence in the loading amounts.

Table 6.5 - Experimental conditions and adsorbed amounts of breakthrough experiments performed on MIL-100(Cr)EtAp.

Run	*T* (K)	Helium flow rate (mL(STP).min^{-1})	Mixture pressure (kPa)	m_{ads} (mg)	Partial loading (g.100g$_{ads}^{-1}$)				Total loading (g.100g$_{ads}^{-1}$)
					22DMB	23DMB	3MP	*n*HEX	
EtAp_a1	343	41.6	0.6	376	0.8	1.0	1.2	1.5	4.5
EtAp_a2	383				0.1	0.2	0.25	0.3	0.9
EtAp_b1	343	13.8	6		3.2	4.1	4.7	6.4	18.3
EtAp_b2	383				0.5	0.6	0.7	1.1	2.9

Table 6.6 shows the selectivity of the hexane isomers calculated relatively to the less adsorbed compound 22DMB. The highest value is around 3.0 for *n*HEX/22DMB at 383 K and 0.6 kPa. Between 3MP/23DMB the values never exceed 2.5 but this value was obtained at 383 K where the amounts adsorbed are too low.

Table 6.6 - Selectivities of hexane isomers in MIL-100(Cr)EtAp.

Run	T (K)	Mixture pressure (kPa)	Selectivities		
			*n*HEX/22DMB	3MP/22DMB	23DMB/22DMB
EtAp_a1	343	0.6	1.9	1.5	1.3
EtAp_a2	383		3.0	2.5	2.0
EtAp_b1	343	6	2.0	1.5	1.3
EtAp_b2	383		2.2	1.4	1.2

Fig. 6.13 depicts the breakthrough curves. The breakthroughs show a certain degree of separation with a roll-up phenomenon characteristic of competitive adsorption of the guest molecules in the structure, except at 343 K and 0.58 kPa due to the very low partial pressure. Note that more than 60 min were required to attain the adsorption equilibrium in the breakthrough curves at 343 K.

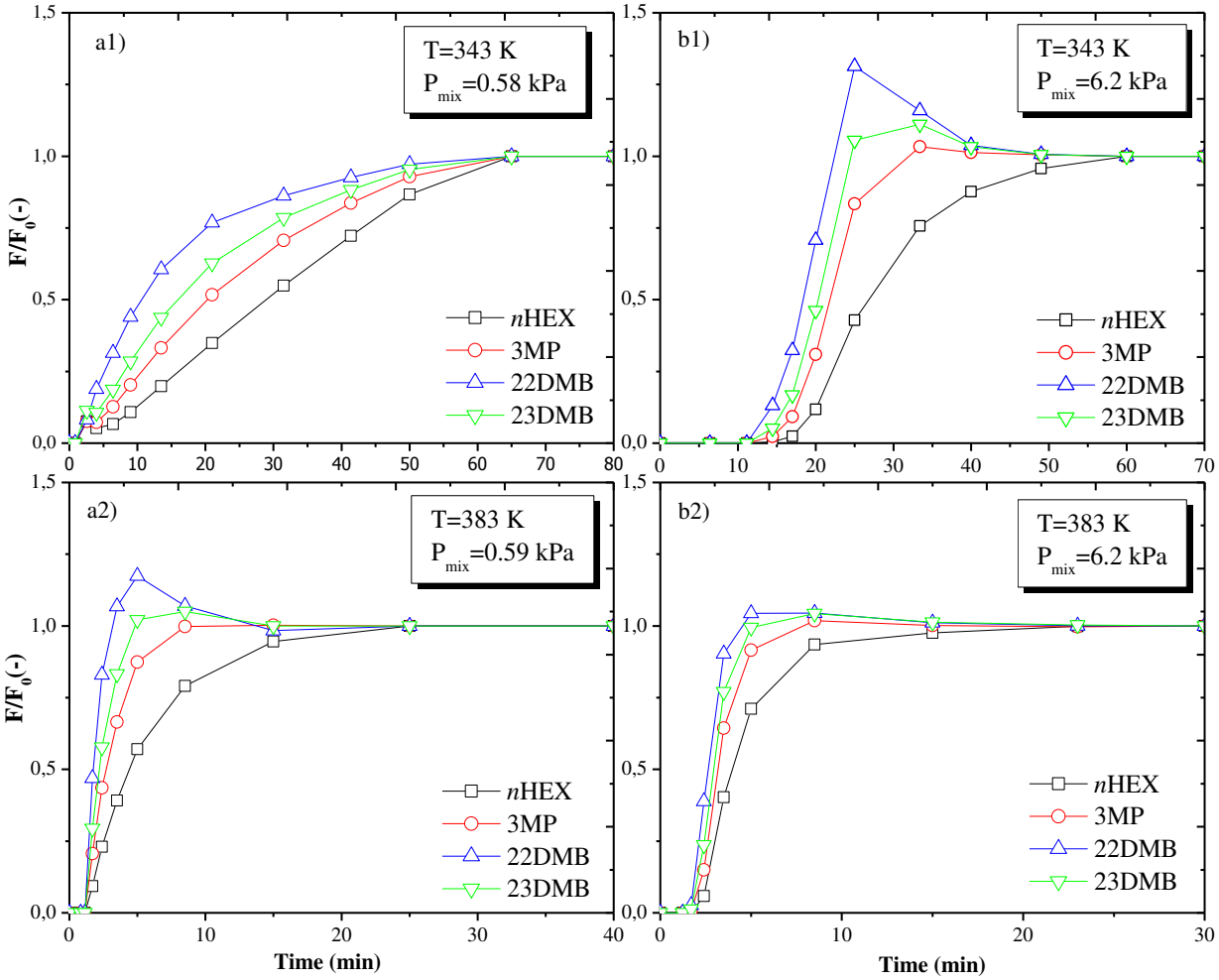

Figure 6.13 - Breakthrough curves of the quaternary equimolar mixture of hexane isomers in MIL-100(Cr) grafted with Ethylamine pure. (a1) pp = 0.58 kPa, T = 343 K; (b1) pp = 6.2 kPa, T = 343 K; (a2) pp = 0.59 kPa, T = 383 K; (b2) pp = 6.3 kPa, T = 383 K.

6.2.3. MIL-100(Cr) MEDA

6.2.3.1. Experimental Section

Synthesis

The preparation method of the MIL-100(Cr) Methyl ethylene diamine (MEDA) sample followed the sample process as the one used to prepare the MIL-100(Cr) Ethylamine sample but replacing ethylenediamine by MEDA. The material of MIL-100(Cr)MEDA was synthesized by J. E. Eubank *et al.*, in ILV and after sent to the LSRE–IPB for the breakthrough experiments. Accordingly

6.2.3.2. Results and Discussion

Prior to the breakthrough experiments, MIL-100(Cr)MEDA was placed in its powdered form under vacuum (10 kPa) in an oven overnight at 383 K. Within this set of experiments, 536 mg of sample was packed with ceramic wool in a stainless steel column (Length = 8 cm, diameter = 4.6 mm). The studies were performed with a quaternary equimolar mixture of hexane isomers *n*HEX/3MP/23DMB/22DMB at 343 K and two partial pressures 1.6 kPa and 10 kPa. Table 6.7 indicates the experimental conditions and adsorbed amounts calculated from the profiles of the breakthrough curves.

Table 6.7 - Experimental conditions and adsorbed amounts resulting from the breakthrough experiments performed in MIL-100(Cr) MEDA.

Run	*T* (K)	Helium flow rate (mL(STP).min^{-1})	Mixture pressure (kPa)	m_{ads} (mg)	Partial loading (g.100g$_{ads}^{-1}$)				Total loading (g.100g$_{ads}^{-1}$)
					22DMB	23DMB	3MP	*n*HEX	
MEDA_a1	343	37.3	1.6	536	1.8	2.6	3.2	4.9	12.5
MEDA_b1		14.0	10		3.6	5.1	6.4	8.9	24.0

Table 6.8 shows a total adsorbed amount around 24 wt% at 343 K and 10 kPa and the half value at 1.6 kPa. The sorption hierarchy is the same as the order of the normal boiling points of the compounds. In Table 6.8 are reported the selectivities using the reference compound 22DMB. The selectivity linear/di-branched (*n*HEX/22DMB) was around 2.7 at 343 K and 1.6 kPa, decreasing to a value of 1.4 for the ratio 23DMB/22DMB.

Table 6.8 - Selectivities of hexane isomers in MIL-100(Cr) MEDA.

Run	T (K)	Mixture pressure (kPa)	Selectivities		
			23DMB/22DMB	3MP/22DMB	*n*HEX/22DMB
MEDA_a1	343	1.6	1.4	1.8	2.7
MEDA_b1		10	1.4	1.8	2.5

Fig 6.14 shows the quaternary breakthrough curves. 200 min were required to reach the saturation of the bed at 343 K and 1.6 kPa, while for 10 kPa the same happens in 80 min. The values of the selectivities are comparable with other materials such as zeolites but the amount adsorbed is considerably higher.

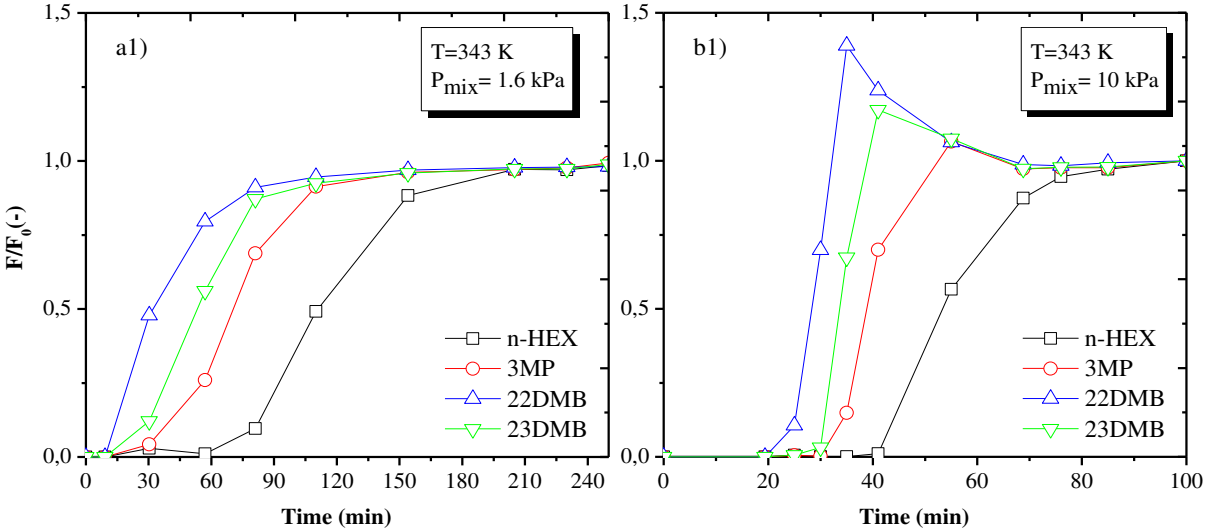

Figure 6.14 - Quaternary breakthrough curves of the hexane isomers in MIL-100(Cr)MEDA at 343 K. (a1) pp = 1.6 kPa and (b1) pp = 10 kPa.

6.3. Structure of MIL-127(Fe)

The iron(III) 3,3',5,5-azobenzenetetracarboxate MIL-127(Fe) is an MOF phase isostructural to the indium-trimmer building blocks based Soc-MOF [6]. Here, Fe(III)-octahedral trimmers sharing one central μ_3-oxo anion form trimeric building blocks similar to those of MIL-100(Fe). Fig 6.15 represents the crystal structure of this microporous rigid cubic architecture. The framework topology consists on the linkage of each trimer unit (Fig 6.15a) by a six carboxylate bonds (Fig. 6.15b). It delimited a 3D microporous (5 – 7 Å) system (cage size superior than 10 Å) that consists of an alternative of hydrophilic parts (trimmer of Fe) or hydrophobic ones (spacer).

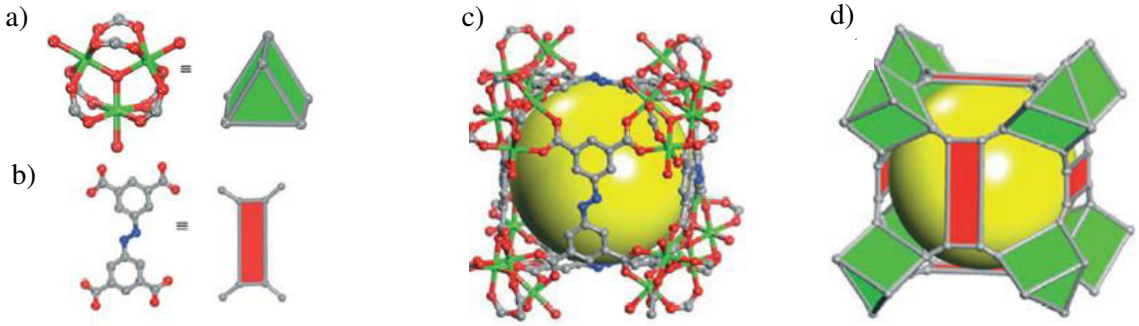

Figure 6.15 - Structure of the Indium-Trimmer Building Blocks: (a) trimmer of iron carboxylate [$Fe_3O(CO_2)(H_2O)_3$]; (b) organic linker (3,3', 5,5'–azobenzenotétracarboxilato); (c) Ball-and-stick and (d) polyhedral views of the cuboidal cage of the framework Fe-Azobenzenetetracarboxylic. Fe (green); C (grey); N (blue); O (red); Internal cage size (yellow sphere; Hydrogen atoms, water molecules, and $[NO_3]^-$ ions are omitted for clarity [6].

6.3.1. Experimental Section

6.3.1.1. Synthesis

This material was synthesized at the *Institut Lavoisier* by Hubert Chevreau. The synthesis consists on the reaction of 3.27 g of Fe(III) perchlorate hexahydrated (9.2 mmol), 3.3 g of 3,3',5,5'-azobenzenetetracarboxylic acid (synthesized at the lab [5], 9.3 mmol) in 415 mL of DMF and 2.7 mL of hydrofluoric acid 5M at 423 K in a Teflon flask. The obtained orange crystals have a chemical formula $[Fe_3O(C_{16}N_2O_8H_6)_{1,5}(H_2O)_3](H_2O)_3(NO_3)]$. The as-synthesized solid was placed in DMF (100 mL) under stirring for 5 h at ambient temperature. The final product was kept overnight at 373 K.

6.3.2. Results and Discussion

A set of breakthrough experiments was performed at 343, 373 and 423 K for high (6 kPa) and low partial pressure (0.6 kPa). 420 mg of sample was packed in a stainless steel column (Length = 8 cm, diameter = 4.6 mm). Previously to the breakthrough experiments, the sample of MIL-127(Fe) was placed in its powdered form under vacuum (10 kPa) in an oven during 15 h at 423 K for solvent removal. A quaternary equimolar mixture of hexane isomers *n*Hex/3MP/23DMB/22DMB was used for the adsorption studies. Table 6.9 shows the experimental conditions and the amount adsorbed of each component.

Table 6.9 - Experimental conditions and amounts adsorbed of the hexane isomers in MIL-127(Fe).

Run	*T* (K)	Helium flow rate (mL(STP).min^{-1})	Mixture pressure (kPa)	m_{ads} (mg)	Partial loading (g.100g$_{ads}^{-1}$)				Total loading (g.100g$_{ads}^{-1}$)
					22DMB	23DMB	3MP	*n*HEX	
MIL-127_a1	343	13.9	0.6	420	0.08	0.09	0.10	0.56	0.82
MIL-127_a2	373				0.07	0.08	0.07	0.43	0.65
MIL-127_a3	423				0.03	0.04	0.05	0.48	0.59
MIL-127_b1	343		6		0.33	0.44	0.54	6.05	7.36
MIL-127_b2	373				0.23	0.34	0.44	5.77	7.16
MIL-127_b3	423				0.28	0.44	0.65	5.27	6.64

For this material the maximum amount adsorbed is around 7.4 wt% at 343 K and 6 kPa, where the linear *n*HEX is predominantly adsorbed. Fig 6.16 shows the quaternary breakthrough curves of the hexane isomers in MIL-127(Fe) for 343, 373 and 423 K.

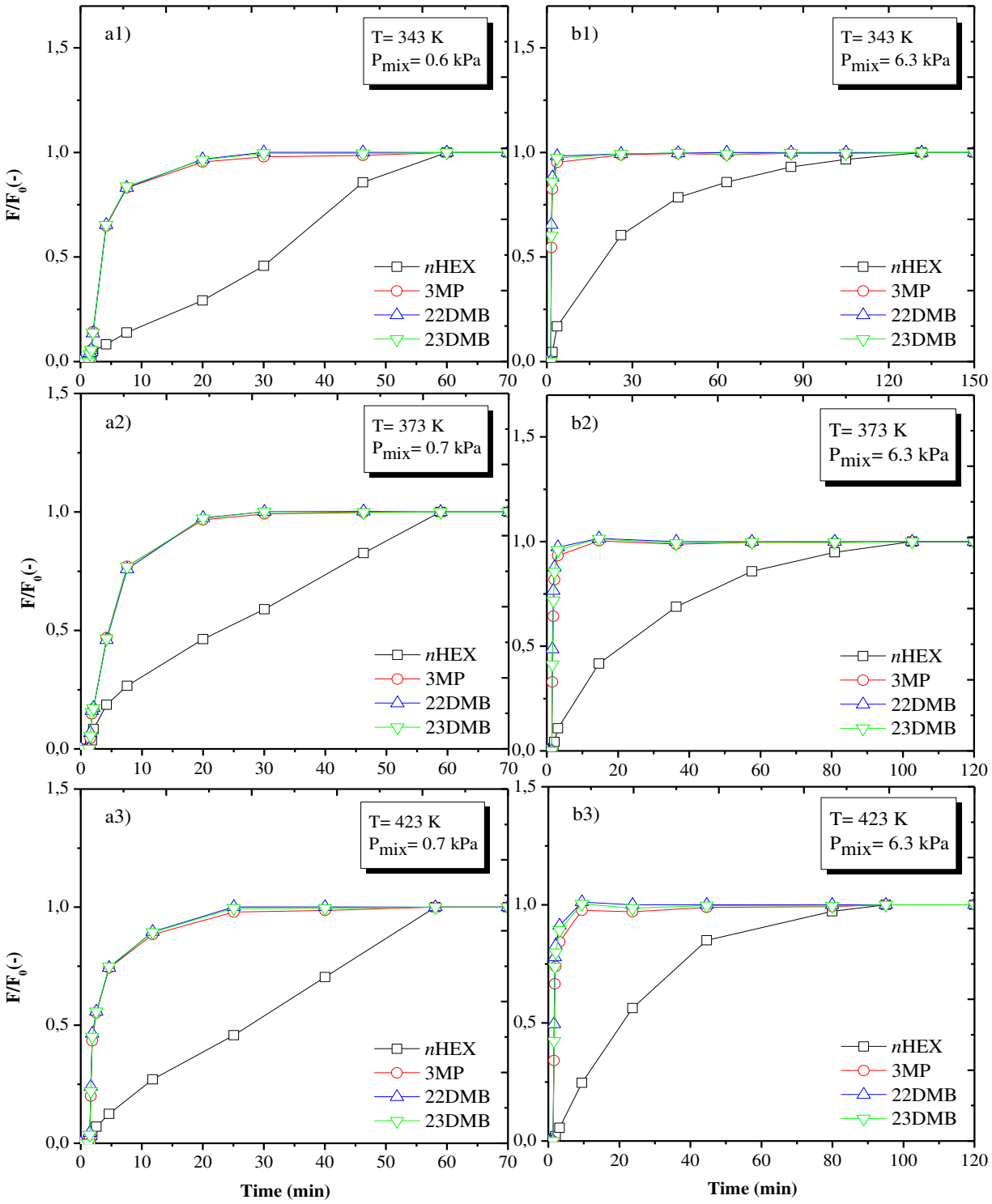

Figure 6.16 - Quaternary equimolar breakthrough curves of the hexane isomers in MIL-127(Fe) at 423 (a1) pp = 0.6 kPa, T = 343 K; (b1) pp = 6.3 kPa, T = 343 K; (a2) pp = 0.7 kPa, T = 373 K; (b2) pp = 6.3 kPa, T = 373 K; (a3) pp = 0.7 kPa, T = 423 K; (b3) pp = 6.3 kPa, T = 423 K.

It is clear from the Fig. 6.16 that *n*HEX is the only compound that adsorbs. This feature gives to the material an important role as a molecular sieve material to separate *n*HEX from the other isomers. Another interesting feature is that the *n*HEX breakthrough profile shows a slow approach to equilibrium meaning that also for this compound the sorption is dominated by a strong resistance to mass transfer probably because the size of *n*HEX is similar to the pores dimensions of the material, which difficult the access to the framework.

6.4. Structure of MIL-125

Titanium terephthalate MIL-125 or $Ti_8O_8(OH)_4$-$(O_2C$-C_6H_4-$CO_2)_6$ exhibits a rigid quasi-cubic tetragonal structure, [7] with cell parameters a = 18.654(1) Å and c = 18.144(1) Å, unit cell volume = 6313.9(1) $Å^3$ and the *I 4/m m m* (n° 139) space group. The 3D connection of the Ti oxoclusters and the terephthalate anions delimits two types of microporous cages corresponding to the octahedral (Fig. 6.17, yellow sphere) and tetrahedral (Fig. 6.17, green sphere) extended vacancies of the parent cubic centred structure with accessible diameters 12.55 and 6.13 Å, respectively [7]. The cages are accessible through triangular windows with a free aperture within the 5-7 Å range [7]. The surface areas estimated by the BET and Langmuir method are: S_{BET} = 1550(20) $m^2.g^{-1}$ and S_{Lang} = 1950(10) $m^2.g^{-1}$, respectively.

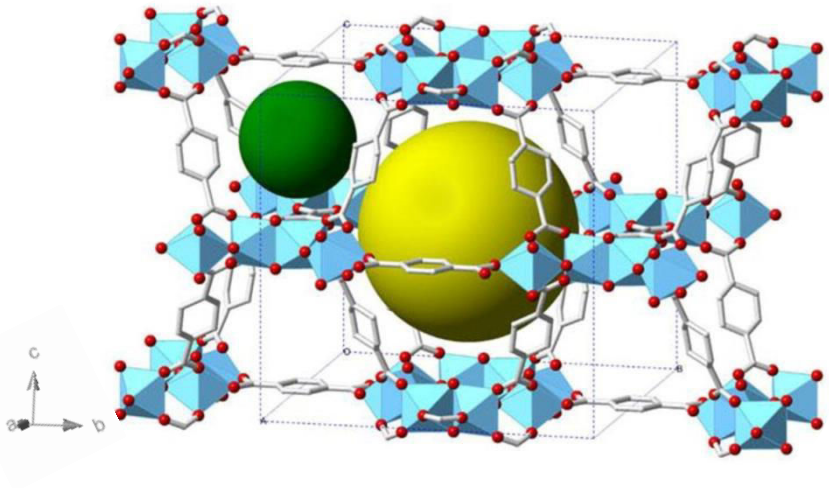

Figure 6.17 - Polyhedral view of a unit cell of MIL-125 [8]. Ti octahedral (Blue), Carbon (grey), oxygen (red); octahedral (yellow sphere) and tetrahedral (green sphere) vacancies.

6.4.1. MIL-125–NH_2

6.4.1.1. Experimental Section

Synthesis

The functionalized amino form of MIL-125 was obtained and denoted MIL-125-NH_2. The synthesis was performed using a mixture of 20 mL of dry DMF and 5mL of methanol, to which 1.5 mL of titanium(IV) isopropoxide (5 mmol) and 1.5 g of 2-aminoterephthalic acid (8.3 mmol) were added. The resulting slurry was placed in a Teflon-lined solvothermal Parr bomb of 125 mL at 423 K overnight. Finally, the yellow powder was recovered by filtration. This material was synthesized at ILV by Dr. Florence Ragon and sent to LSRE–IPB for the sorption experiments.

6.4.1.2. Results and Discussion

Before the screening sorption tests, MIL-125–NH_2 was activated in its powdered form in a vacuum oven at nearly 10 kPa bar during 15 h at 423 K. 194 mg of this sample was mixed with ceramic wool to minimize pressure drop problems. The breakthrough experiments were performed at 373 and 423 K for high (6 kPa) and low partial pressure (0.6 kPa). Table 6.10 shows the experimental conditions and the amount adsorbed of each component.

Table 6.10 - Experimental conditions and amounts adsorbed of the hexane isomers in MIL-125–NH_2.

Run	*T* (K)	Helium flow rate (mL(STP).min^{-1})	Mixture pressure (kPa)	m_{ads} (mg)	Partial loading (g.100g_{ads}^{-1})				Total loading (g.100g_{ads}^{-1})
					22DMB	23DMB	3MP	*n*HEX	
NH_2_a1	373	36.8	0.6	194	0.79	1.19	1.53	2.27	5.79
NH_2_a2	423				0.36	0.51	0.66	1.06	2.60
NH_2_b1	373	13.8	6		1.94	2.76	3.39	4.51	12.61
NH_2_b2	423				0.70	1.34	1.55	2.58	6.18

The maximum adsorbed amount is close to 13 wt% at 373 K and 6 kPa. The affinity order follows once again the same as the boiling points: 22DMB < 23DMB < 3MP < *n*HEX. Table 6.11 shows selectivities that range from 2.6 for *n*HEX/22DMB to 1.3 for 23DMB/22DMB.

Table 6.11 - Selectivities of hexane isomers in MIL-125-NH_2.

Run	*T* (K)	Mixture pressure (kPa)	Selectivities		
			23DMB/22DMB	3MP/22DMB	*n*HEX/22DMB
NH_2_a1	373	0.6	1.4	1.8	2.6
NH_2_a2	423		1.3	1.6	2.4
NH_2_b1	373	6	1.3	1.6	2.0
NH_2_b2	423		1.4	1.6	2.3

Fig. 6.18 shows the quaternary breakthrough curves of the hexane isomers in MIL-125–NH_2 at 373 and 423 K for 0.6 and 6 kPa.

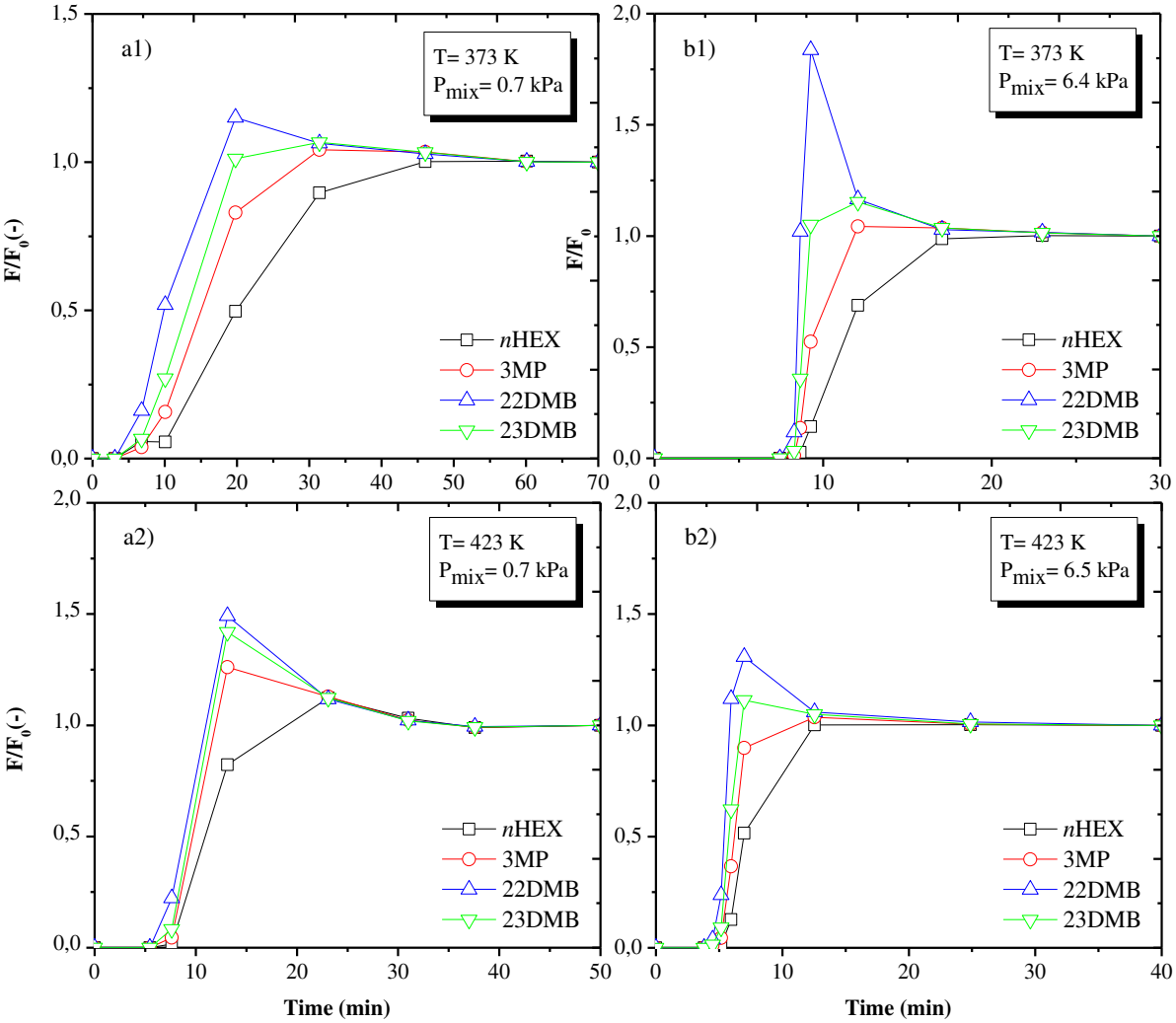

Figure 6.18 - Quaternary breakthrough curves of the hexane isomers in the MIL-125–NH_2; (a1) pp = 0.7 kPa, T = 373 K; (b1) pp = 6.4 kPa, T = 373 K; (a2) pp = 0.7, T = 423 K; (b2) pp = 6.5 kPa, T = 423 K.

It is obvious that a roll-up phenomenon characteristic of competitive adsorption of guest molecules occurs within this structure. The access windows of MIL-125-NH$_2$ possess a free aperture between 5 and 7 Å, which therefore might limit the accessibility to the bulkiest of the hexane isomers (kinetic diameters of *n*HEX, 3MP, 23DMB and 22DMB = 4.3, 5.0, 5.6 and 6.2, respectively). So, if the *n*HEX might easily migrate in both cages, 3MP, 22DMB and 23DMB might be adsorbed preferentially in the larger cage, which could explain the better adsorption of *n*HEX relatively to the other components.

6.5. Conclusions

Several micro and mesoporous rigid MOFs were successfully synthesized and characterized including MIL-100(Cr), MIL-100(Cr) functionalized by PSM with amines, MIL-125–NH_2 and MIL-127(Fe). The screening studies of the hexane isomers separation show that the hexane isomers are typically adsorbed with a selectivity order similar to the one found for the normal boiling points of the compounds: *n*HEX > 3MP > 23DMB > 22DMB. The experimental selectivities were similar to those ones obtained with zeolite BETA (3 for the *n*HEX/22DMB ratio and 1.4 for the 23DMB/22DMB ratio). The exception lies in the MIL-127(Fe) MOF where *n*HEX is exclusively adsorbed in the framework, in agreement with a remarkable molecular sieve effect similar to one observed in zeolite 5A. Finally, the adsorbed amounts are, in most cases, considerably higher than classic adsorbents such as activated carbons or zeolites, which is a characteristic feature of MOFs consequence of their higher porosity. For example, MIL-100(Cr) is able to adsorb up to 27 wt% of alkanes at 343 K and 10 kPa, which is almost the double compared with the zeolite 5A for *n*HEX.

6.6. References

1. *P. Wright, Microporous framework solids, Roy. Soc. of Chem, United Kingdom, 2008.*

2. *G. Férey, C. Serre, C. Mellot-Draznieks, F. Millange, S. Surblé, J. Dutour, I. Margiolaki, A Hybrid Solid with Giant Pores Prepared by a Combination of Targeted Chemistry, Simulation, and Powder Diffraction, Angew. Chem. Int. Ed., 43 (2004) 6296-6301.*

3. *G. Férey, C. Serre, T. Devic, G. Maurin, H. Jobic, P.L. Llewellin, G. Weireld, A. Vimont, M. Daturi, J.S. Chang, Chem. Why hybrid solids capture greenhouse gases?, Soc. Rev. 40 (2011) 550–562.*

4. *T. Trung, N. Ramsahye, P. Trens, N. Tanchoux, C.Serre, F. Fajula, G. Férey, Adsorption of C5–C9 hydrocarbons in microporous MOFs MIL-100(Cr) and MIL-101(Cr): A manometric study, Micropor. Mesopor. Mater., 134 (2010) 134-140.*

5. *S. Wang, X. Wang, L. Li, R. C. Advincula,* Design, Synthesis and Photochemical Behavior of Poly(benzyl ester) Dendrimers with Azobenzene Groups Throughout Their Architecture, *J. Org. Chem. 69 (2004) 9073–9084.*

6. *Y. Liu, J. F. Eubank, A. J. Cairns, J. Eckert, V. C. Kravtsov, et al., Assembly of Metal–Organic Frameworks (MOFs) Based on Indium-Trimer Building Blocks: A Porous MOF with soc Topology and High Hydrogen Storage, Angew. Chem. Int. Ed, 46 (2007) 3278–3283.*

7. *M. Dan-Hardi, C. Serre, T. Frot, L. Rozes, G. Maurin, C. Sanchez, and G. Férey; A New Photoactive Crystalline Highly Porous Titanium (IV) Dicarboxylate; J. AM. CHEM. SOC., 131 (2009) 10857–10859.*

8. *S. Kim, J. Kim, H. Kim, H. Cho, W. Ahn, Adsorption/catalytic properties of MIL-125 and NH2-MIL-125, Catalysis Today, 204 (2013) 85– 93.*

7.

Conclusions and Suggestions for Future Work

This work was devoted to explore the potential of porous MOFs to adsorb and separate gaseous mixtures. In this particular case we were interested in the separation of hexane isomers, since not all of them have the same RON (Research Octane Number), and that has influence in the improvement of the octane number of the gasoline.

For that purpose several MOFs were synthesized at *Institut Lavoisier de Versailles*, characterized and further analysed for their adsorption and separation capacity in Laboratory of Separation and Reaction Engineering. The synthesis was performed at the milligram scale in new functionalized porous materials, namely: UiO-66(Zr)(–NO_2, –Br and –NH_2), MIL-100(Cr)(–ethylamine and –methyl ethylene diamine), MIL-125–NH_2, MIL-127(Fe), ZIF-8, MIL-53(Fe)(–$(CF_3)_2$ and –$2CH_3$) and the MIL-88B–$2CF_3$. The functionalization was used to modulate the pore size of the materials and to limit or to increase the cages and windows, with the aim to improve the separation of hexane isomers. A set of screening studies was performed to evaluate the performance of the studied MOFs in terms of adsorption capacity and selectivities through breakthrough experiments.

Concerning the UiO-66(Zr) functionalized MOFs (–NO_2, –Br and –NH_2) studied in Chapter 3, it was found an uptake reaching 15 wt% with a reverse shape selectivity order (22DMB>23DMB>3MP>*n*HEX) characteristic of the UiO-66(Zr) framework with some differences between the functionalized structures. Particularly, the UiO-66(Zr)–Br solid demonstrates better selectivity at low uptakes 22DMB/*n*HEX (around 3) than for high uptakes

(around 1.3). The selectivity 22DMB/3MP is very small (between 1.0 and 1.1). In the case of the MOF UiO-66(Zr)–NO_2 the selectivities 22DMB/*n*HEX are smaller relatively to the UiO-66_Br (around 1.8), but the selectivity between the 22DMB/3MP is slightly higher (around 1.3). However, in the case of the UiO-66(Zr)–NH_2 a slight alteration on the tendency order changing from reverse for normal is observed. The UiO-66(Zr)–NH_2 satisfies the criteria for upgrading conventional TIP processes since high RON di-branched paraffins exhibit a significant selectivity relatively to the low RON parents (monobranched and linear ones) at high uptake.

Relatively to the ZIF-8 studied in Chapter 4, it was found a potential MOF to separate linear *n*HEX from the other branched isomers due to the high loading of the *n*HEX (around 25 wt% at 313 K and 10 kPa) relatively to the other isomers (practically zero). This high uptake of *n*HEX can be explained by the important accessible pore volume of ZIF-8. The estimated heat of sorption was around 32.8 $kJ.mol^{-1}$. Binary experiments with the isomers 3MP/22DMB demonstrate a poor separation with a practically negligible sorption. Accordingly, we can consider ZIF-8 as an efficient adsorbent to separate linear *n*HEX from the branched isomers. This fact places the ZIF-8 as a remarkable candidate to compete with some molecular sieves, such as zeolite 5A.

The flexible MOFs MIL-53(Fe) functionalized (–$2CH_3$ and –$(CF_3)_2$) and the MIL-88B(Fe)–$2CF_3$were studied in Chapter 5 and present an uptake ranging from 1 (for the MIL-53(Fe)–$2CH_3$) to 6 wt% for the structures MIL-53(Fe)–$(CF_3)_2$ and MIL-88B(Fe)–$2CF_3$. The MIL-53(Fe)–$2CH_3$ demonstrates low affinity with the hexane isomers with a small retention time within the column. The framework MIL-53(Fe)–$(CF_3)_2$ and MIL-88B(Fe)–$2CF_3H_3$ exhibit similar adsorption capacity, however their big difference is the selectivity that each ones offer. Through the MOF MIL-53(Fe)–$2CF_3$ we obtained a maximum selectivity $S_{nHEX/22DMB}$=4. The separation of the mono and di-branched isomers, through the MIL-88B(Fe)–$2CF_3$is only $S_{3MP/22DMB}$=1.3 at 393 K and 0.5 kPa.

The studies performed in the MIL-53(Fe)–$(CF_3)_2$ show the more interesting results found in this work since 22DMB is practically excluded from the framework giving rise to a molecular sieve effect relatively to the other mono and linear isomers. According to our objectives, this result indicates that the MIL-53(Fe)–$(CF_3)_2$ is a promising candidate for the improvement of the octane number of actual TIP processes.

The screening studies in rigid MOFs studied in Chapter 6 show that the hexane isomers adsorb in all materials with a selectivity order similar to the one found for the normal boiling points of the compounds: *n*HEX>3MP>23DMB>22DMB. The exception is found in MOF MIL-127(Fe) where only *n*HEX is able to enter in the framework giving rise to a molecular sieve effect similar to the one observed in ZIF-8. The amounts adsorbed are considerably high (above 20 wt%) which is a feature characteristic of MOFs when compared to classic adsorbents such as activated carbons or zeolites. For example in MIL-100(Cr) the amounts adsorbed reach 27 wt% at 343 K and 10 kPa, in MIL-100(Cr) MEDA 24 wt% at 343 K and 10 kPa and in MIL-100(Cr) ethylamine 18 wt% at 343 K and 6 kPa. In the case of MIL-100(Cr) the value is practically the double of the one found in zeolite 5A for the sorption of *n*HEX. In the MOFs where all the isomers are free to adsorb it is observed selectivities similar to the ones found in classic materials such as for example zeolite BETA ranging from 3 for the ratio *n*HEX/22DMB to a value around 1.4 for the ratio 23DMB/22DMB. It should be also noted that the results observed for MIL-127(Fe) are very interesting since they demonstrate again the interesting feature of porous solids which is the capability of some frameworks to exhibit molecular sieve effects.

As a final conclusion this work demonstrates that MOFs can be efficient separators of hexane isomers. Flexible MOFs such as the MIL-53(Fe)–$(CF_3)_2$ and ZIF-8 and the rigid MIL-127(Fe) can give rise to molecular sieve effects. The functionalized UIO-66(Zr) keeps the reversal shape selectivity effect already demonstrated in a previous cooperation between LSRE and ILV. The large pore rigid frameworks such as the MIL-100(Cr) show a normal trend of selectivity as other type of materials but it can adsorb large amounts of mass (above 20 wt%) which confers them a great feature. For octane enhancement strategies in petrochemical industries such as the TIP processes these results prove that MOF ZIF-8 can separate with a molecular sieve effect *n*HEX from the branched isomers and MIL-53(Fe)–$(CF_3)_2$ to separate 22DMB from the other mono branched isomers with a similar molecular sieve effect. So, the combination of the MOFs ZIF-8 and MIL-53(Fe)–$(CF_3)_2$ into an adsorption system can give rise to the complete fractionation of a mixture of hexane isomers through adsorption, which is the first result shown in literature. The major drawback is that the separation 3MP/22DMB in MIL-53(Fe)–$(CF_3)_2$ is obtained at the low temperature of 313 K and low partial pressures. This means that an improvement should be done for the MOF be capable to do the separation at higher temperatures and partial pressures.

Suggestions for Future Work

The first suggestion for future work is to synthesize at a multi gram scale the best MOFs studied especially the MIL-53(Fe)–$(CF_3)_2$ and to test it in a pilot plant operating in a PSA, TSA or purge displacement cycle to study the effect of operational parameters for the separation of hexane isomers. It is also imperative to perform a detailed kinetic and equilibrium studies to develop a mathematical model of simulation. Moreover studies in a layered bed with MOFs ZIF-8/ MIL-53(Fe)–$(CF_3)_2$ can give rise to the complete fractionation of a mixture of hexane isomers. This process can be called "Fractionation of hexane isomers mixtures using MOFs", where for example a mixture 3MP/22DMB/*n*HEX is separated first with ZIF-8, filtering the majority of *n*HEX and the rest of the mixture (3MP/22DMB) separated with MIL-53(Fe)–$(CF_3)_2$. So, the suggestion is the design of a suitable industrial adsorption cyclic separation process in a layered or mixed bed of ZIF-8 and MIL-53(Fe)–$(CF_3)_2$ (Pressure Swing Adsorption – PSA, Isobaric Displacement Processes – IDP or Simulated Moving Bed - SMB).